UNIVERSITÀ DEGLI STUDI DI PAVIA

Dottorato di Ricerca in Scienze della Terra e dell'Ambiente (XXXIV Ciclo)

Coordinatore: Chiar.mo Prof. Roberto Sacchi

EXPLOITING THE PAVIA TERRITORY PLANT BIODIVERSITY FOR THE DISCOVERY OF PROTEASOME MODULATORS

Tutor: Prof.ssa Emanuela Martino

Tesi di dottorato di
Valeria Cavalloro

Summary

The research

Since ancient times, natural organisms or their derivatives are used as foods, cosmetics and medicines. Today it is well recognized that natural products are essential for human life: they are used as food, raw materials for medicines, improving our health and well-being. Accordingly, secondary metabolites, mainly thanks to their great chemical diversity, play a fundamental role in the discovery of bioactive compounds.

Starting from these considerations, along my PhD journey, I focused on the valorization of both the vascular and the lichen flora of Pavia countryside with the double aim to preserve the territory where I live and to discover new effective drugs. To reach the goals, based on the information available so far, we studied both the vascular flora and lichens, following the strategy briefly here below explained.

As a first step of the work, a database reporting all the 3D structures of the secondary metabolites produced by the plants growing in the Pavia territory was set up. This database could be a tool suitable for speeding up the identification of biologically active metabolites able to interact with specific targets. Briefly, through a literature survey and consulting the databases already available, all the most common plants growing in our territory have been associated to their secondary metabolites. In this way, a new database, reporting the metabolites produced by the most common plants growing in our territory called Secondary Metabolites Search (S.M.S.) was built. So far, this database collects the 2D and 3D structures of more than 5000 compounds produced by plants growing in our territory. For a full botanical description, in the near future the database will be further implemented by reporting the producing organism and inserting the link to Floritaly, the portal to the Italian flora. The database allows an easy download of all the data, thus simplifying the research on natural products in different fields, including computational applications. Moreover, the S.M.S. structure will allow an easy aggregation of data coming from other Italian Flora, so it could represent an embryo for a DB reporting the secondary metabolites produced by all the plants growing in Italy. The preparation of database has been possible thanks to the collaboration with Professor Stefano Martellos of University of Trieste (Department of Life Science).

With the database in hands, a first attempt to use it to valorize the biodiversity of our territory was performed, following an already well-founded strategy: the use of pharmaceutical botany to valorize the biodiversity of a selected territory.

Thanks to the Erasmus traineeship program, I had the opportunity to spend three months at Inte:Ligand (Vienna, Austria) and to collaborate with Professor Sharon Bryant. During my stay at Inte:ligand, I focused on proteasome inhibitors, as new potential anticancer drugs. To select molecules potentially able to inhibit proteasome, a pharmacophoric model was set up and it was used for the virtual screening of all the molecules reported in the previously described database. In this way, seven metabolites potentially able to inhibit proteasome have been identified (Table 1).

Table 1: Molecules identified as potential proteasome inhibitors and their producing organisms.

Name	Source
Kaempferol-3-O-β-D-glucoside-7-O-α-L-rhamnoside	*Eryngium campestre* L.
6-methoxykaempferol-3-O-glucoside	*Artemisia annua* L.
Aucubin-10-O-β-D-glucosyl	*Scrophularia canina* L.
Cyanidin-3-O-arabinoside	*Vaccinium myrtillus* L.
Kaempferol-3-O-α-L-rhamnopyranosyl(1-2)-β-D-galactopyranoside	*Blackstonia perfoliata* (L.) Huds.
Vicianin	*Vicia segetalis* Thuill. AND *Vicia sativa* L.
Kaempferol-3-O-α-L-arabofuranoside	*Prunus spinosa* L.

None of the overmentioned metabolite has been studied so far for its ability to modulate proteasome.

To validate our model we collected *P. spinosa* flowers and *A. annua* aerial parts, purchased *V. sativa* seeds, an extract of *V. myrtillus* fruits and two commercially available metabolites: Cyanidin-3-O-arabinoside and Kaempferol-3-O-alpha-L-arabofuranoside.

Regarding *A. annua* aerial parts and *V. sativa* seeds, an appropriate extract has been prepared and its fractionation has been performed to isolate the metabolites of interest. For both these natural matrices, literature protocols have been firstly applied, the extraction procedure was then optimized, and the obtained extract fractionated. In this way, pure 6-methoxykaempferol-3-O-glucoside and an enriched fraction of vicianin in suitable amounts for further studies have been obtained.

A preliminary biological profile of crude extracts, enriched fractions and pure metabolites, have been drawn, performing MTT, trypan blue (both cell viability tests), and proteasome activity tests. These analyses have been performed at University Milano-Bicocca, thanks to the collaboration with Professor Guido Cavaletti.

Results highlight that *V. sativa* methanolic extract and *V. myrtillus* are active against glioblastoma cell line, after 48h and after 72h, respectively. Multiple Myeloma and Breast cancer cell lines resulted more sensitive to the treatment with the crude extracts. Encouraged by these results, the activity of enriched fractions and pure compounds have been evaluated. Results highlighted that all the compounds are able to inhibit proteasome, demonstrating that the pharmacophoric model previously set up was correct. Moreover, *V. sativa* enriched fraction and Kaempferol-3-O-α-L-arabofuranoside resulted the most effective ones, making them suitable candidates for undergoing to drug development process.

In the meantime, a study of the lichen flora of Pavia countryside was performed. Despite lichens are often underestimated and the knowledge on these complex organisms is still very poor, during the last years the interest of the scientific community from a medicinal standpoint was grown. Their success in this field is mainly due to their secondary metabolites, whose structures are often absent from other natural matrices. Despite many steps forward have been done in investigating the phytochemical profile of lichens, their characterization is far to be completed. For this reason, the valorization of the lichen flora through the development of a DB of secondary metabolites could be limitative, being only a limited number of structures elucidated so far. We focused our attention on three lichens belonging to Cladonia genus growing in the Pavia territory: *Cladonia foliacea*, *C. furcata* and *C. rangiformis*. These species grow near the Ticino river and therefore their in-depth study from a phytochemical point of view can represent a further step towards the enhancement of our territory. Extractive, analytical, and separative procedures have been developed and their main metabolites isolated and characterized, i.e. (*S*)-usnic and fumarprotocetraric acids from *C. foliacea*, atranorin and rhizomic acid from *C. furcata* and *C. rangiformis*. Crude extracts and the pure metabolites have been investigated for their potential anticancer and antifungal properties.

Results evidenced that all the extracts are able to reduce viability of multiple myeloma, breast cancer, cholangiocarcinoma and glioblastoma cell lines. More in details, RPMI 8226 (multiple myeloma), MCF7 (breast cancer), and EGI-1 (cholangiocarcinoma) resulted more sensitive than U87-MG (glioblastoma). Moreover, (*S*)-usnic acid and fumarprotocetraric acid impaired cell viability in a dose- and time-dependent manner, while atranorin didn't show any effect.

Regarding the assays performed on fungal stains, we found that crude extracts and isolated metabolites are able to reduce viability in *Candida albicans*, *Candida tropicalis*, *Trichophyton rubrum* and *Aspergillus niger* stains. These good results prompted us to further optimize the active metabolites and now the semi-synthesis of a small library of derivatives is ongoing. These new chemical entities could represent new weapons against infections still considered unmet medical diseases and whose complications still causes many deaths.

La ricerca

Storicamente, gli estratti ottenuti da organismi naturali sono stati riconosciuti come la base di medicinali, cosmetici e alimenti. Oggi i prodotti naturali continuano ad essere una risorsa importante per lo sviluppo tecnologico e socioeconomico e per il mantenimento del benessere umano. In questo scenario, i metaboliti secondari giocano un ruolo fondamentale, soprattutto grazie alla loro grande diversità chimica.

Partendo da queste considerazioni, il mio progetto di dottorato si è concentrato sulla valorizzazione della flora sia vascolare che lichenica del territorio pavese, con il duplice obiettivo di preservare il territorio in cui vivo e di individuare nuovi metaboliti secondari biologicamente attivi. Per raggiungere gli obiettivi, sulla base delle informazioni finora disponibili, sono partita studiando la flora vascolare.

Come primo passo del lavoro è stato realizzato un database riportante tutte le strutture 3D dei metaboliti secondari prodotti dalle piante diffuse nel territorio pavese. Questo database potrebbe essere uno strumento utile per velocizzare l'identificazione dei metaboliti biologicamente attivi in grado di interagire con bersagli specifici.

Questa attività è stata svolta in collaborazione con il Professor Stefano Martellos dell'Università di Trieste. Per raggiungere questo obiettivo, tutte le specie più comuni diffuse nel nostro territorio sono state associate ai loro metaboliti secondari attraverso indagini bibliografiche e consultazione di database. Questa attività ha consentito la costituzione di un nuovo database (DB) denominato *Secondary Metabolites Search* (S.M.S.). Il database raccoglie più di 5000 composti isolati dalle specie distribuite nel nostro territorio e li descrive considerando sia la loro struttura 2D che 3D. Per una descrizione botanica completa in futuro il database verrà ulteriormente implementato riportando l'organismo produttore, e inserendo il link a Floritaly, il portale della flora italiana. Il database consentirà un facile download di tutti i dati, semplificando così la ricerca sui metaboliti attivi in diversi campi, comprese le applicazioni computazionali. Inoltre, la struttura di S.M.S. consentirà una facile aggregazione di dati provenienti da altre flore italiane, rappresentando quindi il punto di partenza per un DB riportante i metaboliti secondari prodotti da tutte le piante italiane.

Un altro importante obiettivo del mio progetto di dottorato è sfruttare il database sviluppato per valorizzare la biodiversità del nostro territorio seguendo una strategia già ben fondata: l'utilizzo della botanica farmaceutica per la valorizzazione della biodiversità di un territorio selezionato. In dettaglio, grazie alla collaborazione con la Professoressa Sharon Bryant di Inte:Ligand (Vienna, Austria), è stato messo a punto un modello farmacoforico, utilizzato per lo screening virtuale di tutte le molecole riportate nel DB precedentemente descritto, con l'obiettivo di selezionare quelle potenzialmente in grado di inibire il proteasoma. Questo target è stato selezionato in quanto è il meccanismo alla base di alcuni farmaci antitumorali. Questo ci ha permesso di selezionare sette diversi metaboliti potenzialmente in grado di inibire il target considerato (Tabella 1).

Tabella 1: Molecole identificate come potenziali inibitori del proteasoma e loro fonti.

Nome	Fonte
Kaempferol-3-O-β-D-glucoside-7-O-α-L-rhamnoside	*Eryngium campestre* L.
6-methoxykaempferol-3-O-glucoside	*Artemisia annua* L.
Aucubin-10-O-β-D-glucosyl	*Scrophularia canina* L.
Cyanidin-3-O-arabinoside	*Vaccinium myrtillus* L.
Kaempferol-3-O-α-L-rhamnopyranosyl(1-2)-β-D-galactopyranoside	*Blackstonia perfoliata* (L.) Huds.
Vicianin	*Vicia segetalis* Thuill. AND *Vicia sativa* L.
Kaempferol-3-O-α-L-arabofuranoside	*Prunus spinosa* L.

Nessuno dei metaboliti sopra menzionati è stato già oggetto di studio come modulatore del proteasoma. Dati di letteratura però dimostrano che alcuni metaboliti strutturalmente correlati a quelli selezionati sono già stati identificati come inibitori del proteasoma, rendendoci ottimisti sulla bontà del modello sviluppato.

Per convalidare il nostro modello, in seguito abbiamo raccolto fiori di *P. spinosa* e parti aeree di *A. annua*, mentre abbiamo acquistato semi di *V. sativa* e un estratto di frutti di *V. myrtillus*. Abbiamo anche acquistato due metaboliti puri selezionati dal modello: Cyanidin-3-O-arabinoside da *V. myrtillus* e Kaempferol-3-O-alpha-L-arabofuranoside da *P. spinosa*.

Sia la droga di *A. annua* che di *V. sativa* sono state successivamente sottoposte a frazionamento per isolare i metaboliti di interesse. Per entrambe queste matrici naturali sono stati dapprima applicati protocolli di letteratura. Successivamente, è stata eseguita l'ottimizzazione sia delle procedure di estrazione che di frazionamento, consentendoci di ottenere il 6-metossi-kaempferol-3-O-glucoside puro e una frazione arricchita di vicianina, entrambi in quantità adeguate agli studi biologici.

Una volta ottenuti i grezzi, le frazioni arricchite e i metaboliti puri, sono state effettuati saggi MTT, Trypan blue (entrambi test di vitalità cellulare) e test di attività del proteasoma su tre diverse linee cellunari: RPMI 8226 (Mieloma Multiplo), MCF7 (tumore al seno) e U87-MG (glioblastoma) . Queste analisi sono state eseguite grazie alla collaborazione con il Professor Guido Cavaletti, Università di Milano-Bicocca.

I profili biologici preliminari eseguiti sulle tre differenti linee cellulari hanno evidenziato che solo gli estratti di *V. sativa* dopo 48 ore e di *V. myrtillus* dopo 72 ore sono risultati attivi contro il glioblastoma. Le linee cellulari di Mieloma Multiplo e di cancro al seno, invece, sembrano rispondere in modo simile al trattamento con gli estratti grezzi. Incoraggiati da questi risultati, dopo lo *screening* preliminare degli estratti grezzi, sono state eseguite le analisi biologiche delle frazioni arricchite e dei composti puri su linee cellulari di Mieloma Multiplo. I risultati hanno evidenziato che tutti i composti sono in grado di inibire il proteasoma, dimostrando che il modello farmacoforico precedentemente costruito era corretto. Inoltre, la frazione arricchita di *V. sativa* e

Kaempferol-3-O-α-L-arabofuranoside sono risultati i più efficaci, rendendoli candidati idonei per essere sottoposti al processo di sviluppo di farmaci.

Parallelamente a quanto descritto, è stata portata avanti anche la valorizzazione della flora lichenica del territorio pavese. Nonostante i licheni siano spesso sottovalutati e le conoscenze su questi complessi organismi siano ancora molto scarse, negli ultimi anni l'interesse della comunità scientifica, dal punto di vista medicinale, è cresciuto. Il loro successo in chimica farmaceutica è dovuto principalmente ai loro metaboliti secondari, le cui strutture sono spesso assenti da altre matrici naturali. Nonostante siano stati fatti molti passi avanti nello studio del profilo fitochimico di molti licheni, la loro completa caratterizzazione è ancora lontana dal completamento. Per questo motivo la valorizzazione della flora lichenica attraverso lo sviluppo di un DB di metaboliti secondari potrebbe essere limitativa, essendo molte strutture ancora da scoprire.

Abbiamo quindi deciso di focalizzare la nostra attenzione su tre licheni appartenenti al genere Cladonia che crescono nel nostro territorio, ovvero *Cladonia foliacea*, *C. furcata* e *C. rangiformis*. Queste specie sono state scelte in quanto crescono nei pressi del fiume Ticino e quindi il loro approfondimento fitochimico può rappresentare un ulteriore passo verso la valorizzazione del nostro territorio. In particolare, abbiamo messo a punto procedure estrattive, analitiche e separative per caratterizzarli. Abbiamo successivamente isolato e caratterizziamo i loro principali metaboliti, ovvero (*S*)-acido-usnico e acido fumarprotocetrarico da *C. foliacea* e atranorina e acido rizonico da *C. furcata* e *C. rangiformis*. Successivamente abbiamo analizzato i grezzi e i metaboliti puri sia considerando la loro attività nei confronti di linee cellulari tumorali che nei confronti di ceppi fungini.

I risultati hanno evidenziato che tutti gli estratti di licheni sono in grado di ridurre la vitalità nelle linee cellulari testate in maniera dose-dipendente. In dettaglio, le linee RPMI 8226 (mieloma multiplo), MCF7 (carcinoma mammario), ed EGI-1 (colangiocarcinoma) sono risultate più sensibili di U87-MG (glioblastoma). Inoltre, in tutte le linee cellulari testate, sia l'(*S*)-acido usnico che l'acido fumarprotocetrarico hanno ridotto la vitalità cellulare in modo dose e tempo dipendente, mentre l'atranorina non ha mostrato alcun effetto.

Anche i saggi eseguiti sui ceppi fungini hanno portato a buoni risultati. Infatti, sia gli estratti grezzi che i metaboliti puri sono stati in grado di ridurre la vitalità di *Candida albicans*, *Candida tropicalis*, *Trichophyton rubrum* e *Aspergillus niger*. Tali risultati ci hanno spinto ad ottimizzare ulteriormente i metaboliti attivi ed è ora in corso la semi-sintesi di una piccola libreria di derivati.

Queste nuove entità chimiche potrebbero rappresentare nuove armi contro le infezioni ancora considerate *unmet medical need* e le cui complicanze sono ancora associate ad un alto tasso di mortalità.

List of abbreviations

ACN	Acetonitrile
AIs	AutoInducers
ATR	Atranorin
AUC	Area Under the Curve
BSTA	N,O-Bis(trimethylsilyl)trifluoroacetamide
BTZ	Bortezomib
DB	Database
DCM	Dichloromethane
CTRL	Control
DoE	Design of Experiment
DPD	4,5-dihydroxy-2,3 pentane-dione
Ef	Enriched fraction
EF	Enriched factor
FBS	Fetal Bovine Serum
FDA	Food and Drug Administration
FPCA	Fumarprotocetraric Acid
FT	Fourier Transform
FTIR	Fourier Transform InfraRed
Hex	Hexane
HPLC	High Pressure Liquid Chromatography
IC	Invasive Candidiasis
IFIs	Invasive Fungal Infections
IR	Infrared
LBDD	Ligand-based Drug Discovery
L/L E	Liquid/Liquid Extraction
MASE	Microwave Assisted Solvent Extraction
MBD	Myeloma Bone Disease

MM	Multiple Myeloma
MTT	3-(4,5-Dimethylthiazol-2-yl)-2,5-Diphenyltetrazolium Bromide
mw	Microwave
MW	Molecular Weight
NA	Not Active
NADD	Nature Aided Drug Discovery
NDM-1	New Delhi metallo-β-lactamase-1
NHDF	Normal Human Dermal Fibroblasts
NMR	Nuclear magnetic resonance
NP	Natural Product
PDA	Photodiode Diode Array
PDB	Protein Data Bank
PLE	Pressurized Solvent Extraction
QS	Quorum Sensing
R_f	Retention Factor
r.t.	Toom Temperature
SAR	Structure-Activity Relationship
SBDD	Structure-based Drug Discovery
SLE	Solid–Liquid Extraction
SMILES	Simplified Molecular-Input Line-Entry System
S.M.S.	Secondary Metabolites Search
SFE	Supercritical Fluid Extraction
TCA	Trichloroacetic acid
TEA	Triethylamine
TMS	Trimethyl silane
TFA	Trifluoroacetic acid
t-SNE	T-distributed Stochastic Neighbor Embedding
TLC	Thin Layer Chromatography
UA	Usnic Acid

UASE   Ultrasound-assisted Solvent Extraction

UPP   Ubiquitin-Proteasome Pathway

UV   UltraViolet

1. Introduction

1.1 Nature aided drug discovery (NADD)

Over the centuries, life on hearth has changed and different living beings have developed several ways to protect themselves from the external damages. This statement can be considered true both for the animal and for the plant kingdom and it can explain why several trees, grass and shrubs are able to produce different kinds of compounds to face both the biotic and the abiotic damage. Moreover, natural matrices are able to produce molecules for attractive or defensive purposes or to be useful in the interspecific competition. All compounds produced with these aims belong to the class of secondary metabolites and have been the basis of medicine since ancient time, as witnessed by the well-known Chinese or African traditional medicines [1–6]. Thanks to their chemical diversity, secondary metabolites can be considered a limitless source of interesting active molecules, thus their study can bring to the discovery of a very high number of new drugs [7].

One of the most important examples of the success of Nature Aided Drug Discovery (NADD) can be found in the Nobel Prize in Physiology or Medicine of 2015 [8]. This has been conferred to Professor Tu Youyou for the discovery of artemisinin, a sesquiterpene lactone from *Artemisia annua*. This finding has been reached starting from an ethnobotanical approach, being the natural matrix used against malaria since ancient time. Recent works postulated that artemisinin acts by alkylating essential malarial proteins thanks to the free radical intermediate generated by the cleavage of the endoperoxide catalyzed by intra parasitic heme-iron. Treatments containing an artemisinin derivative are now standard treatments against malaria, a disease affecting hundred million people worldwide [1,9–11].

Secondary metabolites can also be considered as synthons for the synthesis of complex molecules. For example, paclitaxel, a potent anticancer drug, is obtained by chemical modification of 10-deacetylbaccatin, a tetracyclic diterpenoid extracted from the needles of *Taxus* genus [12].

Beside the already mentioned ethnobotanical approach, NADD can be performed following different strategies:

- Random approach: serendipity plays a key role in the discovery. One of the most successful randomic approaches is the High Throughput Screening (HTS) which foresee the analysis of a very high number of compounds on different targets to identify the active ones [13];
- Phytochemical approach: the plant to study is chosen for its already known metabolomic content. An example of this approach can be found in the neurodegenerative area and, particularly, in a study where *Ginko biloba* extract has been chosen because of its content in bioactive metalloproteins for the treatment of Alzheimer Disease or other degenerative disorders [14];
- Taxonomic approach: the specie is chosen for its belonging family. This approach finds its main application considering important fungal genera such as *Penicillium* and *Aspergillus*. Thus, fungi belonging to these genera can be interesting sources of antimicrobial agents [15];
- Chemotaxonomic approach: it arises from the union of the taxonomic and phytochemical approaches, so the plant is chosen due to its belonging family and phytochemical

11

content. For example, some active alkaloids are particularly concentrated in some families (Raunuculaceae, Berberidaceae, Papaveraceae), so plants belonging to these families could be potential sources of these metabolites active in different areas, i.e. cancer, antimicrobial and on the Central Nervous System [16];

- Ecological approach: the plant is chosen for its ability to protect itself from external damages. In recent years, this approach has led to select extremophile plants because able to withstand to extreme climatic conditions and to quench toxic ROS [17];

- Ethnobotanical approach: the plant is chosen for its well-known use by the indigenous population. Evidence demonstrates that an ethnobotany-guided plant collections can bring to a higher rate of positive results, compared to a random approach [18].

- Informatics approach: the plant is chosen via chemoinformatic analysis, usually after virtual screening. This is the most modern approach and foresee the exploitation of specific software which allows to screen high number of secondary metabolites on ad hoc models which can retrieve only the compounds virtually able to bind a selected target [19].

For the purpose of this thesis work, this latter strategy requires a more thorough description.

As mentioned before, the success of NADD finds its main reason in the heterogeneous chemical space covered by natural products (NPs) whether compared with synthetic molecules. The 83% of the chemical scaffolds found in nature are unique, due to the lack of commercially available synthons or prohibitive synthetic procedures [20]. Thus, the screening of libraries of compounds deriving from natural sources remains a worthy procedure for the identification of new hit compounds. Taking into account this assumption, many works report on the isolation of a high number of secondary metabolites produced by a selected genus or a selected flora to allow the subsequent High Throughput Screening (HTS) analysis [21]. This approach has led to many successes both in terms of identification of new potent drugs, like Taxol [22], both in terms of valorization and conservation of the considered biodiversity and related benefits to the local people [23]. Despite these important goals, this approach has also important drawbacks, being the isolation of every secondary metabolite required for the screening time consuming and expansive. Considering this, an evolution of the HTS approach has led to the development of virtual libraries reporting the 3D structure of secondary metabolites. Thus, these libraries are suitable for Virtual Screening (VS). This more modern approach has rapidly gained a foothold in the NADD arena and many libraries reporting the 3D structures of secondary metabolites have appeared [24].

Among them, one of the most used is ZINC, a free database provided by the Irwin and Shoichet Laboratories in the Department of Pharmaceutical Chemistry at the University of California, San Francisco (UCSF) [25]. It collects almost one billion of commercially available compounds for VS purposes. Among the different subsets present in the database, four can be considered natural products-related and are summarized in Table 1.

Table 1: Subsets present in ZINC database related to natural products.

Name	Description	Estimated Size (purchasable)
Nonhuman-metabolites	Primary metabolites - also known as metabolites, not reported in humans	2034 (944)
Metabolites	Primary metabolites of any species, including humans	52538 (11096)
Natural-products	Natural products, also known as secondary metabolites, i.e. explicitly excluding metabolites	80617 (48164)
Biogenic	Made by nature, including primary metabolites (metabolites) and secondary metabolites (natural products)	135335 (61592)

Of note, natural-products subsets derived from the collaboration of 20 different companies and organizations like Analyticon Discovery, Herbal Ingredients In-Vivo Metabolism and Specs Natural Products demonstrating that the collaboration among different realities can brings to great goals. The result of this collaboration has been exploited in several works. Among them, an important example is represented by a recent article focused on one of the most urgent medicinal needs of our decade, antimicrobial resistance. In this work, natural-products subsets have been exploited for VS purposes to select potential New Delhi metallo-β-lactamase-1 (NDM-1) inhibitors. Thus, NDM-1 is one of the enzymes responsible of bacterial resistance against β-lactam antibiotics. At the end, Authors identify carnosic acid, a diterpenoid mainly produced by rosemary and sage, as interesting allosteric NDM-1 inhibitor (IC$_{50}$= 27.07 μM). After verifying their results via fluorescence experiments, Authors finally conclude that carnosic acid is a potential NDM-1 inhibitor and it is a promising drug for the treatment of NDM-1 producing pathogens [26].

Despite this important and successful example of data aggregation, nowadays there is no globally accepted community resource for NPs, leading to numerous libraries. In a recent work, 123 databases of NPs have been identified in literature, all different in terms of organization, data reported and scope [27]. Furthermore, beside all these databases reported in literature, as many or even more in-house libraries exists, which can be exploited only by a few numbers of co-workers [28]. Considering the published libraries, the 85% focus on data concerning terrestrial plants. Among this 85%, 63% are general DB and did not specify the geographic origin of the collected data, while 23% reports on plants from Asia, 12% from Africa, 2% from America and only 1% from Europe (Figure 1).
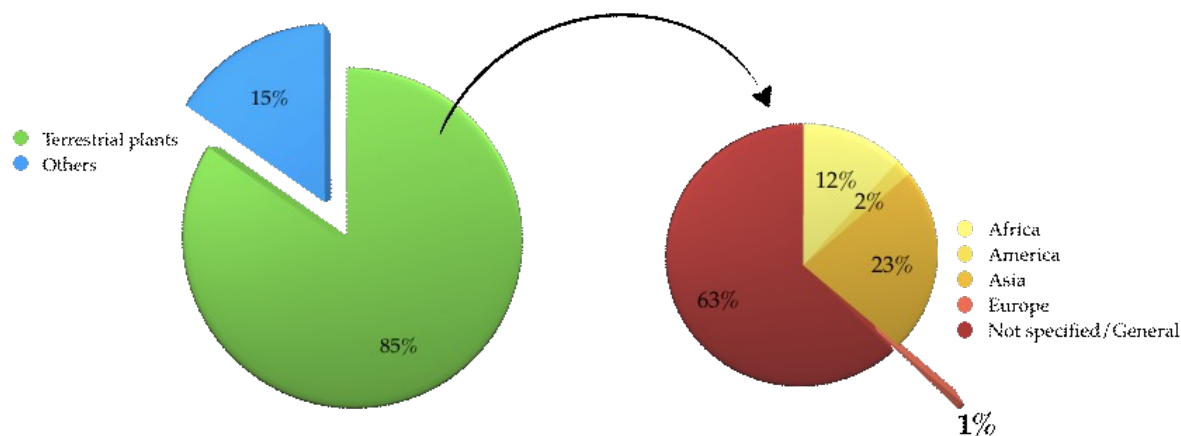
Figure 1: Characteristic and geographic origin of the libraries reported in literature.

This data makes us understand how Europe's biodiversity is largely under considered in the NADD scenario. The reason may lie in the less rooted influence of traditional medicine on our life, in comparison to the well known Chinese or African traditional medicine.

This underestimation hides an inestimable wealth. Thus, the Mediterranean part of Europe is recognized as a global biodiversity hotspot [29,30]. In Europe, the pharmacopoeias of folk practitioners as well as medicinal doctors contain thousands of medicines made from natural matrices, i.e. roots, bark, leaves, herbs, flowers and others, like in Chinese, Ayurvedic, Unani and other systems. Unfortunately, because of the great exploitation of the European land, nowadays many medicinal plants are becoming extinct and, although considerable efforts have been made, biodiversity decline and the associated loss of vital ecosystem services continues to be a major concern in the region.

Nowadays the first community resources which allows to search or analyze data concerning NPs are raising. Particularly, Natural Products Online is an open source project hosting the COlleCtion of Open Natural ProdUcTs (COCONUT) one of the biggest and best annotated resources for NPs completely freely available. It collects data from 50 different DBs and currently contains 426895 unique structures [31]. Simple searches are possible by molecule name, molecular structure, substructures and others. Moreover, several data can be found, like the overview, representations, synonyms, molecular properties and descriptors, known stereochemical variants, references and notes.

All the libraries already mentioned can be applied to chemoinformatics software which allows to set up models able to predict if molecules can be considered ligands of a selected target. This analysis is important because it allows to evaluate which metabolites are potentially active without purchasing or isolating each one of them. This can be translated into a more economic and rapid screening of the metabolites we want to consider. The informatic approach can be divided in two different strategies: the structure-based drug discovery (SBDD) and the ligand-based drug discovery (LBDD) (Figure 2).

In the first case, the 3D structure of the selected target is known thanks to crystallographic, spectroscopic or homology studies, so we can identify its active site and perform docking studies.

This approach allows to identify the most important interactions that a generic ligand has to institute with the target.

In the second case, the 3D structure of target is not known, so the identification of the promising molecules can be performed by comparing their 3D structures with the ones of known ligands. In this case, two different models can be set up: pharmacophoric model and Quantitative Structure-Activity Relationship (QSAR) model. In the pharmacophoric model the 3D structures of known ligands are overlapped to identify the most important and maintained groups (H bond acceptor or donors, hydrophobic features, etc.). In the QSAR model, known ligands are introduced in a grid and the most important features identified thanks to proper probes. On note, this is the only approach, which allows not only to evaluate the affinity of the selected molecules, but also their activity and pharmacokinetic properties.
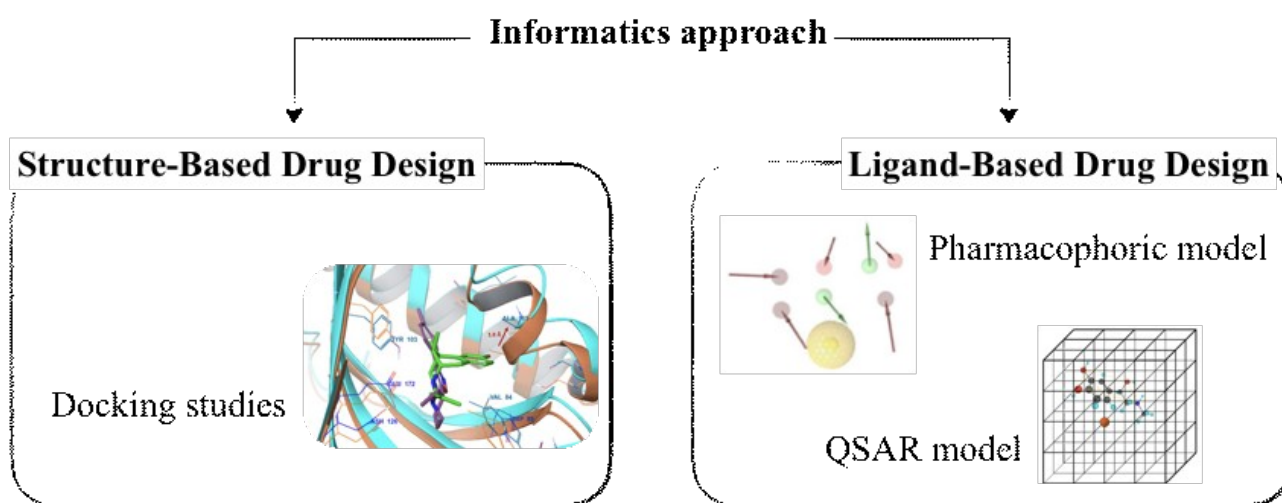

Figure 2: Different strategies in the informatics approach.

Recent software also allows to combine SBDD and LBDD approaches, for example by generating a pharmacophoric model starting from the interaction of a known ligand with the binding site of the target.

1.2 NADD and cancer

Natural products (NPs) found applications in many disease areas with few exceptions, i.e. antihistamines, diuretics, and hypnotics, but probably the most important one is cancer [32–34].

Cancer is the second leading cause of death worldwide [35]. The International Agency for Research on Cancer (IARC) estimated that annually more than 10 million people in the world are affected by cancer and this value is expected to increase over the years [36]. Nowadays, academia and pharma-company are particularly focused on the discovery of new molecular entities active against tumor disease since chemotherapy remains the first-choice treatment for more patients. Thus, innovative and effective treatments for this pathology have been demonstrated to be an urgent medical need [37].

The first anticancer NP approved by the Food and Drug Administration has been vincristine in 1963 for the treatment of lymphomas [38]. This is an alkaloid extracted from *Catharanthus roseus*, which acts by inhibiting the microtubule formation in mitotic spindle, resulting in an arrest of dividing cells at the metaphase stage. From that moment on always more metabolites has been approved as anticancer agents [39–42].

Thus, among the 247 new chemical entities approved as anticancer agents from 1981 to 2019, 185 are small molecules among which 10.2% are NPs (alone or in phytocomplex), 23.2% derived from NPs, 50.5% have been inspired from NPs and only 15.7% are classifiable as totally synthetic [43]. All the non-modified NPs approved by FDA as anticancer agents in the considered period are reported in Table 2.

Table 2: Unmodified NPs approved by FDA as anticancer agents from 1981 to 2019

Generic name	Trade name	Year	Source
Aclarubicin	Aclacin	1981	*Streptomyces galilaeus*
Aminolevulinic acid	Levulan	2000	Animals and plants
Angiotensin II	Delivert	1994	Animals
Aplidine	Aplidin	2018	*Aplidium albicans*
Arglabin	?	1999	*Artemisia glabella*
Homoharringtonine	Ceflatonin	2012	*Cephalotaxus fortunei*
Ingenol mebutate	Picato	2012	*Euphorbia peplus*
Masoprocol	Actinex	1992	*Larrea divaricatta*
Paclitaxel	Taxol	1993	*Taxus brevifolia*
Paclitaxel liposomal	Lipusu	2003	*Taxus brevifolia*
Paclitaxel nanoparticles	Abraxane	2005	*Taxus brevifolia*
Paclitaxel nanoparticles	Nanoxel	2007	*Taxus brevifolia*
Paclitaxel nanoparticles	Genexol-PM	2007	*Taxus brevifolia*
Paclitaxel nanoparticles	PICN	2014	*Taxus brevifolia*
Pentostatin	Nipent	1992	*Streptomyces antibioticus*
Peplomycin	Pepleo	1981	*Streptomyces verticillus*
Romidepsin	Istodax	2010	*Chromobacterium violaceum*
Trabectedin	Yondelis	2007	*Ecteinascidia turbinata*

As evidenced in Table 2, during the last years, there have been some significant approvals of secondary metabolites for the treatment of cancer. These metabolites have been extracted by a great variety of natural matrices, among which we can recognize three fungi belonging to *Streptomyces* genus, one bacterium (*Chromobacterium violaceum*) and two marine organisms (*Aplidium albicans* and *Ecteinascidia turbinate*). The most represented natural source are the plants. Thus, 11 of the 18 NPs approved have been extracted from plants, i.e. *Artemisia glabella, Cephalotaxus fortunei, Euphorbia peplus, Larrea divaricatta* and *Taxus brevifolia*. All their structures are reported in Figure 3.
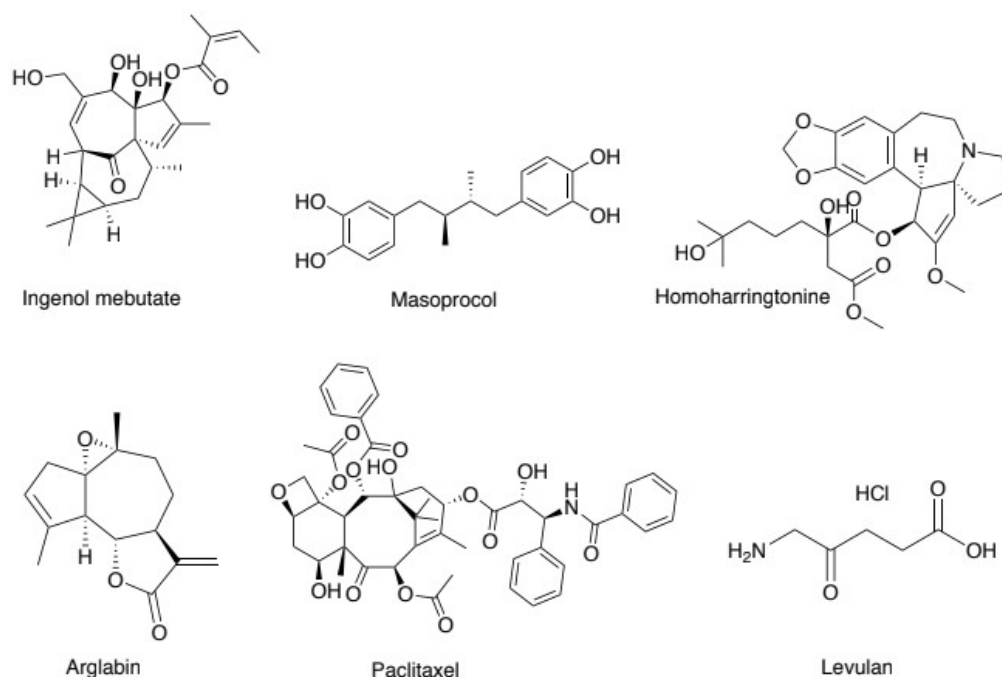
Figure 3: Chemical structures of NPs extracted from plants approved by FDA.

As evidenced by Figure 3, the approved metabolites are characterized by a great chemical diversity. This characteristic is strictly correlated to the possibility to interfere with different biological pathway, like by inhibiting the disassembly of microtubules (Paclitaxel), antibody-dependent cellular cytotoxicity (Ingenol mebutate), inhibiting protein synthesis by acting on ribosomes (Homoharringtonine) and so on [44,45].

Beyond the already approved NPs, many other metabolites are now in early drug discovery process or in clinical development, also for aggressive and orphan cancers like glioblastoma [46]. Thus, nowadays 38 NPs are under investigation for the treatment of aggressive forms of glioblastoma. Among them 17 are now in clinical trials and they all act with different mechanism of action involving apoptosis and autophagy, cell cycle/repair mechanism, proliferation and differentiation, angiogenesis, EMT/STAT3 pathway and microenvironment.

Cancer cells produce proteins that promote both cell survival and proliferation, and/or inhibit mechanisms of cell death. A central component of this cellular protein-degradation machinery is the ubiquitin proteasome pathway, which plays and essential role in preventing the accumulation of misfolded or toxic proteins. For this reason, proteasome has been studied as target for fighting cancers. Proteasome inhibitors approved so fare are effective in patients with myeloma, but side-effects are frequent and acquired resistance is possible. Scientific community is working for finding new proteasome inhibitors with a better biological profile and to understand the mechanisms of resistance. In the following paragraph, this mechanism will be briefly described.

1.3 Proteasome

During cell life, a lot of proteins act as activators/inhibitors of several process or represents the building blocks of different structures. Thus, an equilibrium between protein synthesis and degradation is necessary to allow cell homeostasis. Protein degradation is performed thanks to two different pathways: lysosomal system, responsible for the 10-20% of the protein degradation, and Ubiquitin-Proteasome Pathway (UPP), responsible for the other 80-90% [47].

The UPP acts with a very complex mechanism. First of all, the protein to be degraded is marked by one or more ubiquitins, small proteins (76 aminoacids, 8kDa) able to bind the aminic group of the substrate's lysine residue via an isopeptidic bond thanks to their final carboxylic group. Three different enzymes catalyze this process: E1 activating the ubiquitin, E2 acting as a transferase and moving the ubiquitin to the protein to be degraded and E3, a ligase, allowing the isopeptidic bond. Once marked, the protein can reach proteasome, a multi catalytic complex, that compartmentizes the lysis in 20S core [48–50].

The 20S core is a fundamental part of the multicatalytic complex and it is composed by four rings arranged to form a tunnel in which the protein to be degraded will pass. The two external rings are composed by seven α-subunits (red in Figure 4) while the other two internal rings are composed by seven β-subunits (blue and gray in Figure 4). Inside the 20S core, three β-subunits act as catalytic sites and hydrolyze different kind of aminoacidic chains: (i) β5 is the Chymotrypsin-like and cuts hydrophobic and aromatic residues; (ii) β2 is the Trypsin-like and cuts basic residues; (iii) β1 is the Caspase-like and cuts the acidic residues [51–54].

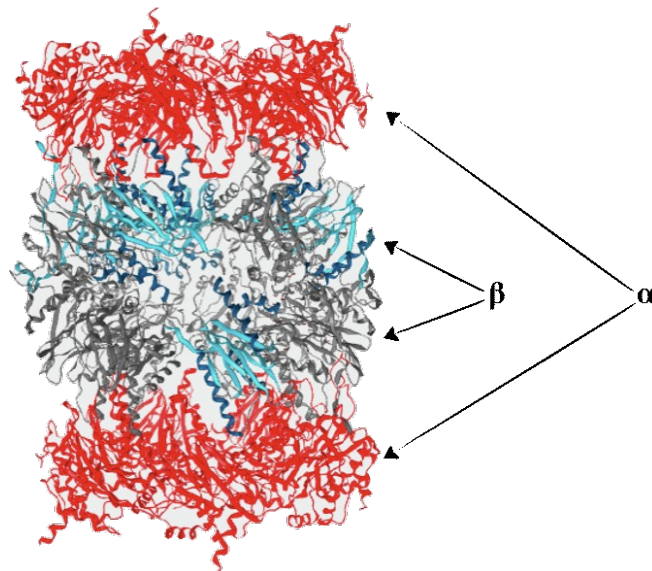**Figure 4:** Crystal structure of proteasome 20S core. α-subunits are reported in red while β-subunits are reported in blue-grey.

The 20S core can be coupled with some regulator domains among which the most frequent one is 19S. This later structure can bind both the extremity of the tunnel formed by 20S core or only its entrance. The complex obtained from the coupling between 20S core and 19S factor is called 26S

(1500–2000 kDa) (Figure 5). This second complex regulates the 20S core function and allows the substrate's entering in the catalytic site by allowing protein's unfolding [55,56].
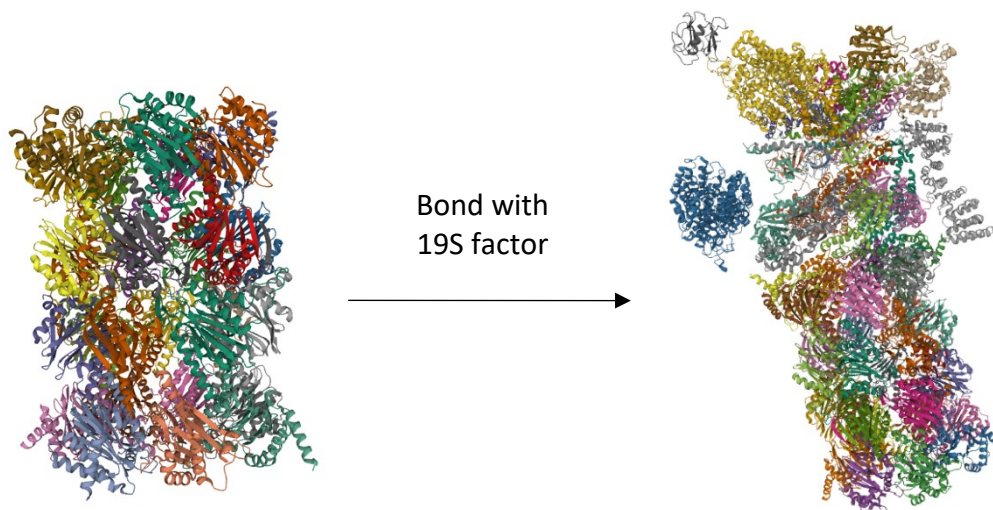

Bond with
19S factor

Figure 5: Crystal structure of 20S core and 26S complex

At the beginning, molecules inhibiting proteasome were exploited to study the function of the multicatalytic complex itself. Then became evident that these molecules caused apoptosis in leukemic cell lines. Studies have deepened this aspect and nowadays there are three different proteasome inhibitors approved for the clinical uses against Multiple Myeloma (MM): Bortezomib (Velcade®), Carfilzomib (Kyprolis®) and Ixazomib (Ninlaro®) (Figure 6) [57]. MM is a malignant tumor concerning plasma cells, and represents about 1% of all the malignancy and 10% of the hematologic ones. Among the risk factors, age is probably the most important one, since 66% of patients are more than 65 years old and only 1% of them are less than 40 years old. Chemical and physical agents, like pesticides, petroleum derivate and ionizing radiations, represent another important risk factor. Neoplastic plasma cells infiltrate bone marrow where they find a favorable microenvironment promoting cell proliferation and adhesion [58]. During the development of MM, plasma cells in bone marrow rise from 3% to more than 10%, leading to anemia, leucopenia and thrombocytopenia. Other clinical features of MM are osteoclasts activation and osteoblasts inhibition leading to bone resorption, hyperkalemia and bone fractures, pathological condition called myeloma bone disease (MBD) [59–61].
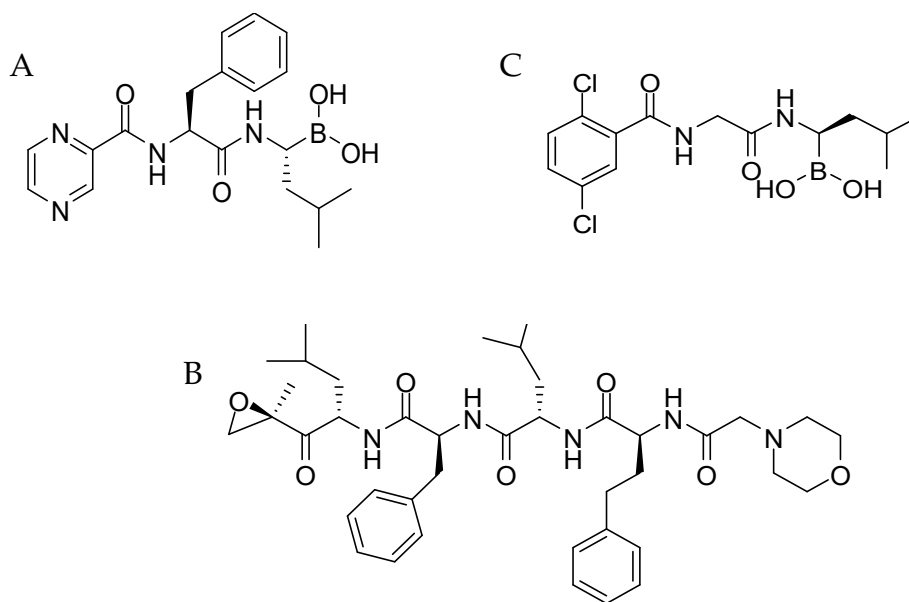
Figure 6: Structure of Bortezomib (A), Carfilzomib (B) and Ixazomib (C).

Bortezomib (BTZ) is the first proteasome inhibitor FDA-approved acting against Multiple Myeloma (MM) and Mantle Cell Lymphoma and it is a dipeptide boronic acid [62]; Carfilzomib is a second-generation inhibitor belongs to the epoxyketone and, in opposition with BTZ, it owns an irreversible effect [63]; Ixazomib belongs to the same class of BTZ and presents significant clinical advantages like the possibility to be orally assumed [64]. These compounds binds the β5 subunit leading to growth arrest in the G1 phase of the cell cycle causing apoptosis in cancer cells [65]. Unfortunately, all the drugs acting as proteasome inhibitors actually in commerce are associated to severe side effects like, among all, neurotoxicity. This can cause a dose reduction or a complete suspension of the therapy.

Besides the above-mentioned drugs already approved, other proteasome inhibitors are in clinical trial. Among them, one of the most interesting one is Salinosporamide A (Marizomib), a densely functionalized γ-lactam-β-lactone belonging to the family of Salinosporamides and extracted from obligate marine bacteria *Salinispora tropica* and *Salinispora arenicola*. It entered phase I human clinical trials for the treatment of multiple myeloma only three years after its discovery in 2003. Nowadays it is also in clinical trial for the treatment of glioblastoma, one of the most aggressive and lethal cancer [66,67].

Moreover, many other secondary metabolites are able to inhibit proteasome. Among them, polyphenols (i.e. (-)-Epigallocatechin-3-gallate, tannic acid, apigenin, quercetin, etc) are the most represented ones (Figure 7) [68,69].
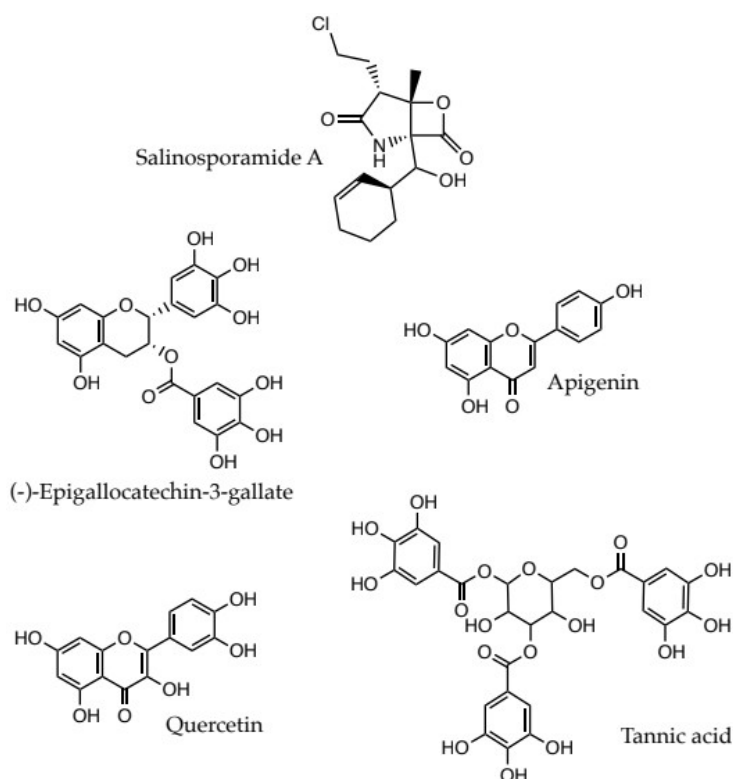
Figure 7: Chemical structure of metabolites able to inhibit proteasome.

Considering the great interest for proteasome inhibitors of the scientific community, efforts to identify its 3D structure have been done. At the beginning, researchers could only predict proteasome 3D structure thanks to homology studies based on proteasome isolated from *Mus musculus* and *Bos taurus*. Thus, these species own amino acid sequences with a high percent identity when compared to the corresponding primary structures of the human proteasome.

In 2009, a pharmacophore model was developed for the design of proteasome inhibitors. The result was a model with seven features: two hydrogen bond acceptors and two donors, one ionizable positive and two ionizable hydrophobic features. This work allowed the identification of three dipeptide boronic acid showing a very interesting profile as proteasome inhibitors [70].

Next, in 2014, a combined approach to identify novel covalent proteasome inhibitors was developed. This strategy merged pharmacophore modeling, molecular docking calculations, and molecular dynamics. The best pharmacophoric model obtained contains the same hydrogen-bond acceptors/donor of the previous model, but also one hydrophobic group and several excluded volumes [71,72].

During the following years, molecular docking was intensively used in the discovery and optimization of human proteasome inhibitors, but the crystal structure obtained with crystallographic techniques of this target have been available only in 2015. Nowadays almost 200 crystals of human proteasome exist in Protein Data Bank, both as single crystals and as co-crystals with activators and inhibitors. These new weapons could represent an important boost to speed up the research in proteasome inhibitors.

1.4 Extraction techniques in NADD programs

Once identified a potential active metabolite, a crucial step in its isolation is the development of an ad hoc extractive method. Over the years different Solid–Liquid Extraction (SLEs) approaches have been developed, which are now classified in conventional or innovative methodologies [73]. In the first case, SLE is performed by conventionally heating the natural matrix in the presence or not of solvent and with or without stirring. Examples of conventional methodologies are maceration, percolation, Soxhlet and steam distillation and they are usually related to long extraction time, and high solvent consumption. For this reason, different more efficient alternatives have been developed, like for example, Microwave-assisted Solvent Extraction (MASE), Ultrasound-assisted Solvent Extraction (UASE), pressurized solvent extraction (PLE), and supercritical fluid extraction (SFE) [74]. These unconventional approaches exploit innovative technologies to facilitate the extractive procedures and the recovery of the product of interest [73,75–77].

Among the different innovative extractive techniques, MASE is one of the most interesting one, as evidenced by the increasing number of scientific works, which exploit it (Figure 8).
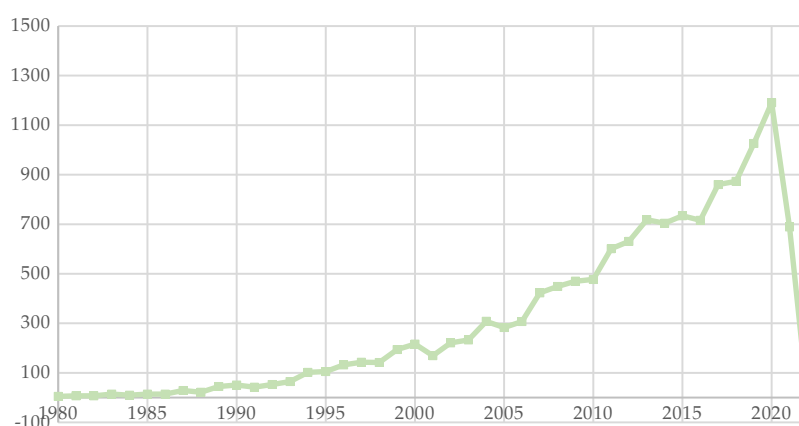
Figure 8: Number of scientific papers reporting on MASE from 1980 until august 2021 (Source: Scopus).

The effectiveness of MASE derived from the synergistic effect of two different mechanisms. On one hand, microwaves (mw) increase the dipolar rotation and ionic conductivity of polar liquids (i.e. solvents or intracellular water) which results in a rise of the system temperature. On the other hand, mw causes vaporization of the intracellular water leading to dehydration of the cellular wall and increasing of the intracellular pressure causing cell wall and membranes disruption [78].

Efficiency of MASE can be also improved operating at high pressure, exploiting ionic liquid of with particular modified instrumentations [75,76,79,80]

An example of the effectiveness of MASE can be found in our recent articles, which will be briefly discussed in chapter 4.

As we reviewed in a book chapter (Appendix, paper 1), ovens specifically designed for MASE are now available and derive from domestic ones. They can be classified both considering if

they are monomodal and multimodal, or if they work with open or closed vessels systems. A monomodal (or single-mode) system permits to focus the radiation on a restricted zone allowing the generation of a stronger electric field. Conversely, in a multimodal (or multi-mode) system, the microwave radiation is randomly dispersed, allowing the extraction of a higher amount of natural matrix [81]. Both these systems can exist as open vessel apparatus, where the extraction is conducted at ambient pressure, or closed vessel apparatus, which allows to control pressure and temperature during the extraction [82]. To develop a new MASE method, different parameters has to be kept in mind. Among the most important ones, we can find solvent, solvent-drug ratio, temperature, time, pressure and, microwave power. In detail, solvent should be selected not only by considering its ability of selectively solubilize the metabolite of interest, but it should also be selected based on its ability to absorb mw. Thus, solvent can be classified as high absorbance (i.e. dichloromethane, ethyl acetate, and hexane), medium absorbance (i.e. water, butanol, and acetonitrile) or low absorbance (i.e. ethanol, methanol, and propanol). Other parameters should be set up considering a balance between the effectiveness of the method and the stability of the metabolites. Thus, high pressure, power, and temperature are usually related to higher efficiency and lower time, but they could also cause the degradation of some metabolites.

Moreover, each of these parameters should not be considered alone, but they are all linked together. To reach this aim and to consider also the interactions among the different variables, a Design of Experiment (DoE) approach may be applied. This systematic statistic-based tool allows to speed up the set-up of the procedure by identifying the best experimental conditions with the minimum number of runs both in the academic and industrial fields [83,84].

In conclusion, MASE is a versatile technique allowing reduction of time and solvent consumed, while enhancing efficiency, reproducibility, and robustness. For these reasons, it has rapidly risen during the latest decades mostly in the early stage of the drug discovery process or, more generally, when a high number of samples have to be processed. Unfortunately, this technique has also some drawbacks. Thus, many variables have to be kept in mind during the setup of a new method and oven for industrial scale are not already available.

2. Valorization of the vascular flora of Pavia countryside

2.1 The biodiversity of Pavia countryside

Pavia is a city located in north-western Italy. It has an extension of 2970 km^2 and a density of 183.88 ab/km^2. It is crossed by Ticino and Po rivers, which divide the province into three areas: Pavese (north-east) and Lomellina (north-west), both in the Po Valley, and Oltrepò (south), in the Apennine territory (Figure 9).
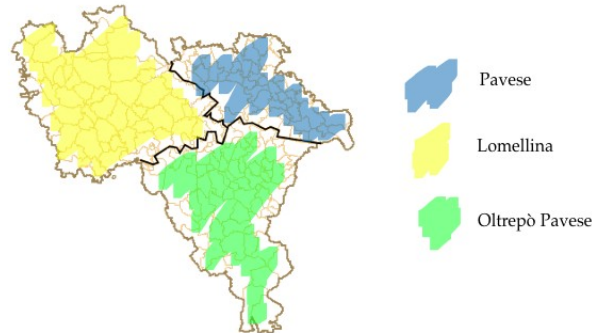

Figure 9: Pavia countryside divided into its three areas.

These rivers coupled with the proximity of Apennine and Alps, make Pavia countryside a very rich territory in terms of biodiversity. Moreover, the considered territory is characterized by the presence of dry-acidic continental open habitats, considered by the European Red List Classification endangered or vulnerable [85]. These habitats are now the subject of a LIFE Program of the European Union [86,87].

From 1970 Pavia countryside is also enriched by the foundation of an integral reserve called Bosco Siro Negri [88–91]. The Reserve host a small surviving strip of Po Valley forest characterized by a total suspension of all management activities since the end of World War II. It is a deciduous forest where, among the different species, some of the most represented are *Quercus robur*, *Acer campestre*, *Corylus avellana* and *Crataegus monogyna*. To have a wider comprehension of the biochemical mechanisms occurring in these species, and to give our contribution to the characterization of the plants growing in Bosco Siro Negri, we decided to investigate the correlation between pectin and mesophyll conductance during leaf development of these dicotyledonous deciduous species. Thus, recent evidences seem to suggest that there is a correlation between these polymers and CO_2 diffusion [92,93]. In detail, we demonstrated that in *A. campestre*, *C. monogyna* and *Q. robur* to higher value of pectin corresponded higher mesophyll conductance, while an opposite behavior was observed in *C. avellana*. The results obtained so far were reported in a recent publication (Appendix, paper 2). The leaves of this latter plant were further investigated considering the variation of their content in secondary metabolites. Particularly, we investigated wild or cultivated species under different nutrient supplies.

Quercitrin and Myricitrin were selected as marker and results suggested their higher production in wild species with no nutrient supplies (Appendix, paper 3). This evidences further increment the importance of the preservation of the reserve Bosco Siro Negri, being the wild species growing there valuable source of secondary metabolites.

As the different habitats present in our province can suggest, the vascular flora of Pavia is one of the most floristically diversified, but, in the meanwhile, also the most neglected in north-western Italy. Thus, from *Flora ticinensis* (Nocca & Balbis, 1816, 1821) and *il Prospetto delle Piante fanerogame ritrovate nella Provincia Pavese* (Rota, 1847), we have to wait almost 170 years until a new checklist reporting the flora of this territory was published. In fact, in 2016 Ardenghi and Polani published *La flora della provincia di Pavia (Lombardia, Italia settentrionale)* in which they identify 2273 taxa growing in Pavia countryside [94]. All the species were described considering their family, distribution, abundance, harvesting location, and other of their main characteristics. Among the 2273 taxa, 183 (8%) are considered extinct, 651 (28.6%) very rare, 194 (8.5%) rare, 349 (15.4%) not common, 78 (3.4%) locally common, 297 (13.1%) common, and 119 (5.2%) very common, while the others are considered "*Taxa dubia et excludenda*". (Figure 10).
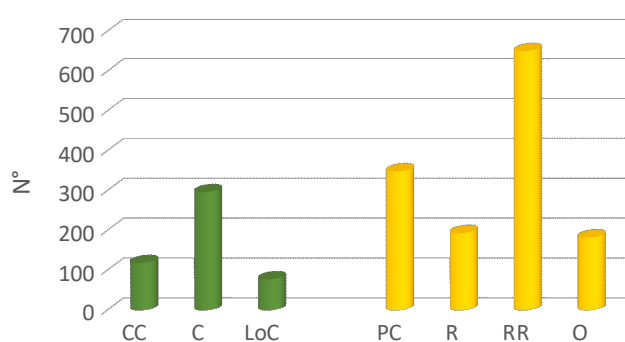
Figure 10: Distribution of taxa classified as very common (CC), common (C), locally common (LoC) (green) and of taxa classified as less common (PC), rare (R), very rare (RR) and extinct (0) (yellow).

This paper will constitute the starting point of the present work. Thus, the main goal of my PhD project is the valorization of Pavia biodiversity by identifying biologically active secondary metabolites produced by the plants growing in this territory.

To reach this aim, we set up a proper database reporting all the plants growing in the Province of Pavia and their main characteristics. Moreover, this database will allow the researchers to easily obtain all the information concerning the secondary metabolites produced by those plants. In line with previous research of my supervisor, the first application of the database consisted in the search of novel anticancer drugs, since tumors are the second cause of death worldwide and many of them are still considered unmet clinical diseases. Moreover, the World Health Organization estimates that the number of cases is expected to considerably increases during next years [95]. Specifically, we focused on proteasome as target. As discussed in the introduction section, proteasome inhibitors have a great potential as anti-cancer molecules, but only three of them reached the clinical stage and they are associated to severe side effects [96].

The identification of secondary metabolites active against cancer may be a useful tool for valorizing the biodiversity of our territory. This approach has been successfully applied to other areas.

2.2 Development of the database of secondary metabolites produced by plant growing in Pavia territory

The first part of my PhD program consisted in building up an Excel data sheet reporting all the taxa already collected in *La flora della provincia di Pavia (Lombardia, Italia settentrionale)* by Ardenghi and Polani [94]. Once the data have been collected and organized, a preliminary selection of the taxa has been performed. In the Excel data sheet only the taxa whose abundance was sure have been reported, thus avoiding those reported in the section "*Taxa dubia et excludenda*". In the same data sheet for all of the selected taxa, their main characteristics like Family, Red List Classification and synonyms have been inserted. After this first selection, the number of taxa remained high (1871 taxa), and therefore the different taxa have been grouped and then filtered: the species whose harvesting would represent a danger have been excluded, and only the species locally common, common and very common have been considered. As a result, a total of 494 taxa have been selected and used for the subsequent part of the work.

As a second step of my PhD project, I implemented the data sheet collecting the already identified secondary metabolites produced by the plants selected in the first part of the work. To reach this aim, the online database called Dr Duke's Phytochemical and Ethnobotanical Databases [97] (by now on called Dr. Duke's DB) has been consulted and a literature survey performed, based on Web of Science. Dr Duke's DB is a freely available database, which allows plant, chemical, bioactivity, and ethnobotany searches. Metabolites have been associated to the 28% of the selected taxa, based on Dr. Duke's DB, and to 58% of the taxa, based on literature survey. For the 14% of the taxa no information about the secondary metabolites produced is available. Results are summarized in Figure 11. To sum up, 5715 secondary metabolites have been associated to their producing plants and inserted with a unique code in another excel data sheet. Only the secondary metabolites have been considered. Amino acids, fatty acids and sugars have been excluded, thus avoiding compounds that could cause false positive results in the following part of the work. To complete the database I was building, the Simplified Molecular-Input Line-Entry System (SMILES) code has been associated to each compound. SMILES code is a line notation for describing the structure of chemical species and so it is a useful tool to quickly obtain the 3D chemical structure of the considered molecules. To obtain them, we exploited several free online databases like PubChem, ChemSpider, FooDB and Wikipedia.
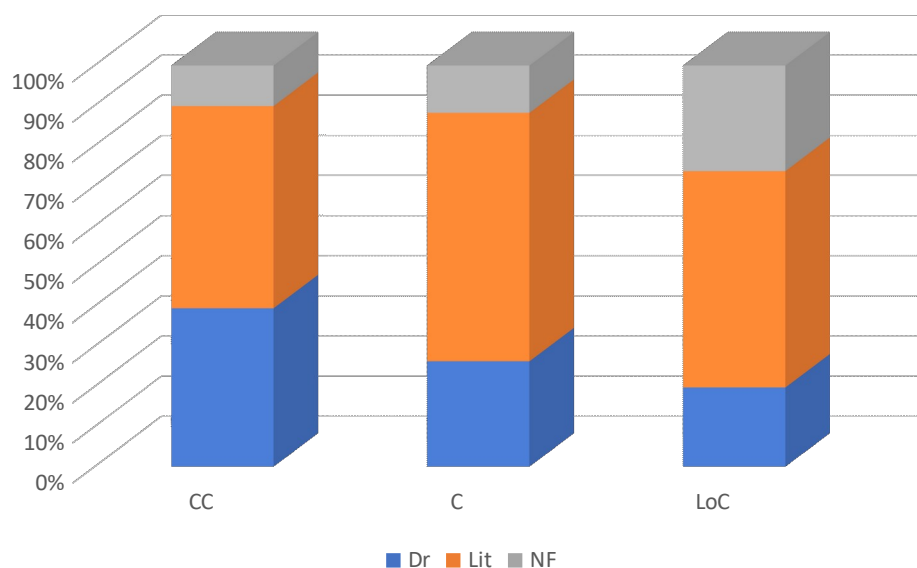
CC = very common
C = common
LoC= locally common

Figure 11: Percent distribution of scientific sources for metabolites identification (Dr= Duke's Phytochemical and Ethnobotanical Databases; Lit= literature; NF= Not Found).

The subsequent *t*-SNE (T-distributed Stochastic Neighbor Embedding) analysis (Figure 12) evidenced that 5715 molecules reported in the first draft of the new database allows to cover a wide chemical space. This is an essential requirement of a versatile database, potentially useful for a NADD program.
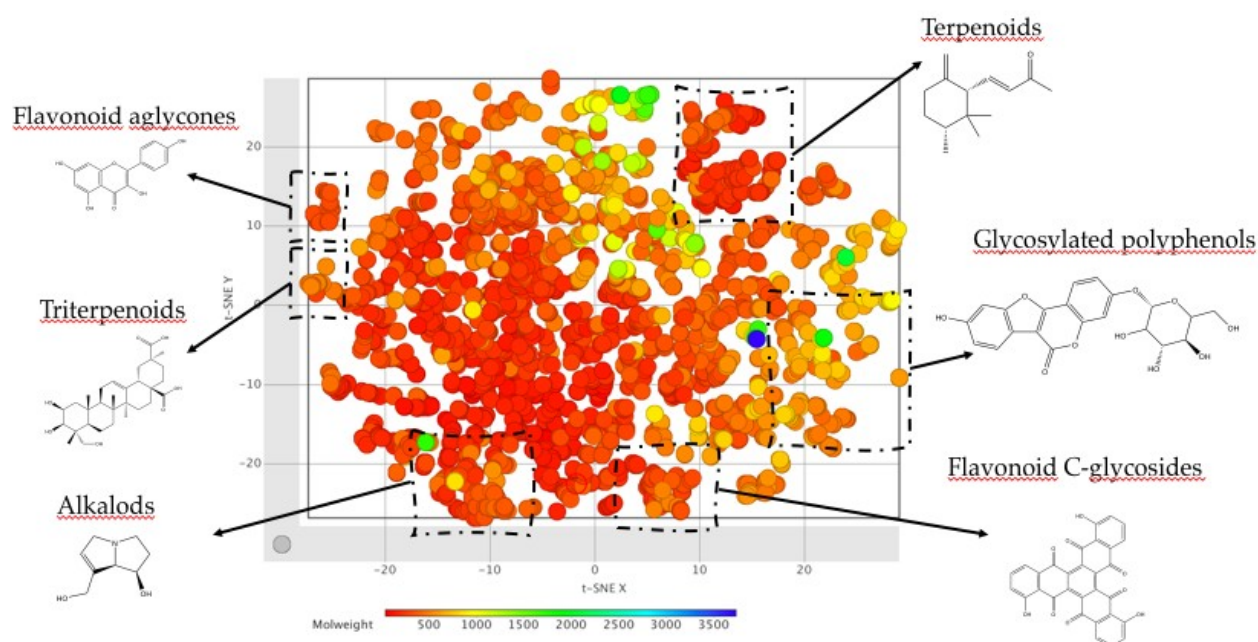

Figure 12: 3D representation of t-SNE analysis.

The first draft of the database, as excel data sheets, represented the starting point for building the demo, called Secondary Metabolites Search (S.M.S.). This activity was possible thanks to the collaboration with Professor Martellos and collaborators of the University of Trieste.

The "database demo" was built considering that: (i) it should allow an easily aggregation of data concerning other territories and (ii) its interface must be intuitive to be easily consulted. Therefore, we added to each metabolite both IUPAC name and categories, thus assigning an unambiguous name to each metabolite and allowing the aggregation also of other DBs reporting only the class. In addition, we have developed an easy interface and enriched the chemical information with synonyms, exact mass, molecular weight, chemical formula, m/z and elemental analysis. Once the "database demo" has been completed, it was called Secondary Metabolites Search, a Logo drawn and a web site built. The DB is still under development, but it will be soon published online. Its logo is reported in Figure 13.

Figure 13: Logo of the final web site.

2.3 Virtual screening vs Proteasome of the library of secondary metabolites

The collection of metabolites (in its demo version) was then used for a virtual screening with the double aim to verify if it could really represent an effective tool to identify biologically active metabolites and to discover compounds for fighting cancer. If successful, the herein proposed database may represent a relevant tool to valorize the Pavia territory and its biodiversity.

To identify secondary metabolites potentially able to inhibit proteasome and therefore active as anticancer agents a virtual screening (VS) approach was followed. The rationale behind this decision can be found in the statement by Paul Ehrlich (1854-1915) "*corpora non agunt nisi fixata*" which means that molecules have to establish specific interactions with their target to explicit a specific activity. As stated in the introduction, interactions that molecules have to establish with proteasome to inhibit it have already been well-characterized. Thus, the co-crystals present in the Protein Data Bank (PDB) evidenced that the main inhibitors' binding site is the β5 subunit (Chymotripsin like subunit). During my stay at Inte:Ligand (Vienna, Austria), within the Erasmus traineeship program, I had the opportunity to collaborate with Professor Sharon Bryant. I

learnt to use the Ligand Scout software to set up and validated a proper pharmacophoric model. More in details, I exploited three different libraries:

- L1, a library containing 32 molecules represented by: three drugs already in clinic (Bortezomib, Ixazomib and Carlfizomib) and other known proteasome inhibitors downloaded from ChEMBL (ChEMBL1944494) with related activity values;
- L2, a library containing 16 known proteasome activators;
- L3, a library containing 1400 decoys obtained using DUD-E software.

In detail, L2 and L3 have been considered as decoys.

Despite dozens of inhibitors are known, only L1 has been considered to obtain a good active/decoy ratio.

At the beginning, attempts have been done considering the pharmacophoric model generated via a structure-based approach from the three co-crystal structures of the drugs (PDB codes: 4R67 for Carlfizomib, 5L5F for Bortezomib and 5FL7 for Ixazomib). Unfortunately, the obtained models were too specific, and their modifications allowed to obtain models able to retrieve from the library of metabolites only Ochratoxin A, a known highly toxic compound.

For this reason, we decided to move to a ligand-based approach. In detail, L1 was clustered obtaining 15 different clusters, among which seven containing more than one molecule. The pharmacophoric models for each of these seven clusters were generated.

For each model the ROC curve was generated and cluster 7 (CL7) selected as the best one. Unfortunately, it did not retrieve any of the secondary metabolites of the library, evidencing that a simplification was necessary. The elimination of the most external features allowed to obtain a good model (CL7_II), but unfortunately it did not retrieve any of the drugs during the validation procedure. Further modification consisting in deleting three excluded volumes made the model (CL7_III) able to retrieve Carlfizomib, even if it caused a slight worsening of the ROC curve (Figure 14).
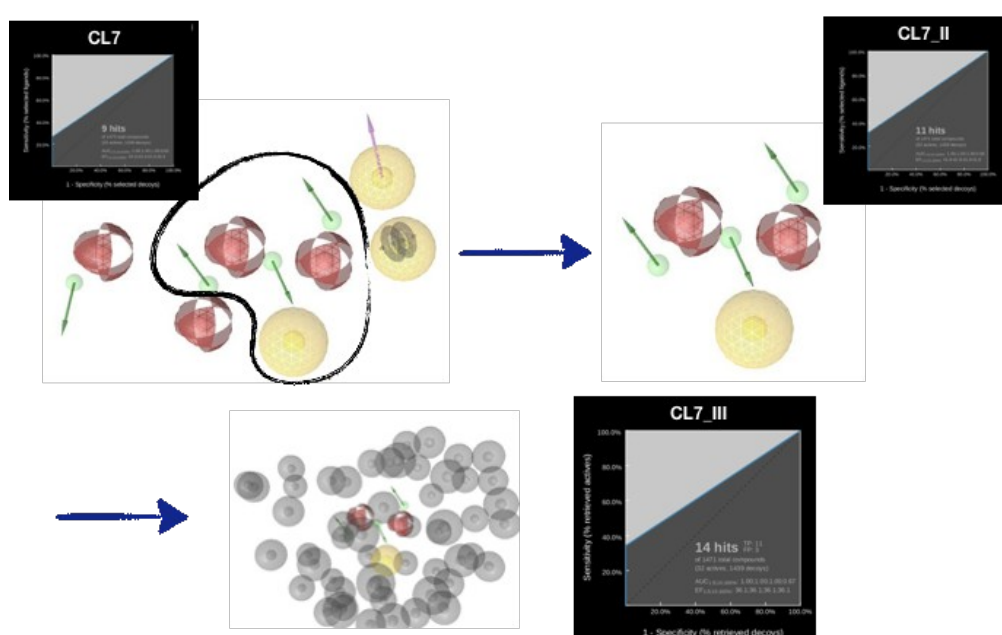
Figure 14: Optimization of the pharmacophoric model deriving from cluster 7.

CL7_III was so selected to screen the library of secondary metabolites. Retrieved molecules are summarized in Table 3 and Figure 15.

Table 3: Potential proteasome inhibitors and their sources.

Code	Name	Source
MVPV02178	Kaempferol-3-O-β-D-glucoside-7-O-α-L-rhamnoside	*Eryngium campestre* L.
MVPV04227	6-methoxykaempferol-3-O-glucoside	*Artemisia annua* L.
MVPV02411	Aucubin-10-O-β-D-glucosyl	*Scrophularia canina* L.
MVPV01905	Cyanidin-3-O-arabinoside	*Vaccinium myrtillus* L.
MVPV02611	Kaempferol-3-O-α-L-rhamnopyranosyl(1-2)-β-D-galactopyranoside	*Blackstonia perfoliata* (L.) Huds.
MVPV01541	Vicianin	*Vicia segetalis* Thuill. AND *Vicia sativa* L.
MVPV01548	Kaempferol-3-O-α-L-arabofuranoside	*Prunus spinosa* L.

MVPV02178
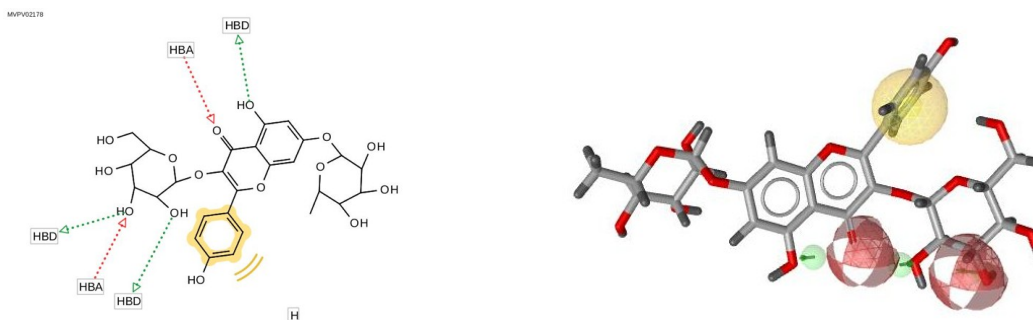
MVPV04227
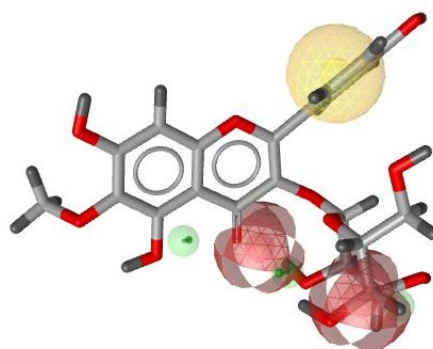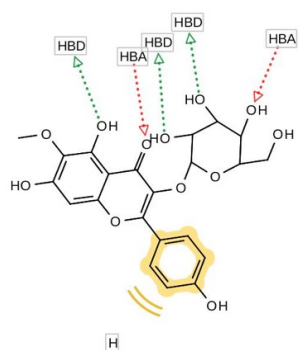
MVPV02411
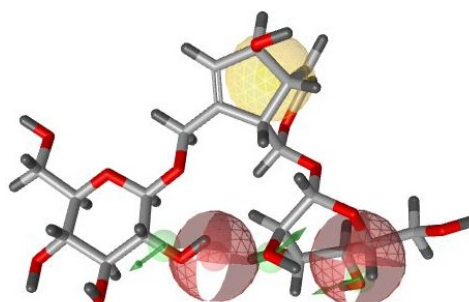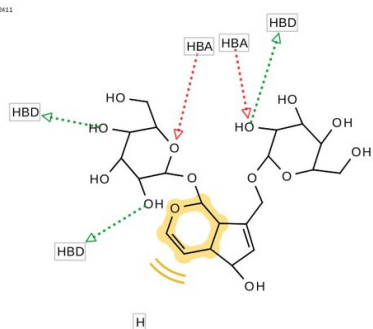
MVPV01905
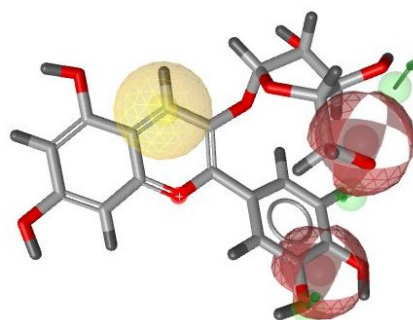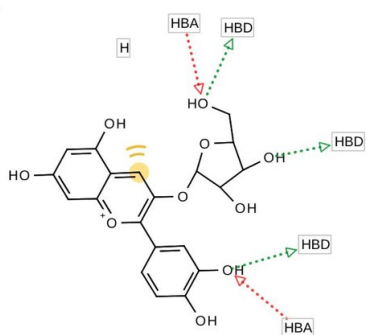
MVPV02611
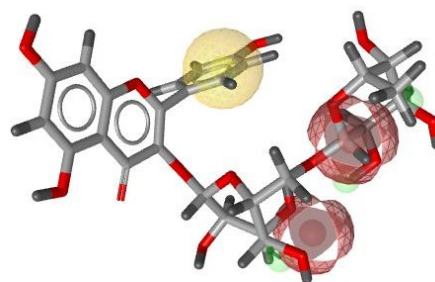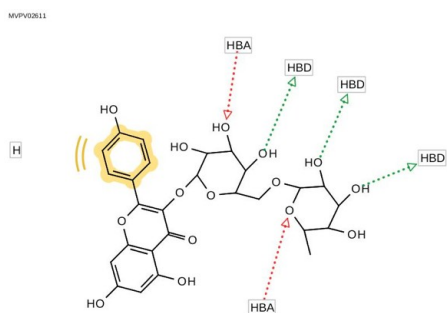
MVPV01541
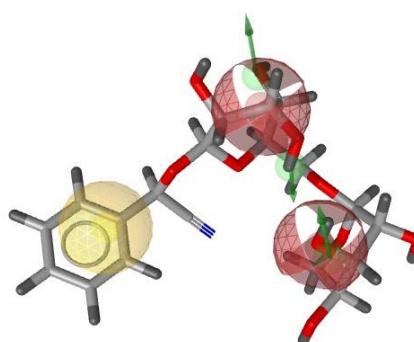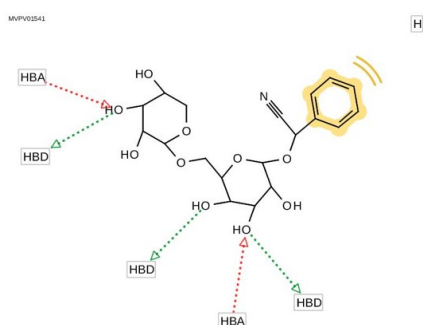
MVPV01548
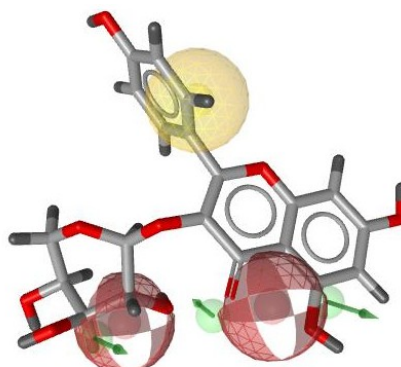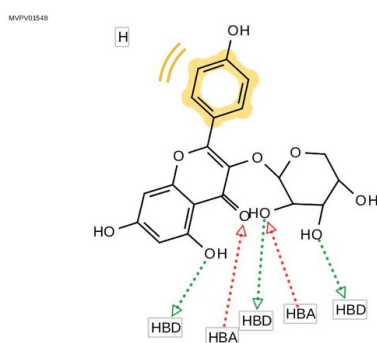
Figure 15: Structures of the selected molecules and their fitting in the pharmacophoric model

Further docking studies suggest that they all occupy the same binding pose of Carlfizomib.

Of note, none of the selected metabolites were already known proteasome inhibitors, but many works report on the ability of flavonoids to inhibit proteasome [98,99]. For example, Kaempferol is a known inhibitor, but none of the paper found in literature analyze the effect of sugar moiety that in my model fits very well [100]. Another paper assesses that Cyanidin-3-glucoside binds proteasome with an IC_{50} = 12.6 μM [101]. Therefore, we can conclude that the results of the VS are in line with the poor literature data available. We then decided to go further,

changing the paradigm: we leaved the theoretical studies for gaining experimental data to support the results obtained from the virtual screening.

Briefly, (1) Cyanidin-3-O-arabinoside was purchased and its activity compared with an extract of the fruits of *Vaccinium myrtillus* rich in anthocyanins, kindly provided by Indena S.p.A. (Milan, Italy); (2) Kaempferol-3-O-alpha-L-arabofuranoside was purchased, and its activity compared with *P. spinosa* flower extract. *P. spinosa* flowers have been collected by us and then the extract prepared according to literature procedures; (3) extracts of the *A. annua* aerial parts (collected by us) and of *V. sativa* seeds (purchased) have been prepared and the metabolites 6-methoxykaempferol-3-O-glucoside and Vicianin isolated and properly characterized.

Extraction procedures and compound characterization are discussed in the following paragraph.

2.4 Isolation of the selected metabolites

2.4.1 6-Methoxykaempferol-3-O-glucoside from Artemisia annua *L.*

Artemisia annua L., also known as a sweet wormwood, is an annual herbaceous specie native from Asia and Southeast Europe, now naturalized in many countries including Italy (Figure 16). It belongs to Asteraceae family, and it prefers warm and sunny conditions (optimal temperature: 20-25°C).

Figure 16: *Artemisia annua* L.

A. annua blooms form June to July. Its flowers are small, yellow and the green stalk can reach up to 30-200 cm [102]. Characteristic trade of *A. annua* is the intensive aromatic scent of its leaves. It is mainly known for its antimalarial properties, being its sesquiterpene lactone artemisinin the first-choice treatment for this pathology. It has been demonstrated that, extracts of *A. annua* also show antibacterial, antioxidant, anti-parasitic, anti-cancer and antifungal effects [103].

This plant was selected because its aerial parts produced the metabolite suggested by VS, i.e. 6-methoxykaempferol-3-O-glucoside, also known as Patuletin-3-O-glucoside. The aerial part of *A. annua* was collected in August 2020 on the left bank of Ticino river at the Becca's bridge (coordinates: 45.144, 9.223, 55.90).

After the identification of the plant, the aerial parts (flowers and leaves) were dried, separated from the stem, grounded with a blade mill, thus obtaining an homogeneous powder.

Afterward, 10 grams of the powder have been macerated using a mixture of 4 methanol: 1 water at room temperature (2 cycles, 4h each), according to literature procedure [104]. Next, the same natural matrix underwent to a second maceration using the same conditions but with solvents in a different ratio (1:1). The combined extracts were simplified via liquid/liquid extraction (L/L E) suspending the raw extract in water, and sequentially extracting with hexane (5 cycles, to eliminate metabolites with low polarity like chlorophyll and sesquiterpenes), diethyl ether (3 cycles, to eliminate aglycon polyphenols), and ethyl acetate (5 cycles). Based on literature evidences, this last fraction is the one of interest, being ethyl acetate able to extract glycosylated polyphenols, so it was anhydrified with Na_2SO_4 and evaporated under reduced pressure.

This latter organic fraction was analyzed *via* High Performance Liquid Chromatography (HPLC). A proper HPLC-UV/PAD method suitable both for the extract analysis and for the separation of the main metabolites was set up. To find the best chromatographic conditions, we screened Chromolith SpeedROD RP-18 endcapped (50x4.6mm, monolithic) column with several mobile phases. In detail, we used combinations of methanol or acetonitrile with water, both added with formic acid (0.1%) or trifluoracetic acid (TFA, 0.05%). The best results in terms of time of analysis, peak shape, and peak resolution were achieved under gradient elution conditions, using a mobile phase composed of acetonitrile and water added with TFA (0.5%, v/v). This method allowed the resolution of the main peaks and it was transferred to a (semi)preparative scale to isolate the most abundant peaks. Once obtained a suitable amount, the MS analysis of the main metabolites isolated was performed, allowing the identification of the peak with retention time 4.5 min (the most intensive one) as the one representing patuletin-3-O-glucoside (Figure 17).
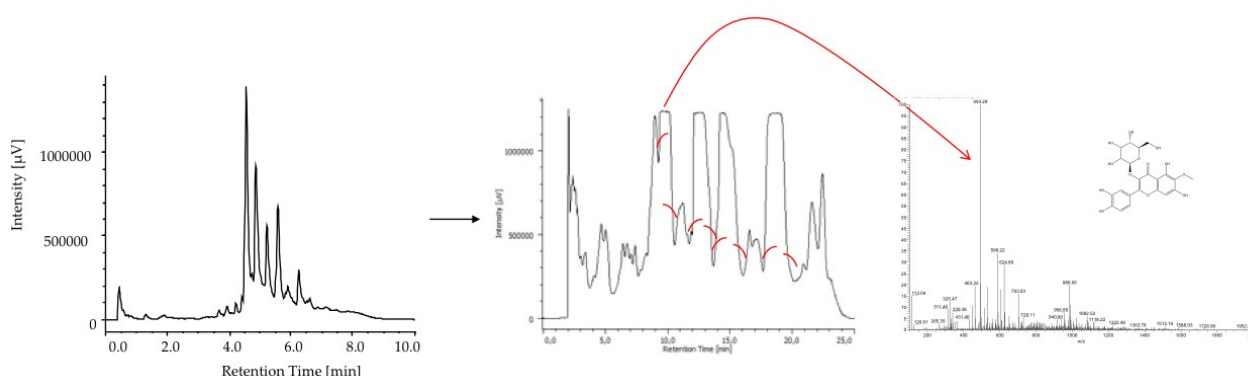
Figure 17: Analytical and semi-preparative profile of the ethyl acetate fraction.

With a standard sample of patuletin-3-O-glucoside in hand, both the extraction and the isolation procedures have been optimized. We repeated the literature procedure keeping separated

the macerate obtained with 4 MeOH: 1 H_2O form the one obtained from 1 MeOH: 1 H_2O and extracted them as previously described via L/L E. By the comparison of the yields the HPLC profiles of the extract obtained with ethyl acetate fraction, we concluded that the extraction with 1 MeOH: 1 H_2O is not relevant for isolating the metabolite of interest (Table 4).

Table 4: Yield of the ethyl acetate fraction: comparison between the two solvent mixtures.

MeOH:H_2O ratio	EtOAc yield
4:1	3.7%
1:1	0.2%

Accordingly, for improving the extraction yield of patuletin-3-O-glucoside, we exploited a microwave assisted solvent extraction (MASE) using a mixture of 4 MeOH: 1 H_2O mixture. As highlighted in the introduction section, this extraction technique may increase the effectiveness of the extraction by reducing the required time and amount of solvent. In detail, we kept constant the temperature (60°C) and matrix: solvent ratio (1:2) and varied the number of cycles and the solvent renewal. Each extract was subjected to L/L extraction and results compared in terms of yield of EtOAc fraction to avoid interferences with different metabolites. Results are summarized in Table 5.

Table 5: EtOAc fraction extraction yields basing on the MAE procedure

Method	Temperature	Time	Amount of solvent (4MeOH : 1H_2O)	EtOAc yield
MASE 1	60°C	3x15 min (45 min tot)	3x50 mL (150 mL)	2.8%
MASE 2	60°C	5x15 min (75 min tot)	5x50 mL (250 mL)	5.2%
MASE 3	60°C	3x20 min (60 min tot)	3x50 mL (150 mL)	3.2%
MASE 4	60°C	5x15 min (75 min tot)	1x50 mL (50 mL)	2.0%
MASE 5	60°C	5x15 min (75 min tot)	2x50 mL (100 mL)	2.4%

To sum up, the best results have been achieved applying five mw heating cycles and renewing the solvent after each cycle (method MASE 2). In this way, the yield of the EtOAc fraction was substantially increased and the extraction time reduced (from 16 h of the initial method to 75 min). Once identified the best extractive method, we moved to the optimization of the isolation of patuletin-3-O-glucoside. As first attempt, a semi-preparative HPLC separation of

the EtOAc fraction was performed. Unfortunately, this procedure is not suitable for the scale up process due to the large number of injections required. Therefore, we decided to further simplify the organic fraction.

A preliminary Thin Layer Chromatography (TLC) analysis has been performed, being TLC a simple and rapid method for qualitative or semi-quantitative evaluations of extracts that allows a lower time of analysis and lower solvent consumption comparing to HPLC analysis. Initially a mobile phase (4 Toluene : 3 EtOAc : 3 MeOH : 0.1 HCOOH) commonly used in our laboratory for the analysis of polyphenols has been tested. Unfortunately, R_f value was too high (R_f=0.55) and the spots were not completely resolved. The mobile phase was then properly modified, reducing the polarity. Using a mobile phase consisting in 5 Toluene : 3 EtOAc : 2 MeOH : 0.1 HCOOH, patuletin-3-O-glucoside showed a spot with R_f value of 0.3. This elution conditions are suitable for flash chromatography.

Flash chromatography performed with 5 Toluene : 3 EtOAc : 2 MeOH : 0.1 HCOOH as MP allowed the obtaining of a fraction rich in patuletin-3-O-glucoside which was next subjected to (semi)preparative HPLC. Even if the HPLC separation was still necessary, the preliminary flash chromatography allows to perform fewer injections, resulting in a lower time and solvent consumption.

At the end of the purification process, patuletin-3-O-glucoside was obtained in suitable amount for the chemical and biological characterization.

The chemical structure was then confirmed by NMR, MS and polarimetric analyses ($[\alpha]_D$ = - 9.5, c 0.5, MeOH). The NMR and MS spectra are reported in the experimental section.

2.4.2 Extraction of Vicianin from Vicia sativa *L.*

Vicia sativa L. is one of the most common annual legumes growing in temperate areas, and it belongs to the Fabaceae family (Figure 18).

Figure 18: *Vicia sativa* L.

Native from the Middle East, *V. sativa* is now cultivated in many areas of the world especially in Ethiopia, Mexico, Turkey, and Spain, and it is also widespread in Italy. The best growing conditions are in areas with medium-low rainfall, but it withstands cold winter or aridity,

and also poor or hard soils [105]. This characteristic makes *V. sativa* a good ecological fertilizer with a low environmental impact [106].

The plants of the genus *Vicia* have been known since ancient times for their therapeutic properties. In ancient Greece and Rome they were used as diuretic and expectorant, and later application has spread for the treatment of numerous diseases such as Parkinson's, hypertension, liver cirrhosis and other disorders [107].

Seeds, one of the most interesting part of the plant, are easily available [108]. They are widely used as feed for livestock and can also be part of human diet as a rich source of starch, proteins, minerals, and other components such as tannins, and flavonoids [105]. Moreover, seeds also produce vicianin, the metabolite with potential proteasome inhibition properties, as suggested by VS. To isolate this metabolite, a first set of experiments have been exploited.

The first literature maceration of the seeds considered involved 2 consecutive extractions, with renewal of the solvent, at room temperature with an aqueous solution of 10% trichloroacetic acid (TCA) [109]. The second method considered foresaw a maceration with an aqueous solution of methanol 80% [110].

Consistently, two 2.5 g aliquots of powdered natural matrix were extracted by maceration using the two different solvents, keeping constant the drug / solvent ratio of 5% w/v, the temperature (r.t.) and the time (6h). The first extraction was carried out using an aqueous solution of 5% TFA, while the second was carried out using an 80% methanol as the extracting solvent. For the first method it was decided to replace the aqueous solution of 10% TCA with an aqueous solution of 5% TFA given the absence of acid in the laboratory. The percentage was therefore lowered due to the greater acidity of TFA compared to TCA. The extracts so obtained were then evaporated under reduced pressure. The procedure was repeated 3 times and the extraction yields were calculated as indicated in Table 6.

Table 6: Preliminary extractions yields with TFA 5% and MeOH 80% as extractive solvents at r.t.

Solvent	Yield
TFA 5%	32.4%
MeOH 80%	12.0%

To obtain quick answers regarding the vicianin content in the crude extracts, a screening was firstly carried out to identify the most suitable mobile phase for the TLC analysis. Since a reference standard of vicianin was not commercially available, the identification of the suitable mobile phase (MP) was carried out exploiting amygdalin as external standard. Thus, as can be seen from the structures reported in figure 19, the two molecules differ only for the presence of an extra -CH_2-OH group of the amygdalin. It is therefore expected that in a TLC analysis the R_f value of the amygdalin is slightly lower as it is more polar and therefore more retained by the stationary phase.
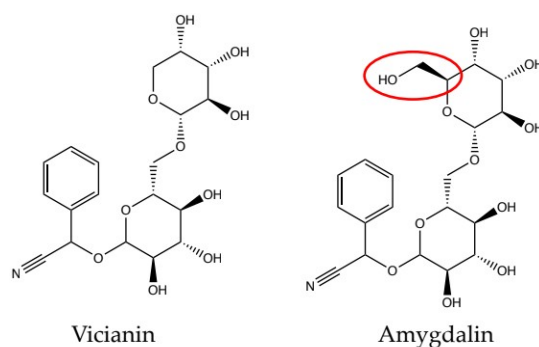
Figure 19: Chemical structure of vicianin and amygdalin.

Different attempts were carried out using eluent mixtures with different polarities (Table 7). Particularly, two mobile phases seemed to be suitable for both the analysis and the scale up in flash chromatography for the subsequent purification, consisting of DCM: MeOH in 8: 2 ratio and EtOAc: Acetone: Chloroform: MeOH: H_2O in 4: 3: 1.2: 1: 0.8 ratio.

Table 7: Screening of mobile and stationary phases for TLC analysis

Mobile Phase	Stationary phase	R_f value
9DCM: 1MeOH	Silica	0
5AcOEt: 5(CH₃)₂CO	Silica	0
9DCM: 1MeOH 0.1 HCOOH	Silica	0
DCM:MeOH 8:2	**Silica**	**0.4**
8DCM: 2MeOH: 0.1 HCOOH	Silica	No resolution
7DCM: 3MeOH	**Silica**	**0.3**
7DCM: 3MeOH: 0.1 HCOOH	Silica	No resolution
8AcOEt: 2MeOH	Silica	0.2
8AcOEt: 2MeOH: 0.1HCOOH	Silica	0.2
7AcOEt: 3MeOH	Silica	0.2
7AcOEt: 3MeOH: 0.1HCOOH	Silica	0.2
7AcOEt: 3MeOH	Allumina	No resolution
7DCM: 2MeOH: 0.1HCOOH	Allumina	No resolution
4AcOEt: 3(CH₃)₂CO: 1.2 CHCl₃: 1 MeOH: 0.8H₂O	**Silica**	**0.3**

Simultaneously to the identification of the mobile phase, a screening of a proper stain for the visualization of the spot of interest was also performed. Among the different stains tested like ceric ammonium molibdate (IV) (Hanessian's Stain), bromocresol green and permanganate, this latter one resulted to be the best one. With the TLC method in our hand, we were able to compare the two crude extracts previously obtained. Results highlighted that while in the extract obtained exploiting MeOH 80% as solvent a spot was identified as vicianin thanks to the comparison with amygdalin, no interesting spots were identified in the crude obtained using TFA 5%. This result makes us speculate that the metabolite of interest was not stable in that extractive conditions. The reason may lie in the presence of an acetal group, which is labile in acidic conditions. The hypothesis that vicianin had degraded was further valorized by the results of the cell vitality test (See paragraph 2.5). Thus, the hydroalcoholic extract resulted to be much more active than the other one.

Given the promising results in terms of activity obtained through the hydroalcoholic extraction, we kept the drug / solvent ratio constant (5% w/v), while we varied the following conditions: extractive method (Maceration and MASE), hydroalcoholic mixture, temperature (rt, 70°C, 80°C) and time (2 + 2 + 12 hours; 5 + 5 + 5 minutes) (Table 8).

Table 8: Yields deriving from the different extractive procedures.

Method	Solvent	Temperature	Time	Yield
MAC 1	80% MeOH	70°C	2h-2h-12h	14%
MAC 2	80% MeOH	r.t.	2h-2h-12h	12%
MAC 3	MeOH	rt	2h-2h-12h	10%
MAC. 4	EtOH	rt	2h-2h-12h	10%
MASE 1	80% MeOH	80°C	3x5 min	15%
MASE 2	EtOH	80°C	3x5 min	12%

As can be seen from Table 8, the extractive yields are comparable, however, the extraction carried out using microwaves is very advantageous in terms of time. Moreover, the crude extracts obtained were analyzed by TLC which highlighted how the presence of water in methods Mac 1, Mac 2 and MASE 1 strongly affected the complexity of the phytocomplex. Given the proven efficiency of mw, it was therefore decided to follow a MASE 2 approach.

Once the crude extract was obtained, it was then fractionated and purified. Several steps were performed.

In a preliminary liquid-liquid extraction, the yellow-green crude was solubilized in water and three sequential washes with DCM were applied. However, the results obtained were not optimal as the organic phase partially extracts vicianin. It was therefore decided to opt for two solvents with increasing polarity, the first washing was carried out with three cycles of hexane which, given the low polarity, is expected to retain all the non-polar compounds present in the crude without extracting the metabolite of interest, while the second wash was carried out with three cycles of ethyl acetate. The results obtained by washing the crude with these two solvents allow us to obtain a less complex mixture, thus suitable for the following flash chromatography (MP: 8DCM: 2MeOH).

After the chromatographic separation and in order to isolate vicianin, a crystallization of the fractions containing the metabolite of interest with methanol-toluene 1: 1 was carried out, which led to obtain of a crystalline solid [109,110]. NMR analysis seems to confirm the presence of vicianin, however obtained in very low amount and with limited purity. For this reason, a second attempt has been performed, which foresaw to perform a flash chromatography directing on the crude extract and exploiting the 4 EtOAc: 3 Acetone: 1.2 Chloroform: 1 MeOH: 0.8 H_2O mobile phase and repeating the crystallization. Also in this case NMR analysis revealed that the solid obtained was only a fraction enriched in vicianin (Figure 20), even if this time its amount was sufficient for further biological analysis.
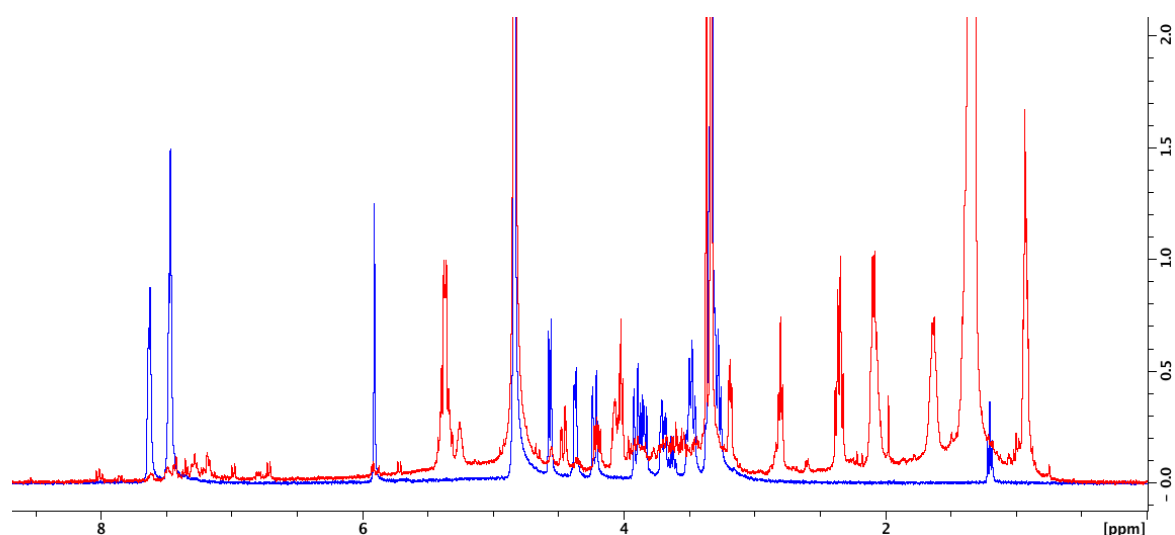
Figure 20: Comparison between NMR spectra of amygdalin (blue line) and vicianin enriched fraction (red line).

To definitively confirm the presence of vicianin, a UHPLC-MS method was setup. In detail, we preliminary treat this enriched fraction (Ef) with N,O-Bis(trimethylsilyl)trifluoroacetamide (BSTA) and kept the solution at room temperature overnight. This procedure allowed the persilylation of the product, making it more suitable for an MS analysis. Results confirm the

presence of the persilynated product, and so the Ef was subjected to biological tests (See paragraph 2.5)

Simultaneously, pretreatments of the natural matrix were performed to obtain better results in terms of purity of the sample.

Thanks to the analogy with amygdalin, the hypothesis that vicianin was found in greater concentration in the integument seed was formulated [111]. Therefore, 5 g of seeds were therefore powdered with a blade mill and finely sieved (sieves from the mash of 0.25 and 0.5 mm) to separate the albumen (central part) from the integument (external part). The two separate portions, respectively weighing 300 mg for the albumen and 300 mg of the integument, were extracted following the optimized method. The TLC analysis seems to confirm the literature hypothesis, however, no significant difference between the composition of the two powders was noted. It was therefore decided not to carry out this separation to avoid material lost.

Subsequently, a second kind of pre-treatment of the natural matrix was performed. In detail, the natural matrix was washed before carrying out the extraction with 3 different solvents in sequence. The first wash was carried out with hexane, the second with DCM and the third with ethyl acetate. A small scale test was carried out exploiting mw (ramp: 2 minutes, time: 5 minute, power: 200 W, pressure: 250 PSI, temperature: 80 ° C for Hex and EtOAc and 40 ° C for DCM).

The absence of vicianin in the washing solvents was verified both by TLC and IR analysis. Thus, in the amygdalin spectrum (Figure 21 A) there is a wide band at 3555.13 cm^{-1} which can be attributed to the vibration of the OH groups of the glycosidic moiety. The low intensity absorptions at 2928.38 cm^{-1} are attributable to the stretching of the aromatic C-H. The bands at 1661.37 and 1608.34 cm^{-1} are the result of the stretching vibrations of the C = C double bond of the aromatic ring while the stretching vibrations of the CO bonds, from the ether and hydroxyl groups are observed at 1275.68 and 1047.16 cm^{-1}, respectively. Moreover, an intense absorption band can be observed at 699.07 cm^{-1} which are related to the vibration of the C-H. Finally, no band around 2200 cm^{-1} for the CN group is detectable, due to its low intensity [112]. On the other hand, in the spectra of the washes the main bands associated with the structure of amygdalin are absent. In detail, in the spectra of washes with hexane and DCM the band at 3555.13 cm^{-1} is absent, while the band at 2928.38 cm^{-1} is absent in all the spectra (Figure 21 B, C and D). Therefore, the IR analysis allow to exclude the presence of vicianin in the Soxhlet washing solvents. However, the TLC analysis of the crude obtained from the washed seeds did not reveal the presence of the metabolite of interest. This make us postulate that the long time required for Soxhlet extraction (one day for each wash) cause the enzymatic degradation of the metabolite of interest. For this reason, none of the pre-treatment tested resulted suitable for the extraction of vicianin.
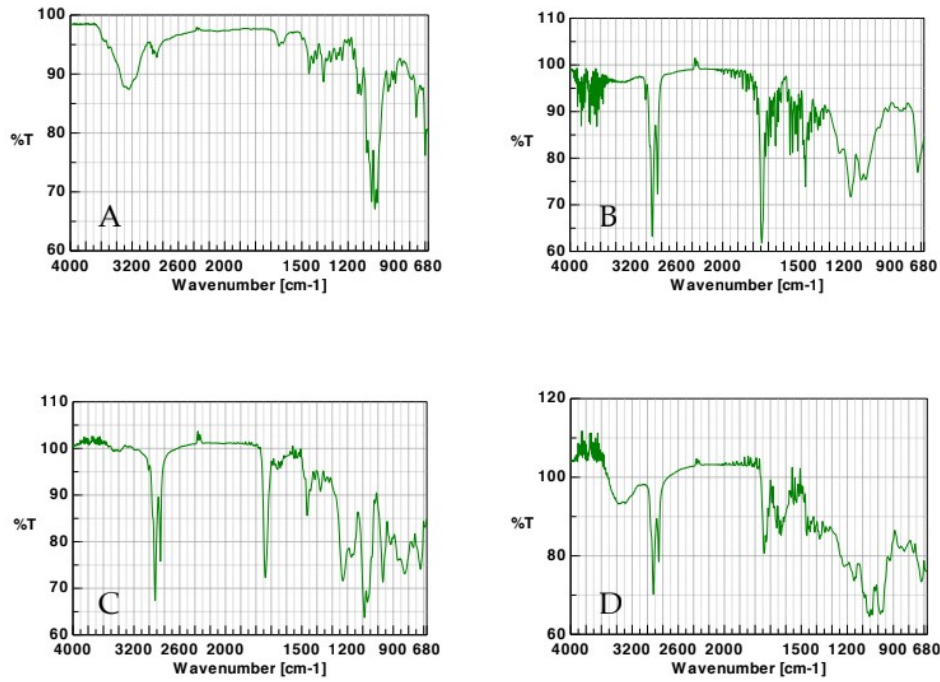
Figure 21: IR spectra of amygdalin (A) and the washes obtained with Hex (B), DCM (C), and AcOEt (D)

To resume, optimized extraction protocols for both patuletin-3-Oglucoside and vicianin are reported in Figure 22.
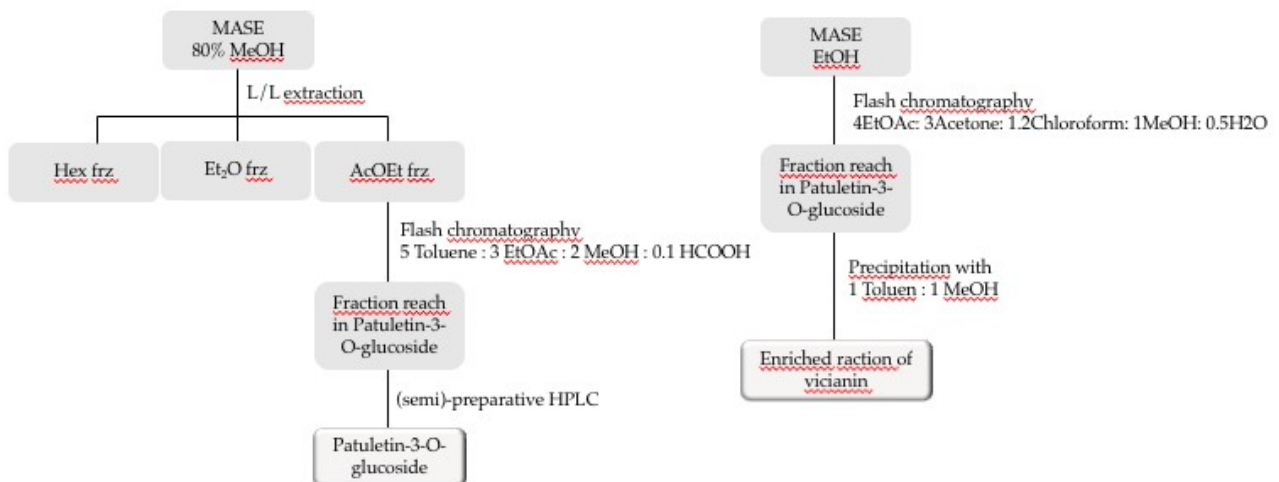
Figure 22: Optimized extraction protocols for both patuletin-3-Oglucoside and vicianin

At the end of the extraction and fractionation procedures reported in paragraphs 2.4.1 and 2.4.2, crude extracts **1-4**, 1 EFs and 3 pure compounds (Table 9) were available for further biological investigations.

Table 9: Mixtures, EFs and pure compounds underwent to biological investigations.

Source	Name
Artemisia annua L.	Crude extract **1**
	6-methoxykaempferol-3-O-glucoside
Vaccinium myrtillus L.	Crude extract **2**
	Cyanidin-3-O-arabinoside
Vicia sativa L.	Crude extract **3**
	Fraction enriched in vicianin
Prunus spinosa L.	Crude extract **4**
	Kaempferol-3-O-α-L-arabofuranoside

2.5 Biological investigation

An initial screening of the crude extracts was performed on three different cell lines: RPMI 8226 (Multiple Myeloma), MCF7 (breast cancer) and U87-MG (glioblastoma). Results obtained are summarized in Table 10. Results of *Vicia sativa* acidic extracts have not been reported being resulted not active in all the tested conditions.

Table 10: IC$_{50}$ values

Artemisia annua L. _ Crude extract **1**			
	24h	**48h**	**72h**
RPMI 8226			
MCF7		Ongoing	
U87-MG			

Vaccinium myrtillus L._ Crude extract **2**			
	24h	**48h**	**72h**
RPMI 8226	54.84 µg/mL	39.42 µg/mL	16.84 µg/mL
MCF7	45.25 µg/mL	14.21 µg/mL	12.87 µg/mL
U87-MG	NA	NA	145.78 µg/mL

Vicia sativa L. _ Crude extract **3**			
	24h	**48h**	**72h**
RPMI 8226	734.72 µg/mL	146.94 µg/mL	103. 01 µg/mL
MCF7	485.21 µg/mL	237.39 µg/mL	150.22 µg/mL
U87-MG	NA	219.81 µg/mL	39. 09 µg/mL

Prunus spinosa L. _ Crude extract **4**			
	24h	**48h**	**72h**
RPMI 8226	378.61 µg/mL	188.29 µg/mL	161.88 µg/mL
MCF7	345.57 µg/mL	161.52 µg/mL	103.15 µg/mL
U87-MG	NA	NA	NA

NA = not active

Results reported in the previous table evidence that all extracts are active against RPMI 8226 and MCF7 with similar trend, whereas only *Vicia sativa* methanolic extract after 48h and *Vaccinium myrtillus* after 72h showed an effect against U87-MG cell lines.

Encouraged by the results obtained in the crude extracts screening, the investigation was extent to EFs and pure compounds, especially focusing on RPMI 8226 cell line, in light of the consideration that the compounds are the result of a VS on proteasome. The considered cell line derives from the peripheral blood of a 61 year old male affected by MM. Both cell viability (with MTT and Trypan blue test) and proteasome activity after the treatment with different compounds have been evaluated.

Best results have been obtained after the treatment with the Ef of vicianin. Thus, this Ef is able to significantly reduce both cell viability and proteasome activity, encouraging us to further fractionate it in the near future (Figure 23).
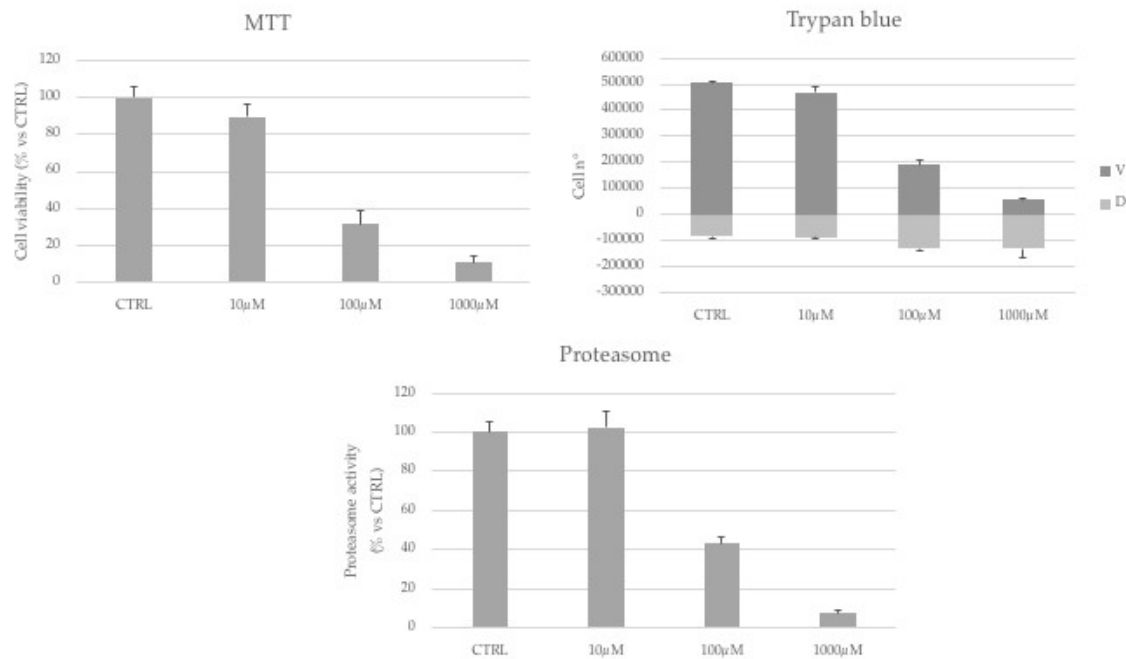
Figure 23: Results of MTT (A), Trypan blue (B) and proteasome activity (C) assays after the treatment with vicianin enriched fraction. Results are compared to untreated controls (CTRL).

Similar considerations can be done for Kaempferol-3-O-α-L-arabofuranoside (also known as Juglanin), the metabolite produced by the flowers of *Prunus spinosa*. This compound is able to reduce cell viability in a dose dependent manner (Figure 24 A and B) and to significantly inhibit proteasome (Figure 24 C). In detail, the considered target exhibits activity reduced by almost 40% at a concentration of 50μM in comparison with a control.
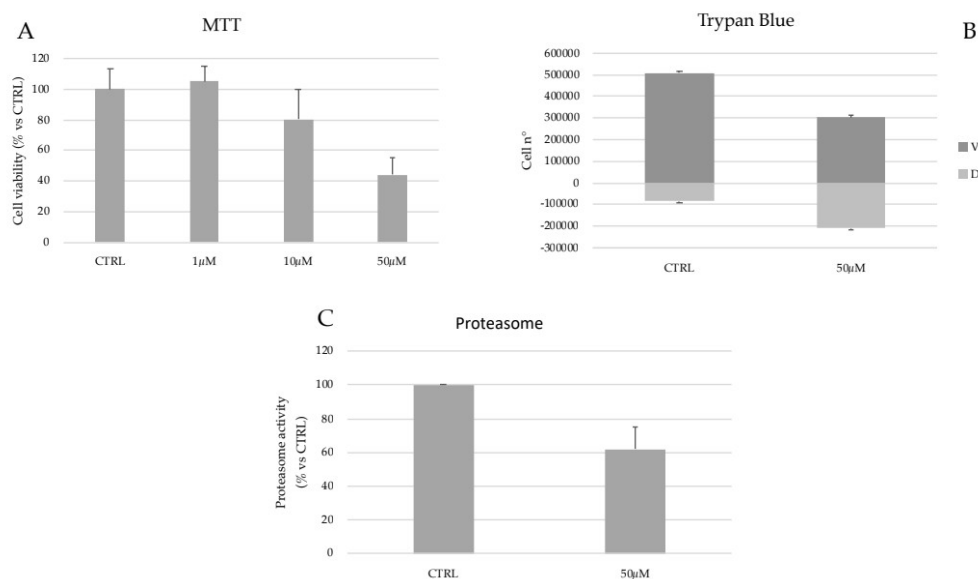
Figure 24: Results of MTT (A), Trypan blue (B) and proteasome activity (C) assays after the treatment with Kaempferol-3-O-α-L-arabofuranoside. Results are compared to untreated controls (CTRL).

The biological profile of both these compounds highlights that they can be considerate promising hit compounds to develop new anticancer drugs. Of note, this is the first time vicianin has been identified as possible weapon in the anticancer arena. Moreover, studies are ongoing to identify suitable modification of its cyanogenic group to avoid the correlated in vivo toxicity and maintaining the activity [113].

Different considerations can be done for 6-methoxykaempferol-3-O-glucoside (Patuletin-3-O-glucoside). Thus, the biological investigations highlighted that this metabolite extracted by the aerial parts of *Artemisia annua* is able to slight inhibit proteasome at non cytotoxic concentration.

In conclusion, all the compounds derived from the VS of the Demo Database resulted able to inhibit proteasome, with the only exception of Cyanidin-3-O-arabinosid. It resulted not active both in reducing cell viability, both in inhibiting the target of interest. This result is not coherent with literature data, which identify Cyanidin-3-O-glucoside (kuromanin), as a proteasome inhibitor whose IC$_{50}$ is 12.6 μM [114]. This unexpected result could be associated to the degradation of the compound, being cyanidins susceptible to variations of temperature, pH, presence of oxygen and light [115]. Further investigation for corroborating this hypothesis is ongoing.

Taken together, the results confirmed that the pharmacophoric model postulated during my stay in Inte:ligand is correct and that the database herein proposed may be useful for identifying new actives. Therefore, we screened the compounds of the database on another target.

2.6 Virtual screening vs LsrK of the library of secondary metabolites
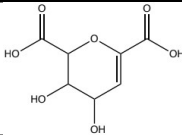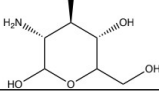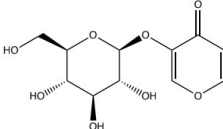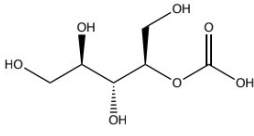
The developed database can be used for the screening on a plethora of different target. As a demonstration of the versatility of the set up library, a second VS on a different target has been performed, changing not only the protein but also the pathology. In this second case, we considered another threat for human health: antimicrobial resistance.
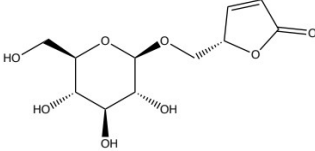
Over the last decades, multidrug-resistant bacteria have been extensively observed. These persistent pathogens predominantly grow in complex heterogeneous structures enmeshed in a self-produced exopolysaccharide matrix, called biofilms. Biofilm formation confers additional resistance to bacteria, commonly referred to as community resistance, which can have a 1000-fold higher tolerance to antibiotics than the same organisms in a planktonic state [116,117].

The communication among the different microorganisms constituting the biofilm is entrusted by the quorum sensing (QS) signaling. The messengers of QS are the so-called autoinducers (AIs). Among the different AIs, the AI-2 signaling allows for interspecies communication and all the compounds belonging to this class have a common precursor, named 4,5-dihydroxy-2,3 pentane-dione (DPD). The phosphorylation of hydrated linear DPD by the kinase LsrK is a crucial step in triggering the QS cascade. Thus, LsrK represents a valuable target in fighting the multidrug resistance bacteria (Appendix, paper 4).

Being the 3D structure of LsrK available on the PDB, we followed a protocol similar to the one reported in Paragraph 2.3 to develop a pharmacophoric model for the identification of potential LsrK inhibitors. After the VS of the library of secondary metabolites, five different molecules have been identified as promising (see table 11)

Table 11: Potential proteasome inhibitors and their sources

Code	Name	Structure	Source
MVPV01801	Daucic acid		*Daucus carota* L.
MVPV04563	Glucosamine		*Capsella bursa-pastoris* L. AND *Urtica dioica* L.
MVPV02430	Erigeroside		*Bellis perennis* L.; *Erigeron annuus* (L.) Desf. AND *Erigeron sumatrensis* Retz.
MVPV00162	2-Carboxyarabinitol		*Medicago sativa* L.; *Mentha spicata* L.; *Cirsium arvense* (L.) Scop; *Equisetum arvense* L.; *Erodium cicutarium* (L.) L'Hér AND *Plantago lanceolata* L.

| MVPV02238 | Ranunculin | | *Ranunculus bulbosus* L.; *Helleborus foetidus* L.; *Ranunculus repens* L.; *Ranunculus acris* L. AND *Ranunculus sceleratus* L. |

Some of the selected molecules are commercially available. Harvesting, extraction and fractionation of the other retrieved natural matrices are ongoing. Of note, this is the first time a VS based on a pharmacophoric model has been performed on LsrK. If the inhibitory activity of the selected molecules will be confirmed, they would represent an inestimable weapon against multi-drug resistance bacteria.

To conclude, in this part of the work, our main goal was to valorize the vascular flora of the province of Pavia. To reach this aim we developed a DB reporting all the 3D structures of the produced metabolites and exploited it to identify possible agents to fight cancer and antimicrobial resistance. More in general, the DB can be exploited to identify new ligands of a plethora of different targets and can also be exploited to make "deep botanical investigations", being all the metabolites linked with their producing organism.

3. Valorization of the lichen flora of Pavia countryside

3.1 Lichens in medicinal chemistry

To further valorize the biodiversity of Pavia countryside, I also studied a completely different flora, the lichen one.

Lichens represent more than 20% of the world's fungal biodiversity [118]. The term was coined more than 2000 years ago by the Greek philosopher Theophilus to indicate the unidentified organisms that grow on the bark of plants [119]. Today, lichens are known to be symbiotic associations between a photobionts (algae) and a microbionts (fungi): the alga produces carbohydrates and other nourishment, while the fungus provide protection from drying and against solar radiation. This partnership allows the lichen to survive even in difficult environmental conditions and to colonize different habitats. They are able to colonize various substrates and can grow on rocks, barks, on wood, soil, mosses, on other lichens, as well as on artificial substrates such as cement, glass, and plastics. The dense lichen layer suggests a possible role of these organisms as a protective coating, especially against possible environmental attacks [120]. Despite this extreme range of ecological adaptations, many lichens are sensitive to changes in their optimal ecological conditions and don't grow in non-native habitats [121]. Moreover, lichens are bio-accumulators and are highly sensitive to specific pollutants. Effects of pollution in lichens are evident considering that their number is decreasing, mainly because of the disruption of the symbiotic association. Therefore, lichens are used as bioindicators according to their presence / absence in the environment [122–124].

Lichens can be divided into three distinct groups: foliose, fruticose, and crustose. Foliose lichens exhibit a lobed leaf appearance and extend in a horizontal layer above the substrate surface. Fruticose lichens appear as a shrubby shape and their overall appearance is similar to a bush. Finally, crustose lichens remain very attached to the substrate. In nature, lichens grow very slowly. Their radial growth is measured in millimeters per year. In general, most of the foliose species grow by 0.5–4 mm per year, the fruticose ones 1.5–5 mm per year and the crustose species 0.5–2 mm per year.

In traditional medicine, lichens were used in Asia, ancient Egypt, and Rome mainly for the treatment of respiratory, skin, obstetric, gynecological, and digestive diseases [119,125].

During the last years, the interest in studying lichens as potential source of drugs has undoubtedly grown, as demonstrated by the number of scientific papers. The main reason relies in the characteristics of their secondary metabolites, whose structures are often absent in the other natural matrices. From a structural standpoint, they can be classified in four chemical classes: monocycles, depsides, depsidones and dibenzofurans (Figure 25). A review of the literature evidenced that many of the metabolites identified so far are biologically active and that most of them showed anticancer (table 12), antimicrobial (table 13) and antifungal (Table 14) properties.

Supported by literature data, we decided to explore also the lichen flora. The first idea was to build up a proper Database, collecting all the information regarding lichens and their metabolites, following the same scheme discussed above for the vascular flora. Nevertheless, considering that the knowledge on these complex organisms is still very poor, and that few

metabolites have been isolated and properly characterized, we felt this approach was not the right one and changed the perspective.
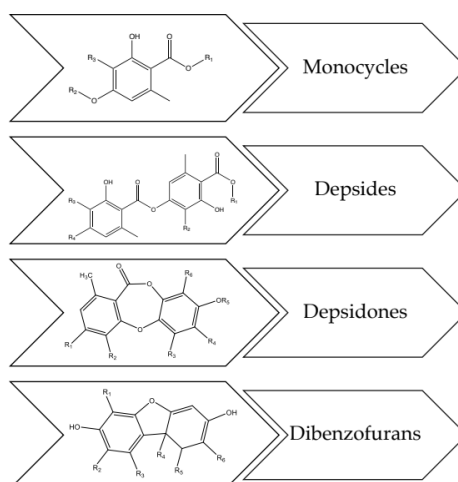
Figure 25: class of secondary metabolites produced by lichens.

My research in the lichens field started from lichens spontaneously growing in Pavia countryside. Lichens belonging to *Cladonia* genus are particularly abundant and easy to collect. They are fruticose lichens, which can have two kinds of thallus: primary horizontal thallus (squamulous or rarely crusty, sometimes disappears) and secondary vertical thallus (podetia) [126]. The three main species I studied in my thesis project are *Cladonia foliacea*, *C. furcata* and *C. rangiformis*. These species spontaneously grow near the Ticino river and their in-depth study from a phytochemical standpoint may be useful for the valorization of our territory.

The work was organized as follow:

- collection of *Cladonia foliacea*, *C. furcata* and *C. rangiformis* thanks to the collaboration with Dr Gabriele Gheza, lichenologist at the University of Pavia, Department of Earth and Environmental Science;
- develop of extractive, analytical, and separative procedures to characterize the main metabolites;
- evaluation of anticancer and antimicrobial properties of extracts and isolated metabolites.

Table 12: Anti-cancer activity of lichen metabolites reported in literature.

	FeMX	UACC-62	U87MG Glioblastoma	A2780 Ovaric cancer	HT-29 Colon carcinoma	MCF-7 breast arcinoma	HeLa Cervical cancer	A549 Lung carcinoma	DU-145 Prostate cancer	LS174 Colon carcinoma
	Melanome									
Orsellinic acid						[127]				
Methyl-orsellinate						[128]				
Lecanoric acid						[128]	[129]	[129]		[129]
Giroforic acid	[130]			[131]	[132]	[131]	[131]			
Evernic acid	[133]									[133]
Barbatic acid						[134]	[134]	[134]	[134]	
Atranorin	[135]	[136]	[137]	[131]	[131]	[137]	[131]	[137]	[137]	[130]
Stictic acid					[132]	[138]				
Norstictic acid	[139]	[136]								[139]
Protocetraric acid		[136]								
Fumarprotocetraric acid	[130]									[130]
Psoromic acid		[136]	[140]							
(R)-usnic acid	[139]	[136]	[141]	[131]	[131]	[142]	[133]	[133]	[133]	[139]
(S)-usnic acid						[142]				

Table 13: Anti-bacterial activity of lichen metabolites reported in literature.

	Bacillus megaterium	*B. cereus*	*B. subtilis*	*E. coli*	*Pseudomonas aeruginosa*	*Salmonella choleraesuis*	*Salmonella enterica typhimurium*	*Staphylococcus aureus*	*Sarcina lutea*	*Mycobacterium tuberculosis*	*Klebsiella pneumoniae*
Orsellinic acid	[143]	[143]	[143]	[143]	[143]	[143]	[143]	[143]	[143]		
Methyl-orsellinate										[144]	
Lecanoric acid	[143]	[143]	[143]	[143]	[143]	[143]	[143]	[143]	[143]	[144]	
Giroforic acid			[145]	[145]				[146]			[145]
Evernic acid			[133]	[133]				[133]			[133]
Barbatic acid			[147]		[147]			[147]			
Atranorin		[148]	[149]	[150]				[149]	[150]	[144]	[150]
Stictic acid			[145]	[145]				[145]			[145]
Norstictic acid	[143]	[143]	[143]	[143]	[143]	[143]	[143]	[143]	[143]	[144]	
Protocetraric acid	[143]	[143]	[143]	[143]	[143]	[143]	[143]	[143]	[143]	[144]	
Iporotocetraric acid		[150]	[150]	[150]				[150]	[150]		[150]
Fumarprotocetraric acid		[148]	[148]	[151]				[148]	[150]		[151]
Psoromic acid											
(R)-usnic acid	[143]	[143]	[143]	[143]	[143]	[143]	[143]	[143]	[143]	[144]	
(S)-usnic acid		[148]	[148]					[152]			

Table 14: Anti-fungal activity of lichen metabolites reported in literature.

	Aspergillus flavus	*Aspergillus nidulans*	*Aspergillus niger*	*Candida albicans*	*Candida glabrata*	*Candida krusei*	*Candida tropicalis*	*Fusarium moniliforme*	*Trichoderma viridae*	*Trichophyton mentagrophytes*
Orsellinic acid	[143]	[143]	[143]	[143]	[143]	[143]	[143]	[143]	[143]	[143]
Methyl-orsellinate										
Lecanoric acid	[143]	[143]	[143]	[143]	[143]	[143]	[143]	[143]	[143]	[143]
Giroforic acid	[145]			[145]						
Evernic acid	[133]			[133]						
Barbatic acid										
Atranorin	[130]		[153]	[130]	[154]					[153]
Stictic acid	[145]			[145]						
Norstictic acid	[143]	[143]	[143]	[143]	[143]	[143]	[143]	[143]	[143]	[143]
Protocetraric acid	[143]	[143]	[143]	[143]	[143]	[143]	[143]	[143]	[143]	[143]
Iporotocetraric acid										
Fumarprotocetraric acid	[130]			[130]	[154]					
Psoromic acid										
(R)-usnic acid	[143]	[143]	[143]	[143]	[143]	[143]	[143]	[143]	[143]	[143]
(S)-usnic acid					[148]					

3.2 Preparation of extract from Cladonia lichens and analytical investigation

Considering that one the most studied and well described metabolite produced by lichens is usnic acid (UA) and that it is also produced by *Cladonia* genus, the first activity of this part of the project consisted in the isolation of UA from *C. foliacea* collected near Ticino river.

UA is a dibenzofuran derivate owning an asymmetric center, which make two enantiomers possible (Figure 26). Of note, two enantiomers of one molecular entity may show different pharmacological and toxicological profiles. Both UA forms occur in nature depending on the producing organism. For example, *Usnea* genus produces only (*R*)-UA, *Alectoria* genus only (*S*)-UA, while *Flavocetraria* genus produces a mixture of two enantiomers [155,156]. Sometimes lichens belonging to the same genus produce different enantiomeric forms. This is the case of *Cladonia* genus, in which *C. arbuscula* and *C. mitis* produce (*R*)-UA, *C. uncialis* and *C. foliacea* produce (*S*)-UA and *C. stellaris* produces a mixture of both [156,157]. Under a biological point of view, these two enantiomers show different profile. Thus, they are active on different fungal and bacterial stains and on different cancer cell line. Moreover, they also show different behaviour in terms of allergenicity and toxicity [156].

(+)-*(R)*-Usnic Acid   (-)-*(S)*-Usnic Acid
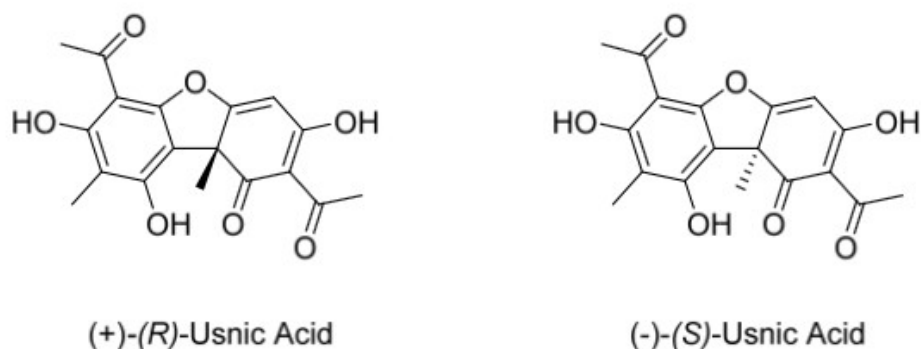
Figure 26: Chemical structure of usnic acid enantiomers.

Between the two enantiomers, (*S*)-UA is surely the less studied one. Considering this, the first step in the valorization of this genus is to set up a quick and exhaustive method to extract this metabolite from *C. foliacea*. To reach our aim and basing on our previous experience, we developed a MASE methodology easily applicable to the extraction of (*S*)-UA from *C. foliacea* exploiting a design of experiments (DoE) approach. This method is based on statistical calculations and it allows to identify the best experimental conditions with the minimum number of runs. Moreover, DoE facilitates the broad understanding of the investigated process [158,159]. Moreover, we set up a proper HPLC method in order to allow a rapid analysis of the samples.

The experimental plan described in Paper 5 (see appendix) allowed us to identify a MASE protocol to quantitatively extract (*S*)-UA, using ethanol and heating twice at 80°C under mw irradiation for 5 min. The procedure is simple, rapid, low cost, versatile and suitable for the scale up procedure. Moreover, the selected solvent, EtOH, has several advantages: (i) it is classified as green solvent; (ii) it has non-toxic properties; (iii) having a low boiling point, it is easily removable from a solution; (iv) it is considered a universal solvent, as its molecular structure allows the dissolution of polar, hydrophilic and non-polar, hydrophobic compounds.

For these reasons, the same extraction conditions were also applied for the extraction of *C. furcata* and *C. rangiformis*. To better compare the phytochemical profile of the three species, we decided to exploit two different solvents: ethanol, being the one selected by the DoE experiments,

and AcOEt. This choice was driven by the consideration that EtOH is a high mw adsorption (ε'= 24.3 and ε''= 22.87) while AcOEt is a low microwave adsorption (ε'= 6.02 and ε''= 0).

Dried samples of *C foliacea*, *C. rangiformis*, and *C. furcata* were grounded, extracted and the crude evaporated under reduced pressure to calculate the extraction yield (Table 15).

Table 15: Extraction yields after the extraction of Cladonia genus with different solvents.

	Extraction yields (%)	
	EtOH	AcOEt
C. foliacea	6.73 %	2.50 %
C. rangiformis	7.18 %	3.16 %
C. furcata	7.90 %	3.00 %

The extraction yields of the three *Cladonia* species show a comparable trend, with higher values for the ethanolic crude extracts. This data demonstrates and confirms that ethanol, having a higher dielectric constant, absorbs microwaves more easily and therefore has higher extraction power.

However, considering the different nature of the two solvents considered, we decided to continue the characterization considering the crude extracts obtained by both the solvents.

With all the crude extracts in our hands, we developed TLC and RP-HPLC-UV/PAD-ESI/MS methods to obtain their analytical fingerprints, useful both as a control of the quality of the extracts and as a starting point for future purification studies.

The identification of the MP for the first chromatographic technique was made through the analysis of different mixtures with the addition or not of acidic or basic additives. Evidences highlighted that only by adding an acidic additive, specifically 0.1% formic acid, and a mixture of 4 hexane: 6 diethyl ether a good chromatographic resolution was obtained.

In parallel with the selection of the best TLC MP, an HPLC method was developed by further optimizing the one described in the previously published paper (appendix, paper 5).

To optimize the method, different elution conditions were tested (methanol, acetonitrile, water, with or without formic acid or orthophosphoric acid) by adopting different gradient modes on two different columns (Symmetry C18 and XBridge Phenyl). The best results in terms of peak resolution, peak shape and time of analysis were obtained using an XBridge Phenyl column (5 μm, 4.6 × 150 mm) under gradient elution conditions, using water + 0.05 % (v/v) of orthophosphoric acid (solvent A) and acetonitrile (solvent B) and with a flow of 1 mL/min. Furthermore, the optimal concentration for the injection of the samples was 1 mg/mL.

The developed fast and inexpensive chromatographic method resulted suitable for the complete resolution of the metabolites produced by the three species of *Cladonia*, i.e. *C. foliacea, C rangiformis*, and *C. furcata*. Resulting chromatograms are reported in Figure 27.
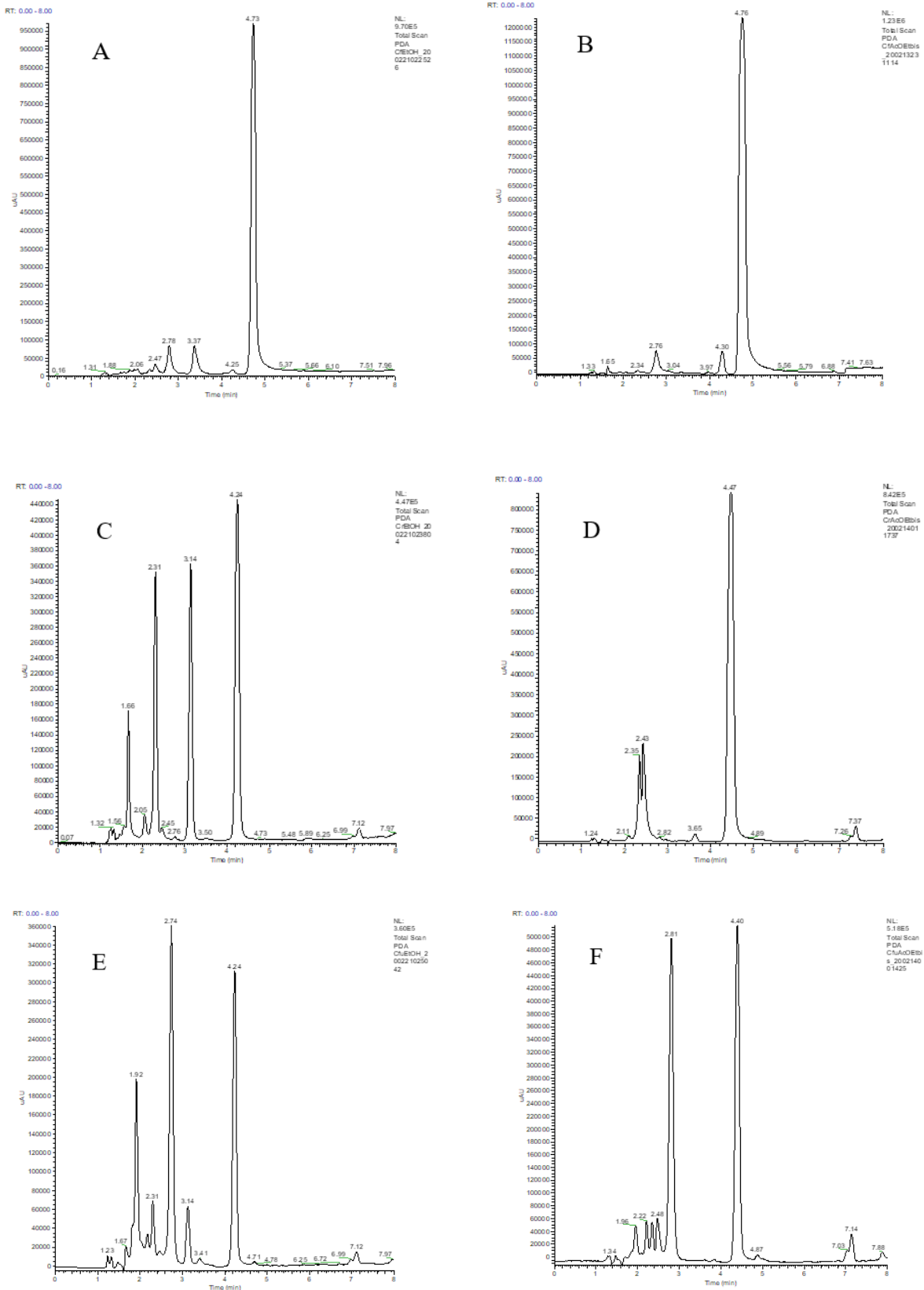
Figure 27: Chromatograms EtOH *C. foliacea* (A), AcOEt *C. foliacea* (B), EtOH *C. rangiformis* (C), AcOEt *C. rangiformis* (D), EtOH *C. furcata* (E), and AcOEt *C. furcata* (D) extracts (PAD *view*).

The number and the intensity of the peaks confirmed the higher extraction power of EtOH. Furthermore, the retention times and the UV and MS spectra of the different peaks highlighted that *C. rangiformis* and *C. furcata* contain several common metabolites, including, above all, the peak with the most intense absorption. Trace of the same peak is also present in *C. foliacea*. Regarding the species *C. rangiformis* and *C. furcata*, other metabolites were also found to be in common, in particular the peaks with $m/z = 369$ and $m/z = 197$, both present in higher amount in *C. rangiformis* (Figure 28).
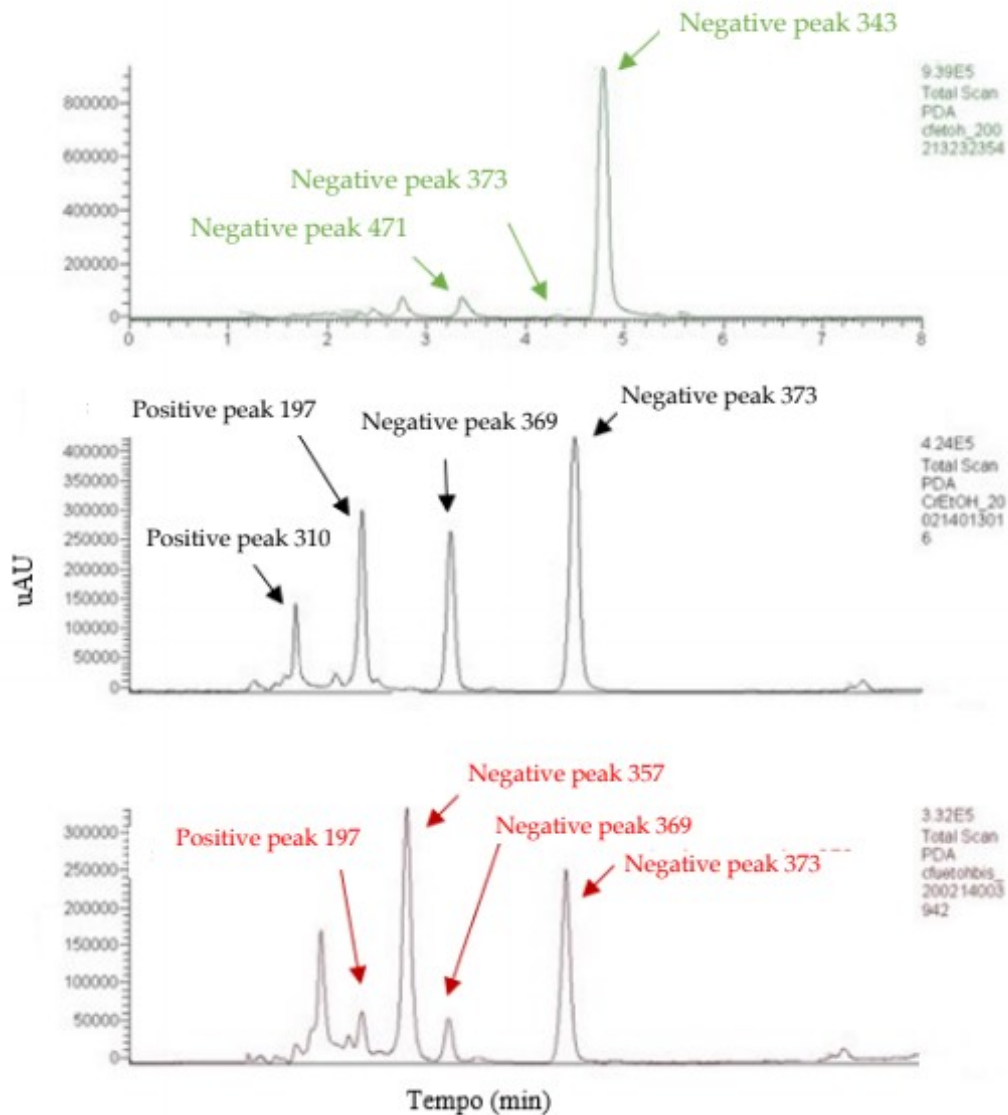
Figure 28: Chromatograms of EtOH extracts of *C. foliacea* (green) *C. rangiformis* (black) and *C. furcate* (red).

3.3 Isolation and identification of the main metabolites

Once the crude extracts obtained by the three different lichen species was obtained, the purifications of the most abundant metabolites were performed.

At the beginning, we focus our attention on (*S*)-UA from *C. foliacea*. Thus, the procedure published in the previous paper (see appendix A, paper 5), was long and expensive, so we decided to optimize it.

After different attempts, the best procedures foresaw a first decantation of the ethanolic crude extract in methanol, a subsequent centrifugation to separate the solid and its final crystallization. This latter procedure is carried out by solubilizing in the minimum quantity of chloroform at room temperature and subsequently adding ethanol, in 1: 2 ratio respectively. This solvent mixture allowed the precipitation of yellow-orange UA crystals. Crystallization is a very advantageous solids purification technique since crystal growth is slow and selective.

Starting from 10 g of natural matrix, 74 mg of compound were obtained with a purity> 99% and a product yield of 0.75%.

The chemical structure was then confirmed by NMR and MS analysis and determination of the specific optical rotational power (Na lamp 589 nm) which resulted in a value of $[\alpha]_D$= - 472 (0.5% w/v, CHCl$_3$). This data confirms that only one enantiomer is present in *C. foliacea*, namely (-)-(*S*)-UA.

Another known secondary metabolite produced by *C. foliacea* is the fumarprotocetraric acid (FPCA), which belongs to the class of depsidones.

Starting from the assumption that UA is soluble in chloroform and insoluble in alcohols, while FPCA has the opposite solubility trend, it was decided to exploit the supernatant obtained after precipitation of UA in MeOH for the isolation of this metabolite.

This fraction properly dried, was subjected to an L/L extraction with EtOAc. The anhydrified organic phase was evaporated under reduced pressure and subjected to a precipitation always exploiting the afore mentioned crystallizing mixture (1 chloroform: 2 EtOH). After an hour, suspended white particles were observed. The centrifugation was then carried out at 3000 rpm for 10 minutes, thus making the separation of a white powder possible.

This precipitate was confirmed to be FPCA by comparing its NMR and MS spectra with those found in the literature.

Once isolated the two main metabolites produced by *C. foliacea*, we move to identify the main metabolites produced by both *C. rangiformis* and *C. furcata*. Being the first specie more abundant in our lab, we exploited the crude deriving from it for the fractionation procedure.

Comparing the chromatograms obtained by TLC and HPLC analysis, it was possible to note that the main metabolite is present in greater quantities in the ethyl acetate extract.

It was therefore decided to extract 10 g of *C. rangiformis* with this solvent. Upon evaporation at reduced pressure of the crude obtained, it was noted that the precipitation of a colorless solid was triggered during the concentration of the mixture. It was therefore decided to favor this phenomenon by leaving the suspension so obtained overnight at 4°C. A TLC analysis of the white solid so obtained highlighted that it was not a pure compound, so a further investigation

was carried out to complete its isolation. After screening of different precipitation, chloroform allowed to obtain a grayish powder whose purity was suitable for subsequent analysis.

NMR and MS analysis of the compound allowed its identification as atranorin (ATR), belonging to the class of depsides. HPLC analysis demonstrated that this metabolite was abundant one both in *C. rangiformis* and *C. furcata*, but it was also present in trace in the extract of *C. foliacea*. Another intensive peak present in the ethanolic extract of *C. rangiformis* and *C. furcata* has a retention time = 2.31 min. To isolate the metabolite eluted at that time, a liquid-liquid extraction of the crude ethanolic extract was performed, using dichloromethane (DCM) as organic phase. Specifically, the extract was dissolved in DCM and seven L/L extractions were performed with water. After removal of the solvent under reduced pressure, the obtained oil was chromatographed. The proper mobile phase was identified testing different mixtures of diethyl ether and hexane, always added with 0.1% of formic acid. The best MP was identified as a gradient elution from 3 Et$_2$O: 7 Hex to 9 Et$_2$O: 1Hex plus the acidic additive.

After the flash chromatography, the fraction containing the metabolite of interest were put together, evaporated and added with hexane, triggering the precipitation of the pure compound in suitable amount for MS and NMR analysis, which allowed to identify it as rhizonic acid. It is interesting to note that this metabolite had never been isolated from either *C. rangiformis* or *C. furcata* before. Unfortunately, the amount of metabolite extracted was not sufficient for biological analysis.

The structure of all the identified molecules is reported in Figure 29.
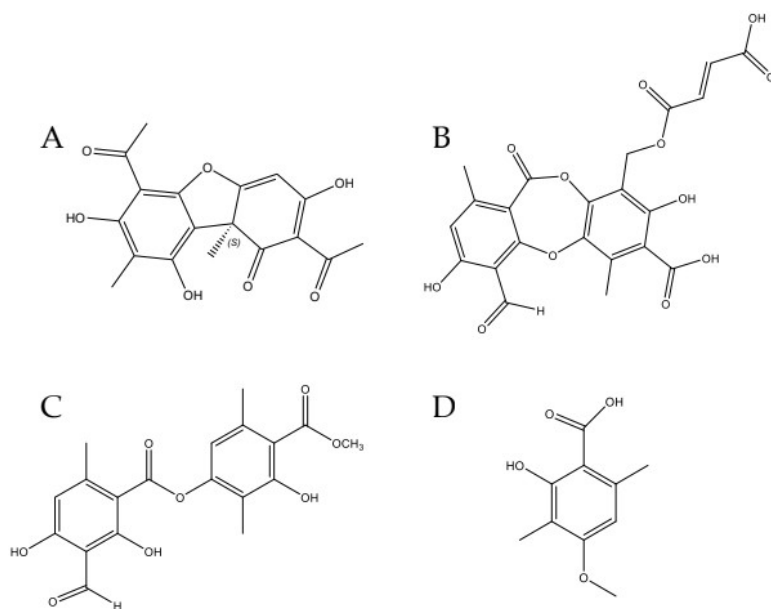
Figure 29: Chemical structure of (S)-Usnic acid, (A), Fumarprotocetraric acid (B), Atranorin (C), and Rhizonic acid (D).

Once the main metabolites of each lichen have been identified and chemically characterized, their biological profile has been deepened on anticancer and antifungal cell lines and strains, in line with the main research areas of the team I work with.

3.4 Investigation of anticancer properties

Although the mechanism of action of lichen secondary metabolites on cancer cells are not well understood yet, studies have evidenced that some metabolites have cytotoxic effects against cancerous cell lines, including breast, lung and colon cancer. This cytotoxic effect is often due to an apoptosis induction, angiogenesis regulation and to the modulation of various transcription factors, cell cycle and proliferation.

To investigate the anticancer potential of lichens belonging to Cladonia genus, a screening on four different cell lines representative of different tumors was performed, once again in collaboration with Professor Guido Cavaletti's group. The activity against the following cancer cell lines have been considered: RPMI 8226 (MM), MCF7 (breast cancer), EGI-1 (cholangiocarcinoma), and U87-MG (glioblastoma) cell lines, since they are representative of unmet medical diseases.

As evidenced in Figure 27, the crude extracts obtained using ethanol and ethyl acetate differs for both the relative abundance of the peaks and for the nature of the extracted metabolites. For this reason, we decided to analyze each lichen by extracting them exploiting both these solvents. The biological assays selected for this preliminary screening were MTT, for its rapidity and versatility, and proteasome activity test. The results of the latter were negative in all the tested conditions, demonstrating that lichen metabolites do not affect the activity of this target. On the other hand, results of the MTT test were very promising and they are summarized in Figure 30.
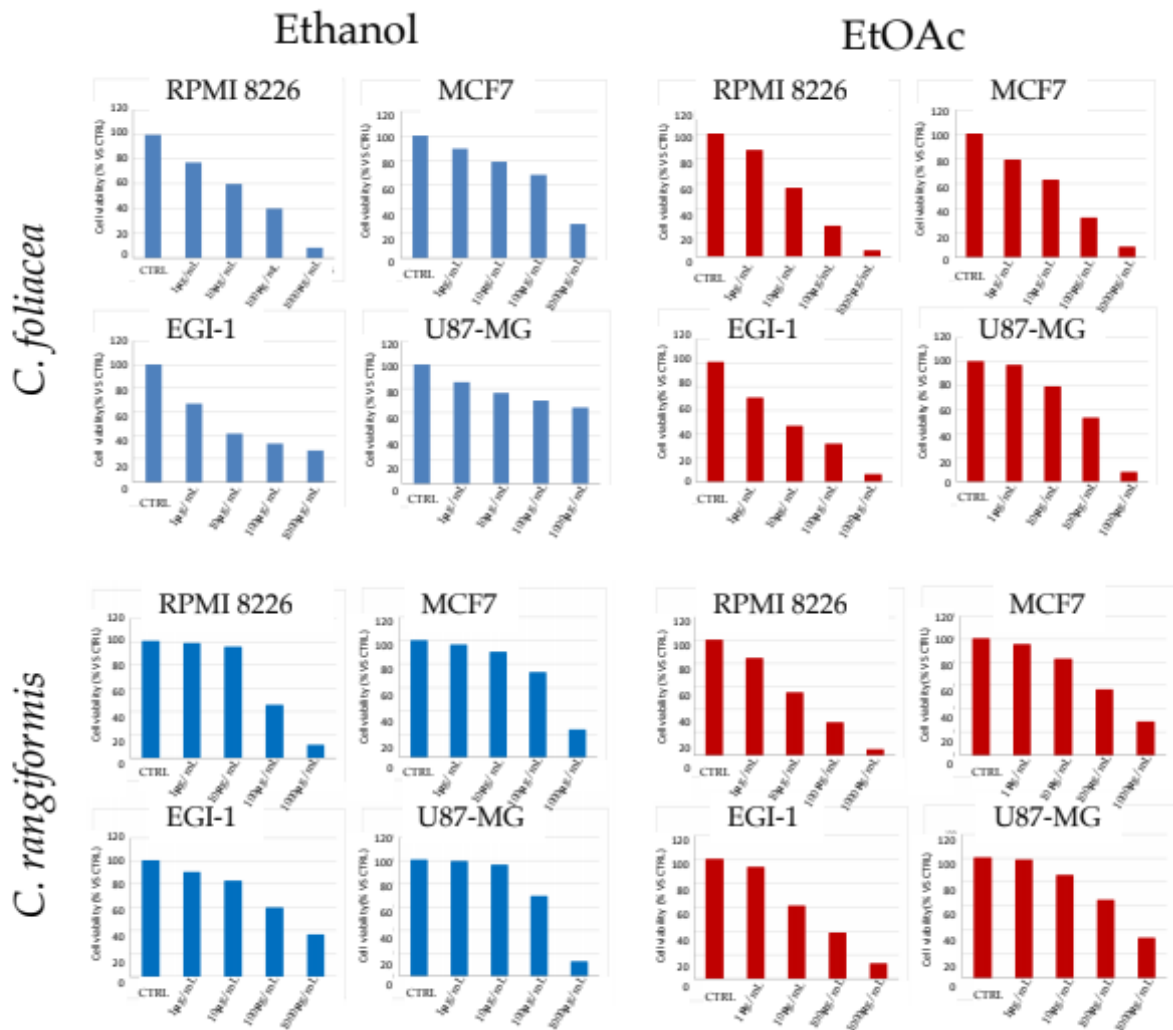
Figure 30: Cell viability of RPMI 8226, MCF7, EGI-1, and U87-MG cell lines after the treatment with *C. foliacea* and *C. rangiformis* crude extracts.

As evidenced by the results reported above, all the extracts are able to reduce viability in the tested cell lines in a dose dependent manner. EtOAc extracts generally resulted more active than the corresponding alcoholic crude extracts and RPMI 8226, MCF7, and EGI-1 resulted more sensitive than U87-MG.

Encouraged by these results, we investigated the biological profile of the isolated metabolites. The IC_{50} values are reported in Table 16.

Table 16. IC$_{50}$ values of tested metabolites at different time.

Cell line	(S)-UA (IC$_{50}$ μM)		
	24h	48h	72h
RPMI-8226	49.4	29.0	14.5
MCF-7	316.6	37.8	23.3
EGI-1	377.6	98.8	40.7
U87-MG	572.2	26.1	5.8

Cell line	FPCA (IC$_{50}$ μM)		
	24h	48h	72h
RPMI-8226	27.5	0.4	0.02
MCF-7	< 150	78.3	25.4
EGI-1	97.4	2.7	1.9
U87-MG	< 150	< 150	< 150

Cell line	Atranorin (IC$_{50}$ μM)		
	24h	48h	72h
RPMI-8226			
MCF-7	< 150 μM		
EGI-1			
U87-MG			

In all the tested cell lines, both (*S*)-UA and FPCA impaired cell viability in a dose- and time-dependent manner, while atranorin didn't show any effect.

As evidenced by the IC$_{50}$ values, (-)-(*S*)-UA generates an effect strongly time-dependent. Thus, at 24h, the mostly affected line is the MM one, while at 72h, the Glioblastoma cells are the most affected ones. Results obtained have been compared to those of (+)-(*R*)-UA against MCF-7 and U87-MG cell line reported in literature. Although (-)-(*S*)-UA and (+)-(*R*)-UA have a comparable activity against MCF-7 cell line (IC$_{50}$ of (*R*)- enantiomer at 72h = 18,9μM) [160], it has to be highlighted that the (*S*)-UA is far more effective against U87-MG cell line than the (*R*)-enantiomer (IC$_{50}$ at 48h =12mM) [141], with an eudismic ratio ≈ 460. This evidence further supports the in-depth investigation of the biological profile of this underestimated enantiomer.

On the other hand, FPCA resulted very interesting for the viability impairment of both EGI-1 and RPMI 8226 cell line. Particularly, the IC$_{50}$ value at 72h on RPMI 8226 is 20nM, making this compound a promising hit in the fight against cancer. Consistently, Structure-Activity Relationship (SAR) studies are ongoing to improve its biological profile. To this aim, other metabolites belonging to the class of depsidones will be extracted to analyze the effect of different substituent on the biological profile.

Regarding *C. rangiformis,* the crude extract showed a good cytotoxic activity towards both EGI-1 and RPMI 8226 cell lines, but its main metabolite atranorin is totally inactive. Therefore, it is reasonable to hypothesize that the activity may be due to other metabolite/s present in traces. To deep this issue, a bioguided assay fractionation is ongoing, with the double aim to identify novel anticancer agents, and to better define the phytochemical profile of this species.

3.5 Investigation of antifungal properties

More than 500 fungal species causing human mycosis are known worldwide. These are infections caused by fungi, mainly by yeasts and mold [161].

Antifungal therapy is based on the biochemical differences between fungi and mammals. The main difference is the cell wall, which is a constituent only of fungal cells. Other differences between the two cellular structures lays in the sterols constituting the cell membrane: cholesterol in mammals and ergosterol in fungi. The minimal difference between the two molecules represents the biochemical basis of selective toxicity [162].

Drugs that inhibit the biosynthesis of the bacterial cell wall, such as penicillins and cephalosporins, are part of antifungal chemotherapy. Other biochemical targets of antifungal agents are DNA, the mitotic spindle and interference with the intermediate metabolism [163].

Despite many progresses have been performed in the treatment against fungal infections, this pathology still remains a threat for human being. Thus, billions of people are infected with pathogenic fungi and among these 1.5 million die every year worldwide. The result of the infection depends on several factors: the pathogenicity of the fungus, the host's immune system and the site of infection. 80% of deaths are caused by various species of *Candida*, *Aspergillus* and *Cryptococcus* [162].

Another menace comes from drug resistance. Example can be found in fluconazole, a fungistatic and fungicidal drug commonly prescribed. The resistance mechanisms developed mainly include increase in drug efflux pumps, alterations or overexpression of the drug target and the development of alternative metabolic pathways for the production of ergosterol [164]. Accordingly, new therapeutic options are still necessary to contrast this pathology. To evaluate the antifungal potential of lichen, we followed the same approach described before for the evaluation of the anticancer properties. This activity has been performed with Professor Solveig Tosi and collaborators of the Department of Earth and Environmental Science, University of Pavia.

Firstly, both ethanolic and EtOAc extracts of each lichen have been screened on a panel of fungal strains. Selected strains are *Candida albicans*, *Candida tropicalis*, *Trichophyton rubrum* and *Aspergillus niger*, being them the cause of aggressive infections. Particularly, *Candida* is a commensal fungus, which can be found on the skin, mucosal surface and internal organs. It is the cause of three kind of candidiasis: thrush, vaginal candidiasis, and invasive candidiasis (IC). IC is a deep-seated infection that can affect the lungs, blood, heart, brain, eyes, bones and other organs and it is responsible for 46-75% of invasive fungal infections (IFIs). Candidiasis causes 40% of death in immunocompromised patients [161].

Results of the screening of the extracts on the panel of fungal strains are reported in Table 17.

Table 17. MIC values of tested crude extracts.

	C. foliacea (**MIC** mg/mL)	
	EtOH	**AcOEt**
Candida albicans	> 2	2
Candida tropicalis	**0.03**	> 2
Trichophyton rubrum	> 2	> 2
Aspergillus niger	> 2	> 2
	C. rangiformis (**MIC** mg/mL)	
	EtOH	**AcOEt**
Candida albicans	2	2
Candida tropicalis	2	**0.25**
Trichophyton rubrum	> 2	2
Aspergillus niger	2	> 2
	C. furcata (**MIC** mg/mL)	
	EtOH	**AcOEt**
Candida albicans	> 2	2
Candida tropicalis	1	2
Trichophyton rubrum	> 2	> 2
Aspergillus niger	> 2	> 2

Of particular interest resulted *C. foliacea* ethanolic extract for its effect against *Candida tropicalis*. For this reason, (*S*)-UA and FPCA have been tested, in comparison with Amphotericin B, an effective antifungal drug, commonly used as standard (Table 18).

Table 18. MIC values of tested pure compounds.

	(*S*)-UA	FPCA	Amphotericin B
Candida albicans	> 0.2 mg/mL (> 580 μM)	> 0.2 mg/mL (> 423 μM)	0.1 mg/mL (108 μM)
Candida tropicalis	**0.003 mg/mL (8.72 μM)**	> 0.2 mg/mL (> 423 μM)	> 0.2 mg/mL (> 216 μM)
Trichophyton rubrum	**0.2 mg/mL (580 μM)**	**0.2 mg/mL (423 μM)**	**0.2 mg/mL (216 μM)**
Aspergillus niger	> 0.2 mg/mL (> 580 μM)	> 0.2 mg/mL (> 423 μM)	**0.0125 mg/mL (13.5 μM)**

Results shows that (*S*)-UA has a very interesting profile against *Candida tropicalis* and *Trichophyton rubrum*, both the causes of skin mycosis. For this reason, we decided to perform SAR studies. Firstly, its enantiomer (*R*)-UA (purchased) was tested. Also in this case, *Candida tropicalis*

was the fungus whose viability was mostly affected by the treatment (MIC = 0.00625 mg/mL ≡ 18.15 µM).

After a focused literature survey, a class of UA derivatives have shown wound healing properties, a possible synergistic activity with the antifungal one. The semisynthetic molecules reported in the paper were enamines coming from the reaction between (*R*)-UA and a primary amine [165].

Consistently, we synthetized a small focused library composed by both (*S*)-UA and (*R*)-UA derivatized with three different amino acids, e.g. serine-O-Me, phenylalanine and tyrosine.

The optimized synthetic procedure is reported in scheme 1, while all the obtained derivatives are reported in Table 19.
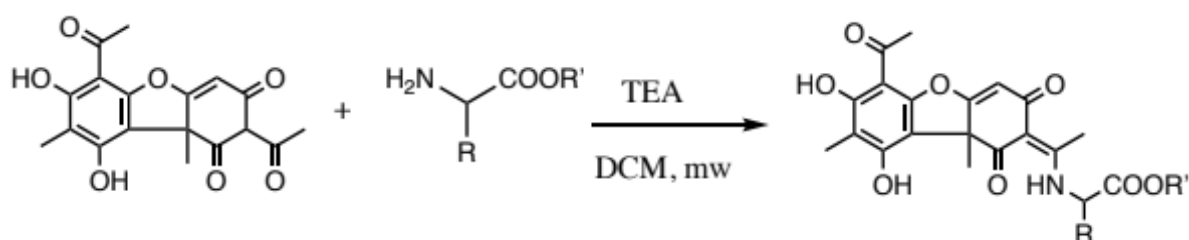
Scheme 1: Synthetic protocol for the semi-synthesis of UA derivatives.

Table 19: Obtained UA derivatives and related yields.

R		
	1A Yields: 54%	**1B** Yields: 46%
	2A Yields: 87%	**2B** Yields: 72%
	3A Yields: 45%	**3B** Yields: 80%

3.6 Future directions

Starting from the good results until now obtained, further biological investigations are ongoing. Specifically, we are evaluating the anticancer profile of *C. furcata* crude extract and the bioguided assay fractionation of *C. rangiformis* is ongoing.

Moreover, after obtaining all the semisynthetic derivatives, we are now evaluating their biocompatibility. In detail, an MTT test on Normal Human Dermal Fibroblasts (NHDF) has been performed and preliminary results demonstrate that all the compounds are biocompatible in the tested concentrations. Future steps will consist in performing the gap closure cell motility assay, based on the employment of a Petri μ-Dish[35 mm, low] (Ibidi, Giardini, Italy) as wound healing test and evaluating their antifungal activity.

4. Other projects

4.1 *Marrubium vulgare* L.

Beside the main line of research described in chapter 2 and 3, during my PhD curse I also conclude other side projects, always related to NADD and to the application of MASE.

The first project consisted in the application of DoE for optimizing the extraction procedure of *Marrubium vulgare* L. aerial parts (Appendix, paper 6). *M. vulgare* is an annual herbaceous plant belonging to Lamiaceae family, also known as white/common horehound [166]. It is an herbal remedy presents in several European Pharmacopoeias whose chemotaxonomic marker is marrubiin. The content of this metabolite may change in response to biotic and abiotic stress [167,168].

In order to evaluate changes in marrubiin content of *M. vulgare* aerial parts, the following experimental plan was drown: (i) a HPLC-UV/PAD methodology for marrubiin quantitation was set up; (ii) a proper MASE procedure was identified by applying DoE statistical approach; (iii) *M. vulgare* aerial parts grown under abiotic stress induced by increasing concentrations of $CuSO_4$ (a model agent for abiotic stress) were analyzed (Figure 31).

Thanks to the application of DoE, we were able to analyze the effect of solvent, time, temperature and their interactions on the extractive process performing few numbers of experiments.
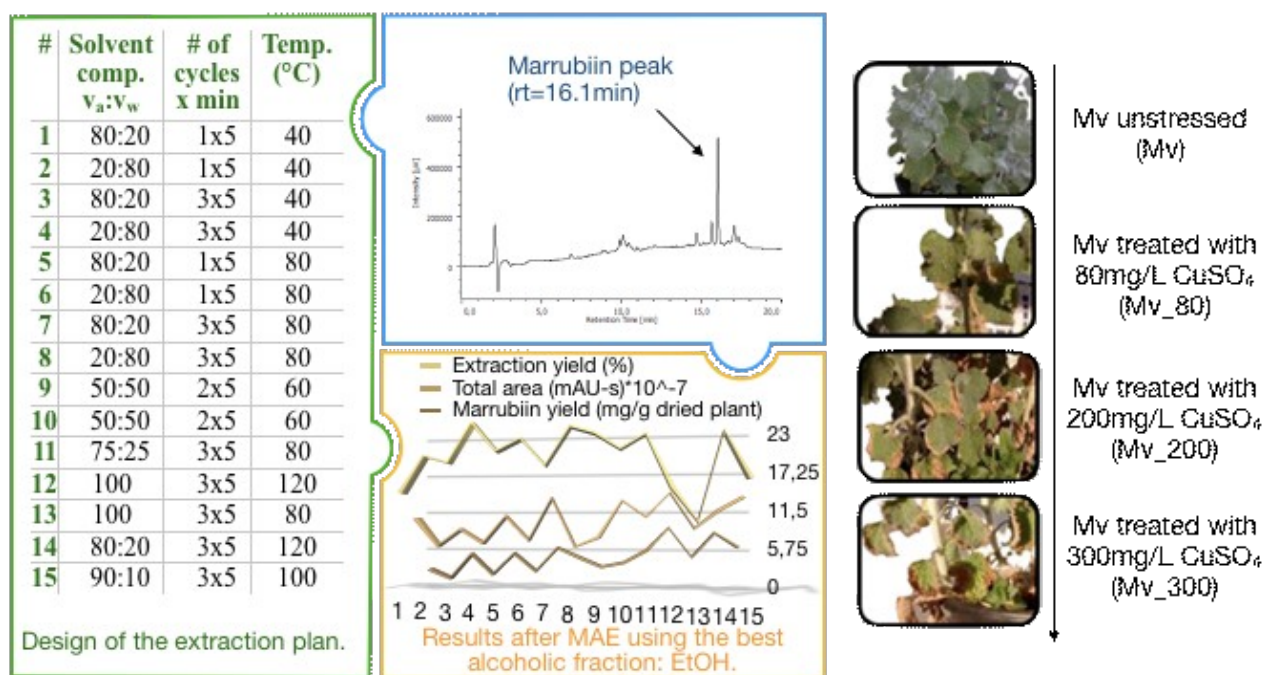

Figure 31: HPLC chromatogram (Blue), DoE plan (green) and related results (yellow) and pictures of *M. vulgare* aerial parts under different abiotic stress.

The extraction method which ensured the exhaustive extraction of marrubiin consisted in 120°C, 100% ethanol, for 15min. The developed methodology was successfully applied to matrices

grown in greenhouse conditions and under copper (II) induced stress. A decreasing production of marrubiin was evidenced in connection with treatment of $CuSO_4$.

In conclusion, an efficient methodology for the extraction and determination of marrubiin in large sets of samples of *M. vulgare* was developed, demonstrating that marrubiin is an easily detectable marker useful for evaluating the reaction to stress of the producing plant.

4.2 *Hibiscus sabdariffa* **L.**

Hibiscus sabdariffa L. is an annual herbaceous subshrub belonging to the Malvaceae family [169]. This plant is also known as roselle, red sorrel or karcadè and it has been widely studied for its biological properties.

At the beginning of this work we optimize the extraction of *Hibiscus sabdariffa* calyces in order to obtain a phytocomplex with enhanced antioxidant activity. To reach this aim we compared three different extractive methods, maceration, UASE and MASE, keeping constant the solvent (ethanol 80%). Both maceration and UASE were conducted in dark or light conditions, while MASE was performed only in dark condition, being the only status allowed by the oven. Moreover, the temperature was chosen basing on the stability of the main metabolites of *H. sabdariffa*, the anthocyanins [170]. The different extraction methodologies were then compared considering both extraction yield and the antioxidant activity. Despite the first response was comparable among the different conditions, the second one was slighted better when the extraction was performed in dark condition. At the end, MASE was selected as the most convenient method, considering that it required only 15 minutes to obtain similar or even better results obtained after 3h of maceration or more than 2h of UASE.

In this study, the optimized extract was loaded in an in situ gelling formulation developed for the treatment of oral mucositis and esophagitis. The in vitro biological tests proved that the formulation was biocompatible and did not reduced the antioxidant and anti-inflammatory properties of the extract.

Beside the development of an *H. sabdariffa* extract with enhanced antioxidant activity, we also investigate this natural matrix by evaluating its anticancer profile.

In detail, recently, we identified an *H. sabdariffa* extract active against Multiple Myeloma (MM) (Appendix, paper 8). The bioguided fractionation of the crude ethanolic extract allowed the identification of a fraction with endowed activity (HsEF). We assessed cell viability (MTT and Trypan blue test), cell migration (Boyden chamber assay), and neurotoxicity (DRG neurotoxicity assay). The promising results prompted us to further fractionate HsEF, obtaining two molecules effective against RPMI-8226 cells without neurotoxic effects at their active concentrations: *Hib-ester* and *Hib-carbaldehyde* (Figure 32). Moreover, both compounds are able to significantly reduce cell migration.
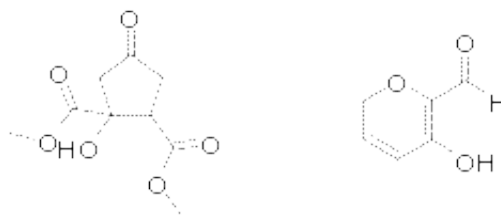
Figure 32: Structure of *Hib-ester* (left) and *Hib-carbaldehyde* (right).

Both *Hib-ester* and *Hib-carbaldehyde* resulted responsible for the cytotoxic effect, which was correlated with apoptotic process. Furthermore, we identified proteasome inhibition as the main mechanism of action. In this case, HsEf was characterized by a very high activity in inhibiting this target. This can be considered as the result of a synergistic effect among metabolites *Hib-ester*, *Hib-carbaldehyde*, and also anthocyanins. Thus, this class of secondary metabolites represented the 0.23% of HsEf and are a class of secondary metabolites endowed with an already known proteasome inhibitory activity. This more potent activity of the enriched fraction compared with the single metabolites demonstrated the potential of HsEf as diet supplement to contrast MM. Regarding the mechanism of action, we proved its inhibition effect on proteasome.

Not less important, we are confident about the safety of the proposed extract, owing to the wide use of *Hibiscus sabdariffa* infusion as beverage since ancient times.

The experimental steps regarding the *H. sabdariffa* project are resumed in Figure 33.
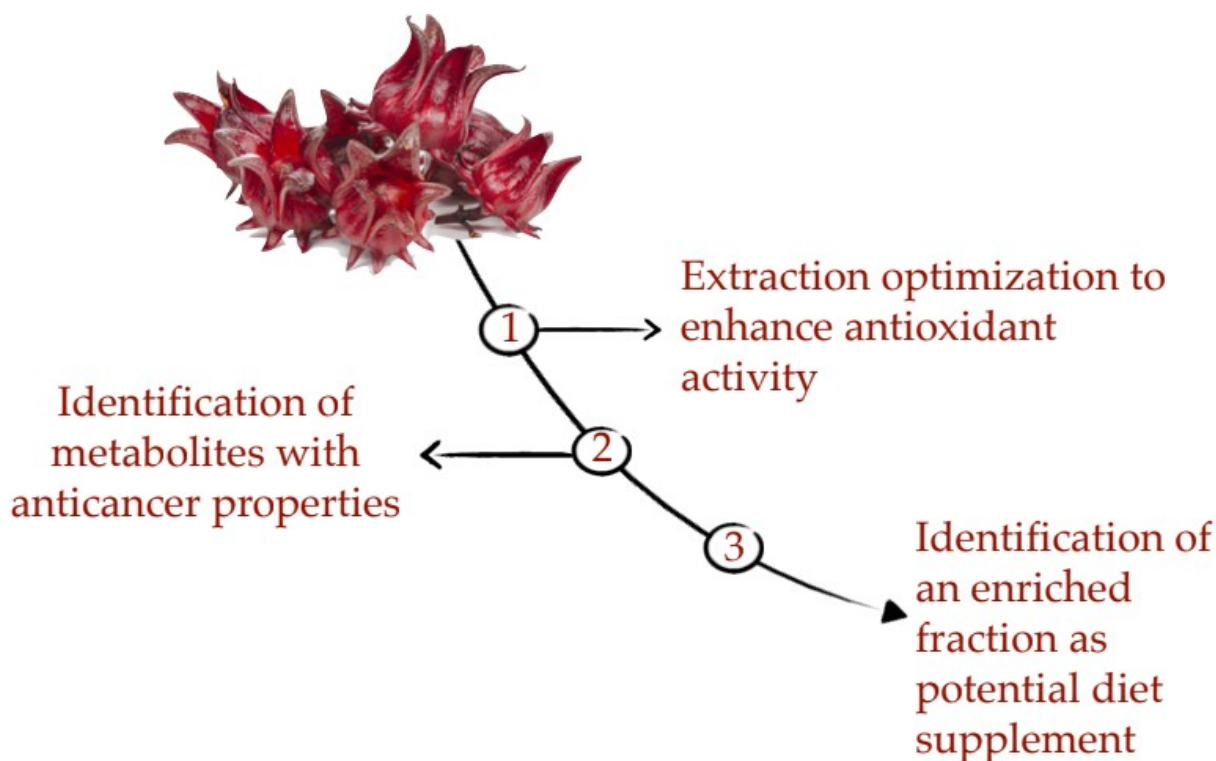
Figure 33: experimental steps regarding the *H. sabdariffa* project

5. Conclusions

The main goal of my PhD journey was the valorization of both the vascular and the lichen flora of Pavia countryside with the double aim to preserve the territory where I live and to discover new effective drugs. To reach these goals, basing on the information available so far, we studied both the vascular and lichen flora, following two different strategies.

Firstly, a database reporting all the 3D structures of the secondary metabolites produced by the plants growing in the Pavia territory was set up. So far, this database collects the 2D and 3D structures of more than 5000 compounds produced by plants growing in our territory and their producing organism are linked to Floritaly, the portal to the Italian flora. The database allows an easy download of all the data, thus simplifying the research on natural products in different fields. Moreover, the DB structure will allow an easy aggregation of data coming from other Italian flora, so it could represent an embryo for a DB reporting the secondary metabolites produced by all the plants growing in Italy.

With the database in hands, a first attempt to use it to valorize the biodiversity of our territory was performed, following an already well-founded strategy: the use pharmaceutical botany to valorize the biodiversity of a selected territory.

Thanks to the Erasmus traineeship program, I had the opportunity to spend three months at Inte:Ligand (Vienna, Austria) and to collaborate with Professor Sharon Bryant. During my stay at Inte:ligand, I focused on proteasome inhibitors, as new potential anticancer drugs. To select molecules potentially able to inhibit proteasome, a pharmacophoric model was set up and it was used for the virtual screening of all the molecules reported in the database. In this way, seven metabolites potentially able to inhibit proteasome have been identified, none of which have ever been studied so far for its ability to modulate proteasome.

To validate our model, we collected or purchased four of the selected natural matrices and obtained relative metabolites of interest. Next, a preliminary biological profile of crude extracts, enriched fractions and pure metabolites, have been drawn, performing MTT, trypan blue, and proteasome activity tests. These analyses have been performed at University Milano-Bicocca, thanks to the collaboration with Professor Guido Cavaletti.

Results confirmed that the pharmacophoric model previously set up was correct. Moreover, *V. sativa* enriched fraction and Kaempferol-3-O-α-L-arabofuranoside resulted the most effective ones, making them suitable candidates for undergoing to drug development process.

In the meantime, a study of the lichen flora of Pavia countryside was performed. Being available literature data not sufficient for the development of a DB, the valorization of this underestimated flora was performed focusing the attention on three lichens belonging to *Cladonia* genus growing in the Pavia territory: *Cladonia foliacea*, *C. furcata* and *C. rangiformis*. Particularly, extractive, analytical, and separative procedures have been developed and their main metabolites isolated and characterized, i.e. (*S*)-usnic and fumarprotocetraric acids from *C. foliacea*, atranorin and rhizomic acid from *C. furcata* and *C. rangiformis*. Crude extracts and the pure metabolites have been investigated for their potential anticancer and antifungal properties.

Results evidenced that all the extracts are able to reduce viability of multiple myeloma, breast cancer, cholangiocarcinoma and glioblastoma cell lines. Moreover, (*S*)-usnic acid and fumarprotocetraric acid impaired cell viability in a dose- and time-dependent manner, while atranorin didn't show any effect.

Regarding the assays performed on fungal strains, we found that crude extracts and isolated metabolites are able to reduce viability in *Candida albicans*, *Candida tropicalis*, *Trichophyton rubrum* and *Aspergillus niger* strains. These good results prompted us to further optimize the active metabolites and now the semi-synthesis of a small library of derivatives is ongoing. These new chemical entities could represent a new weapon against infections still considered unmet medical diseases and whose complications still causes many deaths.

In conclusion, the new database described in this thesis could represent a valuable and versatile tool suitable for speeding up the identification of biologically active metabolites able to interact with specific targets. Moreover, the lichens belonging to *Cladonia* genus herein considered resulted valuable sources of active metabolites to contrast two unmet medical needs: cancer and fungal infections.

Future directions will be represented by the online publication of the database and by a deeper evaluation of the *Cladonia* lichens potential against orphan pathologies.

Thanks to an interdisciplinary approach we were able to achieve all the planned goals and even more. Thus, we were able not only to valorize the vascular flora of Pavia, but also the lichen one. Moreover, new metabolites have been identified as potential agents against unmet medical needs. The herein reported results represent the proof-of-concept that the proposed approach is successful, and its versatility allows the application also to other flora.

6. Experimental section

6.1 Chemical and reagents

All reagents and solvents were obtained by Merck (Italy), Carlo Erba and Panreac. Unless otherwise specified, the commercially available reagents were used as received from the supplier. Reference standards of amygdalin has been purchased by Merck (Milan, Italy), (R)-Usnic acid by Carbosynth (Staad, Switzerland), while Cyanidin-3-O-arabinoside and Kaempferol-3-O-α -L-arabofuranoside from MolPort (Riga, Latvia).

6.2 Instrumentations

Solvent removal has been done with a rotary evaporator (Heidolph Laborota 4000 efficient), compounds weighed with a precision balance (Gibertini E42-B), solid dissolution with ultrasounds (Elma Transsonic T420), while centrifugation has been performed with ALC Centrifugette 4206 (ALC International Srl.) centrifuge.

Microwave assisted solvent extractions (MASE) has been performed exploiting a mono-mode oven (Discover® Lab-Mate instrument, CEM Corporate, Buckingham, UK) equipped with a power and temperature controller. The scaled up procedures were performed on a multimode microwave apparatus (MARSX press, CEM Corporation, Matthews, NC, USA).

Melting points were measured on SMP3 Stuart Scientific apparatus.

HPLC analysis were carried out on a Jasco (Tokyo, Japan) high-performance liquid chromatography ultraviolet photodiode array detection (HPLC-UV/PAD) system equipped with a Jasco AS-2055 plus autosampler, a PU-2089 plus pump and a -2010 plus multi-wavelength detector. Experimental data were acquired and interpreted with Borwin PDA and Borwin chromatograph software (Tokyo, Japan).

Optical rotation values were measured on a Jasco photoelectric polarimeter DIP 1000 using a 0.5dm cell and a sodium lamp (λ=589 nm)

Analytical thin-layer-chromatography (TLC) was carried out on silica gel pre-coated and alluminium-backed plates (Fluka Kieselgel 60 F254, Merk) and visualized by ultra-violet (UV) radiation MinUVIS, DESAGA_Sastedt-GRUPPE (λ=254 and 366 nm), ceric ammonium molibdate (IV) or permanganate stains.

Flash chromatography was performed with Silica Gel 60 (particle size 230-400 mesh, purchased from Nova Chimica).

IR spectra were recorded on a Jasco FT/IR-4100 spectrophotometer with ATR module.

Proton nuclear magnetic resonance (NMR) spectra were recorded on a Bruker Avance 400 spectrometer operating at 400.13 MHz or JEOL JNM-LA 300 at 300 MHz. Chemical shifts (δ) are reported in parts per million with the solvent reference relative to tetramethylsilane (TMS) internal standard.

6.3 Computational analysis

6.3.1 Development of the online database of secondary metabolites

The secondary metabolites produced by the different taxa growing in our territory were identified using already existing database and literature search. In detail, we exploited:

- Dr Duke's Phytochemical and Ethnobotanical Databases: this tool facilitate in-depth plant, chemical, bioactivity, and ethnobotany searches using scientific or common names. [*U.S. Department of Agriculture, Agricultural Research Service. 1992-2016. Dr. Duke's Phytochemical and Ethnobotanical Databases. Home Page, http://phytochem.nal.usda.gov/* http://dx.doi.org/10.15482/USDA.ADC/1239279]
- Free literature search: to find the secondary metabolites produced by the taxa absent from the considered database, we perform a literature search on Web of Science, that is the world's most trusted publisher-independent global citation database. [link: https://apps.webofknowledge.com/WOS_GeneralSearch_input.do?product=WOS&search_mode=GeneralSearch&SID=C4uSwuTgkJfrlPe5ph4&preferencesSaved=]

We associated the Simplified Molecular-Input Line-Entry System (SMILES), that is a line notation for describing the structure of chemical species, to each metabolite.

To obtain both the SMILES code and the belonging class for each metabolite, free online database like PubChem, ChemSpider, FooDB or Wikipedia were exploited.

Finally, thanks to ChemDraw version 16.0.1.4 (61) (Cambridge software, PerkinEmber informatics Inc.) also chemical information like IUPAC name, exact mass, molecular weight, chemical formula m/z and elemental analysis were added. Moreover, an ID number was assigned to both scientific name of the plant and metabolite produced. This makes the data sheet suitable for the online publication.

6.3.2 Virtual screening

Computational work was carried out exploiting LigandScout 4.1 Advanced software (Inte:Ligand GmbH, Vienna, Austria). In ligand-perspective a library containing 32 known inhibitors was clustered and obtained the pharmacophoric model for each cluster containing two molecules or more was generated. The best one was selected considering its Receiver Operating Characteristic (ROC) curve and its Area Under the Curve (AUC) and Enriched Factor (EF) values, and was finally simplified by omitting the most external features and three excluded volumes.

The final model is reported in Figure 34. The retrieved molecules were further analyzed via docking studies on proteasome crystal (PDB code = 4R67) through AutoDock 4.2.

of 1471 total compounds
(32 actives, 1439 decoys)

$AUC_{1;5;10;100\%}$: 1.00;1.00;1.00;0.67
$EF_{1;5;10;100\%}$: 36.1;36.1;36.1;36.1

20.0%   20.0%   40.0%   60.0%   80.0%   100.0%

1 - Specificity (% retrieved decoys)
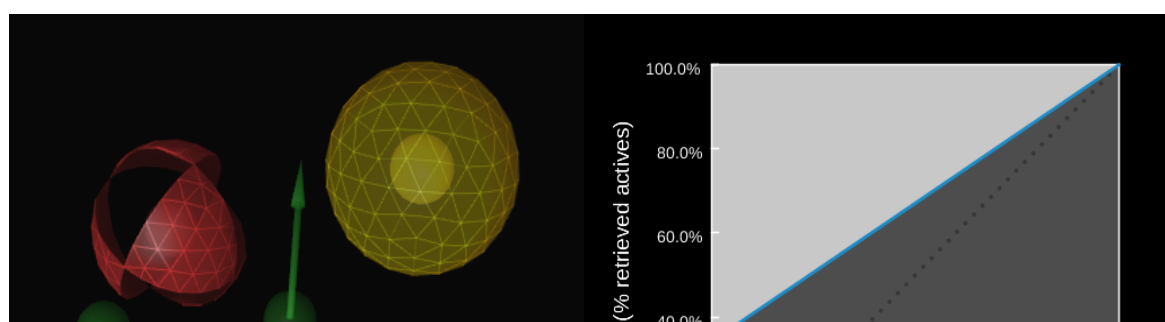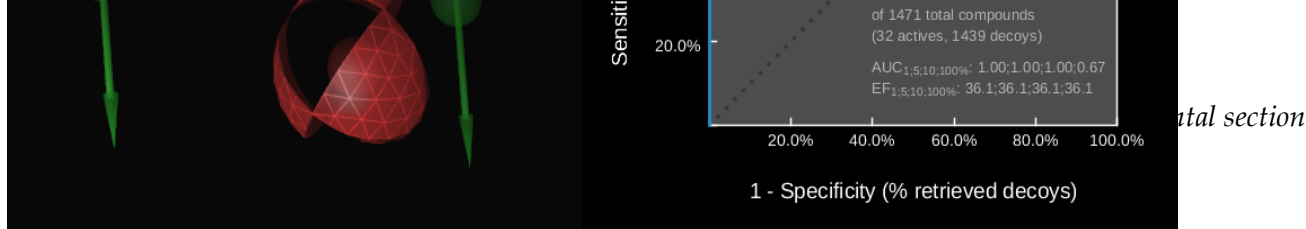
Green arrow = H bond donor
Yellow sphere = Hydrophobic interaction

Figure 34. Pharmacophoric model set up to identify potential proteasome inhibitors and its ROC curve

6.3.3 t-SNE analysis

To perform the t-SNE analysis DataWarrior software (version 5.2.1) has been exploited. In detail, the library of secondary metabolites has been uploaded and the physicochemical characteristics for each metabolites calculated. Next t-SNE analysis have been performed to group the metabolites in a three-dimensional space basing on their similitudes.

6.4 Collection of natural matrices and fractionation procedures

6.4.1 Collecting or purchasing natural matrices of interest

Vicia sativa L.: the metabolite of interest is Vicianin, produced by the seeds. These were purchased from Franchi sementi, golden line. A little aliquot was seeded to correctly verify the identity of the plant.

Prunus spinosa L.: the metabolite of interest is Juglanin, produced by the flowers. The natural matrix was collected in May 2020 in Parco del Ticino. The plants were harvested in two distinct areas near Via Milazzo (Pavia). In the first collection site (coordinates: 45,1714; 9,1693; 58,80), *Prunus spinosa* plants were younger and originated from a recent reforestation area. In the second case (coordinates: 45,170; 9,1700, 74,25) the plants were adult and were located on the banks of the Gravellone stream.

Vaccinium myrtillus L.: the metabolite of interest is Cyanidin-3-O-arabinoside, produced by the fruits. An extract rich in anthocyanins was kindly provided by Indena S.p.A., Milan, Italy.

Artemisia annua L.: the metabolite of interest is Patuletin-3-O-glucoside, produced by the aerial parts. The natural matrix was collected in August 2020 on the left bank of Ticino river at the Becca's bridge (coordinates: 45,144, 9,223, 55,90)

Cladonia foliacea, *C. rangiformis* and *C. furcata*: these lichens were collected in the locality of Bosco della Ghisolfa, Sforzesca district, Vigevano (Pavia); UTM WGS84 32T 494934.5013801; in an acidophilic arid prairie of *Thero-Airion* on siliceous sandy-pebbly substratum.

All the collected natural matrices have been cleaned, left to dry in the air until constant weight and stored in a dark conditions. A voucher speciment of each natural matrix was deposited in the herbarium of the Earth and Environmental Science Department, University of Pavia.

6.4.2 Extraction of 6-methoxykaempferol-3-O-glucoside from A. annua

After the correct identification of *A. annua*, we started the extraction of this natural matrix. At the beginning, dried aerial parts (flowers and leaves) were separated from the stem, grounded and extracted following literature data. Consistently, 10 g of powder has been macerated using a mixture of 4methanol: 1water at room temperature under magnetic stirring (2 cycles, 4h each). Next, the same natural matrix underwent to a second maceration using the same conditions but with solvents in a different ratio (1:1).

The combined extracts were concentrated under reduced pressure and simplified via liquid/liquid extraction suspending the raw extract in water, and sequentially extracting with hexane (5 cycles), diethyl ether (3 cycles), and ethyl acetate (5 cycles).

This latter organic fraction were anhydrified with Na_2SO_4, evaporated under reduced pressure and exploited to set up an HPLC-UV/PAD method suitable both for the sample analysis and for the separation in semi-preparative scale.

Analytical scale:

Samples: 1mg/ml;

Column: Cromolith RP-18e 50-4,6mm;

Mobile phase: TFA 0.05% + acetonitrile

Flow: 2ml/min;

Gradient:

Time	% H_2O + TFA	% ACN
0	95	5
2	90	10
7	70	30
8.5	95	5
11	95	5

Semi-preparative scale:

Samples: 3 mg/ml; solvent: methanol;

Column: Chromolith Semiprep RP-18 (100-10 mm);

Mobile phase: TFA 0.05% + acetonitrile

Flow: 4ml/min;

Gradient:

Time	% H_2O + TFA	% ACN
0	90	5
7	90	10
20	70	30
24	95	5
30	95	5

Once obtained a suitable amount, the MS analysis of the main metabolites isolated was performed, allowing the identification of the most intensive peak as the one representing the metabolite of interest.

After the isolation of the reference standard of 6-methoxykaempferol-3-O-glucoside in our hands, we focus our attention on the optimization of the isolation technique.

Best results have been obtained with a MASE procedure, using 80% methanolic solution, 60°C, 75min, 120 PSI, and maximum potency 200 W. After repeating the liquid/liquid extraction previously described, a flash chromatography using 5 Toluene: 3 EtOAc : 2 MeOH : 0.1 HCOOH as mobile phase was performed. Fractions containing the metabolite of interest were further chromatographed via semi-preparative HPLC obtaining pure 6-methoxykaempferol-3-O-glucoside.

The metabolite of interest was obtained as yellow powder and characterized as follows:

MS spectrum, generated in negative ion mode under constant instrumental conditions (ion spray voltage 5 kV, capillary voltage −12 V, capillary temperature 220°C, and tube lens voltage −60 V). MS/MS data were acquired in Dependent scan mode (Full-scan MS followed by MS/MS of the most intense ion) (Figure 35)
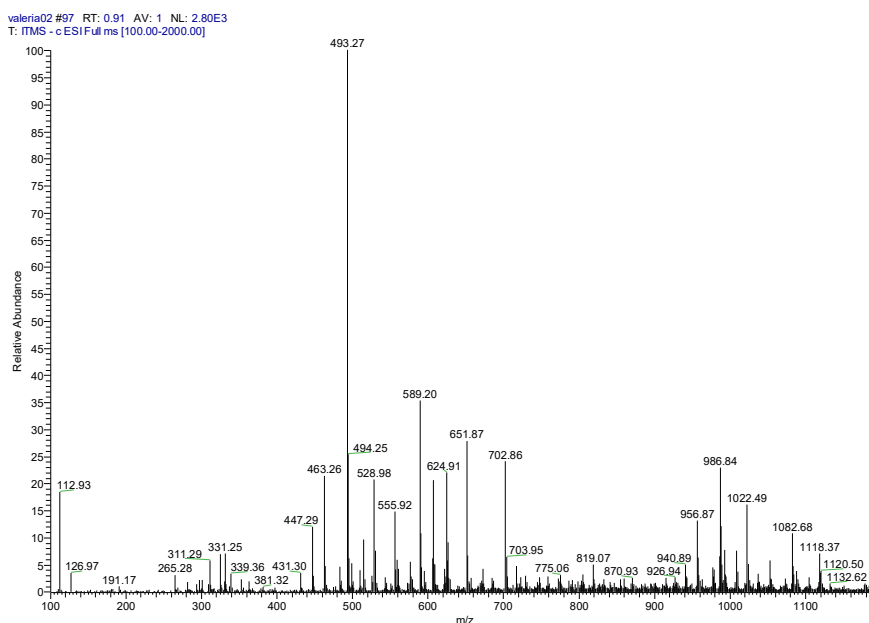
Figure 35. 6-methoxykaempferol-3-O-glucoside MS spectrum

IR spectrum, generated by a Fourier-transform infrared spectroscopy (FTIR) analysis, a Spectrum One Perkin Elmer spectrophotometer equipped with a MIRacle™ ATR device was used. The IR spectra were scanned over a wavenumber range of 4000–650 cm^{-1} with a resolution of 4 cm^{-1} (Figure 36).
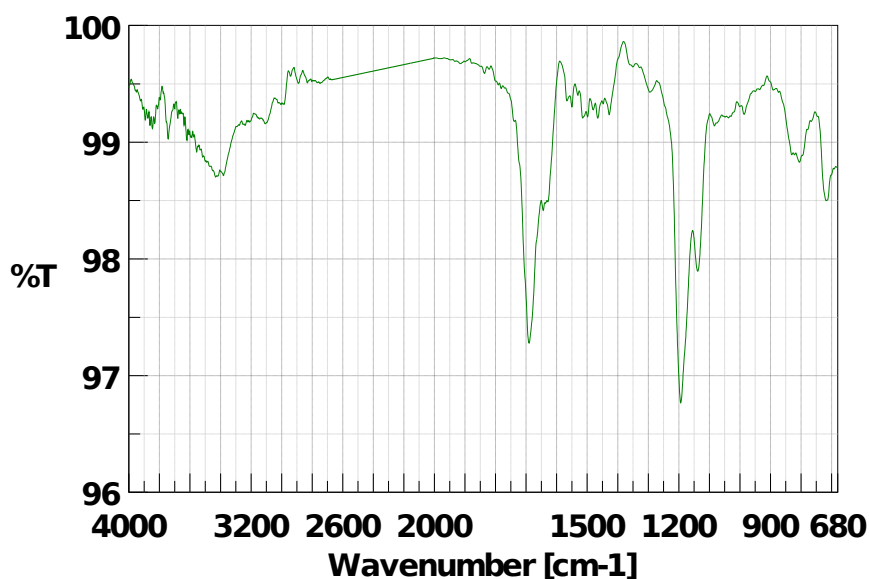
Figure 36. 6-methoxykaempferol-3-O-glucoside IR spectrum

Optical rotatory power, recorded using a Jasco photoelectric polarimeter DIP 1000. The analysis was conducted using a 0.5 dm cell, methanol as solvent (0.5% w/v) and a sodium lamp (λ = 589 nm).

$$[\alpha]_D^{24}=-5.6$$

6.4.3 Extraction of an enriched fraction of vicianin from V. sativa

10 grams of the powdered seeds have been extracted with different procedures.

Best results have been exploiting using MAE and using Ethanol, 80°C, 3 cycles of 5 minutes each, 120 PSI, and maximum potency 200 W.

The crude extract was evaporated under reduced pressure and chromatographed with 4AcOEt: 3Acetone: 1.2 Chloroform: 1 MeOH: 0.8water as mobile phase. All the fractions containing the metabolite of interest were next subjected to crystallization using 1 methanol: 1 toluene as solvent. The enriched fraction so obtained was characterized as follows:

NMR spectroscopy, the Ef was dissolved in MeOD and DMSO-D$_6$ and the ^{1}H-NMR spectra recorded. Results were compared with spectra of amygdalin recorded in the same conditions (Figure 20).

MS analysis, 7 mg of Ef were solubilized in ACN and treated with 500 μL of BSTFA overnight at room temperature. The mixture was injected in an UHPLC-MS system JASCO (Lecco, Italy) X-LC system coupled with a MS spectrometer Thermo Scientific (Milan, Italy) LTQ XL HESI-MS/MS system (linear ion trap).

Results confirmed the presence of vicianin.

Samples: 1mg/ml;

Column: RESTEK-Raptor ARC-18, 1.8 µm. 100 x 2.1 mm;

Mobile phase: HCOOH 0.2% + acetonitrile

Flow: 0.3 ml/min;

Gradient:

Time	% H$_2$O + HCOOH	% ACN
0	90	10
10	0	100
15	0	100
17	90	10
20	90	10

Mass spectrometer used an HESI (Heated Electro Spray Ionization) Probe (3.5 kV) and the spray gas was N$_2$ with a desolvation temperature of 90 °C. Gas flows were adjusted to enhance signals.

HESI Probe: Gas=N$_2$, T=90°C, Voltage=3.5kV; Capillary T=275°C, Voltage=48V, Tube Lens=70V

Tune Settings: Multipole 00 Offset = 2.5V, Lens 0 = - 4.28V, Multipole 0 Offset = -5.12V,

Lens 1 = - 8.91, Gate Lens = - 66.1V, Multipole 1 Offset = - 6.4V, Multipole RF Amplitude

(p-p)= 400V, Front Lens = - 6.0V.

Settings for MS2: Dependent-Scan detection by CID (Collision Induced Dissociation); Isolation Width: ±2 d; Activation Q: 0.250; Activation Time 30.0 msec.

Isolation width for quantitation ±2.5 d.

6.4.4 Isolation of the main metabolites of lichens of Cladonia genus

10g of each lichen has been extracted in a MARSX multimodal microwave oven, with200 mL of AcOEt. The extraction was carried out under the following experimental conditions: 400 Watts; 80 ° C; 120 PSI; ramp time 2 min; holding time: 5 minutes; 2 cycles with solvent renewal. Each extract was analyzed using and HPLC-ESI-MS:

Samples: 1 mg/ml;

Column: XBridge Phenyl 5 µm, 4,6 × 150 mm;

Mobile phase: orthophosphoric acid 0.05% + acetonitrile

Flow: 1 ml/min;

Gradient:

Time	% H$_2$O + H$_3$PO$_4$	% ACN
0	25	75
7	0	100

8	0	100
9	25	75
12	25	75

Instrument conditions were kept constant: atomization voltage of 5 kV, capillary voltage of -12 V and flight tube voltage of -60 V. MS / MS data was acquired in Dependent scan mode (Full-scan MS followed by MS / MS of the most intense ion).

**(S)-Usnic acid:** 10 g of *C. foliacea* were extracted as previously reported.

The raw extract was solubilized in the minimum amount of methanol and left at 4°C overnight. Next, the solid was centrifugated and a mixture of 1 chloroform: 2 ethanol added. Crystallization was promoted by refrigeration. The precipitate was isolated by vacuum filtration with Buchner funnel, washed with cold ethanol and dried in air. 74 mg of pure compound were isolated, with a product yield of 0.75%.

The crystals so obtained were characterized as follows:

HPLC-ESI-MS analysis, comparing the chromatographic peak (t_R = 4.79 min) with that of a standard reference sample and recording its MS specrum, whose main peak was m/z=343 in negative ion mode.

^{1}H-NMR in $CDCl_3$, δ (ppm): 18.86 (s, 1H, O**H**), 13.33 (s, 1H, O**H**), 11.05 (s, 1H, O**H**), 6.00 (s, 1H, OC**H**), 2.70 (s, 3H, COC**H₃**), 2.68 (s, 3H, COC**H₃**), 2.13 (s, 3H, CCC**H₃**), 1.78 (s, 3H, COC**H₃**).

^{13}C-NMR in $CDCl_3$, δ (ppm): 201.78 (**C**OCH₃), 200.33 (**C**OCH₃), 198.06 (**C**O), 191.72 (**C**OH), 179.38 (**C**O), 163.89 (**C**OH aromatic), 157.51 (**C**OH aromatic), 155.21 (aromatic), 109.33 (aromatic), 105.24 (**C**COCH₃), 103.96 (aromatic), 101.53 (aromatic), 98.34 (**C**H), 59.08 (**C**CH₃), 32.13 (**C**CH₃), 31.29 (CO**C**H₃), 27.90 (CO**C**H₃), 7.54 (C**C**H₃).

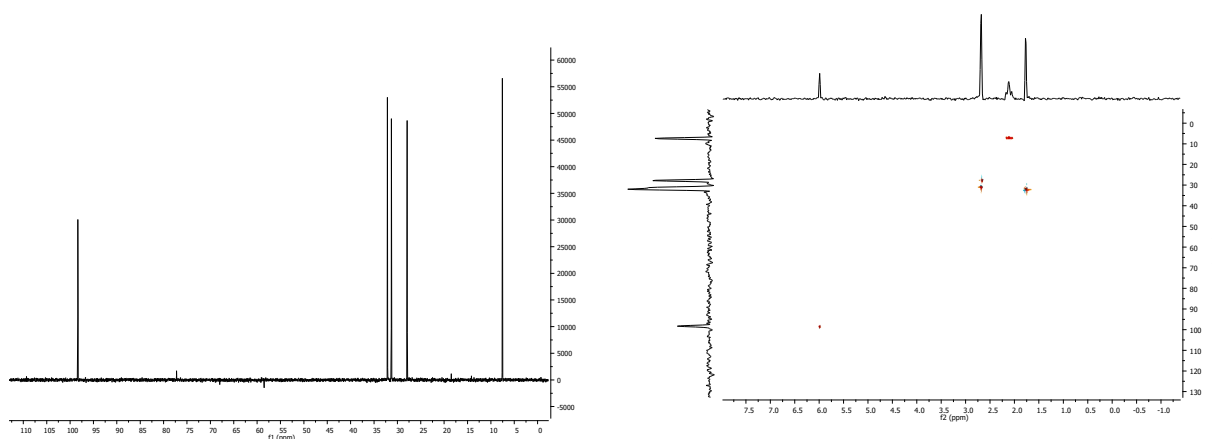**DEPT-135 and HSQC** spectra in CDCl₃ are reported in Figure 37

Figure 37: DEPT-135 (left) and HSQC (right) spectra of (S)-usnic acid

Optical rotatory power, recorded using a Jasco photoelectric polarimeter DIP 1000. The analysis was conducted using a 0.5 dm cell, chloroform as solvent (0.5% w/v) and a sodium lamp (λ = 589 nm).

$$[\alpha]_D^{24} = -472$$

Fumarprotocetraric acid: 10 g of *C. foliacea* were extracted as previously reported.

The raw extract was solubilized in the minimum amount of methanol and left at 4°C overnight. The supernatant was evaporated under reduced pressure and subjected to a L/L extraction with EtOAc. The anhydrified organic phase was evaporated under reduced pressure and subjected to a precipitation exploiting 1 chloroform: 2 EtOH. After an hour, the suspended white particles were centrifugated at 3000 rpm for 10 minutes, thus making the separation of a white powder possible. 14 mg of pure compound were isolated, with a product yield of 0.14%.

The solid so obtained were characterized as follows:

^{1}H-NMR in DMSO-d_6, δ (ppm): 10.57 (s, 1H, COH), 6.82 (s, 1H, CH), 6.62 (s, 1H, CHCH), 6.62 (s, 1H, CHCH), 5.28 (s, 2H, CH$_2$), 2.46 (s, 3H, CH$_3$), 2.42 (s, 3H, CH$_3$).

ESI/MS: Negative peak of m/z=470.8.

Atranorin: 10 g of *C. rangiformis* were extracted as previously reported.

Upon evaporation at reduced pressure of the raw extract, precipitation of a colorless solid was triggered. The suspension was left at 4°C overnight. The precipitate was isolated by vacuum filtration with Buchner funnel with sintered glass disc, washed with cold ethyl acetate and dried in air. The obtained solid was then subjected to a second precipitation in chloroform. The precipitate was separated from the supernatant by vacuum filtration with a Buchner funnel. The filtrate was dried under reduced pressure, obtaining 35 mg of a greyish powder (yield = 0.35%).

The solid so obtained were characterized as follows:

ESI/MS: negative peak of m/z=372.9.

^{1}H-NMR in $CDCl_3$, δ (ppm): 12.59 (s, 1H, OH), 12.53 (s, 1H, OH), 11.98 (s, 1H, OH), 10.40 (s, 1H, COH), 6.55 (s, 1H, CH), 6.44 (s, 1H, CH), 4.02 (s, 3H, OCH$_3$), 2.72 (s, 3H, CH$_3$), 2.58 (s, 3H, CH$_3$), 2.13 (s, 3H, CH$_3$).

HSQC in $CDCl_3$ is reported in figure 37
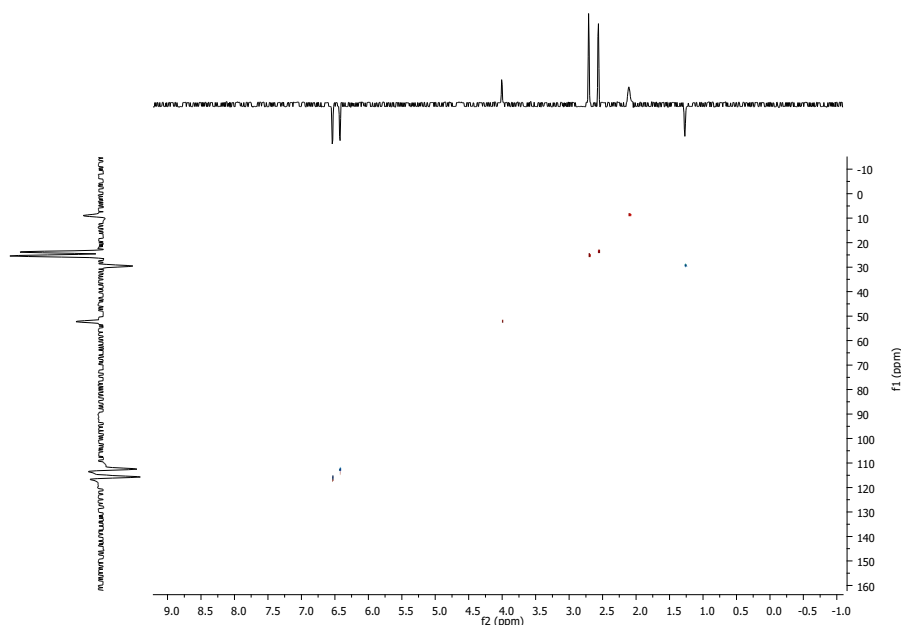
Figure 38: HSQC spectrum of atranorin

Rhizonic acid: 10 g of *C. rangiformis* were extracted with EtOH as previously reported.

The crude extract was subjected to a liquid / liquid extraction with DCM, performing six sequential extractions with 200 ml of solvent. The organic phase was subjected to anhydrification with Na_2SO_4, filtered and evaporated at reduced pressure.

The 48.6 mg so obtained were subjected to purification by flash chromatography with a gradient mobile phase:

3 diethyl ether: 7 hexane + 0.1% formic acid

5 diethyl ether: 5 hexane + 0.1% formic acid

8 diethyl ether: 2 hexane + 0.1% formic acid

9 diethyl ether: 1 hexane + 0.1% formic acid

12 mg of the A8 - A13 fraction were collected and subjected to precipitation in hexane. The precipitate was separated obtaining 6 mg of pure compound (yield = 0.06%).

The solid so obtained were characterized as follows:

ESI/MS: negative peak of m/z= 197.

¹H-NMR in $CDCl_3$, δ (ppm): 12.05 (s, 1H, **COOH**), 6.23 (s, 1H, **CH**), 5.10 (s, 1H, **COH**), 3.94 (s, 3H, **OCH₃**), 2.48 (s, 3H, **CH₃**), 2.13 (s, 3H, **CH₃**).

¹³C-NMR in $CDCl_3$, δ (ppm): 172.59 (**COOH**), 163.17 (**COH** aromatico), 157.99 (**COCH₃** aromatico), 140.16 (**CCH₃** aromatico), 110.52 (**CCH₃** aromatico), 108.47 (**CCOOH** aromatico), 105.27 (**CH** aromatico), 51.82 (**OCH₃**), 24.09 (**CH₃**), 7.64 (**CH₃**).

HSQC in $CDCl_3$ is reported in Figure 39
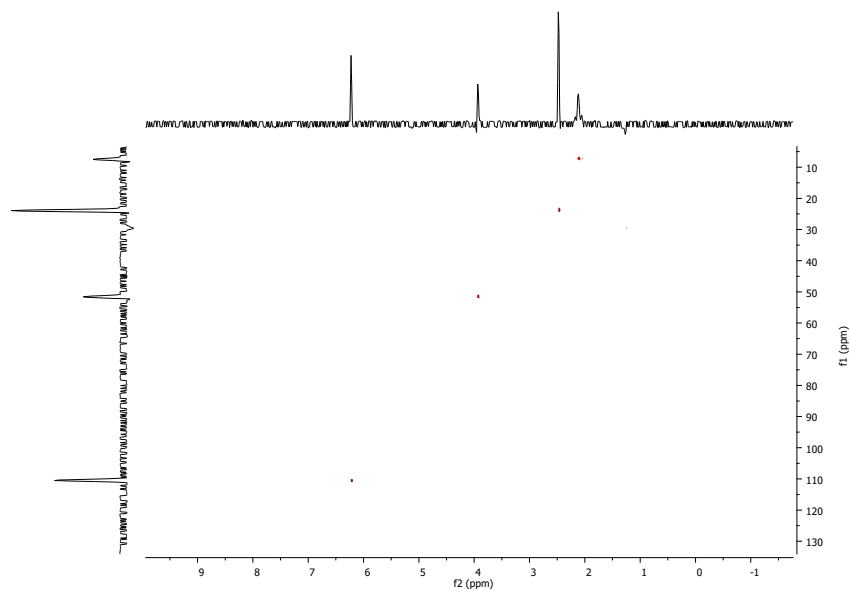
Figure 39: HSQC spectrum of rhizomic acid

6.5 Semisynthetic procedure

A mixture of UA (1 eq.), amino acid (1.5 eq.), and triethyl amine (2 eq.), in EtOH (5 mL) was irradiated with a microwave power of 60 watts at 90 °C for 2 cycled of 5 min each under magnetic stirring. The reaction workup was performed as follows: the mixture was evaporated under reduced pressure, then the solid was dissolved in water, washed with hexane (3 cycles) and extracted with dichloromethane (3 cycles). Then the organic phase was evaporated to dryness.

1A: ^{1}H NMR 400 MHz (CDCl$_3$) 1.64 (s, 3H, CH$_3$-13), 2.03 (s, 3H, CH$_3$-16), 2.65 (s, 3H, CH$_3$-15), 2.68 (s, 3H, CH$_3$-18), 3.52 (q, J = 6.7 Hz, 1H, CH-2′), 3.90 (s, 3H, CH$_3$-1′), 4.17 (m, 2H, CH$_2$-3′), 5.62 (s, 1H, CH-4), 11.50 (br s, 1H, OH), 13.32 (s, 1H, OH), 13.80 (br s, 1H, NH).
$$[\alpha]_D^{24}=¿ = +28 \text{ (c= 0.5\%, DCM)}.$$

1B: ^{1}H NMR 400 MHz (CDCl$_3$) 1.73 (s, 3H, CH$_3$-13), 2.12 (s, 3H, CH$_3$-16), 2.64 (s, 3H, CH$_3$-15), 2.68 (s, 3H, CH$_3$-18), 3.52 (q, J = 6.7 Hz, 1H, CH-2′), 3.88 (s, 3H, CH$_3$-1′), 4.17 (m, 2H, CH$_2$-3′), 5.84 (s, 1H, CH-4), 11.50 (br s, 1H, OH), 13.32 (s, 1H, OH), 13.80 (br s, 1H, NH).
$$[\alpha]_D^{24}=¿ = -47 \text{ (c= 0.5\%, DCM)}.$$

2A: ^{1}H NMR 400 MHz (CDCl$_3$) 1.69 (s, 3H, CH$_3$-13), 2.10 (s, 3H, CH$_3$-16), 2.32 (s, 3H, CH$_3$-15), 2.68 (s, 3H, CH$_3$-18), 3.05 (dd, J = 7.2 Hz, 14 Hz, 1H, CH$_2$-3′), 3.50 (dd, J = 4.8 Hz, 14 Hz, 1H, CH$_2$-3′), 4.51 (m, 1H, CH-2′), 5.78 (s, 1H, CH- 4), 6.70 (d, J = 8.4 Hz, 2H, CH-5′, CH-9′), 7.02 (d, J = 8.4 Hz, 2H, CH-6′, CH-8′), 12.19 (s, 1H, OH), 13.37 (br s, 2H, OH, NH).

$$[\alpha]_D^{24}=¿ = + 70 \ (c= 0.5\%, \ DCM).$$

2B: ^{1}H NMR 400 MHz (CDCl$_3$) 1.62 (s, 3H, CH$_3$-13), 2.02 (s, 3H, CH$_3$-16), 2.24 (s, 3H, CH$_3$-15), 2.60 (s, 3H, CH$_3$-18), 2.96 (dd, J = 7.2 Hz, 14 Hz, 1H, CH$_2$-3'), 3.22 (dd, J = 4.8 Hz, 14 Hz, 1H, CH$_2$-3'), 4.37 (m, 1H, CH-2'), 5.69 (s, 1H, CH- 4), 6.64 (d, J = 8.4 Hz, 2H, CH-5', CH-9'), 7.01 (d, J = 8.4 Hz, 2H, CH-6', CH-8'), 12.11 (s, 1H, OH), 13.30 (br s, 2H, OH, NH).

$$[\alpha]_D^{24}=¿ = - 73 \ (c= 0.5\%, \ DCM).$$

3A: ^{1}H NMR 400 MHz (CDCl$_3$) 1.69 (s, 3H, CH$_3$-13), 2.10 (s, 3H, CH$_3$-16), 2.20 (s, 3H, CH$_3$-15), 2.68 (s, 3H, CH$_3$-18), 3.09 (dd, J = 7.2 Hz, 14 Hz, 1H, CH$_2$-3'), 3.42 (dd, J = 4.8 Hz, 14 Hz, 1H, CH$_2$-3'), 4.57 (m, 1H, CH-2'), 5.78 (s, 1H, CH- 4), 7.23 (m, 5H, aromatic), 12.17 (s, 1H, OH), 13.37 (br s, 2H, OH, NH).

$$[\alpha]_D^{24}=¿ = + 40 \ (c= 0.5\%, \ DCM).$$

3B: ^{1}H NMR 400 MHz (CDCl$_3$) 1.61 (s, 3H, CH$_3$-13), 2.01 (s, 3H, CH$_3$-16), 2.10 (s, 3H, CH$_3$-15), 2.60 (s, 3H, CH$_3$-18), 2.96 (dd, J = 7.2 Hz, 14 Hz, 1H, CH$_2$-3'), 3.22 (dd, J = 4.8 Hz, 14 Hz, 1H, CH$_2$-3'), 4.44 (m, 1H, CH-2'), 5.69 (s, 1H, CH- 4), 7.18 (m, 5H, aromatic), 12.07 (s, 1H, OH), 13.31 (br s, 2H, OH, NH).

$$[\alpha]_D^{24}=¿ = - 147 \ (c= 0.5\%, \ DCM).$$

6.6 Biological investigations

6.6.1 Cell cultures

MM RPMI 8226 cells (ATTC, USA) were cultured in Iscove's Modified Dulbecco's Medium (IMDM) medium (Invitrogen, Carlsbad, CA) with 20% FBS, 1% L-glutamine, and 1% Penicillin and Streptomycin. Human glioblastoma U87-MG (kindly provided by Dr D. Ballinari, Nerviano Medical Sciences, Nerviano, Italy) cells were cultured in high glucose DMEM (Euroclone, Pero, Italy) supplemented with 10% FBS and 1% Penicillin and Streptomycin. Human breast cancer MCF7 cells and human cholangiocarcinomaEGI-1 cells were cultured in RPMI 1640 medium with 10% FBS, 1% L-glutamine, and 1% Penicillin and Streptomycin.

Cells were incubated at 37°C and 5% CO$_2$ in a humidified incubator.

6.6.2 MTT assays

RPMI 8226 (MM), MCF7 (breast cancer), EGI-1 (cholangiocarcinoma), and U87-MG (glioblastoma) cells were seeded in 96-well plates at 10,000 cells/well density and were treated

with different concentrations of the extracts or pure compounds for 24, 48, and 72h at 37°C. Culture medium was then replaced with a 3-(4,5-dimethylthiazol-2-ys)-2,5-diphenyltetrazolium bromide (MTT) (Sigma-Aldrich, St Louis, MO) 0.5 mg/mL medium solution. After 2h of incubation at 37°C, formazan crystals were solubilized in 100% EtOH and absorbance was read at 560nm in a microplate reader (Biorad, Hercules, CA). Survival cells were calculated normalizing the data to absorbance of non-treated cells.

6.6.3 Trypan blue vital staining

Cells were cultured in 60-mm diameter dish at initial density of 200,000 cells/dish. After 24 h and 48 h of different treatments, RPMI 8226, MCF7, EGI-1, and U87-MG adherent and floating cells were harvested after trypsinization and stained with Trypan blue vital dye. RPMI 8226 cells were harvested and stained with Trypan blue vital dye. Viable and death cells were counted in a Burker hemocytometer under a light microscope (Nikon Eclipse TS100).

6.6.4 Proteasome activity test

Proteasome activity was assessed by N-Succinyl-Leu-Leu-Val-Tyr-7-Amido-4-Methylcoumarin fluorogenic substrate for chymotrypsin-like enzymes (Sigma-Aldrich, S.Louis, MO). In the presence of proteasome, the fluorophore, 7-Amido-4-Methylcoumarin, is released and emits fluorescence. The fluorescence obtained is a measure of proteasome activity.

Cell lysate was obtained and quantified as described in Western blot paragraph, but lysis buffer was prepared without proteases and phosphatases inhibitors (Phenylmethylsulphonyl fluoride, Aprotinine, Sodium pyrophosphate, Sodium orthovanadate). Cell lysate containing 40µg of proteins were loaded in dark 96-well plate. Water, 10µl of 10X proteasome buffer and 10µl of proteasome substrate (N-Succinyl-Leu-Leu-Val-Tyr-7-Amido-4-Methylcoumarin) were added to protein solution. Plate were then incubated at 37°C and after 2h fluorescence was measured in a microplate reader (Biorad, Hercules, CA).

6.6.4 Funghi

The fungal strains used were *Candida albicans*, *Candida tropicalis*, *Trichophyton rubrum*, and *Aspergillus niger*.

Fungal strain was collected from Petri dish (diameter 5 cm), and resuspended in sterile tubes containing 10 mL of Sabouraud medium (SAB) and broken coverslips. The tubes were shaken by vortex for 5 minutes to obtain a homogeneous fungal suspension. All subsequent tests will be performed using the obtained suspension 1×10^6 conidia/mL.

To obtain the minimum inhibitory concentration (MIC) multiplate 96-well plates were made as follow:

- 100 μL of fungal suspension was added in each well
- 100 μL of phytocomplex or pure metabolites were added in the first line of well to test the efficacy of product at 50%
- From 200 μL obtained in the first line, after resuspension 100 μL was transferred to line second (product concentration = 25%). With the same method all wells were filled up to a product concentration of 0.001%. Three replicates of each concentration were performed.
- The plates were incubated at 25°C for 7 days and then fungal growth was observed.

7. References

1. Tu, Y. The discovery of artemisinin (qinghaosu) and gifts from Chinese medicine. *Nat. Med.* **2011**, *17*, 1217–1220.

2. Lee, S.-H.; Kim, J.-H. Kinetic and thermodynamic characteristics of microwave-assisted extraction for the recovery of paclitaxel from Taxus chinensis. *Process Biochem.* **2019**, *76*, 187–193.

3. Cai, C.; Wu, Q.; Hong, H.; He, L.; Liu, Z.; Gu, Y.; Zhang, S.; Wang, Q.; Fan, X.; Fang, J. In silico identification of natural products from Traditional Chinese Medicine for cancer immunotherapy. *Sci. Rep.* **2021**, *11*, 3332.

4. Zanvo, S.; Djagoun, C.A.M.S.; Azihou, A.F.; Sinsin, B.; Gaubert, P. Preservative chemicals as a new health risk related to traditional medicine markets in western Africa. *One Heal.* **2021**, *13*, 100268.

5. Mwitari, P.G.; Ayeka, P.A.; Ondicho, J.; Matu, E.N.; Bii, C.C. Antimicrobial Activity and Probable Mechanisms of Action of Medicinal Plants of Kenya: Withania somnifera, Warbugia ugandensis, Prunus africana and Plectrunthus barbatus. *PLoS One* **2013**, *8*, e65619.

6. Mutola, S.; Pemunta, N.V.; Ngo, N.V. Utilization of traditional medicine and its integration into the healthcare system in Qokolweni, South Africa; prospects for enhanced universal health coverage. *Complement. Ther. Clin. Pract.* **2021**, *43*, 101386.

7. Amirkia, V.; Heinrich, M. Natural products and drug discovery: a survey of stakeholders in industry and academia. *Front. Pharmacol.* **2015**, *6*.

8. MLA Facts. NobelPrize.org. Nobel Prize Outreach AB 2021.

9. Maiga, F.O.; Wele, M.; Toure, S.M.; Keita, M.; Tangara, C.O.; Refeld, R.R.; Thiero, O.; Kayentao, K.; Diakite, M.; Dara, A.; et al. Artemisinin-based combination therapy for uncomplicated Plasmodium falciparum malaria in Mali: a systematic review and meta-analysis. *Malar. J.* **2021**, *20*, 356.

10. Xiong, Y.; Huang, J. Anti-malarial drug: the emerging role of artemisinin and its derivatives in liver disease treatment. *Chin. Med.* **2021**, *16*, 80.

11. Zhang, M.; Wang, C.; Oberstaller, J.; Thomas, P.; Otto, T.D.; Casandra, D.; Boyapalle, S.; Adapa, S.R.; Xu, S.; Button-Simons, K.; et al. The apicoplast link to fever-survival and artemisinin-resistance in the malaria parasite. *Nat. Commun.* **2021**, *12*, 4563.

12. Lahlou, M. The Success of Natural Products in Drug Discovery. *Pharmacol. & Pharm.* **2013**, *04*, 17–31.

13. Henrich, C.J.; Beutler, J.A. Matching the power of high throughput screening to the chemical diversity of natural products. *Nat. Prod. Rep.* **2013**, *30*, 1284.

14. Kastenholz, B. Phytochemical Approach and Bioanalytical Strategy to Develop Chaperone-Based Medications. *Open Biochem. J.* **2008**, *2*, 44–48.

15. Larsen, T.O.; Smedsgaard, J.; Nielsen, K.F.; Hansen, M.E.; Frisvad, J.C. Phenotypic taxonomy and metabolite profiling in microbial drug discovery. *Nat. Prod. Rep.* **2005**, *22*, 672.

16. Wang, Y. Needs for new plant-derived pharmaceuticals in the post-genome era: an industrial view in drug research and development. *Phytochem. Rev.* **2008**, *7*, 395–406.

17. Sahli, R.; Rivière, C.; Neut, C.; Bero, J.; Sahuc, M.-E.; Smaoui, A.; Beaufay, C.; Roumy, V.; Hennebelle, T.; Rouillé, Y.; et al. An ecological approach to discover new bioactive extracts and products: the case of extremophile plants. *J. Pharm. Pharmacol.* **2017**, *69*, 1041–1055.

18. Gyllenhaal, C.; Kadushin, M.R.; Southavong, B.; Sydara, K.; Bouamanivong, S.; Xaiveu, M.; Xuan, L.T.; Hiep, N.T.; Hung, N.V.; Loc, P.K.; et al. Ethnobotanical approach versus random approach in the search for new bioactive compounds: Support of a hypothesis. *Pharm. Biol.* **2012**, *50*, 30–41.

19. Thomford, N.; Senthebane, D.; Rowe, A.; Munro, D.; Seele, P.; Maroyi, A.; Dzobo, K. Natural Products for Drug Discovery in the 21st Century: Innovations for Novel Drug Discovery. *Int. J. Mol. Sci.* **2018**, *19*, 1578.

20. Hert, J.; Irwin, J.J.; Laggner, C.; Keiser, M.J.; Shoichet, B.K. Quantifying Biogenic Bias in Screening Libraries. *Nat. Chem. Biol.* **2009**, *5*, 479–483.

21. Takagi, M.; Shin-ya, K. Construction of a natural product library containing secondary metabolites produced by actinomycetes. *J. Antibiot. (Tokyo).* **2012**, *65*, 443–447.

22. Wani, M.C.; Horwitz, S.B. Nature as a remarkable chemist. *Anticancer. Drugs* **2014**, *25*, 482–487.

23. Cao, S.; Kingston, D.G.I. Biodiversity conservation and drug discovery: Can they be combined? The Suriname and Madagascar experiences. *Pharm. Biol.* **2009**, *47*, 809–823.

24. Chen, Y.; Kirchmair, J. Cheminformatics in Natural Product-based Drug Discovery. *Mol. Inform.* **2020**, *39*, 2000171.

25. Sterling, T.; Irwin, J.J. ZINC 15 – Ligand Discovery for Everyone. *J. Chem. Inf. Model.* **2015**, *55*, 2324–2337.

26. Yang, Y.; Guo, Y.; Zhou, Y.; Gao, Y.; Wang, X.; Wang, J.; Niu, X. Discovery of a Novel Natural Allosteric Inhibitor That Targets NDM-1 Against Escherichia coli. *Front. Pharmacol.* **2020**, *11*.

27. Sorokina, M.; Steinbeck, C. Review on natural products databases: where to find data in 2020. *J. Cheminform.* **2020**, *12*, 20.

28. Padhi, S.; Masi, M.; Chourasia, R.; Rajashekar, Y.; Rai, A.K.; Evidente, A. ADMET profile and virtual screening of plant and microbial natural metabolites as SARS-CoV-2 S1 glycoprotein receptor binding domain and main protease inhibitors. *Eur. J. Pharmacol.* **2021**, *890*, 173648.

29. A., Mittermeier, R.A.; Gil, P.R.; Hoffman, M.; Pilgrim, J.; Brooks, T.; Mittermeier, C.G.; Lamoreux, J.; da Fonseca, G.A.B. *Hotspots Revisited*; The University of Chicago Press, Ed.; 2005; ISBN 9789686397772.

30. IUCN Red List of Threatened Species Available online: https://www.iucn.org/resources/conservation-tools/iucn-red-list-threatened-species.

31. Sorokina, M.; Steinbeck, C. COCONUT: the COlleCtion of Open NatUral producTs. (Version 4). *Zenodo* **2020**.

32. Atanasov, A.G.; Zotchev, S.B.; Dirsch, V.M.; Supuran, C.T. Natural products in drug discovery: advances and opportunities. *Nat. Rev. Drug Discov.* **2021**, *20*, 200–216.

33. Waltenberger, B.; Mocan, A.; Šmejkal, K.; Heiss, E.; Atanasov, A. Natural Products to Counteract the Epidemic of Cardiovascular and Metabolic Disorders. *Molecules* **2016**, *21*, 807.

34. Atanasov, A.G.; Waltenberger, B.; Pferschy-Wenzig, E.-M.; Linder, T.; Wawrosch, C.; Uhrin, P.; Temml, V.; Wang, L.; Schwaiger, S.; Heiss, E.H.; et al. Discovery and resupply of pharmacologically active plant-derived natural products: A review. *Biotechnol. Adv.* **2015**, *33*, 1582–1614.

35. Keshavarz-Fathi, M.; Rezaei, N. Cancer Immunoprevention: Current Status and Future Directions. *Arch. Immunol. Ther. Exp. (Warsz).* **2021**, *69*, 3.

36. Ferlay, J.; Colombet, M.; Soerjomataram, I.; Mathers, C.; Parkin, D.M.; Piñeros, M.; Znaor, A.; Bray, F. Estimating the global cancer incidence and mortality in 2018: GLOBOCAN sources and methods. *Int. J. Cancer* **2019**, *144*, 1941–1953.

37. Bray F, C.M.; J, F.; Al, E. Cancer incidence in five continents, Vol XI.

38. Sarker, S.D.; Nahar, L.; Miron, A.; Guo, M. Anticancer natural products. In; 2020; pp. 45–75.

39. Mann, J. Natural products in cancer chemotherapy: past, present and future. *Nat. Rev.*

Cancer **2002**, *2*, 143–148.

40. Jeon, Y.-J.; Kim, S.; Kim, J.H.; Youn, U.J.; Suh, S.-S. The Comprehensive Roles of ATRANORIN, A Secondary Metabolite from the Antarctic Lichen Stereocaulon caespitosum, in HCC Tumorigenesis. *Molecules* **2019**, *24*, 1414.

41. Pereira, R.B.; Evdokimov, N.M.; Lefranc, F.; Valentão, P.; Kornienko, A.; Pereira, D.M.; Andrade, P.B.; Gomes, N.G.M. Marine-Derived Anticancer Agents: Clinical Benefits, Innovative Mechanisms, and New Targets. *Mar. Drugs* **2019**, *17*, 329.

42. Menger, L.; Vacchelli, E.; Adjemian, S.; Martins, I.; Ma, Y.; Shen, S.; Yamazaki, T.; Sukkurwala, A.Q.; Michaud, M.; Mignot, G.; et al. Cardiac Glycosides Exert Anticancer Effects by Inducing Immunogenic Cell Death. *Sci. Transl. Med.* **2012**, *4*, 143ra99-143ra99.

43. Newman, D.J.; Cragg, G.M. Natural Products as Sources of New Drugs over the Nearly Four Decades from 01/1981 to 09/2019. *J. Nat. Prod.* **2020**, *83*, 770–803.

44. Rosen, R.H.; Gupta, A.K.; Tyring, S.K. Dual mechanism of action of ingenol mebutate gel for topical treatment of actinic keratoses: Rapid lesion necrosis followed by lesion-specific immune response. *J. Am. Acad. Dermatol.* **2012**, *66*, 486–493.

45. Lü, S.; Wang, J. Homoharringtonine and omacetaxine for myeloid hematological malignancies. *J. Hematol. Oncol.* **2014**, *7*, 2.

46. Alves, A.L. V.; Gomes, I.N.F.; Carloni, A.C.; Rosa, M.N.; da Silva, L.S.; Evangelista, A.F.; Reis, R.M.; Silva, V.A.O. Role of glioblastoma stem cells in cancer therapeutic resistance: a perspective on antineoplastic agents from natural sources and chemical derivatives. *Stem Cell Res. Ther.* **2021**, *12*, 206.

47. Goldberg, A.L. Protein degradation and protection against misfolded or damaged proteins. *Nature* **2003**, *426*, 895–899.

48. Massaly, N.; FrancÃ¨s, B.; MoulÃ©dous, L. Roles of the ubiquitin proteasome system in the effects of drugs of abuse. *Front. Mol. Neurosci.* **2015**, *7*.

49. Budenholzer, L.; Cheng, C.L.; Li, Y.; Hochstrasser, M. Proteasome Structure and Assembly. *J. Mol. Biol.* **2017**, *429*, 3500–3524.

50. Harshbarger, W.; Miller, C.; Diedrich, C.; Sacchettini, J. Crystal Structure of the Human 20S Proteasome in Complex with Carfilzomib. *Structure* **2015**, *23*, 418–424.

51. Saeki, Y. Ubiquitin recognition by the proteasome. *J. Biochem.* **2017**, mvw091.

52. Tomko, R.J.; Hochstrasser, M. Molecular Architecture and Assembly of the Eukaryotic Proteasome. *Annu. Rev. Biochem.* **2013**, *82*, 415–445.

53. Kunjappu, M.J.; Hochstrasser, M. Assembly of the 20S proteasome. *Biochim. Biophys. Acta - Mol. Cell Res.* **2014**, *1843*, 2–12.

54. Isono, E.; Nishihara, K.; Saeki, Y.; Yashiroda, H.; Kamata, N.; Ge, L.; Ueda, T.; Kikuchi, Y.; Tanaka, K.; Nakano, A.; et al. The Assembly Pathway of the 19S Regulatory Particle of the Yeast 26S Proteasome. *Mol. Biol. Cell* **2007**, *18*, 569–580.

55. Manasanch, E.E.; Orlowski, R.Z. Proteasome inhibitors in cancer therapy. *Nat. Rev. Clin. Oncol.* **2017**, *14*, 417–433.

56. Crawford, L.J.; Walker, B.; Irvine, A.E. Proteasome inhibitors in cancer therapy. *J. Cell Commun. Signal.* **2011**, *5*, 101–110.

57. Okazuka, K.; Ishida, T. Proteasome inhibitors for multiple myeloma. *Jpn. J. Clin. Oncol.* **2018**, *48*, 785–793.

58. Gay, F.; Palumbo, A. Multiple myeloma: management of adverse events. *Med. Oncol.* **2010**, *27*, 646–653.

59. Hameed, A.; Brady, J.J.; Dowling, P.; Clynes, M.; O'Gorman, P. Bone Disease in Multiple Myeloma: Pathophysiology and Management. *Cancer Growth Metastasis* **2014**, *7*,

CGM.S16817.

60. Visconti, R.J.; Kolaja, K.; Cottrell, J.A. A functional three-dimensional microphysiological human model of myeloma bone disease. *J. Bone Miner. Res.* **2021**, jbmr.4404.

61. Mukkamalla, S.K.R.; Malipeddi, D. Myeloma Bone Disease: A Comprehensive Review. *Int. J. Mol. Sci.* **2021**, *22*, 6208.

62. Crawford, L.J.A.; Walker, B.; Ovaa, H.; Chauhan, D.; Anderson, K.C.; Morris, T.C.M.; Irvine, A.E. Comparative Selectivity and Specificity of the Proteasome Inhibitors BzLLLCOCHO, PS-341, and MG-132. *Cancer Res.* **2006**, *66*, 6379–6386.

63. Khan, S.A.; Cohen, A.D. Experimental approaches in the treatment of multiple myeloma. *Ther. Adv. Hematol.* **2011**, *2*, 213–230.

64. Moreau, P.; Rajkumar, S.V. Multiple myeloma—translation of trial results into reality. *Lancet* **2016**, *388*, 111–113.

65. Chen, W.-J.; Lin, J.-K. Induction of G1 Arrest and Apoptosis in Human Jurkat T Cells by Pentagalloylglucose through Inhibiting Proteasome Activity and Elevating p27Kip1, p21Cip1/WAF1, and Bax Proteins. *J. Biol. Chem.* **2004**, *279*, 13496–13505.

66. Gulder, T.A.M.; Moore, B.S. Salinosporamide Natural Products: Potent 20 S Proteasome Inhibitors as Promising Cancer Chemotherapeutics. *Angew. Chemie Int. Ed.* **2010**, *49*, 9346–9367.

67. Di, K.; Lloyd, G.K.; Abraham, V.; MacLaren, A.; Burrows, F.J.; Desjardins, A.; Trikha, M.; Bota, D.A. Marizomib activity as a single agent in malignant gliomas: ability to cross the blood-brain barrier. *Neuro. Oncol.* **2016**, *18*, 840–848.

68. Pettinari, A.; Amici, M.; Cuccioloni, M.; Angeletti, M.; Fioretti, E.; Eleuteri, A.M. Effect of Polyphenolic Compounds on the Proteolytic Activities of Constitutive and Immuno-Proteasomes. *Antioxid. Redox Signal.* **2006**, *8*, 121–129.

69. Marienfeld, C. Inhibition of cholangiocarcinoma growth by Tannic acid. *Hepatology* **2003**, *37*, 1097–1104.

70. Guedes, R.; Serra, P.; Salvador, J.; Guedes, R. Computational Approaches for the Discovery of Human Proteasome Inhibitors: An Overview. *Molecules* **2016**, *21*, 927.

71. Lei, M.; Zhao, X.; Wang, Z.; Zhu, Y. Pharmacophore Modeling, Docking Studies, and Synthesis of Novel Dipeptide Proteasome Inhibitors Containing Boron Atoms. *J. Chem. Inf. Model.* **2009**, *49*, 2092–2100.

72. Li, A.; Sun, H.; Du, L.; Wu, X.; Cao, J.; You, Q.; Li, Y. Discovery of novel covalent proteasome inhibitors through a combination of pharmacophore screening, covalent docking, and molecular dynamics simulations. *J. Mol. Model.* **2014**, *20*, 2515.

73. Borges, A.; José, H.; Homem, V.; Simões, M. Comparison of Techniques and Solvents on the Antimicrobial and Antioxidant Potential of Extracts from Acacia dealbata and Olea europaea. *Antibiotics* **2020**, *9*, 48.

74. Zhang, Q.-W.; Lin, L.-G.; Ye, W.-C. Techniques for extraction and isolation of natural products: a comprehensive review. *Chin. Med.* **2018**, *13*, 20.

75. Li, Y.; Fabiano-Tixier, A.S.; Vian, M.A.; Chemat, F. Solvent-free microwave extraction of bioactive compounds provides a tool for green analytical chemistry. *TrAC Trends Anal. Chem.* **2013**, *47*, 1–11.

76. Kala, H.K.; Mehta, R.; Sen, K.K.; Tandey, R.; Mandal, V. Critical analysis of research trends and issues in microwave assisted extraction of phenolics: Have we really done enough. *TrAC Trends Anal. Chem.* **2016**, *85*, 140–152.

77. Nahar, L.; Uddin, S.J.; Alam, M.A.; Sarker, S.D. Extraction of naturally occurring cannabinoids: an update. *Phytochem. Anal.* **2020**, pca.2987.

78. Vinatoru, M.; Mason, T.J.; Calinescu, I. Ultrasonically assisted extraction (UAE) and microwave assisted extraction (MAE) of functional compounds from plant materials. *TrAC Trends Anal. Chem.* **2017**, *97*, 159–178.

79. Dang, Y.-Y.; Zhang, H.; Xiu, Z.-L. Microwave-assisted aqueous two-phase extraction of phenolics from grape (Vitis vinifera) seed. *J. Chem. Technol. Biotechnol.* **2014**, *89*, 1576–1581.

80. Ayuningtyas, I.N.; Rahmawati, M.; S, S.; Mun'im, A. Optimization of Ionic Liquid-Based Microwave Assisted Extraction to Obtain Trans-resveratrol from Gnetum gnemon L. Seeds. *J. Young Pharm.* **2017**, *9*, 457–462.

81. Vats, T.; Mishra, A. Sustainable Syntheses with Microwave Irradiation. *Encycl. Inorg. Bioinorg. Chem.* **2016**.

82. Marco, B.; Agnese, C.; Giuseppe, T. Quality Preservation and Cost Effectiveness in the Extraction of Nutraceutically-Relevant Fractions from Microbial and Vegetal Matrices. In *Scientific, Health and Social Aspects of the Food Industry*; InTech, 2012.

83. N. Politis, S.; Colombo, P.; Colombo, G.; M. Rekkas, D. Design of experiments (DoE) in pharmaceutical development. *Drug Dev. Ind. Pharm.* **2017**, *43*, 889–901.

84. Garcia, L.; Garcia, R.; Pacheco, G.; Sutili, F.; Souza, R. De; Mansur, E.; Leal, I. Optimized Extraction of Resveratrol from Arachis repens Handro by Ultrasound and Microwave: A Correlation Study with the Antioxidant Properties and Phenol Contents. *Sci. World J.* **2016**, *2016*, 1–10.

85. Gheza, G.; Assini, S.; Lelli, C.; Marini, L.; Mayrhofer, H.; Nascimbene, J. Biodiversity and conservation of terricolous lichens and bryophytes in continental lowlands of northern Italy: the role of different dry habitat types. *Biodivers. Conserv.* **2020**, *29*, 3533–3550.

86. Lazzaro, L.; Bolpagni, R.; Buffa, G.; Gentili, R.; Lonati, M.; Stinca, A.; Acosta, A.T.R.; Adorni, M.; Aleffi, M.; Allegrezza, M.; et al. Impact of invasive alien plants on native plant communities and Natura 2000 habitats: State of the art, gap analysis and perspectives in Italy. *J. Environ. Manage.* **2020**, *274*, 111140.

87. Prisco, I.; Angiolini, C.; Assini, S.; Buffa, G.; Gigante, D.; Marcenò, C.; Sciandrello, S.; Villani, M.; Acosta, A.T.R. Conservation status of Italian coastal dune habitats in the light of the 4th Monitoring Report (92/43/EEC Habitats Directive). *Plant Sociol.* **2020**, *57*, 55–64.

88. Castagneri, D.; Garbarino, M.; Nola, P. Host preference and growth patterns of ivy (Hedera helix L.) in a temperate alluvial forest. *Plant Ecol.* **2013**, *214*, 1–9.

89. Motta, R.; Nola, P.; Berretti, R. The rise and fall of the black locust (Robinia pseudoacacia L.) in the "Siro Negri" Forest Reserve (Lombardy, Italy): lessons learned and future uncertainties. *Ann. For. Sci.* **2009**, *66*, 410–410.

90. Nicola, L.; Tosi, S.; Savini, D. In vitro evaluation of nematophagous activity of fungal isolates. *J. Basic Microbiol.* **2014**, *54*, 1–5.

91. Catoni, R.; Granata, M.U.; Sartori, F.; Varone, L.; Gratani, L. Corylus avellana responsiveness to light variations: morphological, anatomical, and physiological leaf trait plasticity. *Photosynthetica* **2015**, *53*, 35–46.

92. CARRIQUÍ, M.; CABRERA, H.M.; CONESA, M.À.; COOPMAN, R.E.; DOUTHE, C.; GAGO, J.; GALLÉ, A.; GALMÉS, J.; RIBAS-CARBO, M.; TOMÁS, M.; et al. Diffusional limitations explain the lower photosynthetic capacity of ferns as compared with angiosperms in a common garden study. *Plant. Cell Environ.* **2015**, *38*, 448–460.

93. Evans, J.R.; Kaldenhoff, R.; Genty, B.; Terashima, I. Resistances along the CO2 diffusion pathway inside leaves. *J. Exp. Bot.* **2009**, *60*, 2235–2248.

94. Ardenghi, N.M.G.; Polani, F. La flora della provincia di Pavia (Lombardia, Italia settentrionale). 1. L'Oltrepò Pavese. *Nat. Hist. Sci.* **2016**, *3*, 51–79.

95. WHO Cancer Available online: https://www.who.int/health-topics/cancer#tab=tab_1.

96. Gandolfi, S.; Laubach, J.P.; Hideshima, T.; Chauhan, D.; Anderson, K.C.; Richardson, P.G. The proteasome and proteasome inhibitors in multiple myeloma. *Cancer Metastasis Rev.* **2017**, *36*, 561–584.

97. Service., U.S.D. of A.A.R. Dr. Duke's Phytochemical and Ethnobotanical Databases. Available online: https://phytochem.nal.usda.gov/.

98. Chen, D.; Daniel, K.G.; Chen, M.S.; Kuhn, D.J.; Landis-Piwowar, K.R.; Dou, Q.P. Dietary flavonoids as proteasome inhibitors and apoptosis inducers in human leukemia cells. *Biochem. Pharmacol.* **2005**, *69*, 1421–1432.

99. Chang, T.-L. Inhibitory Effect of Flavonoids on 26S Proteasome Activity. *J. Agric. Food Chem.* **2009**, *57*, 9706–9715.

100. Bonfili, L.; Cecarini, V.; Amici, M.; Cuccioloni, M.; Angeletti, M.; Keller, J.N.; Eleuteri, A.M. Natural polyphenols as proteasome modulators and their role as anti-cancer compounds. *FEBS J.* **2008**, *275*, 5512–5526.

101. Ayoub, L.; Aissam, E.; Yassine, K.; Said, E.; Mohammed, E.M.; Souad, A. A specific QSAR model for proteasome inhibitors from Oleaeuropaea and Ficuscarica. *Bioinformation* **2018**, *14*, 384–392.

102. Ding, F.; Ma, T.; Hao, M.; Wang, Q.; Chen, S.; Wang, D.; Huang, L.; Zhang, X.; Jiang, D. Mapping Worldwide Environmental Suitability for Artemisia annua L. *Sustainability* **2020**, *12*, 1309.

103. Ekiert, H.; Świątkowska, J.; Klin, P.; Rzepiela, A.; Szopa, A. Artemisia annua – Importance in Traditional Medicine and Current State of Knowledge on the Chemistry, Biological Activity and Possible Applications. *Planta Med.* **2021**, *87*, 584–599.

104. Marco, J.A.; Sanz, J.F.; Bea, J.F.; Barbera, O. Phenolic constituents from Artemisia annua. *Pharmazie* **1990**, *45*, 382–383.

105. Fu, L.; Liu, L.; Chen, W.; Wang, Q.; Lv, X.; Wang, J.; Ji, Z.; Yu, G.; Liu, Q.; Zhang, X. Physicochemical and functional characteristics of starches from common vetch (Vicia sativa L.). *LWT* **2020**, *131*, 109694.

106. Liu, L.-F.; Li, W.-H.; Li, M.-Y.; Wu, X.-Z.; Yang, F.; Xu, J.-N.; Yuan, C.-S. Chemical constituents from common vetch (Vicia sativa L.) and their antioxidant and cytotoxic activities. *Nat. Prod. Res.* **2020**, *34*, 3205–3211.

107. Salehi, B.; Abu-Reidah, I.M.; Sharopov, F.; Karazhan, N.; Sharifi-Rad, J.; Akram, M.; Daniyal, M.; Khan, F.S.; Abbaass, W.; Zainab, R.; et al. Vicia plan ts—A comprehensive review on chemical composition and phytopharmacology. *Phyther. Res.* **2021**, *35*, 790–809.

108. Huang, Y.F.; Gao, X.L.; Nan, Z.B.; Zhang, Z.X. Potential value of the common vetch (Vicia sativa L.) as an animal feedstuff: a review. *J. Anim. Physiol. Anim. Nutr. (Berl).* **2017**, *101*, 807–823.

109. Ressler, C.; Tatake, J.G. Vicianin, Prunasin, and β-Cyanoalanine in Common Vetch Seed as Sources of Urinary Thiocyanate in the Rat. *J. Agric. Food Chem.* **2001**, *49*, 5075–5080.

110. Lizotte, P.A.; Poulton, J.E. Identification of (R)-Vicianin in Davallia trichomanoides Blume. *Zeitschrift für Naturforsch. C* **1986**, *41*, 5–8.

111. Krafft, C.; Cervellati, C.; Paetz, C.; Schneider, B.; Popp, J. Distribution of Amygdalin in Apricot (Prunus armeniaca) Seeds Studied by Raman Microscopic Imaging. *Appl. Spectrosc.* **2012**, *66*, 644–649.

112. Jaszczak-Wilke, E.; Polkowska, Ż.; Koprowski, M.; Owsianik, K.; Mitchell, A.E.; Bałczewski, P. Amygdalin: Toxicity, Anticancer Activity and Analytical Procedures for Its Determination in Plant Seeds. *Molecules* **2021**, *26*, 2253.

113. Tsanov, V.; Tsanov, H. Theoretical Analysis for the Safe Form and Dosage of Amygdalin Product. *Anticancer. Agents Med. Chem.* **2020**, *20*, 897–908.

114. Dreiseitel, A.; Schreier, P.; Oehme, A.; Locher, S.; Rogler, G.; Piberger, H.; Hajak, G.; Sand, P.G. Inhibition of proteasome activity by anthocyanins and anthocyanidins. *Biochem. Biophys. Res. Commun.* **2008**, *372*, 57–61.

115. Cevallos-Casals, B.A.; Cisneros-Zevallos, L. Stability of anthocyanin-based aqueous extracts of Andean purple corn and red-fleshed sweet potato compared to synthetic and natural colorants. *Food Chem.* **2004**, *86*, 69–77.

116. Khatoon, Z.; McTiernan, C.D.; Suuronen, E.J.; Mah, T.-F.; Alarcon, E.I. Bacterial biofilm formation on implantable devices and approaches to its treatment and prevention. *Heliyon* **2018**, *4*, e01067.

117. Davies, D. Understanding biofilm resistance to antibacterial agents. *Nat. Rev. Drug Discov.* **2003**, *2*, 114–122.

118. Zambare, V.P.; Christopher, L.P. Biopharmaceutical potential of lichens. *Pharm. Biol.* **2012**, *50*, 778–798.

119. Varol, M. Lichens as a Promising Source of Unique and Functional Small Molecules for Human Health and Well-Being. In; 2019; pp. 425–458.

120. Bhattacharyya, S.; Deep, P.R.; Singh, S.; Binata, N. Lichen Secondary Metabolites and Its Biological Activity. *Am. J. pharmatech Res.* **2016**, *6*.

121. *Lichen Secondary Metabolites*; Ranković, B., Ed.; Springer International Publishing: Cham, 2019; ISBN 978-3-030-16813-1.

122. Samanta, S.K.; Singh, O. V; Jain, R.K. Polycyclic aromatic hydrocarbons: environmental pollution and bioremediation. *Trends Biotechnol.* **2002**, *20*, 243–248.

123. Grynkiewicz, M.; Polkowska, Ż.; Namieśnik, J. Determination of polycyclic aromatic hydrocarbons in bulk precipitation and runoff waters in an urban region (Poland). *Atmos. Environ.* **2002**, *36*, 361–369.

124. Sarret, G.; Saumitou-Laprade, P.; Bert, V.; Proux, O.; Hazemann, J.-L.; Traverse, A.; Marcus, M.A.; Manceau, A. Forms of Zinc Accumulated in the Hyperaccumulator Arabidopsis halleri. *Plant Physiol.* **2002**, *130*, 1815–1826.

125. Sargsyan, R.; Gasparyan, A.; Tadevosyan, G.; Panosyan, H. Antimicrobial and antioxidant potentials of non-cytotoxic extracts of corticolous lichens sampled in Armenia. *AMB Express* **2021**, *11*, 110.

126. Im., Z.B.; Czeppego, Z. The lichen genus Cladonia (Cladoniaceae, lichenized Ascomycota) from Spitsbergen. *Pol. Polar Res.* **2006**, *27*, 207–242.

127. Bashyal, B.P.; Wijeratne, E.M.K.; Faeth, S.H.; Gunatilaka, A.A.L. Globosumones A−C, Cytotoxic Orsellinic Acid Esters from the Sonoran Desert Endophytic Fungus Chaetomium globosum 1. *J. Nat. Prod.* **2005**, *68*, 724–728.

128. Bogo, D.; Matos, M. de F.C.; Honda, N.K.; Pontes, E.C.; Oguma, P.M.; Santos, E.C. da S.; Carvalho, J.E. de; Nomizo, A. In vitro Antitumour Activity of Orsellinates. *Zeitschrift für Naturforsch. C* **2010**, *65*, 43–48.

129. Ristić, S.; Ranković, B.; Kosanić, M.; Stanojković, T.; Stamenković, S.; Vasiljević, P.; Manojlović, I.; Manojlović, N. Phytochemical study and antioxidant, antimicrobial and anticancer activities of Melanelia subaurifera and Melanelia fuliginosa lichens. *J. Food Sci. Technol.* **2016**, *53*, 2804–2816.

130. Kosanić, M.; Ranković, B.; Stanojković, T.; Rančić, A.; Manojlović, N. Cladonia lichens and their major metabolites as possible natural antioxidant, antimicrobial and anticancer agents. *LWT - Food Sci. Technol.* **2014**, *59*, 518–525.

131. Bačkorová, M.; Bačkor, M.; Mikeš, J.; Jendželovský, R.; Fedoročko, P. Variable responses of different human cancer cells to the lichen compounds parietin, atranorin, usnic acid and gyrophoric acid. *Toxicol. Vitr.* **2011**, *25*, 37–44.

132. Pejin, B.; Iodice, C.; Bogdanović, G.; Kojić, V.; Tešević, V. Stictic acid inhibits cell growth of human colon adenocarcinoma HT-29 cells. *Arab. J. Chem.* **2017**, *10*, S1240–S1242.

133. Kosanić, M.; Manojlović, N.; Janković, S.; Stanojković, T.; Ranković, B. Evernia prunastri and Pseudoevernia furfuraceae lichens and their major metabolites as antioxidant, antimicrobial and anticancer agents. *Food Chem. Toxicol.* **2013**, *53*, 112–118.

134. Reddy, S.D.; Siva, B.; Kumar, K.; Babu, V.S.P.; Sravanthi, V.; Boustie, J.; Nayak, V.L.; Tiwari, A.K.; Rao, C. V.; Sridhar, B.; et al. Comprehensive Analysis of Secondary Metabolites in Usnea longissima (Lichenized Ascomycetes, Parmeliaceae) Using UPLC-ESI-QTOF-MS/MS and Pro-Apoptotic Activity of Barbatic Acid. *Molecules* **2019**, *24*, 2270.

135. Ranković, B.; Kosanić, M.; Manojlović, N.; Rančić, A.; Stanojković, T. Chemical composition of Hypogymnia physodes lichen and biological activities of some its major metabolites. *Med. Chem. Res.* **2014**, *23*, 408–416.

136. Brandão, L.F.G.; Alcantara, G.B.; Matos, M. de F.C.; Bogo, D.; Freitas, D. dos S.; Oyama, N.M.; Honda, N.K. Cytotoxic Evaluation of Phenolic Compounds from Lichens against Melanoma Cells. *Chem. Pharm. Bull. (Tokyo).* **2013**, *61*, 176–183.

137. Mallavadhani, U.V.; Tirupathamma, R.S.; Sagarika, G.; Ramakrishna, S. Isolation, Chemical Modification, and Anticancer Activity of Major Metabolites of the Lichen Parmotrema mesotropum. *Chem. Nat. Compd.* **2019**, *55*, 825–831.

138. ISMED, F.; TAHER, M.; ICHWAN, S.J.A.; BAKHTIAR, A.; HUSNUNNISA, H. Screening of some Sumatran medicinal plants and selected secondary metabolites for their cytotoxic potential against MCF-7 and HSC-3 cell lines. *J. Res. Pharm.* **2019**, *23*, 770–776.

139. Ranković, B.; Kosanić, M.; Stanojković, T.; Vasiljević, P.; Manojlović, N. Biological Activities of Toninia candida and Usnea barbata Together with Their Norstictic Acid and Usnic Acid Constituents. *Int. J. Mol. Sci.* **2012**, *13*, 14707–14722.

140. Emsen, B.; Aslan, A.; Togar, B.; Turkez, H. In vitro antitumor activities of the lichen compounds olivetoric, physodic and psoromic acid in rat neuron and glioblastoma cells. *Pharm. Biol.* **2016**, *54*, 1748–1762.

141. Emsen, B.; Aslan, A.; Turkez, H.; Joughi, A.; Kaya, A. The anti-cancer efficacies of diffractaic, lobaric, and usnic acid: In vitro inhibition of glioma. *J. Cancer Res. Ther.* **2018**, *14*, 941.

142. Ebrahim, H.Y.; Akl, M.R.; Elsayed, H.E.; Hill, R.A.; El Sayed, K.A. Usnic Acid Benzylidene Analogues as Potent Mechanistic Target of Rapamycin Inhibitors for the Control of Breast Malignancies. *J. Nat. Prod.* **2017**, *80*, 932–952.

143. Hanuš, L.O.; Temina, M.; Dembitsky, V.M. Antibacterial and antifungal activities of some phenolic metabolites isolated from the lichenized ascomycete Ramalina lacera. *Nat. Prod. Commun.* **2008**, *3*, 233–236.

144. Honda, N.K.; Pavan, F.R.; Coelho, R.G.; de Andrade Leite, S.R.; Micheletti, A.C.; Lopes, T.I.B.; Misutsu, M.Y.; Beatriz, A.; Brum, R.L.; Leite, C.Q.F. Antimycobacterial activity of lichen substances. *Phytomedicine* **2010**, *17*, 328–332.

145. Ranković, B.; Mišić, M.; Sukdolak, S. The antimicrobial activity of substances derived from the lichens Physcia aipolia, Umbilicaria polyphylla, Parmelia caperata and Hypogymnia physodes. *World J. Microbiol. Biotechnol.* **2008**, *24*, 1239–1242.

146. Kosanic, M.; Rankovic, B.; Stanojkovic, T.; Vasiljevic, P.; Manojlovic, N. Biological activities and chemical composition of lichens from Serbia. *EXCLI J.* **2014**, *13*, 1226–38.

147. Selvaraj, G.; Tinabaye, A.; Ganesan, T.; Ananthi, R.; Kumar, S.S.; Arulmozhi, S. In vitro

antimicrobial activity of barbatic acid and its acetyl derivative of barbatic acid isolated from usneaflexilis(south india). *Int. J. Sci. Eng. Res.* **2016**, *7*, 45–48.

148. Qureshi, M.N.; Numonov, S.; Aisa, H.A. Total polyphenolic compounds, total flavonoids, GC-MS analysis of volatile constituents, evaluation of antioxidant and antimicrobial activities of Prunus dulcis nuts. *Pak. J. Pharm. Sci.* **2019**, *32*, 1461–1466.

149. Amanzadeh, Y.; Hajimehdipoor, H.; Abedi, Z.; Khatamsaz, M. Chemical constituents of Amygdalus spp. oil from Iran. *Res. J. Pharmacogn.* **2016**, *3*, 29–33.

150. Neeraj, V.; Behera, B.; Parizadeh, H.; Sharma, B. Bactericidal activity of some lichen secondary compounds of Cladonia ochrochlora, Parmotrema nilgherrensis & Parmotrema sancti-angelii. *Int. J. Drug Dev. Res.* **2011**, *3*, 222–232.

151. Milovanovic, N.; Kostic, D.; Milovanovic, V.; Djordjevic, A.; Stojanovic, G. Antimicrobial activity of the secondary metabolites of the genus Bryoria - a review. *Facta Univ. - Ser. Physics, Chem. Technol.* **2018**, *16*, 183–189.

152. Studzińska-Sroka, E.; Hołderna-Kędzia, E.; Galanty, A.; Bylka, W.; Kacprzak, K.; Ćwiklińska, K. In vitro antimicrobial activity of extracts and compounds isolated from Cladonia uncialis. *Nat. Prod. Res.* **2015**, *29*, 2302–2307.

153. PIOVANO, M.; GARBARINO, J.A.; GIANNINI, F.A.; CORRECHE, E.R.; FERESIN, G.; TAPIA, A.; ZACCHINO, S.; ENRIZ, R.D. EVALUATION OF ANTIFUNGAL AND ANTIBACTERIAL ACTIVITIES OF AROMATIC METABOLITES FROM LICHENS. *Boletín la Soc. Chil. Química* **2002**, *47*.

154. Butler, M.S. The Role of Natural Product Chemistry in Drug Discovery †. *J. Nat. Prod.* **2004**, *67*, 2141–2153.

155. KINOSHITA, Y.; YAMAMOT0, Y.; YOSHIMURA, I.; KUROKAWA, T.; HUNECK, S. Distribution of optical isomers of usnic and isousnic acids analysed by HPLC. *Journal-Hattori Bot. Lab.* **1997**, *83*, 173–178.

156. Galanty, A.; Paśko, P.; Podolak, I. Enantioselective activity of usnic acid: a comprehensive review and future perspectives. *Phytochem. Rev.* **2019**, *18*, 527–548.

157. SMEDS, A.I.; KYTÖVIITA, M.-M. Determination of usnic and perlatolic acids and identification of olivetoric acids in Northern reindeer lichen (Cladonia stellaris) extracts. *Lichenol.* **2010**, *42*, 739–749.

158. Marrubini, G.; Fattorini, P.; Previderé, C.; Goi, S.; Sorçaburu Cigliero, S.; Grignani, P.; Serra, M.; Biesuz, R.; Massolini, G. Experimental design applied to the optimization of microwave-assisted DNA hydrolysis. *J. Chromatogr. A* **2012**, *1249*, 8–16.

159. Moldovan; Iurian; Puscas; Silaghi-Dumitrescu; Hanganu; Bogdan; Vlase; Oniga; Benedec A Design of Experiments Strategy to Enhance the Recovery of Polyphenolic Compounds from Vitis vinifera By-Products through Heat Reflux Extraction. *Biomolecules* **2019**, *9*, 529.

160. Mayer, M.; O'Neill, M.A.; Murray, K.E.; Santos-Magalhães, N.S.; Carneiro-Leão, A.M.A.; Thompson, A.M.; Appleyard, V.C.L. Usnic acid: a non-genotoxic compound with anti-cancer properties. *Anticancer. Drugs* **2005**, *16*, 805–809.

161. Pathakumari, B.; Liang, G.; Liu, W. Immune defence to invasive fungal infections: A comprehensive review. *Biomed. Pharmacother.* **2020**, *130*, 110550.

162. Roemer, T.; Krysan, D.J. Antifungal Drug Development: Challenges, Unmet Clinical Needs, and New Approaches. *Cold Spring Harb. Perspect. Med.* **2014**, *4*, a019703–a019703.

163. Lee, Y.; Puumala, E.; Robbins, N.; Cowen, L.E. Antifungal Drug Resistance: Molecular Mechanisms in Candida albicans and Beyond. *Chem. Rev.* **2021**, *121*, 3390–3411.

164. Allen, D.; Wilson, D.; Drew, R.; Perfect, J. Azole antifungals: 35 years of invasive fungal infection management. *Expert Rev. Anti. Infect. Ther.* **2015**, *13*, 787–798.

165. Bruno, M.; Trucchi, B.; Burlando, B.; Ranzato, E.; Martinotti, S.; Akkol, E.K.; Süntar, I.; Keleş, H.; Verotta, L. (+)-Usnic acid enamines with remarkable cicatrizing properties. *Bioorg. Med. Chem.* **2013**, *21*, 1834–1843.

166. Amri, B.; Martino, E.; Vitulo, F.; Corana, F.; Kaâb, L.B.-B.; Rui, M.; Rossi, D.; Mori, M.; Rossi, S.; Collina, S. Marrubium vulgare L. Leave Extract: Phytochemical Composition, Antioxidant and Wound Healing Properties. *Molecules* **2017**, *22*, 1851.

167. Sahpaz, S.; Garbacki, N.; Tits, M.; Bailleul, F. Isolation and pharmacological activity of phenylpropanoid esters from Marrubium vulgare. *J. Ethnopharmacol.* **2002**, *79*, 389–392.

168. El Bardai, S.; Morel, N.; Wibo, M.; Fabre, N.; Llabres, G.; Lyoussi, B.; Quetin-Leclercq, J. The Vasorelaxant Activity of Marrubenol and Marrubiin from Marrubium vulgare. *Planta Med.* **2003**, *69*, 75–77.

169. Chin, K.; Qi, Y.; Chin, K.L.; Malekian, F.; Berhane, M.; Gager, J. Biological Characteristics , Nutritional and Medicinal Value of Roselle , Hibiscus Sabdariffa Biological Characteristics , Nutritional and Medicinal Value of Roselle , Hibiscus Sabdariffa. *Agric. Res. Ext. Cent.* **2016**, *70813*, 603–604.

170. Almahy, H.A.; Abdel-Razik, H.H.; El-Badry, Y.A..; Ibrahim, E.M. Ultrasonic Extraction of Anthocyanin's as Natural Dyes from Hibiscus Sabdariffa (Karkade) and its Application on Dying Foodstuff and Beverages in Kingdom Of Saudi Arabia. *Am. J. Biol. Pharm. Res.* **2015**, *2*, 168–174.

Appendice

Paper 1

Chapter

Microwave-Assisted Solid Extraction from Natural Matrices

Valeria Cavalloro, Emanuela Martino, Pasquale Linciano and Simona Collina

Abstract

The extraction of secondary metabolites from plants, and natural sources in general, is a cornerstone in medicinal chemistry and required the development of sustainable extraction techniques. Microwave-Assisted Solid Extraction (MASE) is a promising extractive methodology being more effective than traditional extraction techniques. It offers higher and faster extraction performance ability with less solvent consumption and protection toward thermolabile constituents. For these reasons, MASE resulted in a suitable extractive methodology in all aspects, including economical and practical, compared to traditional extraction techniques, especially over Soxhlet or solid–liquid extraction. In this chapter, a brief theoretical background about the use of microwave energy for extraction has been presented for better understanding. Then, the potential of MASE for the extraction of secondary metabolites from natural resources, for evaluating the plant productivity and for evaluating the quality of the natural matrices will be reviewed. The discussion is supported by reporting recent applicative examples of MASE applied to the extraction of the most representative chemical classes of secondary metabolites, with a special focus on some drugs or compounds of pharmaceutical and nutraceutical interest.

Keywords: MASE, plant material, natural matrices, secondary metabolite, bioactive compounds, plant productivity

1. Introduction

Nature Aided Drug Discovery (NADD) represents the most ancient approach in finding new active compounds for fighting human diseases, and still today it plays a crucial role in drug discovery [1]. New chemical entities (NCE) from natural derivation represent a relevant slice among the drugs approved by Food and Drug Administration (FDA) and the European Medicines Agencies (EMA) for commercialization and administration on humans [2]. More than half the total anti-infective drugs approved in the last forty years resulted from a NADD approach and a similar trend can be observed for anticancer drugs, where 41% of them derived from natural sources and only 16% are classifiable as totally synthetic small molecules [2]. Moreover, the Global Herbal Medicine Market Size is expected to increase to USD 129 billion by 2023, according to Market Research Future [3].

The success of NADD finds its main reason in the wider and heterogeneous chemical space covered by natural products whether compared with synthetic derivatives. The 83% of the chemical scaffolds found in natural compounds are

1

unique and absent in synthetic NCE, due to the lack of commercially available synthons or cumbersome and prohibitive synthetic procedures [4]. Thus, the screening of libraries of compounds derived from natural sources still remains a worthy procedure for the identification of new and unexplored NCE. Besides, marine sources or lichens are still almost uninvestigated and might therefore represent an inestimable treasure of new potential drugs [5–7].

The natural compounds of interest in NADD are secondary metabolites that are not directly involved in the essential functions of the cell cycle and duplication processes and are characterized by high structural variability. From a structural standpoint, they are classified into alkaloids, terpenoids, saponins, lignans, flavonoids, and tannins [8]. Secondary metabolites are produced in different amounts for vexillary functions or defensive responses to biotic or abiotic stress being involved in the system of plant defense [9]. For this reason, specific secondary metabolites may be considered as markers of the plant health and may be used to evaluate the quality of the selected natural matrix and the effects that the environmental factors have on it. The evaluation of their content in natural sources, as well as their recovery, require the exploitation of ad hoc extractive procedures since secondary metabolites are mainly present in the intracellular domain. Thus, appropriate extraction procedures involve the rupture of the cell wall and cellular membranes, thus favoring the passage of the secondary metabolites into the extraction solvent, from which they can be recovered.

Over the years different protocols and techniques have been developed for the extraction of metabolites from natural matrices, named Solid–Liquid Extraction (SLEs). SLEs are classified in conventional (or traditional) and non-conventional (or innovative) methodologies [10]. In conventional methodologies, SLE is performed by heating the natural source with conventional heating sources (i.e., flame, heating plate, or mantle) in the presence or not of solvent and with or without stirring. Examples of conventional methodologies are maceration (digestion, infusion, and decoction), percolation, and Soxhlet or steam distillation. Solvents, or generally mixtures of solvents, with wide grades of polarity such as methanol, ethanol, acetone, ethyl acetate, trichloromethane, hexane, *etc*. are employed. Nevertheless, conventional extraction methods usually require a large volume of solvents, long extraction time, and high temperature. Such harsh extraction conditions may lead to thermal or chemical degradation of the metabolites, thus resulting in a low yield of the final extract. Moreover, the upscaling at an industrial level would be impracticable, owing to energy consumption, technological inaccessibility, and environmental considerations [11]. Conversely, non-conventional methodologies exploit innovative chemical–physical principles and cutting-edge technologies to facilitate the extractive procedures and the recovery of the product of interest from the natural source. Varied energy sources and extractive principles may be exploited and, therefore, specific equipments are needed. Microwave-assisted Solid Extraction (MASE), ultrasound-assisted extraction (UAE), pressurized solvent extraction (PLE), and supercritical fluid extraction (SFE) are the most frequently non-conventional methodologies extensively used for NADD [11].

In this chapter, the potential of microwave-assisted irradiation for the extraction of secondary metabolites from plants, and natural resources in general, will be discussed, with a special focus on recent applicative examples of the most representative chemical classes.

2. Microwave-Assisted Solid Extraction (MASE)

The physical principles underlying MASE are completely different from those of conventional extraction because microwave irradiation can cause a more effective disruption of the cellular structures (cell walls and cellular membranes) thus

2

favoring the release of the cellular content and speeding up the extraction process. The interaction of microwave irradiation with the solvents, intracellular water, and ions causes an increase of the dipolar rotation and ionic conductivity of molecules with dipolar moments and ions, which results in a rise of the temperature inside the cell. The vaporization of the intracellular water causes the dehydration of the cellular wall and the reduction of its resistance. This, combined with the abrupt increment of the intracellular pressure, leads to the cell wall and membranes disruption, thus facilitating the passage of the secondary metabolites into the extractive solvent [12, 13].

This is the result of a synergistic combination of heat and mass gradient working in the same direction from the inside to the outside of the cell, as confirmed by Scanning Electron Microscopy (SEM) analysis (**Figure 1**) [14].

Monomodal and multimodal microwave systems also referred to as single- or multi-mode systems specifically designed for MASE are nowadays available. A single-mode system permits to focus the microwave radiation on a restricted zone where the sample is subjected to a much stronger electric field. Conversely, in a multimode system, the microwave radiation is randomly dispersed within the microwave cavity, where the sample is irradiated [15]. Both mono- and multi-modal microwave devices comprise a magnetron, which generates microwave radiation, a waveguide, which is used to propagate the microwave from the source to the microwave cavity, the applicator, where the sample is placed and a circulator that allows the microwave to move only in the forward direction. The main difference between the two systems relies on the applicator that in the case of a multimodal system is a closed cavity where the microwaves are randomly dispersed, whereas in the monomodal oven the extraction vessel is directly located in-line with the waveguide [15]. Both systems are effective in extracting metabolites from natural sources, and their use is usually related to the amount of natural matrix. Accordingly, the monomodal system is preferred when the amount of natural source to be treated is relatively low (milligram to gram scale), and vice versa. Microwave extraction may be performed using open or closed extraction vessel systems. The open vessel apparatus originated from a modification of domestic MW ovens. The extraction is conducted at ambient pressure and the vessel is directly connected to a condenser to avoid loss of solvent or volatile components. An evolution of the open vessel apparatus is the Focused Microwave-Assisted Soxhlet (FMASE) which combines the classical Soxhlet extraction (SE) technique with MW irradiation. In the closed vessel system the entire extraction vessel is located within the oven, thus allowing better control of the pressure and temperature during the extraction [16].

The closed-vessel system presents several advantages: i) a higher temperature than open vessel systems can be reached because of the increased pressure inside the vessel raises the boiling point of the solvents used, thus decreasing the time needed for the extraction; ii) the loss of volatile substances is completely avoided because they are confined within the vessel; iii) a low amount of solvent is required because no evaporation occurs and there is little or no risk of airborne contamination thus
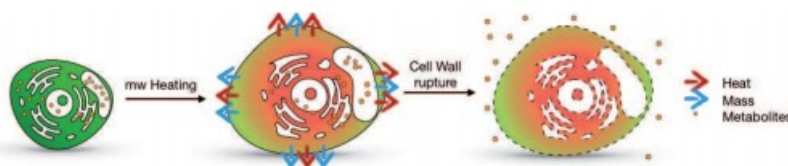

Figure 1.
Microwave heating effect on cells.

3

preventing the oxidation of air-sensitive metabolites; iv) the fumes are contained within the vessel, reducing the hazard of the extractive procedure.

In a closed vessel system high pressure can be reached. The high pressure stimulates various phenomena according to LeChatelier's principle, such as the transition of phase from one form to another, change in reaction dynamics, change in molecular structure, *etc*. hence resulting in the enhancement of extraction efficiency. Accordingly, working under high pressure causes alterations in the structure of some constituents of the cells such as lipids, proteins, enzymes, and outer cell membranes, thus damaging the plant wall and internal structure of the cell and reducing the mass transfer resistance. In this way, the secondary metabolites are released, leaving behind other cellular components. The High-Pressure MASE (HPMAE) is considered a newly emerging technique. It is a time-efficient, convenient, eco-friendly, safe, and energy-efficient extraction method when compared to the traditional or conventional methods of extraction [17].

Nevertheless, the use of closed-vessel systems presents some drawbacks: the amount of samples that can be processed is limited; the addition of reagents or solvents during operation is forbidden and the vessel must be cooled down before it can be opened to avoid loss of volatile constituents [16]. For processing a large amount of material, an open-vessel system is more appropriate. It allows the possibility to add reagents and to refill the solvent during the extraction, and to remove the excess of solvent during the extraction procedure. Moreover, the extraction of thermolabile metabolites is allowed since it usually reaches low temperatures relative to closed-vessel systems. On the other hand, the open-vessel systems ensure less reproducible results compared to the closed-vessel systems and the extraction in open-vessel could require a longer time to obtain results comparable to those achieved in closed-vessel [16].

The microwave energy may be applied also to extraction in solvent-free conditions (Solvent Free Microwave Extraction-SFME) [12]. In this case, the plant material is directly placed into the microwave reactor, without the addition of any solvent. The heating of the water contained by the plant material distends the natural matrices and causes the rupture of the cells releasing their content. This process has been successfully applied for the extraction of the essential oils. After MW heating, the volatile components co-evaporate with the in-situ water contained in the natural matrix; the vapors condense outside the microwave oven into a collector where they separate between essential oils and the aqueous phase. The latter is brought back into the vessel to refresh the amount of water in the sample, whereas the essential oil is collected apart [12].

3. Procedure set-up

The performance of the MASE process is strictly related to the operative conditions employed. Several parameters, such as solvent, solvent-drug ratio, temperature, time, pressure, microwave power, water content, and characteristic of the matrix must be optimized in setting up a MASE procedure. Each of these parameters should not be considered alone, but they are all linked together and the comprehension of the effects and influences of these factors is pivotal for MASE efficiency. A brief discussion about the role of these parameters in the design of a MASE protocol is herein reported.

3.1 Solvent

The selection of the solvent plays a crucial role in MASE, as well as in other conventional extraction processes, and several solvent parameters (solubility of

4

the analyte, penetration, interaction with the matrix, dielectric constant, and mass transfer kinetic process) should be considered to perform the right choice. *In primis*, the solvent should assure the highest solubility of the analyte of interest while excluding undesired matrix components. However, conversely to the traditional extractive procedures, the chosen solvent must be able to absorb the microwave radiation and to convert it into heat. This depends on the dielectric constant and the dielectric loss of the solvent. Thus, in microwave application, solvents are usually classified in low, medium, or high absorbance whether they absorb at 300 W (i.e. carbon chlorides, 1,4-dioxane, tetrahydrofuran, diethyl ether, ethyl acetate, pyridine, toluene, chlorobenzene, xylenes, and hexane), 200 W (i.e. water, DMF, NMP, butanol, acetonitrile, HMPA, ketones, o-dichlorobenzene, 1,2-dichloroethane, 2-methoxy ethanol, acetic acid, and trifluoroacetic acid) or 100 W (i.e. DMSO, ethanol, methanol, propanol, nitrobenzene, formic acid, ethylene glycol), respectively. For low absorbing solvents, the heating rate can be increased by mixing with solvents with a higher dielectric constant or by adding salts to the mixture [18]. Recently, increasing interest in ionic liquids as MASE solvents or modifiers has been observed. Ionic liquids are organic salts with low melting points, and they are usually liquid at room temperature. They are characterized by extremely low vapor pressure, high stability and can solubilize both polar and non-polar metabolites. Moreover, they have the advantage to be eco-friendly solvents, although their extensive use is limited due to the high commercial costs. Another emerging eco-friendly alternative is the use of deep eutectic solvents. They possess physical and chemical properties similar to the ionic liquids, but they show better biodegradability, toxicity profiles, and solubility properties. Lastly, the content of water in the sample should be taken into account since it influences the heating rate and facilitates the transport of the analytes into the solvent at higher rates [19].

As stated in the previous paragraph, a Solvent-Free Microwave Extraction (SFME) is also possible. This procedure foresees the direct irradiation with MW of the plant material, fresh or rehydrated. A crucial role is played by the content of water in the sample, because it is the heating of such water to cause the rupture of the cells of the plant material, favoring the release of the content. This process is mainly applied for the extraction of volatile compounds such as essential oil. The oil evaporates by azeotropic distillation with the water contained in the sample. After cooling outside of the microwave reactor the oil separates from the water and can be collected through a modified Clevenger apparatus. Water is refluxed back into the microwave oven to allow the continuous extraction of the oil from the sample [12].

3.2 Liquid-Solid (L/S) ratio

Another important parameter to consider in the set-up of a MASE protocol is the ratio between the amount of sample and the volume of solvent. The latter should be enough to cover the sample during the entire process, especially when the matrix swells during the extraction process. Although in conventional extraction higher is the volume of solvent, higher is the yield of the extract, in MASE larger volume of solvent may result in more energy and time to heat the suspension and in a lower yield due to a non-uniform distribution and exposure to microwave. Usually, an L/S from 10:1 to 20:1 (mL/mg) is found to be the right ratio in many extractive processes reported in the literature [20].

Strictly correlated to the L/S ratio is the stirring rate since it affects the mass transfer process in MASE. However, the significance of this parameter is rarely explored. By stirring, the mass transfer barrier created by the concentrated compounds in a localized region due to insufficient solvent can also be minimized resulting in better extraction yield. In other words, agitation accelerates the

5

Microwave Heating - Electromagnetic Fields Causing Thermal and Non-Thermal Effects

extraction speed by accelerating the desorption and dissolution of compounds bound to the sample matrix [17].

3.3 Time

Extraction times in MASE lasts from a few minutes up to half an hour, and this represents an advantage for the extraction of thermal or oxygen labile compounds since it avoids the degradation of the compounds of interest [21]. The extraction yield is directly proportional to the extraction time, although it has been observed that this increment is very small for an extremely long time. Moreover, for longer extraction time overheating may occur, especially with high absorbent solvents, thus exposing thermolabile compounds to degradation. Whether longer extraction time is required, consecutive and shorter extraction cycles are preferable. The solvent can be collected after each extraction cycle and a fresh solvent could be added to the residue to guarantee the exhaustion of the matrix. This discontinuous procedure has been applied for the extraction of several secondary metabolites from plant material, allowing an enhanced yield and low decomposition of thermolabile compounds [22].

3.4 Temperature and microwave power

Temperature and MW power are strictly correlated. Power is the driving force of the process since it provides the energy necessary to excite the dipolar moments and the ionic conduction of the constituent of the sample, resulting in a proportional increase of the temperature and promoting the destruction of the natural matrix. Thus, the power of the microwave irradiation has to be carefully dosed in function of the amount of the sample, the solvent employed, the extraction time required, and the chemical stability of the secondary metabolites of interest [23]. Increasing the power results in an improved extraction yield and shorter extraction time. However, this result is true until the reaching of an optimal temperature beyond which a decrease in yield is observed, mainly due to the thermal stability of the target metabolite [24].

Accordingly, the temperature is a key parameter to enhance the efficacy of MASE and to avoid at the same time the degradation of the sample. Thus, the choice of the extraction temperature is strictly related to the properties of the solvent, the chemical stability of the metabolites of interest, and the microwave system used. In particular, at high temperatures the viscosity and the surface tension of the solvent diminish; moreover, the capability to solubilize the analytes, and to wet and penetrate the matrix increase, thus resulting in improved extractive efficacy. Also, when operating in a close-vessel, there is the advantage of heating the solvent above its boiling point, thus leading to a more performing extraction [25].

To conclude, the development of a proper MASE methodology must consider at least four variables: solvent, liquid/solid ratio, temperature, and time. To speed up the set-up of the procedure, the Design of Experiment (DoE) approach may be applied. This is a systematic statistic-based tool to assess the best experimental conditions both in the academic and industrial fields [26]. Thanks to this approach, all the variables and their interactions can be evaluated while doing the minimum number of runs.

Over the years, microwave-assisted extraction has been successfully applied to extract diverse classes of secondary metabolites (i.e. polyphenols, flavonoids, coumarins, terpenoids, cannabinoids, and alkaloids) from natural sources, for evaluating the plant productivity, for extracting bioactive compounds both for drug discovery or for commercial purposes.

6

Here below, studies of plant productivity based on MASE methodology and specific cases of extraction of natural compounds of pharmaceutical and nutraceutical interest will be discussed, with a special focus on resveratrol, terpenoids, and cannabinoids.

4. MASE procedures successfully applied to secondary metabolites extraction

4.1 Evaluation of plant productivity

Numerous applications report about the use of the MW to assist the extraction of organic and organometallic compounds from various matrices (soils, sediments, water samples, botanicals), with special emphasis on environmental applications [27, 28]. Extraction of natural matrices is essential to compare their productivity under different stress conditions [9], harvesting time [29], and places [30]. MASE offers the possibility of performing multiple extractions and therefore, it is suitable for the rapid screening of a numerous set of samples to evaluate the productivity of organisms.

An example is a work performed by Martino et al., regarding the MASE of *Melilotus officinalis,* harvested in different environmental situations, to compare the amount of coumarin and related compounds, and to find the best condition for its cultivation [22]. The Authors developed a rapid, reliable, and reproducible method of extraction from *M. officinalis* inflorescence of coumarin (**Figure 2**), melilotic acid, and o-coumaric acid, considered as productivity markers of the plants. A comparison of different extraction techniques evidenced that MASE is the best procedure in terms of both yields and extraction time [22]. The optimal extraction conditions consisted of two successive irradiations of 5 min each at 50°C, with a cooling step in between, and it resulted suitable for application to large sets of samples [22].

Another example is the setup of a fast and reproducible extraction methodology of vitexin and its isomer isovitexin from *Crataegus monogyna* (**Figure 2**) for evaluating the plant productivity and determining the best ecological conditions for hawthorn cultivation in northern Italy (Lombardy). These metabolites have a high pharmaceutical value due to their anti-hyperalgesic and neuroprotective effects and their activity against oxidative stress, cancer, and inflammation [31].

Within this context, Martino et al. set up a MASE procedure that can be applied for quantitative extraction of both metabolites from *C. monogyna* in just 3 minutes [50% aqueous methanol (v/v), 120°C, 120 W], bringing advantages both in terms of time (3 min *vs* 6 hours) and solvent consumption (0.05 vs 0.10 g/mL) over standard extraction methods [30]. The developed MASE protocol combined with isocratic
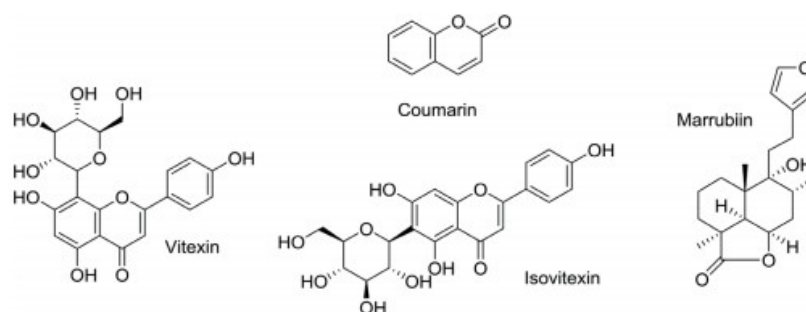

Figure 2.
Secondary metabolites extracted via MASE approach and considered as markers of the plant productivity.

7

HPLC analysis is suitable for the rapid screening of plant materials collected in different environmental conditions, and to determine the best ecological conditions for its cultivation. To extract vitexin and isovitexin from *Crotalaria sessiliflora,* Tang et al. exploited a microwave-assisted cloud-point extraction (MACPE). MACPE combines cloud-point extraction (CPE) with MAE. This has emerged as a technique to extract and separate bioactive compounds from medicinal plants [32]. Of note, using MACPE, hydrophobic compounds present in the aqueous phase can be favorably extracted into the hydrophobic core of micelles [33]. Applying MACPE, vitexin and isovitexin have been obtained in high yields and short times [34].

MASE can also be applied to study the effect of micronutrients or pollutants on secondary metabolites production. Amri et al. investigated the impact of soil copper (II) concentrations on nutrient uptake and the antioxidant system of *Marrubium vulgare*. Owing to waste deposition and agricultural practices, copper (II) tends to accumulate in high and toxic concentrations, leading to an alteration of the vital physiological or biochemical functions of the plants. As it is the case of *M. vulgare,* these effects may have a great impact on human health, since such a plant is used worldwide for its medicinal properties. To perform the study, the Authors selected marrubiin (**Figure 2**) as a reference compound, since it is the main secondary metabolite produced by *M. vulgare* leaves. A MASE protocol was developed for the easy extraction of marrubiin. This procedure allowed to evaluate the quality of a wide range of samples of white horehound. To optimize the process, the Authors used the statistical DoE approach. DoE findings indicated that the highest extraction efficiency of marrubiin with high repeatability was obtained using 100% ethanol at 120°C for 15 min, with significant benefits in terms of extraction times and environmental impact, given that ethanol is completely biodegradable. The MASE methodology may be applied for the characterization of *M. vulgare* herbal drug samples, thus evaluating their exposure to abiotic stress, revealing their phytochemical status, and facilitating the identification of raw materials obtained from a plant grown under stress conditions.

To sum up, MASE procedures is a versatile technique suitable for the evaluation of the plant productivity, and to assess the quality of vegetal matrices, since it is fast, reproducible, suitable for extraction of a large number of samples and requires a low amount of natural matrix.

4.2 Extraction of secondary metabolites for drug discovery or commercial purposes

4.2.1 Alkaloids

Alkaloids are a well-known class of secondary metabolites characterized by basic nitrogen. Over the years, many active alkaloids have been extracted via MW irradiation, e.g. ephedrine alkaloids, cocaine, and ergot alkaloids [35–37]. Unfortunately, results obtained for many of them have been comparable or worst if compared with the traditional method [38]. Nevertheless, microwaves have also spurred the discovery of new active alkaloids at the early stage of drug discovery. MASE protocols can be exploited to extract different alkaloids (examples are reported in **Figure 3**) from different botanicals like tuberous roots, leaves, and seeds [37, 39, 40].

As an example of MASE applied to the extraction of alkaloids, Pan et al. obtained a good recovery of caffeine and polyphenols from the leaves of green tea (*Thea sinensis* L.). MASE provided high extraction and selectivity, required a short time, and less labour-intensive, thus resulting in an efficient method in comparison with the conventional extraction procedures [41].
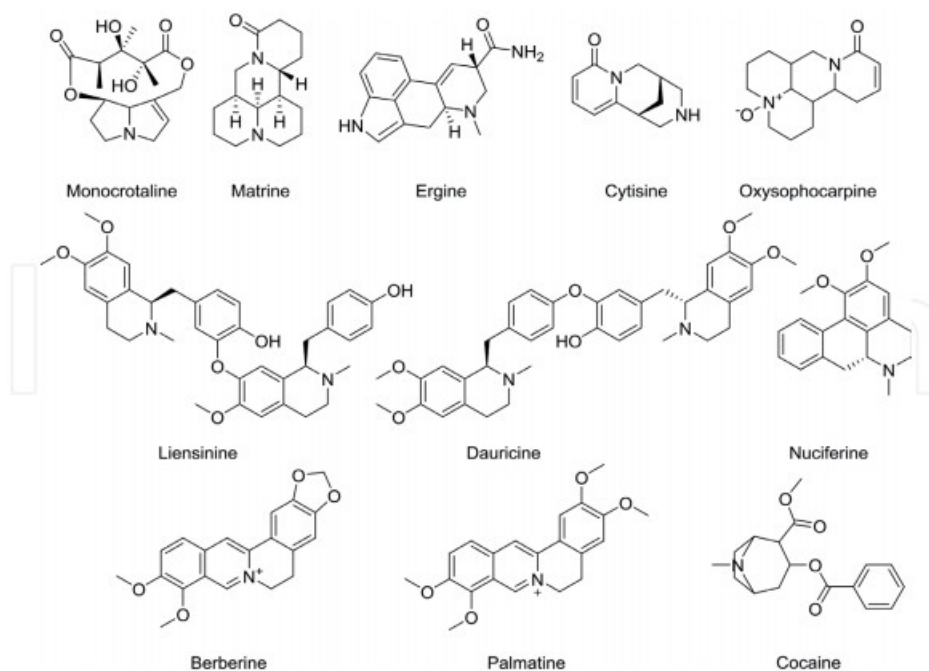
8

Figure 3.
Examples of alkaloids extracted via the MASE approaches.

Xiong et al. developed an efficient MASE protocol, within a drug discovery process, for the isolation of bioactive alkaloids (e.g. liensinine, isoliensinine, neferine, dauricine, nuciferine, **Figure 3**) from *Lotus plumule*. The optimal extraction conditions required a 65% aqueous methanol as a solvent and irradiation at 200 W for 260 seconds [42]. Another interesting example, reported by Zhou et al., is the microwave-assisted aqueous two-phase extraction, useful for rapid and simultaneous extraction and separation of alkaloids. This technique was applied to *Radix Sophorae tonkinensis*. The optimum conditions were summarized as follows: ethanol/Na_2HPO_4 as the extraction solvent, 100 mesh as particle size, 1:75 of S/L ratio, irradiating at 90°C for 5 min [43]. Matrine, sophocarpine, oxymatrine, oxysophocarpine, 5α-hydroxysophocarpine, sophoranol, cytisine, N-methylcytisine, and sophoridine were efficiently extracted.

Recently, Belwal et al. reported an optimized MASE protocol, defined by multicomponent analysis, for the extraction of berberine (**Figure 3**) and polyphenols from diverse species of *Berberis*. The medical properties of berberine (anti-diabetic, hepato-protectant, anti-arthritic, antioxidants, anti-microbial, neuro-protective, and hypo-lipidemic activity) are widely recognized, and it is used in pharmaceuticals and nutraceuticals preparation. In this study, multi-component analysis (MCA) has been used to extract berberine and polyphenols from *B. jaeschkeana* roots under microwave-assisted extraction (MAE) conditions. All the variables, above described, were considered under 42 experiments and the results of the model showed significant model fitness. Under optimized MAE condition, (i.e. 100% methanol, pH 2.0, 598 W, 2 min of irradiation time), the berberine and palmatine (**Figure 3**) contents were recorded in 4.6% and 2.0%, respectively. Under the optimized condition, the yield of alkaloids was found closer to the models' predicted value [34].

Regarding the alkaloids employed as drugs, or of interest for the toxicological use and/or abuse, few extractive procedures by MASE are reported in the literature. As an example, Brachet et al. extracted cocaine and benzoylecgonine from

9

the leaves of *Erythroxylum coca* by MASE. Different solvents, particle size, time, and power were evaluated. Since MeOH is a high absorbing microwave solvent, and cocaine is highly soluble in it, it was found to be the best extraction solvent [36]. Interestingly, MASE found application in the forensic field as a rapid and cleanup-free method for the extraction and quantification of drugs of abuse and the respective metabolites from human fluids and tissues. Fernandez et al. reported the simultaneous extraction of cocaine, benzoylecgonine, cocaethylene, morphine, 6-monoacethylmorphine, and codeine from human urine [44], hair [45], and vitreous humor samples [46]. The MASE procedure reduces the extraction time, avoids the cleanup steps, and allows a quantitative recovery of the drugs.

4.2.2 Stilbene-based polyphenolic compounds

Stilbene-based polyphenolic compounds, i.e. resveratrol, pterostilbene, and piceatannol, are of particular interest from a medicinal chemistry standpoint, having multiple pharmacological activities (**Figure 4**).

In particular, *trans*-resveratrol (3, 5, 4′-trihydroxystilbene) became popular as a result of an attempt to explain the "French paradox" [47]. Resveratrol and other polyphenolic-stilbene derivatives showed a wide range of beneficial physiological properties. They possess antibacterial, anti-inflammatory, hypolipidemic, cardiovascular-hepatoprotective, and anticancer activities [48–50]. In particular, the hypolipidemic and cardiovascular protective activity derived from the agonistic activity against PPARα and PPARγ receptors [51, 52] For all this benefit, resveratrol has attracted the attention of the scientific community and pharmaceutical and nutraceutical industries. Indeed, several drugs and dietary supplements containing resveratrol are commercially available.

Even though resveratrol is produced naturally in plants, the extraction of resveratrol in commercial quantities is a problem, because of its low concentration, multiple steps of isolation and purification, unfriendly environmental issues, and seasonal occurrence [53]. Moreover, the preparation of resveratrol by synthesis is difficult owing to the formation of many unwanted side products [54, 55]. Only recently, the production of resveratrol in heterologous engineered microorganisms
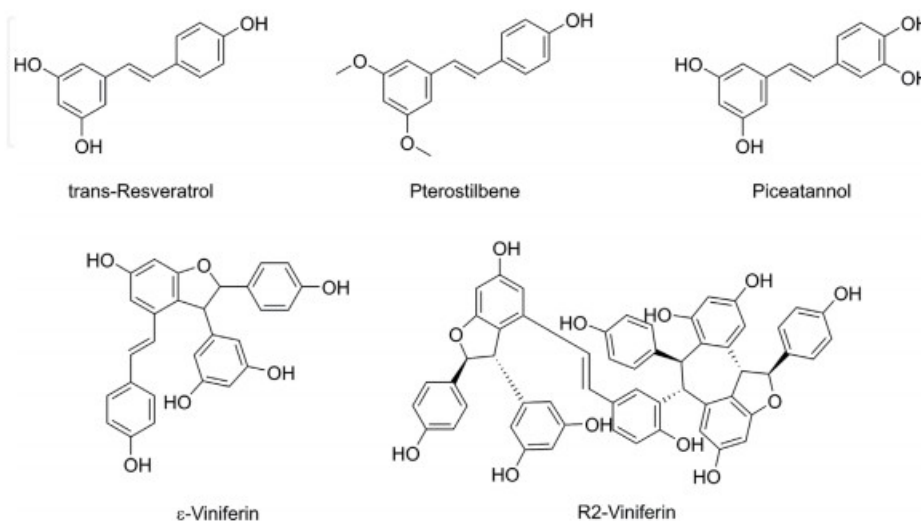

Figure 4.
Chemical structure of polyphenolic-stilbene based secondary metabolites.

10

has been proposed [56]. Thus, resveratrol is still being extracted from wild *Polygonum cuspidatum*'s root (Japanese knotweed), grape skins and seed, and the domestic giant knotweed of China, which is the world's largest producer [53, 56–58]. Garcia-Ayuso *et al.,* in late 1998, found that by applying the MW irradiation to SE, the last of the extraction was drastically reduced from 8 hours to 60 minutes with comparable results to SE in yield. MASE was further optimized by testing solvents and times on bark extraction and compared to SE on the same tree sample. The results suggested that microwave extraction may be more efficient than SE.

The extraction of resveratrol by MASE from different plant materials (i.e. *Arachis repens* and grape seeds) has also been investigated. To exhaustively extract resveratrol from *A. repens*, commonly known as peanut grass, three different methodologies (conventional maceration, ultrasound-assisted extractions, and MASE) have been compared. Although sonication resulted more effectively in the extraction of resveratrol compared to MASE and maceration, MASE showed to be an excellent choice since it extracted high yields in a reduced time [59].

In another study, Dang et al. combined the aqueous two-phase extraction technique (ATPE) with MASE for the extraction of the total polyphenol content, including resveratrol, from grape seeds [60]. Microwave-assisted ATPE (MAATPE) required lower solvent concentration and less time compared with other methods such as refluxing solvent or SE. A higher level of resveratrol was obtained with MAATPE, in contrast to ATPE. The Authors also compared the effectiveness of three solvents (water, water: ethanol (1:1) and ethanol) and three extraction methods, including MASE and ultrasound-assisted extraction (UAE) and the conventional SE. MASE provided a better extraction with water and ethanol (1:1) obtaining extracts very rich in polyphenolic substances, including stilbenes.

Lastly, MASE has successfully applied also for the extraction of other polyphenolic-stilbene based compounds such as pterostilbene, mainly found in blueberries and in *Pterocarpus marsupium* heartwood, and ε-viniferin, found in *Vitis coignetiae*, a wild grapevine (**Figure 4**). Kim et al. reported the MASE of pterostilbene, and other derivatives, from *Vitis coignetiae*, using 80% ethanol at 90 W for 15 min, resulting in a stilbenoids overall yield of 0.13%, with pterostilbene the most representative compound in the extract [61]. An optimized protocol (70–150 W for 8–18 min, using 30–50% ethanol) was further developed for the extraction of viniferin from the same drug [48]. Recently, Pinero et al. disclosed a new process for recovering stilbenes from woody vine by-products such as grape stem and cane samples. MASE was carried out under different extraction conditions. The best results were achieved from grape stems, using 80% ethanol in water as an extraction solvent, a temperature of 125°C, an irradiation power of 750 W for 5 min [49].

4.2.3 Terpenoids

4.2.3.1 Artemisinin and paclitaxel

Terpenes and isoprenoids, in general, gained much attention for their physiological functions (i.e., hormones, aliphatic membrane anchors, maintaining membrane structure), ecological roles (i.e., defense compounds, insect/animal attractants), and extensive pharmaceutical applications such as flavors, fragrances, and medicines.

In particular, artemisinin and paclitaxel represented two milestones in the fight against malaria and cancer, respectively. Artemisinin (**Figure 5**) is a sesquiterpene lactone isolated from *Artemisia annua* and it is a first-class drug for the treatment of drug-resistant malaria. The conventional artemisinin extraction procedure requires room temperature, heat-reflux, or SE. Hao et al., in 2002 reported a first attempt to extract artemisinin from *Artemisia annua* by MASE. Several solvents were explored,
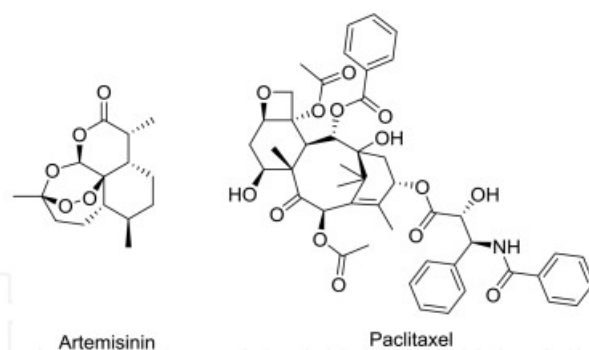
11

Figure 5.
Chemical structures of artemisinin and paclitaxel.

such as ethanol, trichloromethane, cyclohexane, n-hexane, petroleum ether, and two in-house oils. Compared with SE, supercritical CO_2 extraction, and normal stirring extraction, MASE of artemisinin from *Artemisia annua* considerably reduced the processing time to 12 minutes and resulted in a 92.1% extraction rate (compared to several hours and 60% extraction yield obtained with Soxhlet) [50]. Later, Liu et al. applied the MASE for the isolation and quantification of artemisinin in comparison with the traditional protocols. MASE confirmed shorter extraction time necessity, reduced solvent consumption, and higher recovery of artemisinin than conventional procedures. The best extraction solvent was petroleum ether–acetone (4:1 v/v), because of the high solubility of artemisinin and adequate microwave energy absorption, at 50°C. The highest yield of artemisinin achieved was 0.55% in 30 minutes among all the extractive methods used [62].

Recently, Misra et al. developed a rapid and reliable MASE and HPTLC protocol for the analysis of artemisinin. The optimized MASE conditions required 100 mg of dried and grinded drug with a size of 14 mesh dispersed into 10 mL of toluene. The irradiation of the sample at 160 W for 120 seconds led to the extraction of 0.816% of the content of artemisinin.

Paclitaxel (**Figure 5**) is a member of the taxane class, and it is one of the most important anticancer drugs approved for human use against ovarian, breast, and pulmonary cancer.

Although the total synthesis of paclitaxel has been reported, its application for the commercial production of this drug is impracticable. Thus, paclitaxel is still produced by extraction from taxol biomass. The most commonly used methods for the extraction of paclitaxel require the use of methanol at ambient temperature, although other protocols requiring refluxing methanol, 1:1 methanol-chloroform at ambient temperature, and percolation using ethanol or 95% ethanol-water at ambient temperature have been reported. However, these methods require a long time (12–24 h) for a complete extraction. Incorvia-Mattina et al. reported for the first time in 1997 the use of MASE to optimize the efficiency of the extraction of paclitaxel. The effects of the biomass, solvent ratio and water content on taxane recovery were also determined. Under appropriate MASE conditions an extract equivalent to the one obtained by conventional extraction methods was produced [63].

Talebi et al. investigated the use of MASE to extract paclitaxel from the needles of *Taxus baccata L.* The extraction parameters were investigated resulting in 90% aq. MeOH as a solvent, a temperature of 95°C, 7 min of extraction time, and a closed-vessel system as the best performing extractive conditions [64].

Recently, another study for the extraction of paclitaxel from biomass through MASE and based on kinetic and thermodynamic analysis has been carried out. The

12

119

majority of paclitaxel was recovered from the biomass (~99%) within 6 min in a single cycle of microwave-assisted extraction at microwave powers of 50–150 W and temperatures of 30–45°C [64].

4.2.4 Phytocannabinoids

Cannabis sativa L. has always been considered a controversial plant due to its use as both medicine and illicit drug. Nevertheless, Cannabis is a good source of nutrients, fibers, and natural compounds thus, its industrial and pharmaceutical use is undoubtful. Cannabis produces a peculiar class of natural compounds, namely phytocannabinoids. The two most important and renowned phytocannabinoids are the cannabidiol derivatives (i.e. CBD, CBDV, CBDB, and CBDP) [65, 66] and the tetrahydrocannabinol derivatives (i.e. Δ^9-THC, Δ^9-THCV, Δ^9-THCB, and Δ^9-THCP) [66, 67] reported in **Figure 6**. Δ^9-THC is responsible for the recreational use of hemp and therefore its use is banished or tightly regulated by national governments.

CBD-like derivatives are non-psychotropic compounds but with other recognized pharmacological properties such as anti-inflammatory, antioxidant, and anticonvulsant. As an example, Epidiolex, a CBD-based anticonvulsant drug, has been approved in 2018 by Food and Drug Administration for the treatment of seizures associated with Lennox–Gastaut syndrome (LGS), Dravet syndrome, or tuberous sclerosis complex (TSC) in patients 1 year of age and older.

The discovery of a plethora of pharmacological activities ascribed to CBD and other minor phytocannabinoids has increased attention from both scientists and industries for medical, nutraceutical, and cosmetic applications of these cannabinoids.

Several synthetic procedures have been developed and optimized for the industrial preparations of phytocannabinoids and in particular of CBD. However, this process suffers from several drawbacks such as the cost of the starting materials, reagents and solvents, the formation of by-products with consequent cumbersome purification procedures, and the difficulty to control the stereochemistry, the isomerism of the terpenic double bond, and the easy interconversion of CDB into THCs in the synthetic conditions.

Thus, the extraction and purification of phytocannabinoids from *C. sativa* remain the preferred procedure for its cost-effectiveness. Besides, tight monitoring of the chemical consistency of the extracts results therefore mandatory in producing consistent and reliable medical cannabis preparations for human uses. Recently, Nahar et al. reviewed all the procedures adopted at the present for the extraction of naturally occurring phytocannabinoids [68].
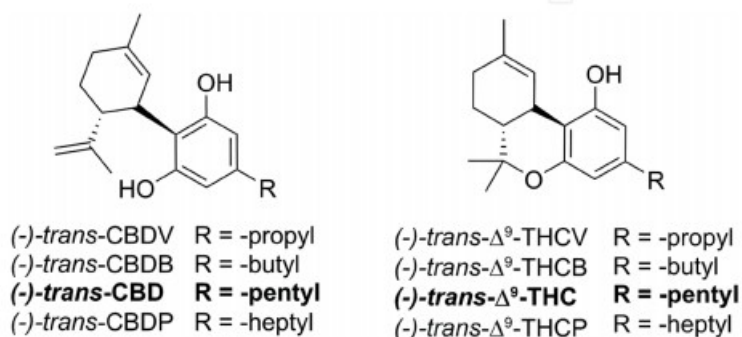

(-)-*trans*-CBDV   R = -propyl
(-)-*trans*-CBDB   R = -butyl
(-)-*trans*-CBD   R = -pentyl
(-)-*trans*-CBDP   R = -heptyl

(-)-*trans*-Δ^9-THCV   R = -propyl
(-)-*trans*-Δ^9-THCB   R = -butyl
(-)-*trans*-Δ^9-THC   R = -pentyl
(-)-*trans*-Δ^9-THCP   R = -heptyl

Figure 6.
Chemical structures of CBD-like and THC-like major phytocannabinoids present in C. sativa.

13

Focusing on MASE, Lewis-Bakekr et al. investigated the potential to directly extract and decarboxylate dried Cannabis material with the microwave reactor [69]. Dried plant material, suspended in ethanol, was subjected to heating with stirring in a microwave reactor at 150° C. Extraction yield for the concentrated resin was in the range of 19.6–24.4% and it resulted directly proportional to the heating time and dependent on the cultivar employed in the process. Interestingly, a complete decarboxylation of the phytocannabinoids was achieved in one step following this process and no acid forms of phytocannabinoids such as Δ^9-THCA and CBDA were detected in the resulting extract. Thus, MASE proves to be a worthy method for extraction and decarboxylation of phytocannabinoids due to the possibility to apply controlled temperatures and shorter extraction times. Moreover, this procedure ensures a more consistent and reproducible *Cannabis* extract with consequent reproducible efficacy of the therapeutic results. Kore et al. investigated and optimized the MASE process applied to *C. sativa* resulting in a patent application where they disclosed an improved method for extracting and decarboxylating cannabinoids from cannabis plant material, before, during, or after extraction [70]. MASE was compared to or used in tandem with other extraction strategies such as ultrasound extraction, SE, and supercritical fluid extraction.

The effect of time and temperature was investigated first. Extraction and decarboxylation of phytocannabinoid resulted in time and temperature dependence. To obtain 100% decarboxylation, the temperature must be sustained over a period without the burning of the cannabis material or the boiling/evaporation of the solvent. Because the solvent of choice is ethanol (b.p. 78°C at 1 atm), to reach a higher boiling temperature (i.e. 100–170°C) the extraction process must be carried out in a sealed vessel and under pressure. 170°C was the highest operative temperature achieved since higher temperatures (>180°C) resulted in the microwave run abortion due to the high pressure reached within the vial.

The extraction of cannabis by MASE at 100°C, 130°C, 150°C, and 170°C for 10 minutes resulted in a 23–25% yield of extract.

Interestingly, it appeared that the addition of a second step, such as SFE, after the MASE did not change the cannabinoid profile in the extract. Thus, MASE alone can perform an almost complete extraction of the cannabinoids from the cannabis plant material. Besides, the extraction and conversion of THCA and CBDA into THC and CBD was better at a temperature above 130°C, than at 100°C.

MASE was compared with the effectiveness of the commonly employed extractive procedure, namely maceration in ethanol, SE, and SFE. The conventional extractive procedures resulted in a low concentration of Δ^9-THC, THCA, and CBD, whereas the addition of the microwave step resulted in a significant increase in the concentration of CBD and THC. As expected, no THCA was detected.

To sum up, a worth general procedure for the extraction and decarboxylation of CBD and THC from cannabis plant material can be thus resumed: i) the drug is weighed and macerated in a mortar; ii) the grinded drug is charged in a microwave vial along with a stir bar; iii) the drug is submerged with ethanol and the vial is sealed; iv) the vial is irradiated with MW using the following conditions [a) Pre-stirring = 30 sec; b) run time = 10 min; c) temperature = 150°C; d) absorption = Normal]; v) the suspension is filtered, and the filtrate concentrated; iv) residual plant material may be subjected (but not necessarily) to SFE.

Drinic et al. extended these studies over other polyphenols and flavonoids as well as phytocannabinoids [71]. In particular, the effects of different extraction parameters, namely ethanol concentration, extraction time and solid/liquid ratio on extraction yield, total phenol content, total flavonoid content, antioxidant activity, reductive capacity, CBD content, and THC content were investigated. For MASE,

14

121

a domestic microwave oven and a round-bottom flask connected with a condenser were used. The solid drug was mixed with the solvent (30, 50, or 70% v/v ethanol) in the selected solid/liquid ratio (S/L = 5, 10, or 15). The extraction was performed irradiating at a potency of 580 W without agitation and for a total extraction time of 10, 20, or 30 min. The results of each extraction were analyzed using response surface methodology. The influence of the three process parameters was investigated on total polyphenols yield, total flavonoids yield, antioxidant activity, and reductive capacity as well. The optimal conditions for the highest CBD content and lowest THC content resulted in 47% ethanol concentration, 10 minutes of extraction time, and an S/L ratio of 5. The model was successfully validated by preparing the Cannabis extract under the calculated conditions.

Alongside the pharmaceutical uses of Cannabis extracts, hemp seeds are widely employed to produce hemp oil. However, the content of Δ^9-THC in the processed hemp seed oils must be under the limits imposed by the jurisdictions of each State. Indeed, although the hemp seeds produce negligible amounts of THC, their outer surface can be contaminated with the enriched in the phytocannabinoids resin secreted by the seeds' bracts. The presence of Δ^9-THC in the final hemp seed products had led to intoxication symptoms in the final consumers. Thus, nowadays the content of THC in hemp products is tightly regulated. Yang et al. investigated the effectiveness of various chemical procedures for the extraction of Δ^9-THC from three brands of hemp seeds and how the extractive methods could influence their commercialization [72]. Four extraction methods were employed, namely, i) microwave extraction, ii) sonication, iii) SE and iv) SFE. As already investigated by Kore et al., the extraction was performed in ethanol at 150°C with stirring, obtaining a complete conversion of CBDA and THCA into the corresponding neutral form. Hemp seeds were macerated in a mortar, transferred into a microwave vessel, and suspended in ethanol. The suspension was irradiated at 150°C with stirring for 20 min in a closed vessel. The yield of the resin (27–38%) achieved was comparable to the other three extraction procedures. In contrast, SE provided higher yields of Δ^9-THC and CBD than the other procedures, resulting in a more robust and appropriate extraction methodology for the testing of hemp seed products. Since the same solvent was used in all the compared extractions, the differences in the number of phytocannabinoids can be attributed to the extraction methods themselves. The results suggest that prolonged heating and solvent cycling in extracting phytocannabinoids from lipid-rich materials such as hemp seeds is mandatory.

5. Conclusion

MASE has rapidly risen during the latest decades as a method for the extraction of secondary metabolites or compounds of pharmaceutical and nutraceutical interest. The use of microwave can generate peculiar, and otherwise impossible to reach extraction mechanisms. As a result, a reduction of the extraction time, improvement of the extraction efficiency, high reproducibility, and robustness of the procedure can be achieved. An increase of the sample throughput is in addition possible, thus it can be considered as the elective technique when a high number of samples have to be processed specially during the first stage of the NADD process, and for evaluating the quality of the natural matrices [9, 29]. For these reasons, MASE has proven to be effective in all aspects, including economical and practical, compared to traditional extraction techniques, especially over SE. Conversely, in MASE the development of the method must be carefully assessed, and all the variables and factors described above must be thoroughly considered to provide some extraction selectivity. Hence,

15

DoE, response surface methodology, and other statistical approaches are of great help to quickly determine the best conditions to achieve the highest yield of the metabolite of interest from the natural source. However, in the past year, the application of MASE in scalable industrial processes has always encountered several limitation due to the presence of some technological barriers, mainly related to the design of safe instrumentation. Thanks to the technological progress witnessed in recent years, the first industrial-scale ovens finally became commercially available [73, 74].

Food, pharmaceutical, and nutraceutical industries would be benefited from this emerging technology of MASE, which is an excellent substitute for traditional methods such as SE, and other environmentally benign technologies. The promise to be the technique that can respond to the necessities in this field will make MASE the extraction method of choice for the next years.

Conflict of interest

The authors declare no conflict of interest.

Author details

Valeria Cavalloro[1], Emanuela Martino[1], Pasquale Linciano[2] and Simona Collina[2*]

1 Department of Earth and Environmental Science, University of Pavia, Pavia, Italy

2 Department of Drug Science, University of Pavia, Pavia, Italy

*Address all correspondence to: simona.collina@unipv.it

IntechOpen

16

Microwave-Assisted Solid Extraction from Natural Matrices
DOI: http://dx.doi.org/10.5772/intechopen.95440

References

[1] Medina-Franco JL. Discovery and Development of Lead Compounds from Natural Sources Using Computational Approaches. In: Evidence-Based Validation of Herbal Medicine. Elsevier; 2015. p. 455-475.

[2] Newman DJ, Cragg GM. Natural Products as Sources of New Drugs over the Nearly Four Decades from 01/1981 to 09/2019. J Nat Prod. 2020 Mar;83(3):770-803.

[3] Herbal Medicine Market Value to Surpass USD 129 Billion Revenue Mark by 2023 at 5.88% CAGR, Predicts Market Research Future. Market Research Future GlobeNewswire. 2019.

[4] Hert J, Irwin JJ, Laggner C, Keiser MJ, Shoichet BK. Quantifying Biogenic Bias in Screening Libraries. Nat Chem Biol. 2009;5(7):479-83.

[5] Popovici V, Bucur LA, Schröder V, Gherghel D, Mihai CT, Caraiane A, et al. Evaluation of the Cytotoxic Activity of the Usnea barbata (L.) F. H. Wigg Dry Extract. Molecules. 2020 Apr;25(8):1865.

[6] Freysdottir J, Omarsdottir S, Ingólfsdóttir K, Vikingsson A, Olafsdottir ES. In vitro and in vivo immunomodulating effects of traditionally prepared extract and purified compounds from *Cetraria islandica*. Int Immunopharmacol. 2008;

[7] McCauley EP, Piña IC, Thompson AD, Bashir K, Weinberg M, Kurz SL, et al. Highlights of marine natural products having parallel scaffolds found from marine-derived bacteria, sponges, and tunicates. J Antibiot (Tokyo). 2020 Aug;73(8):504-25.

[8] Verpoorte R, van der Heijden R, Memelink J. Engineering the plant cell factory for secondary metabolite production. Transgenic Res. 2000;9(4-5):323-43; discussion 321.

[9] Martino E, Della Volpe S, Cavalloro V, Amri B, Kaab LBB, Marrubini G, et al. The use of a microwave-assisted solvent extraction coupled with HPLC-UV/PAD to assess the quality of *Marrubium vulgare* L. (white horehound) herbal raw material. Phytochem Anal. 2019;30(4).

[10] Borges A, José H, Homem V, Simões M. Comparison of Techniques and Solvents on the Antimicrobial and Antioxidant Potential of Extracts from *Acacia dealbata* and *Olea europaea*. Antibiotics. 2020 Jan;9(2):48.

[11] Zhang Q-W, Lin L-G, Ye W-C. Techniques for extraction and isolation of natural products: a comprehensive review. Chin Med. 2018 Dec;13(1):20.

[12] Li Y, Fabiano-Tixier AS, Vian MA, Chemat F. Solvent-free microwave extractionof bioactive compounds providesa tool for green analytical chemistry. Trends Anal Chem. 2013;47:1-11.

[13] Vinatoru M, Mason TJ, Calinescu I. Trends in Analytical Chemistry Ultrasonically assisted extraction (UAE) and microwave assisted extraction (MAE) of functional compounds from plant materials. Trends Anal Chem. 2017;97:159-78.

[14] Xue H, Xu H, Wang X, Shen L, Liu H, Liu C, et al. Effects of Microwave Power on Extraction Kinetic of Anthocyanin from Blueberry Powder considering Absorption of Microwave Energy. 2018;2018.

[15] Vats T, Mishra A. Sustainable Syntheses with Microwave Irradiation. Encycl Inorg Bioinorg Chem. 2016;

[16] Marco B, Agnese C, Giuseppe T. Quality Preservation and Cost

17

Effectiveness in the Extraction of Nutraceutically-Relevant Fractions from Microbial and Vegetal Matrices. In: Scientific, Health and Social Aspects of the Food Industry. InTech; 2012.

[17] Chan C-H, Yusoff R, Ngoh G-C, Kung FW-L. Microwave-assisted extractions of active ingredients from plants. J Chromatogr A. 2011 Sep;1218(37):6213-25.

[18] Ibrahim NA, Zaini MAA. Solvent selection in microwave assisted extraction of castor oil. Chem Eng Trans. 2017;56:865-70.

[19] Xu W, Chu K, Li H, Zhang Y, Zheng H, Chen R, et al. Ionic Liquid-Based Microwave-Assisted Extraction of Flavonoids from Bauhinia championii (Benth.) Benth. Molecules. 2012 Dec;17(12):14323-35.

[20] Du F-Y, Xiao X-H, Xu P-P, Li G-K. Ionic liquid-based microwave-assisted extraction and HPLC analysis of dehydrocavidine in corydalis saxicola Bunting. Acta Chromatogr [Internet]. 2010 Sep;22(3):459-71. Available from: https://akjournals.com/doi/10.1556/achrom.22.2010.3.9

[21] Vigani B, Rossi S, Gentile M, Sandri G, Bonferoni MC, Cavalloro V, et al. Development of a mucoadhesive and an in situ gelling formulation based on κ-carrageenan for application on oral mucosa and esophagus walls. II. Loading of a bioactive hydroalcoholic extract. Mar Drugs. 2019;17(3).

[22] Martino E, Ramaiola I, Urbano M, Bracco F, Collina S. Microwave-assisted extraction of coumarin and related compounds from *Melilotus officinalis* (L.) Pallas as an alternative to Soxhlet and ultrasound-assisted extraction. J Chromatogr A. 2006 Sep;1125(2):147-51.

[23] Xue H, Xu H, Wang X, Shen L, Liu H, Liu C, et al. Effects of Microwave Power on Extraction Kinetic of Anthocyanin from Blueberry Powder considering Absorption of Microwave Energy. J Food Qual. 2018;2018:1-13.

[24] Routray W, Orsat V. Microwave-Assisted Extraction of Flavonoids: A Review. Food Bioprocess Technol. 2012 Feb;5(2):409-24.

[25] Pimentel-Moral S, Borrás-Linares I, Lozano-Sánchez J, Arráez-Román D, Martínez-Férez A, Segura-Carretero A. Microwave-assisted extraction for *Hibiscus sabdariffa* bioactive compounds. J Pharm Biomed Anal. 2018 Jul;156:313-22.

[26] N. Politis S, Colombo P, Colombo G, M. Rekkas D. Design of experiments (DoE) in pharmaceutical development. Drug Dev Ind Pharm [Internet]. 2017 Jun 3;43(6):889-901. Available from: https://www.tandfonline.com/doi/full/10.1080/03639045.2017.1291672

[27] Camel V. Microwave-assisted solvent extraction of environmental samples. TrAC Trends Anal Chem [Internet]. 2000 Apr;19(4):229-48. Available from: https://linkinghub.elsevier.com/retrieve/pii/S0165993699001855

[28] Sanchez-Prado L, Garcia-Jares C, Dagnac T, Llompart M. Microwave-assisted extraction of emerging pollutants in environmental and biological samples before chromatographic determination. TrAC Trends Anal Chem [Internet]. 2015 Sep;71:119-43. Available from: https://linkinghub.elsevier.com/retrieve/pii/S0165993615001442

[29] Granata MU, Bracco F, Catoni R, Cavalloro V, Martino E. Secondary metabolites profile and physiological leaf traits in wild and cultivated *Corylus avellana* under different nutritional status. Nat Prod Res. 2019 Oct;1-8.

[30] Martino E, Collina S, Rossi D, Bazzoni D, Gaggeri R, Bracco F, et al.

18

Influence of the extraction mode on the yield of hyperoside, vitexin and vitexin-2''- O -rhamnoside from *Crataegus monogyna* Jacq. (hawthorn). Phytochem Anal. 2008 Nov;19(6):534-40.

[31] He M, Min J-W, Kong W-L, He X-H, Li J-X, Peng B-W. A review on the pharmacological effects of vitexin and isovitexin. Fitoterapia [Internet]. 2016 Dec;115:74-85. Available from: https://linkinghub.elsevier.com/retrieve/pii/S0367326X16304488

[32] Tang X, Zhu D, Huai W, Zhang W, Fu C, Xie X, et al. Simultaneous extraction and separation of flavonoids and alkaloids from Crotalaria sessiliflora L. by microwave-assisted cloud-point extraction. Sep Purif Technol [Internet]. 2017 Mar;175:266-73. Available from: https://linkinghub.elsevier.com/retrieve/pii/S1383586616307110

[33] Madej K. Microwave-assisted and cloud-point extraction in determination of drugs and other bioactive compounds. TrAC Trends Anal Chem. 2009 Apr;28(4):436-46.

[34] Belwal T, Pandey A, Bhatt ID, Rawal RS. Optimized microwave assisted extraction (MAE) of alkaloids and polyphenols from Berberis roots using multiple-component analysis. Sci Rep [Internet]. 2020 Dec 22;10(1):917. Available from: http://www.nature.com/articles/s41598-020-57585-8

[35] Pellati F, Benvenuti S. Determination of ephedrine alkaloids in Ephedra natural products using HPLC on a pentafluorophenylpropyl stationary phase. J Pharm Biomed Anal. 2008 Sep;48(2):254-63.

[36] Brachet A, Christen P, Veuthey J-L. Focused microwave-assisted extraction of cocaine and benzoylecgonine from coca leaves. Phytochem Anal. 2002 May;13(3):162-9.

[37] Nowak J, Woźniakiewicz M, Klepacki P, Sowa A, Kościelniak P. Identification and determination of ergot alkaloids in Morning Glory cultivars. Anal Bioanal Chem. 2016 May;408(12):3093-102.

[38] Petruczynik A. Analysis of alkaloids from different chemical groups by different liquid chromatography methods. Open Chem [Internet]. 2012 Jun 1;10(3):802-35. Available from: https://www.degruyter.com/view/journals/chem/10/3/article-p802.xml

[39] Xie D-T, Wang Y-Q, Kang Y, Hu Q-F, Su N-Y, Huang J-M, et al. Microwave-assisted extraction of bioactive alkaloids from Stephania sinica. Sep Purif Technol. 2014 Jun;130:173-81.

[40] Ganesapillai M, Singh A, Subba Rao B, De D, Juneja U. EXTRACTION OF ALKALOIDS FROM MICROWAVE DRIED ADATHODA VASICA LEAVES - A COMPARATIVE STUDY. Int J Pharma Bio Sci. 2015;6(1):121-39.

[41] Pan X, Niu G, Liu H. Microwave-assisted extraction of tea polyphenols and tea caffeine from green tea leaves. Chem Eng Process Process Intensif [Internet]. 2003 Feb;42(2):129-33. Available from: https://linkinghub.elsevier.com/retrieve/pii/S0255270102000375

[42] Xiong W, Chen X, Lv G, Hu D, Zhao J, Li S. Optimization of microwave-assisted extraction of bioactive alkaloids from lotus plumule using response surface methodology. J Pharm Anal. 2016 Dec;6(6):382-8.

[43] Zhou S, Wu X, Huang Y, Xie X, Lin Y, Fan H, et al. Microwave-assisted aqueous two-phase extraction of alkaloids from Radix Sophorae Tonkinensis with an ethanol/Na2HPO4 system: Process optimization, composition identification and quantification analysis. Ind Crops Prod. 2018 Oct;122:316-28.

19

Microwave Heating - Electromagnetic Fields Causing Thermal and Non-Thermal Effects

[44] Fernández P, Lago M, Lorenzo RA, Carro AM, Bermejo AM, Tabernero MJ. Microwave assisted extraction of drugs of abuse from human urine. J Appl Toxicol [Internet]. 2007 Jul;27(4):373-9. Available from: http://doi.wiley.com/10.1002/jat.1216

[45] Fernández P, Lago M, Lorenzo RA, Carro AM, Bermejo AM, Tabernero MJ. Optimization of a rapid microwave-assisted extraction method for the simultaneous determination of opiates, cocaine and their metabolites in human hair. J Chromatogr B [Internet]. 2009 Jun;877(18-19):1743-50. Available from: https://linkinghub.elsevier.com/retrieve/pii/S1570023209003055

[46] Fernández P, Seoane S, Vázquez C, Bermejo AM, Carro AM, Lorenzo RA. A rapid analytical method based on microwave-assisted extraction for the determination of drugs of abuse in vitreous humor. Anal Bioanal Chem [Internet]. 2011 Oct 7;401(7):2177-86. Available from: http://link.springer.com/10.1007/s00216-011-5279-6

[47] Rimando AM, Kalt W, Magee JB, Dewey J, Ballington JR. Resveratrol, Pterostilbene, and Piceatannol in Vaccinium Berries. J Agric Food Chem. 2004 Jul;52(15):4713-9.

[48] Kim H-K, Do J-R, Lim T-S, Akram K, Yoon S-R, Kwon J-H. Optimisation of microwave-assisted extraction for functional properties of Vitis coignetiae extract by response surface methodology. J Sci Food Agric. 2012 Jun;92(8):1780-5.

[49] Piñeiro Z, Marrufo-Curtido A, Vela C, Palma M. Microwave-assisted extraction of stilbenes from woody vine material. Food Bioprod Process. 2017 May;103:18-26.

[50] Hao J, Han W, Huang S, Xue B, Deng X. Microwave-assisted extraction of artemisinin from *Artemisia annua* L. Sep Purif Technol. 2002 Sep;28(3):191-6.

[51] Giampietro L, Angelo AD, Giancristofaro A, Ammazzalorso A, Filippis B De, Matteo M Di, et al. Effect of Stilbene and Chalcone Scaffolds Incorporation in Clofibric Acid on PPAR Agonistic Activity. Med Chem (Los Angeles). 2014;10:59-65.

[52] De Filippis B, Linciano P, Ammazzalorso A, Di Giovanni C, Fantacuzzi M, Giampietro L, et al. Structural development studies of PPARs ligands based on tyrosine scaffold. Eur J Med Chem. 2015;89:817-25.

[53] Mei Y-Z, Liu R-X, Wang D-P, Wang X, Dai C-C. Biocatalysis and biotransformation of resveratrol in microorganisms. Biotechnol Lett. 2015 Jan;37(1):9-18.

[54] Quideau S, Deffieux D, Douat-Casassus C, Pouységu L. Plant Polyphenols: Chemical Properties, Biological Activities, and Synthesis. Angew Chemie Int Ed. 2011 Jan;50(3):586-621.

[55] Saraswati S. Velu, Noel F. Thomas, Jean-Frederic F. Weber. Strategies and Methods for the Syntheses of Natural Oligomeric Stilbenoids and Analogues. Curr Org Chem. 2012 Apr;16(5):605-62.

[56] Donnez D, Jeandet P, Clément C, Courot E. Bioproduction of resveratrol and stilbene derivatives by plant cells and microorganisms. Trends Biotechnol. 2009 Dec;27(12):706-13.

[57] Nopo-Olazabal C, Hubstenberger J, Nopo-Olazabal L, Medina-Bolivar F. Antioxidant Activity of Selected Stilbenoids and Their Bioproduction in Hairy Root Cultures of Muscadine Grape (*Vitis rotundifolia* Michx.). J Agric Food Chem. 2013 Dec;61(48):11744-58.

20

[58] Almagro L, Belchí-Navarro S, Sabater-Jara AB, Vera-Urbina JC, Sellés-Marchart S, Bru R, et al. Bioproduction of trans-Resveratrol from Grapevine Cell Cultures. In: Natural Products. Berlin, Heidelberg: Springer Berlin Heidelberg; 2013. p. 1683-713.

[59] Garcia L, Garcia R, Pacheco G, Sutili F, Souza R De, Mansur E, et al. Optimized Extraction of Resveratrol from Arachis repens Handro by Ultrasound and Microwave: A Correlation Study with the Antioxidant Properties and Phenol Contents. Sci World J. 2016;2016:1-10.

[60] Dang Y-Y, Zhang H, Xiu Z-L. Microwave-assisted aqueous two-phase extraction of phenolics from grape (*Vitis vinifera*) seed. J Chem Technol Biotechnol. 2014 Oct;89(10):1576-81.

[61] Kim J-S, Ha T-Y, Ahn J, Kim H-K, Kim S. Pterostilbene from Vitis coignetiae protect H2O2-induced inhibition of gap junctional intercellular communication in rat liver cell line. Food Chem Toxicol. 2009 Feb;47(2):404-9.

[62] Liu C-Z, Zhou H-Y, Zhao Y. An effective method for fast determination of artemisinin in *Artemisia annua* L. by high performance liquid chromatography with evaporative light scattering detection. Anal Chim Acta. 2007 Jan;581(2):298-302.

[63] Mattina MJI, Berger WAI, Denson CL. Microwave-Assisted Extraction of Taxanes from Taxus Biomass. J Agric Food Chem. 1997 Dec;45(12):4691-6.

[64] Lee S-H, Kim J-H. Kinetic and thermodynamic characteristics of microwave-assisted extraction for the recovery of paclitaxel from Taxus chinensis. Process Biochem. 2019 Jan;76:187-93.

[65] Citti C, Linciano P, Forni F, Vandelli MA, Gigli G, Laganà A, et al. Analysis of impurities of cannabidiol from hemp. Isolation, characterization and synthesis of cannabidibutol, the novel cannabidiol butyl analog. J Pharm Biomed Anal. 2019;175.

[66] Linciano P, Citti C, Luongo L, Belardo C, Maione S, Vandelli MA, et al. Isolation of a High-Affinity Cannabinoid for the Human CB1 Receptor from a Medicinal *Cannabis sativa* Variety: Δ9-Tetrahydrocannabutol, the Butyl Homologue of Δ9-Tetrahydrocannabinol. J Nat Prod. 2020;83(1):88-98.

[67] Citti C, Linciano P, Russo F, Luongo L, Iannotta M, Maione S, et al. A novel phytocannabinoid isolated from *Cannabis sativa* L. with an in vivo cannabimimetic activity higher than Δ9-tetrahydrocannabinol: Δ9-Tetrahydrocannabiphorol. Sci Rep. 2019;9(1):1-13.

[68] Nahar L, Uddin SJ, Alam MA, Sarker SD. Extraction of naturally occurring cannabinoids: an update. Phytochem Anal. 2020 Sep;pca.2987.

[69] Lewis-Bakker MM, Yang Y, Vyawahare R, Kotra LP. Extractions of Medical Cannabis Cultivars and the Role of Decarboxylation in Optimal Receptor Responses. Cannabis Cannabinoid Res. 2019 Sep;4(3):183-94.

[70] Kotra LP, Lewis MM, Wasilewski E, Grover H. Decarboxylated Cannabis Resins, Uses Thereof and Methods of Making Same. WO/2018/000094, 2018.

[71] Drinić Z, Vladić J, Koren A, Zeremski T, Stojanov N, Kiprovski B, et al. Microwave-assisted extraction of cannabinoids and antioxidants from *Cannabis sativa* aerial parts and process modeling. J Chem Technol Biotechnol. 2020 Mar;95(3):831-9.

21

Microwave Heating - Electromagnetic Fields Causing Thermal and Non-Thermal Effects

[72] Yang Y, Lewis MM, Bello AM, Wasilewski E, Clarke HA, Kotra LP. Cannabis sativa (Hemp) Seeds, Δ 9 -Tetrahydrocannabinol, and Potential Overdose. Cannabis Cannabinoid Res. 2017 Jan;2(1):274-81.

[73] Li Y, Radoiu M, Fabiano-Tixier A-S, Chemat F. From Laboratory to Industry: Scale-Up, Quality, and Safety Consideration for Microwave-Assisted Extraction. In 2012. p. 207-29.

[74] Périno S, Pierson JT, Ruiz K, Cravotto G, Chemat F. Laboratory to pilot scale: Microwave extraction for polyphenols lettuce. Food Chem. 2016;204:108-14.

22

Paper 2

Reprinted with permission from Emanuela Martino, Mirko Umbero Granata, Rosangela Catoni, Valeria Cavalloro, and Francesco Bracco *Natural product research* **Article accepted**

New insight into pectin effects on mesophyll conductance in four species of deciduous forest

Emanuela Martino, Granata Mirko U*, Rosangela Catoni, Valeria Cavalloro, Francesco Bracco
University of Pavia, Department of Earth and Environmental Sciences, Via S. Epifanio 14, 27100 Pavia, Italy

Granata Mirko Umberto* corresponding author, e-mail: mirkoumberto.granata@unipv.it; ORCID 0000-0002-5234-2163

Francesco Bracco: francesco.bracco@unipv.it ORCID: 0000-0003-1921-2137
Rosangela Catoni: rosangela.catoni@unipv.it, ORCID: 0000-0002-9613-7137
Valeria Cavalloro: valeria.cavalloro01@universitadipavia.it, ORCID: 0000-0002-9759-5148
Emanuela Martino: emanuela.martino@unipv.it ORCID: 0000-0001-9591-4996

Abstract

The amount of pectin in the cell wall is considered a critical element regulating cell wall porosity. Thus, it is likely to influence the diffusional processes particularly that from the substomatal cavities to the carboxylation sites in the chloroplast stroma (*i.e.* mesophyll conductance, g_m). We analyzed in four deciduous species *(Acer campestre, Crateaugus monogyna, Corylus avellana, Quercus robur)* the correlation between pectin and g_m in two phase of leaves development (*i.e.* mature green leaves and senescent leaves). Results showed that in *A. campestre*, *C. monogyna* and *Q. robur* to higher value of pectin in mature green leaves corresponded the higher g_m value. Taking into account this result, we can assume that a higher amount of pectins is associated to an increased cell wall hydrophilicity and elasticity, thus increasing g_m because CO_2 molecules cross the wall dissolved in water. An opposite behavior was observed in *C. avellana*.

Keywords: cell wall, deciduous species, extraction, mesophyll conductance, leaf development, pectin

1. Introduction

Diffusional processes starting from the atmosphere to the sites where biochemical processes occur affect the complex phenomenon of photosynthesis (Clemente-Moreno et al. 2019). The first process, stomatal conductance (g_s), consists of the CO_2 pathway from the atmosphere to the substomatal cavities and the second one, mesophyll conductance (g_m), from here to the carboxylation sites in the chloroplast stroma (Evans et al. 2009; Catoni et al. 2020). Along these steps, anatomical parameters like chloroplast distribution and cell wall thickness are recognized as the most important limitation to CO_2 diffusion through the mesophyll (Peguero-Pina et al. 2017). In particular, cell wall resistance to CO_2 diffusion may depend on at least three physical wall properties: thickness, tortuosity and porosity (Evans et al. 2009). The last one regulates the apoplastic cellular exchange of macromolecules, small metabolites, water and gas (*i.e.* CO_2) (Rondeau-Mouro et al. 2008). Cell wall is composed mainly of polysaccharides (*i.e.* cellulose, hemicellulose, pectin) which contribute up to 90% of cell wall components (Minic and Jouanin 2006). Among polysaccharides, pectin is considered a critical element that controls cell wall elasticity and expansion and is known to regulate porosity (Weraduwage et al. 2016). Pectins are considered one of the most complex natural macromolecules, they are composed by segments of galacturonic acids more or less methyl- and acetyl-esterified (homogalacturonan, HG), by alternating galacturonic acid and rhamnose residues (rhamnogalacturonan I, RGI) branched with side chains of neutral sugars (galactans, arabinans and arabinogalactans) and by HG ramified by complex side chains (type II rhamnogalacturonan, RGII) (Vincken et al. 2003). Both galactan and arabinan side chains on RGI have been proposed to control the cell wall porosity (Forster et al.

133

1
2
3
4
5
6
7
8
9
10
11
12
13
14
15
16
17
18
19
20
21
22
23
24
25
26
27
28
29
30
31
32
33
34
35
36
37
38
39
40
41
42
43
44
45
46
47
48
49
50
51
52
53
54
55
56
57
58
59
60

1996). In particular, in the cell wall, unesterified galacturonic acids in HG interact with calcium and apiose in RGII side chains complexes borate and calcium (Fleischer et al. 1999) to interconnect pectins and create a porous network. Thus, taking into account that the fine chemistry of these networks varies between species and at different leaves development phases (Yokoyama 2020) and, above all, considering the pectin effect on cell wall porosity, the main object of the present work was to analyse the correlation between pectins and mesophyll conductance during leaf development (*i.e.* mature green leaves (IP) *vs* senescent leaves (IIP)) in four dicotyledonous deciduous species (*i.e. Acer campestre* L., *Corylus avellana* L., *Crataegus monogyna* Jacq. and *Quercus robur* L.)

2. Results and Discussion

As regard the methodological aspect the amount of pectin can be significatively affected by the activity of pectinase. For this reason and driven by literature evidences (Zarei et al. 2017), these enzymes were inactivated before extraction by irradiating the powdered natural matrices with microwaves. During this step, the matrices were humified to allow a better efficiency of the system, being water able to absorb these irradiations with good efficiency. After this treatment and adapting literature procedures (Sun et al. 2020), the dried powder was extracted via maceration with acidic water for 2 h, the extracts were diluted with two volumes of ethanol and then kept at 4°C overnight. Finally, pectins were divided from the supernatant by centrifugation, dried and weighted to evaluate the final yield (expressed as mg of dried pectin per gram of dried matrix) Finally, all the pectins were analyzed via Fourier-transform infrared (FTIR) spectroscopy, with the FTIR spectra showing good match with the spectrum of standard (Giusto Faravelli, Milan, Italy) (Figure S1). Spectra showed characteristic peaks at 3301.5, 2912.0, 1727.9 and 1010.9 cm^{-1} corresponding, respectively, to –OH, –CH, C=O of ester and acid, and –COC– stretching of the galactouronic acid.

Overall, the results show a significant variation ($p<0.05$) among the considered species in the pectin amount in the cell wall and between the considered phases (Figure S2). A close correlation was observed between pectin and mesophyll conductance. In fact, cell wall porosity in higher plants is known to be regulated by cell wall composition, particularly by pectins (Rondeau-Mouro et al., 2008), but little information is available for its direct effect on CO_2 diffusion. The correlation between g_m and pectin was confirmed by the simple regression analysis between these two variables (Figure S3). We found significantly correlation in all the species, with an average value of 80% of g_m variations (mean value of the four determinations coefficient) dependent on pectin variations. Pectins are hydrophilic compounds with important capacities to retain water within the cell wall, altering its porosity, permeability and enzyme activity (Panchev et al. 2010), and, a major issue that could significantly affect the diffusion of CO_2 through the cell wall. In particular, in three of the considered species (*A. campestre, C. monogyna* and *Q. robur*) we found that at higher value of pectin corresponded higher g_m value (*i.e.* positive slope in g_m *vs* pectin), so we can assume that a higher fraction of pectins resulted in increased cell wall hydrophilicity and elasticity, thus increasing g_m because CO_2 molecules cross the wall dissolved in water according to Carriquí et al. (2020). However, a different behaviour was observed in *C. avellana* with the simple regression showing a strongly and negative correlation (g_m = - 2.9123 pectin+ 3.9305, R^2 = 0.88) according to the results of Clemente-Moreno et al. 2020 for tobacco plants. Nevertheless, the different behaviour of *C. avellana*, compared to other species, may be subject to further analysis about the pectins trend during the seasons. It is possible to hypothesize a different leaf management during senescence that allow the exploitation of the leaf structures up to the complete leaf abscission. Indeed, hazel is not new to this different type of behaviour in senescence as we previously noted with regard to stomatal conductance (Catoni et al. 2015).

134

1
2
3
4
5
6
7
8
9
10
11
12
13
14
15
16
17
18
19
20
21
22
23
24
25
26
27
28
29
30
31
32
33
34
35
36
37
38
39
40
41
42
43
44
45
46
47
48
49
50
51
52
53
54
55
56
57
58
59
60

In conclusion, the present study showed evidence for a correlation between pectin fraction and mesophyll CO_2 diffusion resistance in an interspecific comparison in four deciduous species. Nevertheless, due to the close relationship between g_m and ETR (electron transport rates) (mean R^2 g_m vs ETR = 0.84) and the correlation between ETR with changes in pectin amount in the cell wall as shown in Figure S4, more studies are required to better infer the exclusive relationship between gm and pectin during the leaf development. Anyway, the results represented an advance in the understanding the mechanisms that regulated g_m, confirming the existence of a general role of pectin proportion in setting effective CO_2 diffusivity in mesophyll.

Acknowledgments

Disclosure statement

No potential conflict of interest was reported by the authors.

References

Carriquí M, Cabrera H, Conesa M, Coopman R, Douthe C, Gago J, Galle A, Galmes J, Ribas-Carbo M, Tomas M. 2015. Diffusional limitations explain the lower photosynthetic capacity of ferns as compared with angiosperms in a common garden study. Plant Cell Environ. 38: 448–460

Catoni R, Granata MU, Sartori F, Varone L, Gratani L. 2015. *Corylus avellana* responsiveness to light variations: morphological, anatomical, and physiological leaf trait plasticity. Photosynthetica 53(1): 35–46

Catoni R, Bracco F, Granata MU, 2020. Analysis of mesophyll conductance in five understory herbaceous species. Physiol Mol Biol Plants 26(2): 261–270.

Clemente-Moreno MJ, Gago J, Diaz-Vivancos P, Bernal A, Miedes E, Bresta P, Liakopoulos G, Fernie AR, Hernandez JA, Flexas J. 2019. The apoplastic antioxidant system and altered cell wall dynamics influence mesophyll conductance and the rate of photosynthesis. Plant J. 99(6): 1031–1046.

Evans JR, Kaldenhoff R, Genty B, Terashima I. 2009. Resistances along the CO_2 diffusion pathway inside leaves. J Exp Bot. 60: 2235–2248.

Fleischer A, O'Neill MA, Ehwald R. 1999. The pore size of nongraminaceous plant cell walls is rapidly decreased by borate ester cross-linking of the pectic polysaccharide rhamnogalacturonan II. Plant Physiol. 121: 829–838

Foster TJ, Ablett S, McCann MC, Gidley MJ. 1996. Mobility resolved C-13 NMR spectroscopy of primary plant cell walls. Biopolymers 39: 51–66.

Minic Z, Jouanin L. 2006. Plant glycoside hydrolases involved in cell wall polysaccharide degradation. Plant Physiol Bioch. 44: 435–449.

Panchev IN, Slavov A, Nikolova Kr, Kovacheva D. 2010. On the water-sorption properties of pectin. Food Hydrocoll. 24(8): 763–769.

Peguero-Pina JJ, Siso S, Flexas, J, Galmes J, Niinemets Ü, Sancho-Knapik D, Gil-Pelegrín E. 2017. Coordinated modifications in mesophyll conductance, photosynthetic potentials and leaf nitrogen contribute to explain the large variation in foliage net assimilation rates across *Quercus ilex* provenances. Tree Physiol. 37: 1084–1094.

Rondeau-Mouro C, Defer D, Leboeuf E, Lahaye M. 2008. Assessment of cell wall porosity in *Arabidopsis thaliana* by NMR spectroscopy. Int J Biol Macromol. 42: 83–92

135

Sun D, Chen X, Zhu C. 2020. Physicochemical properties and antioxidant activity of pectin from hawthorn wine pomace: A comparison of different extraction methods. Int J Biol Macromol 158: 1239–1247.

Vincken J-P, Schols HA, Oomen RJFJ, McCann MC, Ulvskov P, Voragen AGJ, Richard G.F. Visser RGF. 2003. If homogalacturonan were a side chain of rhamnogalacturonan I. Implications for cell wall architecture. Plant Physiol. 132: 1781–1789.

Weraduwage SM, Kim S-J, Renna L, Anozie FC, Sharkey TD, Brandizzi F. 2016. Pectin methylesterification impacts the relationship between photosynthesis and plant growth. Plant Physiol 171: 833–848.

Yokoyama R. 2020. A genomic perspective on the evolutionary diversity of the plant cell wall. Plants 9(9): 1195.

Zarei M, Ahmadi Zenouz A, Saari N, Ghanbari R, Nikkhah M, Vaziri M. 2017. Effect of microwave-assisted extraction on the yield and quality of apple pomace and lemon peel pectins IFRJ 24(6): 2402–2407.
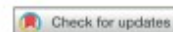
136

Paper 3

Reprinted with permission from Mirko Umbero Granata, Francesco Bracco, Rosangela Catoni, Valeria Cavalloro, and Emanuela Martino, *Natural product research* **2021** *https://doi.org/10.1080/14786419.2019.1682577*

Copyright 2021 Taylor and Francis group

Taylor & Francis
Taylor & Francis Group

SHORT COMMUNICATION

Check for updates

Secondary metabolites profile and physiological leaf traits in wild and cultivated *Corylus avellana* under different nutritional *status*

Mirko Umberto Granata, Francesco Bracco, Rosangela Catoni, Valeria Cavalloro and Emanuela Martino

Department of Earth and Environmental Sciences, University of Pavia, Pavia, Italy

ABSTRACT

Leaf secondary metabolites production and physiological leaf traits were analyzed in *Corylus avellana* wild type (WT) and *cultivar* (*cv.* 'Tonda Gentile Trilobata', TGT) under different nutrient supplies. Three treatments were applied: control treatment with no fertilizer supply (WT$_C$ and TGT$_C$), low nutrient treatment (WT$_{LN}$ and TGT$_{LN}$) and high nutrient treatment (WT$_{HN}$ and TGT$_{HN}$). The analysis of leaf extracts showed a higher concentration of Quercitrin and Myricitrin, with the highest concentrations of both the compounds in WT than TGT. This result can be related to the ecological role of flavonoids, including also antimicrobial properties, which resulted more useful in the understory forest form which hazelnut wild type originates. Therefore, their lower concentration in TGT can be relate to the genetic background of TGT *cultivar* with a lesser intrinsic need to produce such compounds and justified by a usual growth under more controlled environmental conditions, including also pest and disease control.
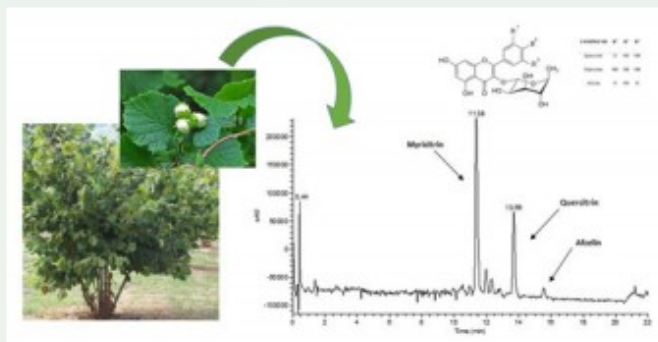
1. Introduction

Corylus avellana L. (hazelnut) is one of the major world's nut crops with a highly positive economic impact. Thus, an appropriate fertilizing program is necessary in order to obtain high yield and high quality in hazelnut (Özenç et al. 2014), affecting also metabolites production and the resistance against pests and diseases (Amtmann et al. 2008). Particularly, several studies show a close relationship between nutrient availability and resources allocation to the production of secondary metabolites (Stark et al. 2007), based on a mutual control between nutritional *status* and metabolic pathways (Amtmann et al. 2008). Secondary metabolites are compounds not directly involved in metabolic process like growth and development, but they are important for plant interaction with the environment in term of adaptation and defense (Ramakrishna and Ravishankar 2011). Beside the survival functions for producing plants, secondary metabolites are also able to set off physiological and pharmacological effects within other living organisms (Martino et al. 2019). In this context, aim of our study was to analyze the effects of different fertilizer supply (NPK fertilizer) at the physiological level and on the secondary metabolites production in the typical form of *C. avellana* occurring in nature and in *C. avellana* cv. 'Tonda Gentile Trilobata', one of the most valuable cultivar worldwide. Both these taxa came from the same geographical area (i.e. north-east Italy) and grew in the same environmental conditions (i.e. common Botanical Garden), assuring us that any observed differences can be attributed only to different fertilized supply as suggested by Sciubba et al. (2014) for different hazelnut *cultivars*. Particularly, we will focus on *C. avellana* leaves, whose extracts have antioxidant and antimicrobial activities. These activities can be attributed to their phenolic constituents, such as flavonoids, caffeic acid and diarylheptanoid derivatives, as well as taxane derivatives (Riethmuller et al. 2013). In this study, taking into account literature data, we will consider and quantify Quercitrin, Myricitrin and Afzelin, their major constituent, to analyze their secondary metabolites production (Figure 1). Hazelnut leaves are considered one of the major waste product derived from the hazelnut cultures, and are the subject of some studies (e.g. Masullo et al. 2015; Prokopenko et al. 2019), although most of these focus on nuts of this species (e.g. Granata et al. 2017). Nevertheless, as far as we know, in the last years, there are no specific studies about the effect of the nutritional *status* on leaf physiology and related production of secondary metabolites in hazelnut.
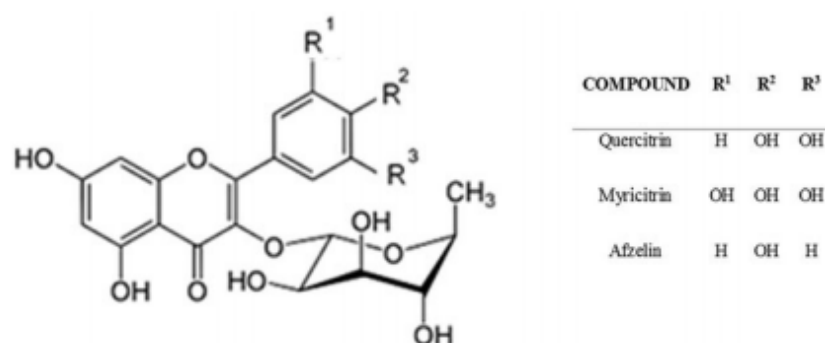

COMPOUND	R¹	R²	R³
Quercitrin	H	OH	OH
Myricitrin	OH	OH	OH
Afzelin	H	OH	H

Figure 1. Molecular structure of Quercitrin, Myricitrin and Afzelin.

2. Results and discussion

The response to different nutritional *status* in term of leaf physiological traits and secondary metabolites production in wild and cultivated *C. avellana* was investigated. Overall, under a physiological point of view we observed an increase of the net assimilation rates and related parameters (i.e. C_E, Φ_{PSII}, and ETR) from control to saplings under high-nutrient supply both in wild and cultivated hazelnut, although this response resulted more evident in the latter (Figures 2 and 3). For instance, Φ_{PSII}, a key parameter related to the carbon fixation efficiency gradually increased from C (0.19 ± 0.01 and 0.17 ± 0.01 in TGT_C and WT_C, respectively) to HN treatments (0.40 ± 0.03 and 0.25 ± 0.01, in TGT_{HN} and WT_{HN}, respectively). The results evidenced
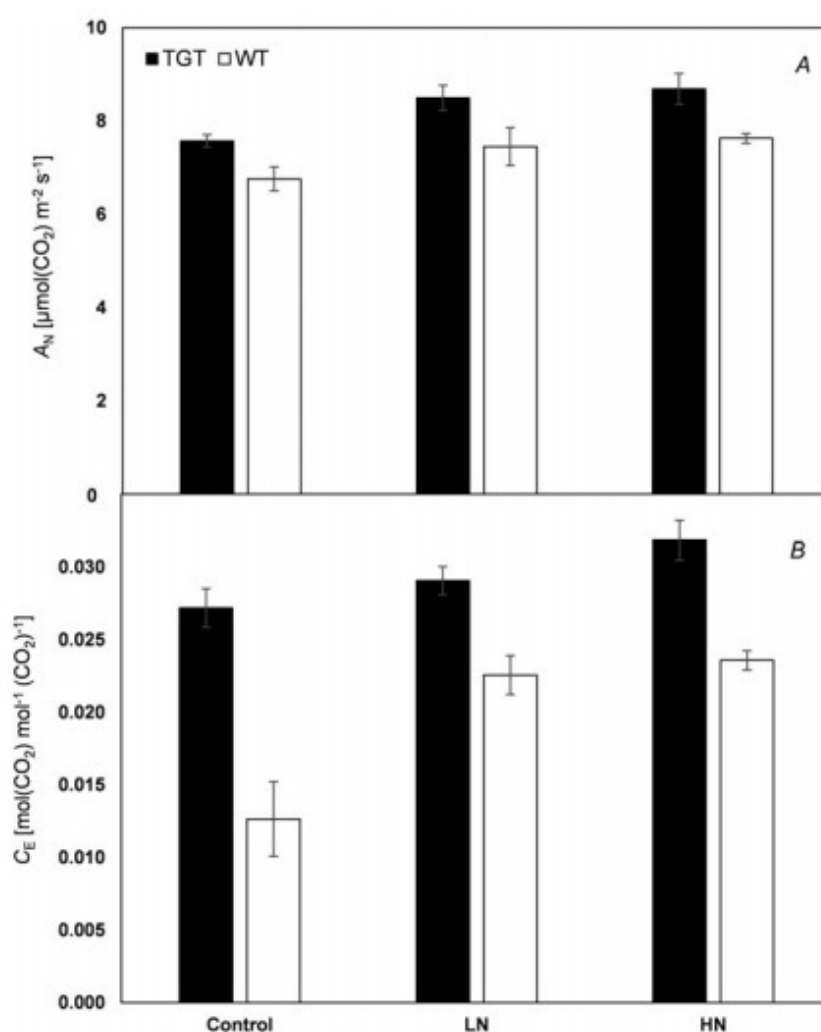

Figure 2. Values of (A) Net assimilation rates (AN) and (B) relative carboxylation efficiency (CE) in control treatment, low nutrient treatment (LN) and high nutrient treatment (HN) of Corylus avellana cv. 'Tonda Gentile Trilobata' (TGT) and Corylus avellana wild type (WT) saplings. Mean values ($\pm$ S.E.) are shown ($n = 60$).

Figure 3. Values of (A) maximum photochemical efficiency of PSII (Fv/FM) and (B) actual photochemical efficiency of PSII (ΦPSII) in control treatment, low nutrient treatment (LN) and high nutrient treatment (HN) of Corylus avellana cv. 'Tonda Gentile Trilobata' (TGT) and Corylus avellana wild type (WT) saplings. Mean values (± S.E.) are shown ($n = 60$).
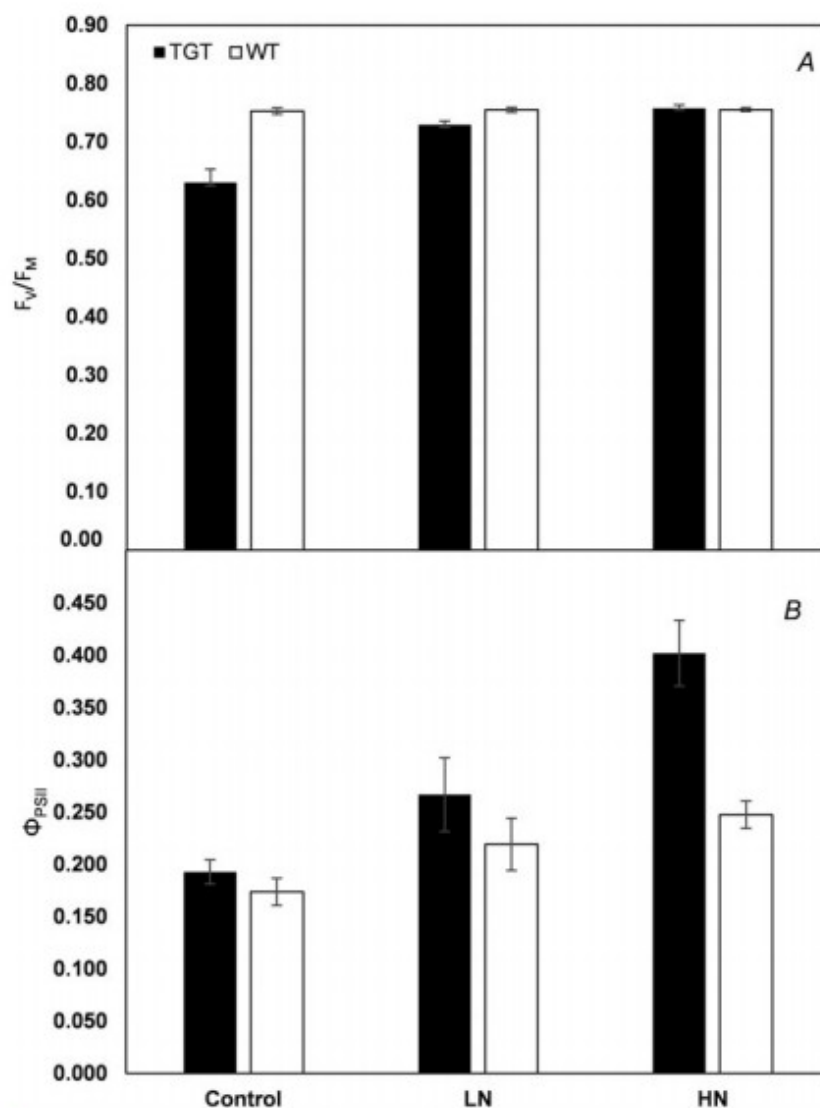
that saplings supplied with higher nutrient availability seem to maximize the allocation of N to RuBisCO improving the photosynthetic activity. The highest net assimilation rates in HN saplings [8.69 ± 0.33 and $7.63 \pm 0.11 \, \mu mol \, (CO_2) \, m^{-2} \, s^{-1}$, in TGT_{HN} and WT_{HN}, respectively] were also sustained by a higher C_E [0.032 ± 0.001 and $0.024 \pm 0.001 \, mol(CO_2) \, mol^{-1}(CO_2)^{-1}$, in TGT_{HN} and WT_{HN}, respectively] and ETR values [199 ± 24 and $107 \pm 6 \, \mu mol(e^-) \, m^{-2} \, s^{-1}$ in TGT_{HN} and WT_{HN}, respectively]. Moreover, the observed values of stomatal conductance in the saplings did not show any significant variations among the treatments for both WT and TGT, confirming that LN and
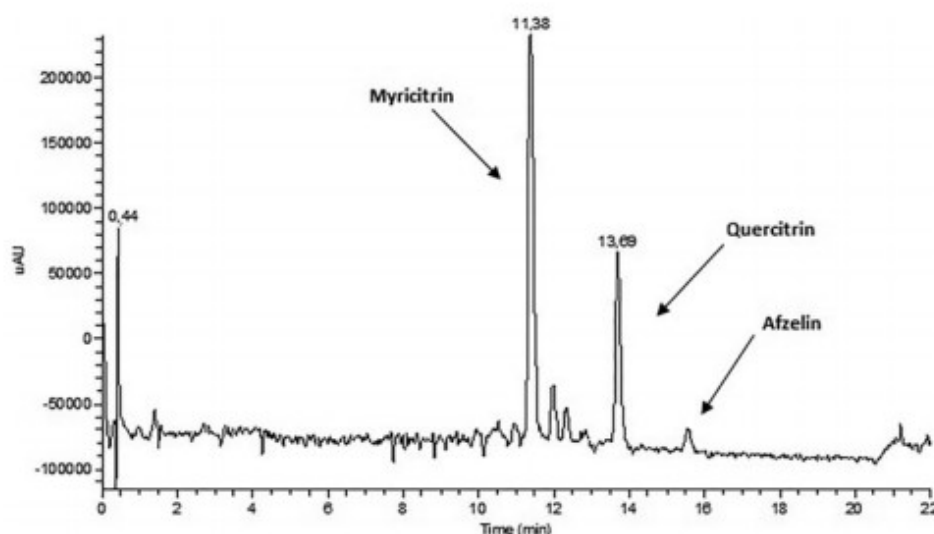
Figure 4. Example of an HPLC-UV/PAD profile of Corylus avellana raw extract (λ = 264 nm).

HN saplings were able to implement mechanisms to increase their photosynthetic efficiency at the biochemical level.

With regard to the analytical characterization of the secondary metabolites profile in hazelnut leaves, an appropriate reverse phase HPLC-UV/PAD method was set up, allowing a rapid and economic analysis of the extracts. Specifically, different elution conditions (Methanol, Acetonitrile, water, with or without Formic Acid) adopting several gradient modes were tested on Chromolith Performance RP-18 endcapped (4.4 × 50 mm). The best results in term of peak resolution, peak shape and time of analysis were achieved with a gradient elution conditions, using water and MeOH both added with formic acid as mobile phase. This method was exploited to record the fingerprint of the extracts, identify the main peaks and quantify the most abundant flavonoids, Quercitrin and Myricitrin, while the quantification of Afzelin was not possible due to its content below the limit of quantification (Figure 4). Next, basing on our previous experience and testing different extraction solvents, we developed a proper Microwave Assisted Solvent Extraction procedure that allowed low time of extraction and low waste of solvent (Rossi et al. 2017). After that, we were able to demonstrate that the considered types of hazelnut under the three different treatments showed the same phenolic profile. With the analytical method in hands and thanks to the external standards, we also set up a calibration curves to quantify Myricitrin and Quercitrin. The results confirmed the well-characterized antioxidant activity of hazelnut leaves (Masullo et al. 2015), and were qualitatively in line with those observed by Amaral et al. (2005) for hazelnut *cultivar* grown in Portugal. Thus, based on these results, the fingerprint of the extracts was not affected by the nature of hazelnut (WT *vs* TGT) and by the nutrient supply (C, LN and HN), while variations at quantitative level were detected as shown in Table 1. In particular, regarding the quantitative comparison between TGT and WT, this last showed a significantly higher concentration both in Quercitrin and Myricitrin (by 27% and 10%, respectively) compared to TGT, and this result can be related to the ecological role of flavonoids. In fact, they exhibit

6 ⊙ M. U. GRANATA ET AL.

Table 1. Values of concentration of Quercitrin and Myricitrin in leaves of Corylus avellana cv. 'Tonda Gentile Trilobata'(TGT) and in Corylus avellana wild type (WT) for the three nutritional treatments: TGTC and WTC = control treatments; TGTLN and WTLN = low nutrients; TGTHN and WTHN = high nutrients.

	Quercitrin	Myricitrin
	mg g^{-1}	mg g^{-1}
TGT_C	0.0095 ± 0.0004a	0.0761 ± 0.0036a
TGT_{LN}	0.0143 ± 0.0006b	0.0754 ± 0.0019a
TGT_{HN}	0.0138 ± 0.0002bc	0.0760 ± 0.0012a
WT_C	0.0191 ± 0.0003d	0.0926 ± 0.0016b
WT_{LN}	0.0153 ± 0.002e	0.0854 ± 0.0006c
WT_{HN}	0.0132 ± 0.008c	0.0713 ± 0.0009d

central functions in various aspects of plant life related to interactions with the environment (Treutter 2006). For instance, they have antimicrobial properties and act as a deterrent for herbivores by limiting assimilation of dietary proteins and inhibiting digestive enzymes (Dixon et al. 2004). In particular, Quercitrin has a high antifungal activity by its autoxidation and the consequent formation of the antifungal agent 3,4-dihydroxybenzoic acid (Pourcel et al. 2007). Thus, the higher concentration of these flavonoids resulted more useful in the wild environment and particularly in the forest understory from which wild hazelnut originates. With regard to the observed differences among treatments in WT and TGT, we founded in wild hazelnut a significant decrease of the concentration of both Quercitrin and Myricitrin from C to HN, while in cultivated hazelnut we found any significant variations in Myricitrin concentrations among treatments and the lowest Quercitrin concentration in TGT_C. Thus, we can highlight, on one hand, an opposite trend of A_N and flavonoids concentration in WT, where to a lower photosynthetic activity (as in WT_C) corresponded a higher Quercitrin and Myricitrin concentration. This result was in line with the carbon/nutrient balance (CNB) hypothesis, according to which plant growing in more nutrient-poor soils can accumulate a higher amount of secondary metabolites due to an excess of carbon available for this metabolic pathway (Flanagan and Van Cleve 1983). On the other hand, the reduced variability among treatments observed for the cultivated hazelnut, along with their lower metabolite concentrations, can be explained by the aforementioned ecological role of flavonoids and related to the genetic background of the TGT *cultivar*. Indeed, due to a usual growth under more controlled environmental conditions, including also pest and disease control, the *cultivar* can be characterized by a lesser intrinsic need to produce such compounds.

A final consideration should be made about beneficial effects on a phytoterapeutic level and the consequent economic implication associated to the use of hazelnut leaves being a waste product. A first aspect to be considered is that in the context of food processing industry a large quantities of both liquid and solid wastes are annually produced, creating serious environmental problems. Thus, in the last years a variety of processes are being developed in order to reuse the waste loads, aiming at converting the waste materials into bio-fuels, food ingredients and other added value bio-products (Makris et al. 2007), reducing in the same time the economic and environmental costs necessary for their containment. In this context, considering the high antioxidant activity found in hazelnut leaves

by means of the presence of phenolic compounds, as confirmed in our study by the high presences of Quercitrin and Myricitrin, its leaves could represent useful sources of bioactive phenolics with phytoterapeutic interest, as confirmed by an already recognized application in folk medicine for the treatments of hemorrhoids, varicose veins, phlebitis, and edema, as a consequence of their astringent, vasoprotective, and antiedema properties and also for their mild antimicrobial effects (Riethmuller et al. 2013).

Disclosure statement

No potential conflict of interest was reported by the authors.

References

Amaral JS, Ferreres F, Andrade PB, Valentão P, Pinheiro C, Santos A, Seabra R. 2005. Phenolic profile of hazelnut (Corylus avellana L.) leaves cultivars grown in Portugal. Nat Prod Res. 19(2):157–163.

Amtmann A, Troufflard S, Armengaud P. 2008. The effect of potassium nutrition on pest and disease resistance in plants. Physiol Plant. 133(4):682–691.

Dixon RA, Xie D-Y, Sharma SB. 2004. Proanthocyanidins – a final frontier in flavonoid research? New Phytol. 165(1):9–28.

Flanagan PW, Van Cleve K. 1983. Nutrient cycling in relation to decomposition and organic-matter quality in taiga ecosystems. Can J Res. 13(5):795–817.

Granata MU, Bracco F, Gratani L, Catoni R, Corana F, Mannucci B, Sartori F, Martino E. 2017. Fatty acid content profile and main constituents of Corylus avellana kernel in wild type and cultivars growing in Italy. Nat Prod Res. 31(2):204–209.

Makris DP, Boskou G, Andrikopoulos NK. 2007. Polyphenolic content and in vitro antioxidant characteristics of wine industry and other agri-food solid waste extracts. J Food Compos Anal. 20:125–132.

Martino E, Della Volpe S, Cavalloro V, Amri B, Kaab LBB, Marrubini G, Rossi D, Collina S. 2019. The use of a microwave-assisted solvent extraction coupled with HPLC-UV/PAD to assess the quality of Marrubium vulgare L. (white horehound) herbal raw material. Phytochem Anal. 30(4):377–384.

Masullo M, Cerulli A, Olas B, Pizza C, Piacente S. 2015. Giffonins A-I, antioxidant cyclized diarylheptanoids from the leaves of the hazelnut tree (Corylus avellana), source of the Italian PGI product "Nocciola di Giffoni". J Nat Prod. 78(1):17–25.

Özenç N, Özenç DB, Duyar Ö. 2014. Nutritional composition of hazelnut (Corylus avellana L.) as influenced by basic fertilization. Acta Agric Scand Sect B Soil Plant Sci. 64:710–721.

Prokopenko Y, Jakštas V, Žvikas V, Georgiyants V, Ivanauskas L. 2019. Hilic MS/MS determination of amino acids in herbs of Fumaria schleicheri L., Ocimum basilicum L., and leaves of Corylus avellana L. Nat Prod Res. 33(13):1961–1963.

Pourcel L, Routaboul J-M, Cheynier V, Lepiniec L, Debeaujon I. 2007. Flavonoid oxidation in plants: from biochemical properties to physiological functions. Trends Plant Sci. 12(1):29–36.

Ramakrishna A, Ravishankar GA. 2011. Influence of abiotic stress signals on secondary metabolites in plants. Plant Signal Behav. 6(11):1720–1731.

Riethmuller E, Alberti A, Toth G, Beni S, Ortolano F, Kery A. 2013. Characterisation of diarylheptanoid- and flavonoid-type phenolics in Corylus avellana L. leaves and bark by HPLC/DAD–ESI/MS. Phytochem Anal. 24:493–503.

Rossi D, Ahmed KM, Gaggeri R, Della Volpe S, Maggi L, Mazzeo G, Longhi G, Abbate S, Corana F, Martino E, et al. 2017. (R)-(-)-Aloesaponol III 8-methyl ether from Eremurus persicus: a novel compound against leishmaniosis. Molecules 22(4):515–519.

Sciubba F, Di Cocco ME, Gianferri R, Impellizzeri D, Mannina L, De Salvador FR, Venditti A, Delfini M. 2014. Metabolic profile of different Italian cultivars of hazelnut (Corylus avellana) by nuclear magnetic resonance spectroscopy. Nat Prod Res. 28(14):1075–1081.

Stark S, Julkunen-Tiitto R, Kumpula J. 2007. Ecological role of reindeer summer browsing in the mountain birch (Betula pubescens ssp. czerepanovii) forests: effects on plant defense, litter decomposition, and soil nutrient cycling. Oecologia 151(3):486–498.

Treutter D. 2006. Significance of flavonoids in plant resistance: a review. Environ Chem Lett. 4(3): 147–157.

Paper 4

Reprinted with permission from Pasquale Linciano, Valeria Cavalloro, Emanuela Martino, Johannes Kirchmair, Roberta Listro, Daniela Rossi, and Simona Collina *J. Med. Chem.* **2021**

https://doi.org/10.1021/acs.jmedchem.0c01282

Copyright 2021 American Chemistry Society

Tackling Antimicrobial Resistance with Small Molecules Targeting LsrK: Challenges and Opportunities

Pasquale Linciano, Valeria Cavalloro, Emanuela Martino, Johannes Kirchmair, Roberta Listro, Daniela Rossi, and Simona Collina*

Cite This: https://dx.doi.org/10.1021/acs.jmedchem.0c01282

Read Online

ACCESS | Metrics & More | Article Recommendations

ABSTRACT: Antimicrobial resistance (AMR) is a growing threat with severe health and economic consequences. The available antibiotics are losing efficacy, and the hunt for alternative strategies is a priority. Quorum sensing (QS) controls biofilm and virulence factors production. Thus, the quenching of QS to prevent pathogenicity and to increase bacterial susceptibility to antibiotics is an appealing therapeutic strategy. The phosphorylation of autoinducer-2 (a mediator in QS) by LsrK is a crucial step in triggering the QS cascade. Thus, LsrK represents a valuable target in fighting AMR. Few LsrK inhibitors have been reported so far, allowing ample room for further exploration. This perspective aims to provide a comprehensive analysis of the current knowledge about the structural and biological properties of LsrK and the state-of-the-art technology for LsrK inhibitor design. We elaborate on the challenges in developing novel LsrK inhibitors and point out promising avenues for further research.
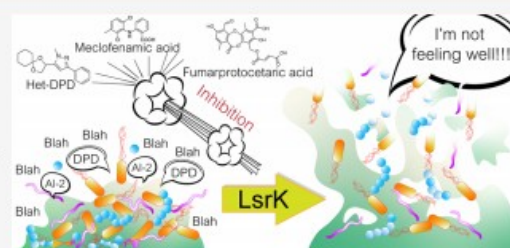
■ INTRODUCTION

Antimicrobial resistance (AMR) and the worldwide increase of superbug infections are recognized by the World Health Organization (WHO) as global concerns for public health and healthcare systems' sustainability.[1,2] AMR infections cause approximately 700 000 deaths annually, and they are expected to become the leading cause of death by the year 2050, especially in low- and middle-income countries.[3−5] Similarly, it is projected that in the year 2050, AMR could lower the global gross domestic product by up to one trillion dollars annually.[6] To challenge this inauspicious outcome, in 2015, the WHO launched the Global Antimicrobial Resistance Surveillance System (GLASS).[7] The primary aim of GLASS is to foster global, national, and regional actions to support AMR's spread surveillance and research.[2,8] Thus, five strategic objectives were set out: (i) promotion of initiatives for raising awareness about this issue, (ii) optimization of the use of antibiotics in both human and animal health, (iii) delineation of global strategies to monitor and contain the spread of resistance, (iv) application of preventive measures to reduce the incidence of infections, and (v) incentivization of investments in the research of new pharmaceutical tools and medicines.[7]

Overuse, inappropriate prescription, and extensive agricultural use of antibiotics have exposed bacteria to intense, selective evolutive pressure. This led to the development of protective mechanisms to inactivate, remove, and, in general, circumvent the toxicity of the antibiotics against bacteria.[8−11] These mechanisms of resistance exploit the reduction of drug permeability,[12] the excretion of the antibiotic through active efflux pumps,[13] the production of antibiotic-inactivating enzymes (i.e., β-lactamases),[14−16] or the formation of biofilms,[17] thus conferring reduced susceptibility to antibiotic activity.

Biofilm formation is the typical virulence mechanism by which bacteria organize in communities, and it is characterized by (i) an extracellular matrix that envelops the microorganism, (ii) the presence of different types of organisms (eukaryotic and prokaryotic), and (iii) an anchoring surface of aggregate colonial bacteria.[17,18] With resistance at the cellular level, biofilms confer additional resistance to bacteria, commonly referred to as community resistance. It is estimated that about 80% of all human bacterial infections are complicated by the formation of biofilms, where bacteria can have a 1000-fold higher tolerance to antibiotics than the same organisms in a planktonic state.[19,20]

The assemblage and "social" organization in a biofilm require bacteria to communicate with the neighbors in order to coordinate efforts and accomplish cooperative activities. The quorum sensing (QS) signaling is the most effective known cell-

A

Figure 1. AI-2 mediated QS cascade and its entanglement with the carbon catabolite repression (CCR) and the phosphoenolpyruvate (PEP)-dependent sugar phosphotransferase system (PTS).

to-cell mechanism that bacteria, both Gram-positive[21,22] and Gram-negative,[23] used to communicate, coordinate and act as a population, thereby gaining some benefits that otherwise were unattainable.[24] Moreover, recent studies indicate that QS can also conversely coordinate the dispersion of the biofilm. This process is activated when nutrients and resources within the biofilm become limited or waste/toxic products accumulate, allowing bacteria to escape from the colony and populate new areas.[25,26]

Besides biofilm formation, QS processes are diverse and depend on the communities' specific needs. Thus, QS may trigger changes in bacteria's physiology,[23,27,28] inducing modification in antibiotic susceptibility,[29] virulence factor production,[30,31] symbiosis, competence,[32] bioluminescence,[33,34] motility, cellular division control,[35] sporulation,[36] and genetic transfer (transformation, conjugation, and transduction).[37] Quenching the QS response thus represents an attractive therapeutic strategy for the treatment of AMR infections. The first experimental evidence of quorum quenching's potential in counteracting the bacterial resistance mechanism dates back to the 1990s. Compound 4-bromo-3-butyl-5-(dibromomethylene)furan-2(5H)-one was discovered to be able to interfere with the N-acyl homoserine lactones (AHL)-mediated QS both in vitro and in vivo,[38] paving the way to the identification and development of several small molecules with anti-QS activity.[39−44] Analogously, mutations on genes involved in QS significantly reduced mutant bacteria's virulence and their capability to form a biofilm.[45,46]

Through modulation/inhibition of QS, several bacterial virulence factors that facilitate human infections can be controlled, and their harmful effects, including mortality, can be reduced. Importantly, because these virulence factors are not essential to bacterial growth and survival, a treatment that does not inhibit bacterial growth will not generate selective pressure. Therefore, the risk of resistance formation can be reduced substantially.[23,47−51] Thus, interfering with the QS has become an appealing strategy to prevent the spread of AMR.[52,53]

■ THE KEY ROLE OF LSRK KINASE IN THE AI-2 MEDIATED QS CASCADE

QS enables bacteria to recognize population density by measuring the accumulation of nonspecific signaling molecules secreted by community members. Only when the population density is high will the accumulation of the signal in the extracellular environment be suitable to activate the response. The messengers of QS are the so-called autoinducers (AIs).[23,54] Conventionally, AIs have been divided into three main categories: (i) N-acyl homoserine lactones (AHLs),[54−56] exploited by Gram-negative bacteria, (ii) oligopeptides,[57] exploited by Gram-positive bacteria,[58] and (iii) autoinducer-2 (AI-2), exploited by both Gram-positive and Gram-negative bacteria.[59] Other QS signals include the (iv) *Pseudomonas* quinolone signal (PQS),[60,61] (v) diffusible signal factor
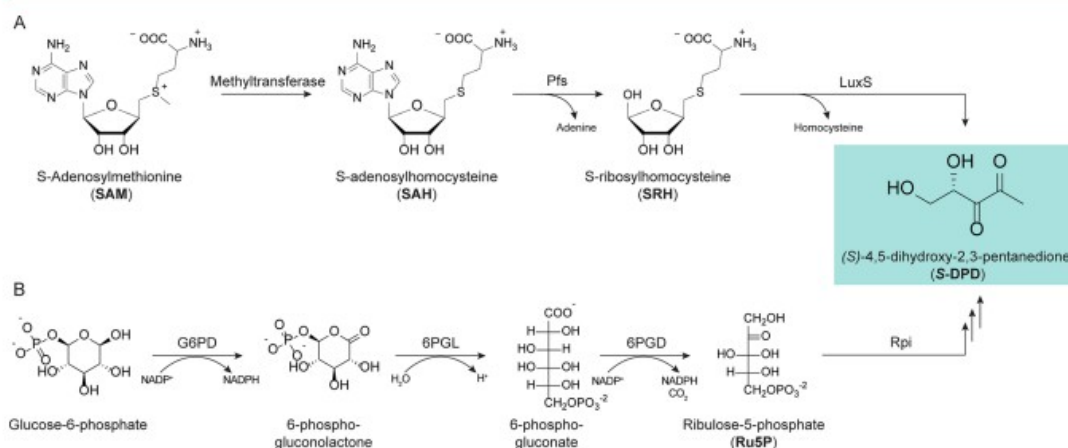
B

Figure 2. Biosynthesis of AI-2 via OPP pathway.

(DSF),[62,63] (vi) γ-butyrolactone,[64] (vii) 2-amino acetophenone (2-AA),[65] and (viii) bradyoxetin.[66]

AI-2 signaling differs from all other QS strategies because it allows for interspecies communication and has been defined as "universal language."[59] The first evidence of the AI-2-mediated signal date back to 1994, when QS activity was observed in bacterial strains lacking the AHL synthase.[34] A few years later, AI-2 activity was detected in a wide range of LuxS-containing species, confirming the role of AI-2 as QS signaling molecules.[67] At present, the synthase responsible for the biosynthesis has been detected in more than 70 bacterial species.[68,69]

All AI-2 compounds share the 4,5-dihydroxy-2,3 pentanedione (DPD) as a common precursor. DPD is biosynthesized in a three-step pathway (Figure 1). In the first step, S-adenosylmethionine (SAM) is demethylated by a methyltransferase to generate S-adenosylhomocysteine (SAH). Because SAH is a potent inhibitor of the methyltransferases itself, in the second step, it is quickly degraded by Pfs (a 5′-methylthioadenosine nucleosidase, MTAN) through the removal of the adenine moiety to form S-ribosylhomocysteine (SRH). In the third step, an S-ribosylhomocysteinase (LuxS) catalyzes the displacement of the homocysteine moiety from SRH to release AI-2 (Figure 1 and Figure 2A).[70−73]

An alternative pathway for the biosynthesis of DPD requires the isomerization (by ribulosephosphateisomerase, Rpi) of D-ribulose-5-phosphate (Ru5P), which results from the catabolism of glucose via the oxidative pentose phosphate (OPP) pathway (Figure 1 and Figure 2B).

However, DPD is not an effective AI-2. DPD itself has never been observed in vitro by MS or NMR analysis. Although DPD is more stable than other autoinducers (such as AHLs and oligopeptides), structural analysis in an aqueous solution of DPD analogues confirmed a complex equilibrium of structurally related compounds. DPD is a highly reactive molecule against electrophiles, and in an aqueous solution, it may undergo a spontaneous cyclization reaction, rearranging in a complex equilibrium of 4-hydroxy-5-methyl-3(2H)-furanone (HMF) derivatives. Linear DPD is in equilibrium with its two cyclic isomers, S-DHMF and R-DHMF (Figure 3). Their hydration at C3 results in the two cyclic, tetrahydrate isomers, S-THMF and R-THMF (Figure 3). This hypothesis was confirmed when the
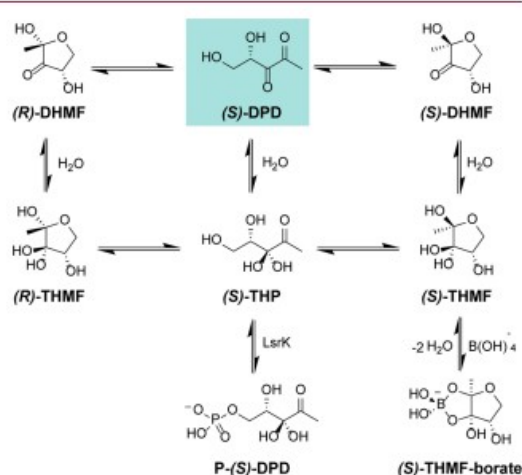

Figure 3. Equilibrium species of AI-2 in an aqueous environment.

first AI-2 was cocrystallized in complex with *Vibrio harveyi* LuxP, revealing the chemical structure of the S-isomer of THMF in the form of borate diester (S-THMF-borate).[74,75] In support of this evidence, (R)-THMF was cocrystallized with the LsrB transporter protein of *Salmonella typhimurium*, *Sinorhizobium meliloti*, and *Yersinia pestis*.[76−78] These results led to the currently accepted model that AI-2 is a set of equilibrium forms of DPD rather than a single molecule. Different forms of AI-2 are manifested under varying environmental conditions.

Although there is evidence supporting the nonenzymatic, spontaneous conversion of DPD to various equilibrium forms of AI-2, a recent study has indicated the presence of alternative synthetic pathways.[79]

Bacteria can selectively recognize the diverse DPD-derivatives triggering specific QS cascades. Moreover, DPDs can be detected by different bacterial species, justifying the adaptable nature of these molecules as universal messengers among bacteria.[74,80]

C

149

Once biosynthesized, AI-2 is actively released in the extracellular space by the proposed YdgG protein, although other unknown mechanisms could be present (Figure 1).[81] Once a threshold concentration of AI-2 in the extracellular environment is reached, *R*-THMF is internalized via the Lsr (LuxS regulated) transporter system, an ATP-binding cassette.[77,82] In the cytoplasm, *R*-THMF, in equilibrium with the hydrated linear DPD (*i.e.*, *S*-THP, Figures 1–2), is further phosphorylated at position 5 by LsrK. Phosphorylation by LsrK drives the equilibrium to the tautomeric form in the linear conformation, producing *S*-THP-phosphate (commonly also known as phospho-DPD or P-DPD, Figure 1).[77,83] The phosphorylation of DPD is the crucial step in the triggering of the QS cascade. P-DPD binds to the transcriptional repressor LsrR, which dissociates from the promoter region of the two divergently transcribed *lsrACDBFG* and *lsrRK* operons. As a result, *lsrACDBFG* transduces the transporters LsrA/C/D, which leads to an increase of the internalization of the signal molecules and, consequently, in sustaining the QS cascade (Figure 1). The activity of LsrR as a repressor of both operons is under negative autoregulation feedback control. When the level of P-DPD within the cell is low, LsrR, in its active state, represses the expression of both the *lsr* and *lsrRK* operons, thus reducing the production of LsrR itself.

Conversely, in the presence of AI-2s, LsrR is inhibited. The transcription of the two operons is activated, leading to speed up the production of all enzymes and transporters involved in the AI-2 mediated QS cascade. This mechanism of autoregulation of LsrR allows the cells of bacteria to respond quickly to the extracellular level of AI-2. Accordingly, with the described mechanism of action, mutants that do not express LsrK cannot activate *lsr* transcription, resulting in reduced expression of the Lsr transporter and extracellular AI-2 accumulation.[84] At the end of its life cycle, P-DPD is degraded by LsrG and LsrF. LsrG catalyzes the isomerization of P-DPD into 3,4,4-trihydroxy-2-pentanone-5-phosphate (P-TPO). LsrF is a thiolase that catalyzes the transfer of an acetyl group from hydrated P-TPO to coenzyme A, releasing dihydroxyacetone phosphate (DHAP) and acetyl-CoA (Figure 1).[85] Accordingly, *lsr* expression is increased in LsrG and LsrF mutants as a result of phospho-AI-2 accumulation.[85,86]

Several studies have been performed to better understand LsrK activity and its importance in bacterial QS. LsrK mutants do not activate *lsr* transcription because of the lack of phospho-AI-2, and, as a consequence, the reduced expression of the Lsr transporter results in extracellular AI-2 accumulation.[87] Furthermore, when LsrK and ATP were added *ex vivo* (*i.e.*, in the extracellular medium) to *Escherichia coli*, *Salmonella typhimurium*, or *Vibrio harveyi* cultures (both in pure cultures and in a synthetic ecosystem), the phosphorylation of AI-2 outside the cells impedes the transport of phospho-AI-2 through the Lsr transporter due to its negative charge. As a result, a reduction in *lsr* expression and QS attenuation was observed (both in the single cultures and in these three species).[88] Exploiting this observation, Rhoads et al. recently synthesized a functionalized biopolymer capsule of alginate and chitosan containing ATP. LsrK, modified with a C-terminal tyrosine tag, was covalently attached to the surface of the capsule. The addition of these capsules in the supernatants of *E. coli* cultures led to a modulation of the QS activity. Thus, these functionalized biopolymers with LsrK, and in a broad sense, other bacterial kinases, may represent a suitable strategy to adopt in human wound dressing to prevent wound infections by the

quenching of AI-2 mediated QS activity.[68] Taken together, these findings suggest that LsrK is an attractive anti-infective target, and they underline how the selective modulation of LsrK could attenuate AI-2 related pathogenesis.

Besides, recent studies have demonstrated the interconnection and control of AI-2 mediated QS with the availability of carbohydrates (e.g., glucose) and their catabolism processes.[89] The transcriptional activity of *lsr* operons is directly controlled by carbon catabolite repression (CCR) by the cyclic AMP (cAMP)-CRP complex. (cAMP)-CRP modulates the transcription of *lsrRK* and *lsr* operon by binding to specific promoter sequences (Figure 1). (cAMP)-CRP works in tandem with the LsrR repressor to regulate AI-2 uptake. Conversely, the AI-2 mediated QS can be indirectly modulated by the phosphoenolpyruvate (PEP)-dependent sugar phosphotransferase system (PTS) (Figure 1). PTS comprises three units: EI, HPr, and EII. The phosphorylation of EI seems to be necessary for the initial uptake of AI-2, although the exact mechanism remains to be determined. Interestingly, crystallographic studies performed by Ha et al. revealed that HPr could directly regulate the activity of LsrK by binding with the kinase.[89] LsrK activity is inhibited when bound to HPr, indicating new linkages between QS activity and sugar metabolism. Therefore, a strong relationship between substrate availability, cell metabolism, and QS processes have been proved, together with the essential role of LsrK is in the QS process.[87,90]

■ STRUCTURE AND CATALYTIC ACTIVITY OF LSRK

From a structural point of view, LsrK belongs to the FGGY carbohydrate kinase family and catalyzes a phosphate group's transfer from ATP to AI-2. Members of this family are widely found in bacterial genomes, and they are involved in the catabolic pathway of carbohydrates. Although discovered in the year 2003 already, LsrK was cloned, for the first time, in 2017.[91] The first three-dimensional structures became available in the following year when Ha et al. reported the first crystallographic structures of *Escherichia coli* LsrK (*Ec*LsrK) cocrystallized with the HPr protein of the phosphotransferase system (PTS).[89] The structures published by Ha et al. include a binary complex of LsrK-HPr at a resolution of 3.00 Å (PDB 5YA0), a ternary complex of LsrK-HPr-ADP at a resolution of 2.70 Å (PDB 5YA2), and a ternary complex of LsrK-HPr-ATP at a resolution of 2.70 Å (PDB 5YA1). The three reported crystallographic structures are similar in terms of structure. Each crystallographic unit consists of two nonsymmetrically arranged molecules of the LsrK-HPr complex (Figure 4A). The two subunits form ionic interactions mediated by two phosphate ions and the side chains of the two specular residues Lys204. However, exclusion chromatography coupled with light scattering analysis suggests that the functional unit of the LsrK-HPr complex may consist of a single monomeric complex.[89]

As observed in the X-ray structure of the three LsrK-HPr complexes, the protein–protein interaction between the two binding partners is dominated by hydrophobic interactions between Phe48 and Leu47 (to a lesser extent) of HPr, and the hydrophobic pocket of LsrK formed by Leu123, Ile148, Leu151, Leu152, Ala155, Tyr162, Met210, and Ala211 (Figure 4B).[89] Phe48 and Leu47 are highly conserved in Gram-negative bacteria, and corresponding hydrophobic residues have been identified in Gram-positive bacteria (e.g., Ile47 and Met48). Besides, the ionic interaction between His15 of HPr and Glu122 of LsrK might represent the main "switch" for the control of the LsrK activity by HPr. His15 is the residue that mediates the
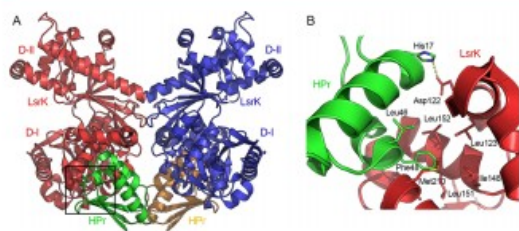
D

Figure 4. (A) Crystal structure of the LsrK-HPr-ATP complex (PDB 5YA1). The two subunits of LsrK are visualized as red and blue cartoons; the two subunits of HPr are displayed as green and ocher cartoons. (B) Close-up on the residues of HPr (green cartoon) involved in the interaction with LsrK (red cartoon). Amino acid residues are reported in stick mode. Yellow dashed lines represent the hydrogen and coordination bonds. Heteroatoms are color-coded (oxygen atoms in red, nitrogen atoms in blue, sulfur atoms in yellow).

phosphate group's transfer from phosphorylated HPr (P-HPr) to the PTS's EIIA protein. In its phosphorylated form, P-HPr carries the phosphate group bound to $N^{\delta1}$ of His15.[92] Thus, Ha et al. proposed that when HPr is in its phosphorylated state, the steric clash and unfavorable repulsive ionic interactions induced by the phosphate group of P-HPr His15 and the negative charge of Asp122 of LsrK might prevent the formation of the LsrK/HPr complex, representing the junction point between the QS activity and sugar metabolism.

Focusing on LsrK, the kinase's overall structure can be divided into two domains: the N-terminal domain (or domain I, D-I, Figure 5A) and the C-terminal domain (or domain II, D-II,
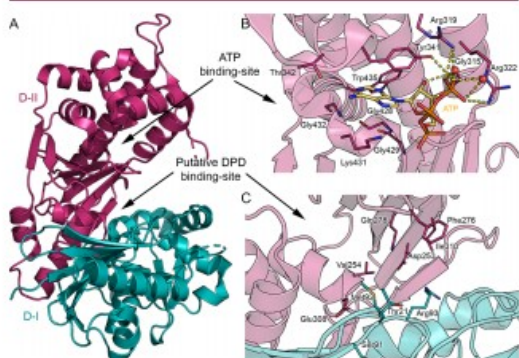
Figure 5. (A) Crystal structure of the LsrK (PDB 5YA1). The two domains D-I and D-II of Lsrk, are visualized as cartoons in teal and magenta, respectively. (B) Close-up of the ATP binding site. ATP is represented in stick mode, with carbon atoms in yellow. (C) Close-up of the putative DPD binding site. Amino acid residues are visualized in stick mode with D-I's and D-II's carbon atoms in teal and magenta, respectively. Yellow dashed lines represent the hydrogen bonds. Heteroatoms are color-coded (oxygen atoms in red, nitrogen atoms in blue, sulfur atoms in yellow, phosphorus atoms in orange).

Figure 5A). This is in accordance with the FFGY superfamily members' architecture and the results of the homology model studies developed by Medarametla et al.[93] The two domains are arranged like the valves of a clamp; the joint is articulated between the α-helices 17 of D-II and the β-sheet formed by strands 1, 2, 3, and 6 of D-I. Upon substrate binding, a long-

range conformational change causes the two valves of the protein to close, thus preventing the entry of the solvent and the priming of the phosphorylation process. Therefore, in analogy to the FGGY carbohydrate kinases, the existence of an open-inactive and a close-active conformational state is also suggested for LsrK.

The three resolved *Ec*LsrK crystallographic structures portrayed the kinase in its open-inactive conformation. All the cocrystallization or soaking attempts performed by Ha et al. in the presence of DPD or an AI-2 antagonist were unsuccessful. Therefore, only the apo form of the LsrK-HPr complex and a complex with ATP-ADP were reported. Additional STD-NMR studies performed by Ha et al.[89] revealed that the LsrK-HPr complex's affinity was higher for ATP than for DPD, thus supporting the above consideration. These experimental observations agree with superimposition studies of the LsrK-HPr complex with the FGGY superfamily member in diverse conformational states (*i.e.*, *ec*XK or *ec*GK), confirming the open-inactive conformation for the newly resolved LsrK-HPr complexes.

The active site of LsrK is located at the cleft between the two domains and contains both the site of interaction for the ATP and the substrate. The ATP site (Figure 5B) is easily identifiable because, in two of the three deposited LsrK X-ray structures, the enzyme is in a ternary complex with ATP (PDB 5YA1) or ADP (PDB 5YA2). ATP and ADP bind near the cleft's opening and interact with residues in domain II, although ATP seems to bind to HisLsrK/HPr more strongly than ADP. The ATP binding site is delineated by α-helices 6, 7, 8, 12, and 14. The adenine base of ATP or ADP is located deep within a hydrophobic pocket formed by Gly428, Gly429, Lys431, Gly432, Trp435, Thr342, and Tyr341. The hydroxyl in position 4 of the ribose forms an H-bond with Gly315. Lastly, the phosphate group of ATP/ADP is exposed to the solvent, and it is involved in a dense network of H-bonds and salt-bridges with Arg319, Arg322, and the solvent (Figure 5B).

The LsrK/HPr crystal structure has been obtained without including DPD or an AI-2 antagonist. To date, the putative binding site of the substrate was only predicted by homology models developed by Medarametla et al.,[93] based on the crystallographic structures of *Ec*GK (PDB 1GLF) and *Ec* L-rhamnulose kinase (PDB 2CGJ) in complex with ADP and glycerol or fructose, respectively (employed as a template for the closed conformation), and on the crystallographic structure of *Ec*XK in complex with xylulose (PDB 3HZ6; used as a template for the open conformation). The substrate's putative binding site is located deeply within the cleft formed by D-I and D-II (Figure 5C). It is enclosed by residues of the two subunits such as Thr21, Ser91, Met92, Arg93, Asp253, Val254, Phe276, Gln278, Glu308, and Ile310 (Figure 5C). Structure-based sequence alignment shows that both the residues of the ATP-binding site as well as the residues of the putative DPD binding site are well conserved among six selected Gram-negative and Gram-positive bacteria (*E. coli*, *Salmonella typhimurium*, *Yersinia pestis*, *Klebsiella pneumoniae*, *Bacillus subtilis*, *Bacillus thuringiensis*, and *Streptococcus* sp.). Because the LsrK binding site pocket depends on the kinase's conformation, the design of effective and specific inhibitors remains challenging. In-depth knowledge of the catalytic mechanism and its variability concerning substrate binding is necessary to successfully guide the rational design of clinically useful inhibitors.

E

Table 1. PROs and CONs of the Biochemical Assay for Monitoring and Quantifying LsrK Activity Developed so Far

biochemical assay	type of screening	PROs	CONs
qTLC	target-based	- direct assay - reproducibility - simple and time-saving - minimum types of equipment used	- poor precision - expensive - use of radiolabeled chemicals - not suitable for HTS
lactate dehydrogenase	target-based	- spectrophotometric assay - kinetic study of LsrK activity - economic - no use of radiolabeled chemicals	- coupled assay - purified recombinant LsrK protein needed - interference with phosphatases
ATP Bioluminescence CLSII kit and Kinase-Glo Max Luminescent kinase kit	target-based	- bioluminescence assay - extremely sensitive - fast and easy to carry out - suitable for HTS - easy to run with high ATP concentrations as a way of selecting against ATP-competitive inhibitors	- expensive - high purity of recombinant LsrK protein needed - sensitive to all the ATP present in the cell-culture - "signal decreaseassay" - sensitive to luciferase inhibitors
ADP-Quest	target-based	- end point or kinetic mode - convenient gain-of-signal with the respect of the ATP-detecting assay - detection around 590 nM, which tends to be less susceptible to inner filter effects	- coupled assay - high purity of recombinant LsrK protein needed
β-galactosidase-based assay	cell-based	- rapid, sensitive, and consistent quantitation of β-galactosidase using a single-reagent addition - performed in either 96- or 384-well plates - performed in both lysogeny broth (LB) and phosphate-buffered saline (PBS) media	- time-consuming - cumbersome when processing large numbers of samples - unspecific β-galactosidase inhibitory activity - not functional in glucose-containing media, due to repression of lsr operon by glucose - the results obtained in one bacterial species cannot always be extrapolated to the other species with the QS system of the same type
luciferase-based assay	cell-based	- fast and simple - highly sensitive - suitable for HTS	- assay kit not commercially available

■ IN VITRO ASSAYS FOR THE EVALUATION OF LSRK ACTIVITY

During the last two decades, several methods and assays have been developed to evaluate the biological activity of LsrK and the testing of small molecules for their inhibitory potential on the kinase (Table 1). In the beginning, the considered kinase activity was assessed by quantitative thin-layer chromatography (qTLC). This is a well-consolidated *in vitro* phosphorylation technique.[94,95] Briefly, to monitor the conversion of ATP to ADP, the kinase is incubated with potential substrates and radiolabeled ATP, and the resulting labeled ADP is quantified by qTLC (Figure 6A). This method was also exploited to evaluate the ability of LsrK to phosphorylate AI-2,[94] and to clarify its mechanism of action.[88,90] Despite the promising results obtained with the qTLC phosphorylation assay, this technique has severe drawbacks. It is expensive, and it requires extra precautions and equipment due to radiolabeled chemicals, and it is not suitable for high throughput screening.

A reliable alternative for the study of the kinetic activity of LsrK is a spectrophotometric assay reported by Zhu et al. Adenosine diphosphate (ADP), produced as a result of the LsrK catalysis, activates the pyruvate kinase to produce pyruvate that is further metabolized by lactate dehydrogenase with consumption of NADH which could be measured spectrophotometrically to determinate the initial velocity of LsrK catalysis (Figure 6B).[84]

During the last years, several assay kits have been developed based on either luminescence or fluorescence. The ATP bioluminescence CLSII kit in kinetic mode (Roche Scientific, Germany) is a bioluminescence-based method that exploits luciferase activity. Luciferase requires ATP as a substrate to produce light (Figure 6C). In the presence of LsrK, the amount of available ATP (and hence the amount of light generated by luciferase) depends on the activity of LsrK, thus enabling the measurement of LsrK inhibition by small molecules.[96] Another luminescence-based method is the Kinase-Glo Max Luminescent kinase assay (Sigma-Aldrich, USA). It correlates ATP
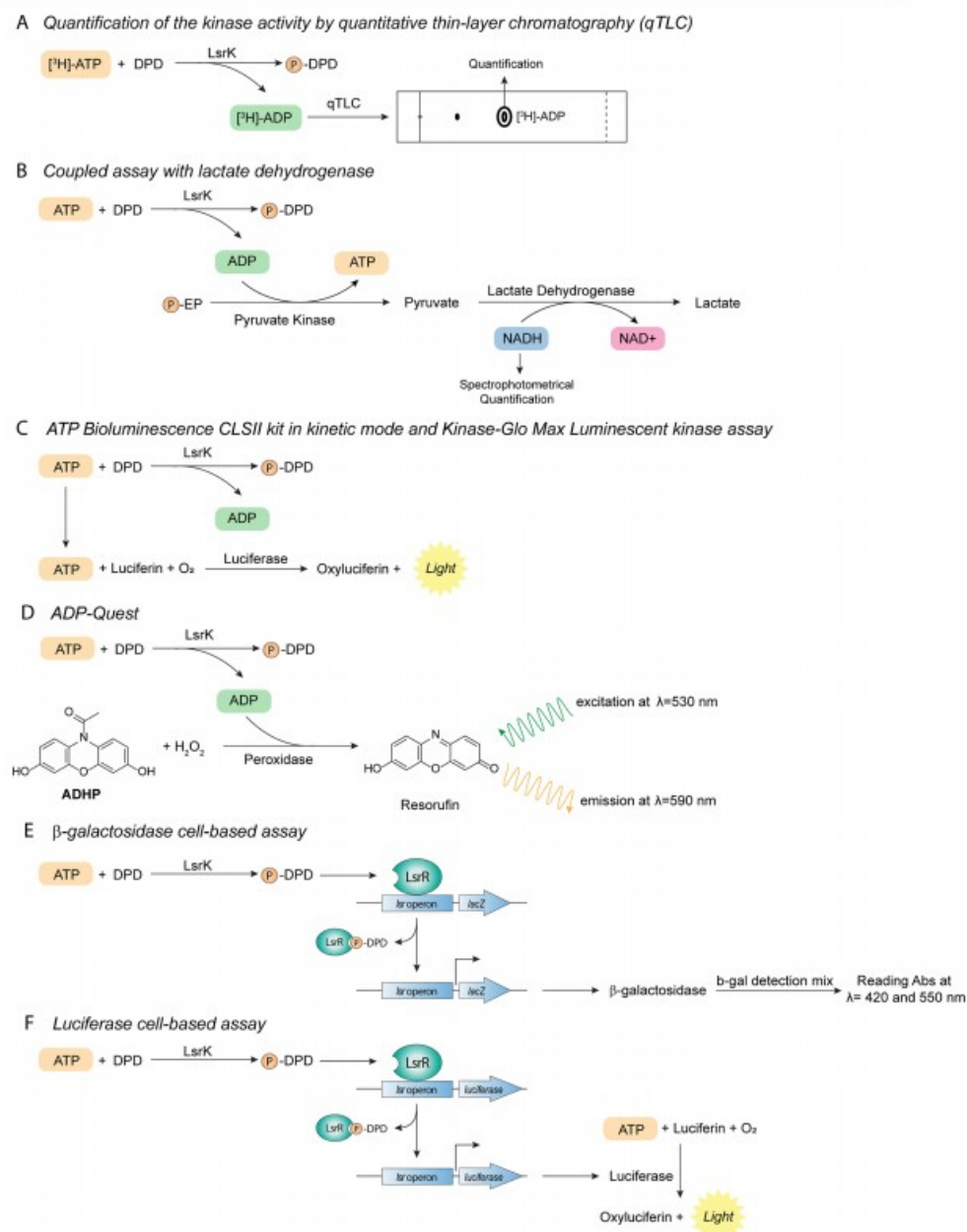
F

Figure 6. Target-based and cell-based in vitro biochemical assays developed so far for quantifying the LsrK inhibition and its effect on QS.

concentration after phosphorylation with the amount of emitted light (Figure 6C). This assay's advantages include a more stable luminescence signal and shorter analysis time, making it suitable for the screen of large compound libraries. It also allows higher ATP concentrations (up to 500 μM), thus making it more versatile.[71,93,97,98] ADP-Quest differs from the two kits described

above as it measures fluorescence. ADP-Quest exploits the ADP produced in the kinase reaction to convert 10-acetyl-3,7-dihydroxyphenoxazine (ADHP), a fluorescent dye precursor the fluorescent resorufin. ADHP is then transformed into the fluorescent molecule (λ = 530 nm for excitation, and λ = 590 nm for emission). Peroxidase catalyzes the latter reaction in the
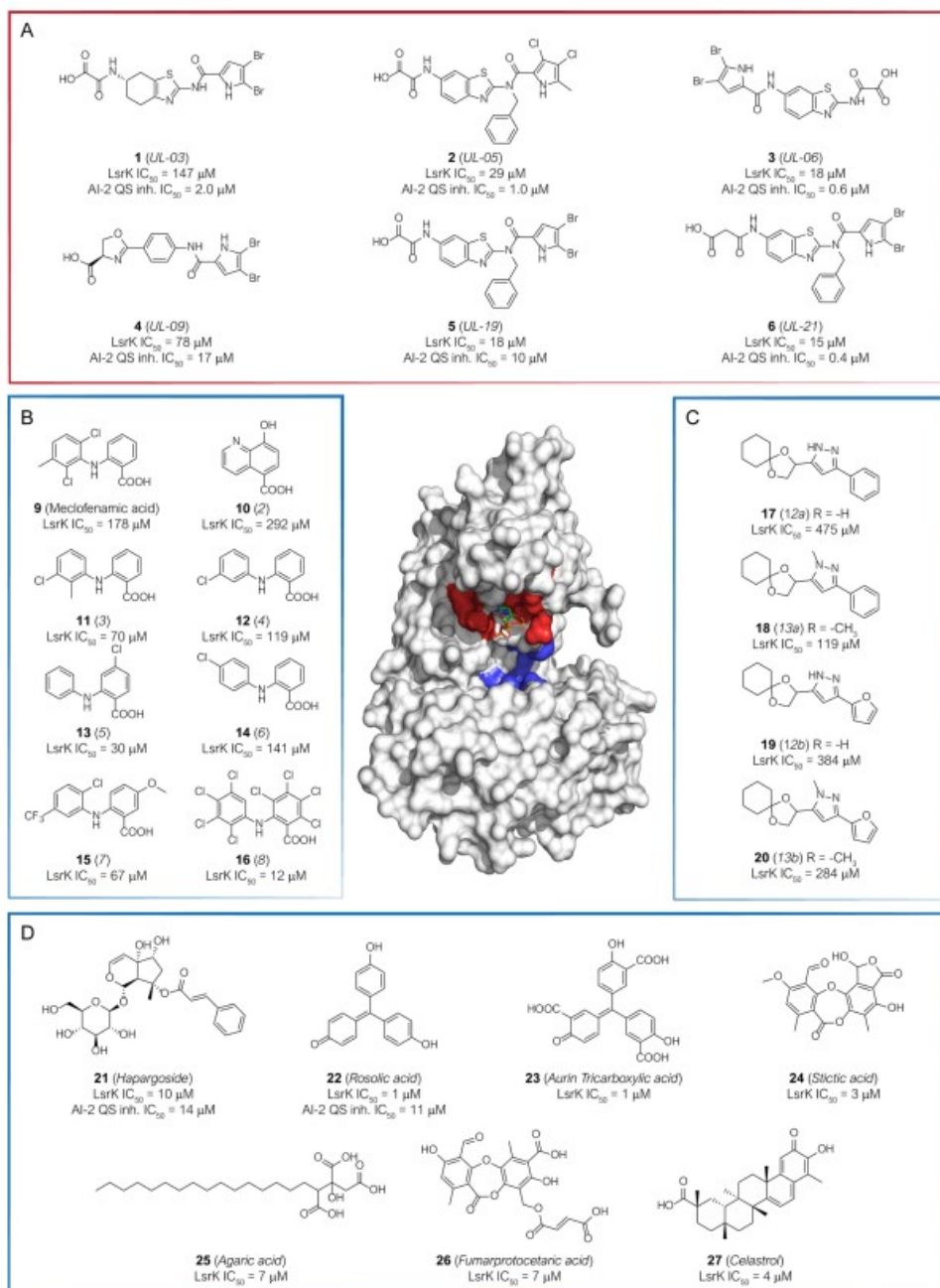
Figure 7. Chemical structure, LsrK inhibitory activity, and AI-2 QS inhibitory activity of the hit compounds identified as LsrK inhibitors so far and mainly discussed in this Perspective. The original numbering of the compounds in the parent paper or the common name for natural compounds is reported in the brackets. The inhibitors directed toward the ATP-binding site (surface colored red in the 3D structure of the protein) are enclosed in the red box. The inhibitors directed toward the putative DPD binding site (surface blue colored in the protein's 3D structure) are enclosed in blue boxes. (A) Primary hits targeting the ATP-binding site, identified by combining target-based and the new luminescent cell-based assay. (B) Hits identified by structure-based virtual screening. (C) DPD-inspired heterocyclic compounds designed in a structure-based approach. (D) Natural and synthetic hits identified by target-based HTS.

H
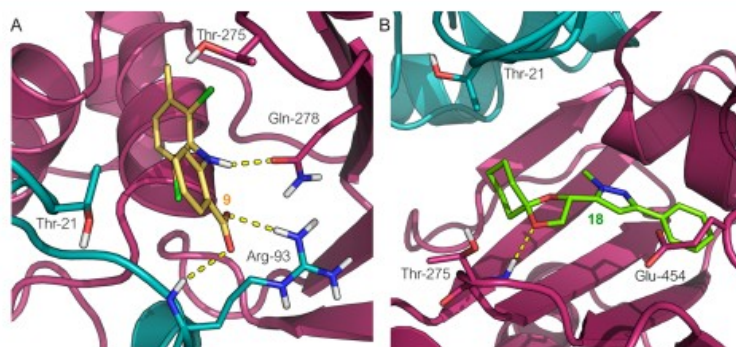
Figure 8. Predicted docking pose of (A) compound **9** (in yellow stick carbon) and of (B) compound **18** (in green stick carbon) at the putative binding site of DPD. Amino acid residues are visualized in stick mode with D-I's and D-II's carbon atoms in teal and magenta, respectively. Yellow dashed lines represent the hydrogen bonds. Heteroatoms are color-coded (oxygen atoms in red, nitrogen atoms in blue, sulfur atoms in yellow, phosphorus atoms in orange).

presence of hydrogen peroxide. The resulting fluorescence is directly proportional to the activity of the enzyme (Figure 6D). ADP-Quest is suitable for high-throughput screening.[88,99]

The assays described above are often coupled with other methods. For example, thermal shift assays are usually performed to confirm the direct interaction of modulators with LsrK.[93,97] Same answers can also be obtained from microscale thermophoresis assays.[97] Furthermore, to evaluate potential modulators' specificity, compounds can be tested with glycerokinase, an enzyme sharing a similarity with LsrK. The same kits and the same conditions used to evaluate LsrK modulation can be used to assess this property.

To study LsrK modulation's effect, QS inhibition can also be evaluated on the whole cell in cellular-based models. This assay is based on the measurement of the level of β-galactosidase activity controlled by the *lsr* promoter. LsrK phosphorylates DPD, and the produced P-DPD activates the *lsr* transcription with the production of β-galactosidase that can be quantified through a specific spectrofluorometric assay (Figure 6E).[100]

Gatta et al. have recently developed a new cell-based assay by engineering *E. coli* strain with a bacterial luciferase operon *luxABCDE* under the control of *lsr*. Thus, when AI-2 activates the QS, the *lux* expression is induced with the final production of light, whereas in the presence of an LsrK inhibitor and/or a QS quenching agent, the expression of the luciferase is inhibited with no production of light (Figure 6F).[101]

■ LSRK INHIBITORS

As stated above, LsrK is almost unexplored from a medicinal chemistry standpoint, and only a few compounds have been identified as LsrK inhibitors (Figure 7).

Gatta et al. reported the identification of a set of LsrK inhibitors with the capability to target the ATP binding pocket of the kinase (compounds **1−6**, Figure 7A).[101] The compounds were fished out from a library of 91 compounds originally designed as ATP-competitive gyrase B inhibitors. The library was first screened against LsrK in a target-based assay and 29 primary hits with IC$_{50}$ values ranging from 8 to 147 μM. The entire library was further assessed for AI-2-mediated QS interference using the new cell-based assay based on luminescence and developed by the same research group. The results obtained from the two assays were compared. Six primary LsrK inhibitors (**1−6**, Figure 7A) were able to inhibit the QS

activation in the cell-based assay with low-sub micromolar IC$_{50}$ (ranging from 0.4 to 17 μM). Interestingly, this cell-based assay fished out additional 18 hits with the potential capability to target other components of the *lsr* pathway.[101]

Medarametla et al. were the first to report a structure-based virtual screening study to identify new AI-2s structurally unrelated LsrK inhibitors and directed to the DPD binding site.[93] In the absence of detailed information on the three-dimensional structure of LsrK, a homology model for predicting the kinase's 3D structure was developed first. Four models of LsrK were developed, taking into account the open and closed conformation and the inclusion or exclusion of ATP. Virtual screening performed on a library of 132 566 compounds resulted in 104 compounds to be in vitro assessed. The primary screening led to identifying two hits compounds (**9**, namely meclofenamic acid and **10**) with an LrsK IC$_{50}$ of 178 and 292 μM, respectively. The two compounds were further used as templates for searching other analogues by catalogue approach. Fourteen commercially available derivatives were selected and assessed for LsrK inhibitor activity, resulting in six derivatives of compound **9** (compounds **11−16**, Figure 7B) with IC$_{50}$ ranging from 12 to 141 μM. A thermal shift assay confirmed the binding of the identified hit to LsrK. Docking of the selected hits suggested an interaction of the compounds with the putative DPD binding site and highlighted potential interactions with the catalytic residues (Arg93, Gln278, and Thr21) that could be exploited for the design of improved inhibitors (Figure 8A).

To identify LsrK inhibitors with a chemical structure distinctive from native DPD, Stotani et al., in a structure-based approach, designed, synthesized, and assessed in vitro the inhibition of LsrK by five small libraries of DPD-inspired heterocyclic derivatives (Het-DPD, Figure 9).[70,71] Taking together the information achieved from a structure−activity relationship (SAR) studies around the main backbone of DPD, a spyrocyclohexyl-dioxolane moiety replaced the portion essential for LsrK-mediated phosphorylation (*i.e.*, the two hydroxyl groups at C4 and C5). In contrast, the diketo group of DPD was embedded in heteroaromatic rings (such as pyrimidine, pyrazole, pyridine, and annulated pyrimidine, Figure 7C).

Among the entire library of compounds investigated by Stotani et al., the pyrazole-containing DPD derivatives **17**, **18**, **19**, and **20** (Figure 7C) emerged as the most promising LsrK inhibitors, with low/medium micromolar IC$_{50}$ against the
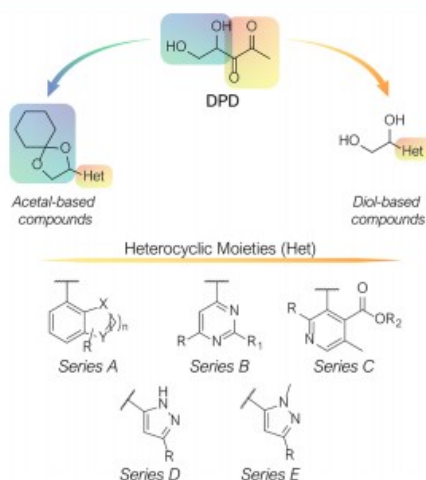
I

Figure 9. DPD-inspired heterocyclic compounds.

purified enzyme (475, 384, 119, and 284 μM, respectively). Docking of these compounds to the putative DPD-binding site was performed using the newly released structure of LsrK bound with ATP (PDB 5YA1).[71] From docking calculation, the DPD diol's protection in a spyro cyclohexyl-dioxolane moiety is essential for activity because, to accommodate the aryl-pyrazole core moiety, the cyclohexyl ring is positioned into the hydrophobic pocket delimited by Thr21 and Phe267, whereas the dioxolane ring establishes electrostatic interaction with the near Thr275 polar residues (Figure 8B). Conversely, the analogues carrying the free diol moiety resulted in less active because they are forced to orient the two hydroxyl groups toward the negative electrostatic potential surface of the binding site formed by Glu454 and Thr456, resulting in an unfavorable repulsion effect.

Interestingly, among the heterocyclic scaffolds explored, solely the pyrazole derivatives resulted in an effective inhibitor of LsrK probably due to the favorable H-bond interactions that the pyrazole ring can establish with critical residues of the binding site. Thus, the simultaneous presence of the dioxolane ring, the pyrazole moiety, and the protection of the diols as acetal seems necessary for LsrK inhibitor activity. The updated SAR considerations might be exploited in the design of other optimized Het-DPD derivatives.

Gatta et al. developed a reliable and robust target-based HTS-assay for the identification of new LsrK inhibitors.[97] This methodology was applied to a library of 2000 chemical compounds containing 50% of known drugs, 30% of natural compounds, and 20% of other bioactive compounds. At the end of the screening campaign, 12 compounds with an LsrK $IC_{50} <$ 10 μM were identified. According to the toxicological and physicochemical studies reported in the literature, eight compounds were discarded for promiscuous activity, toxicity, and impaired chemical-physical properties. Harpagoside (21, LsrK IC_{50} = 10 μM), rosolic acid (22, LsrK IC_{50} = 1 μM), aurin tricarboxylic acid (23, LsrK IC_{50} = 1 μM), and agaric acid (25, LsrK IC_{50} = 7 μM) were further assessed by thermal shift, confirming the binding to LsrK for the first three compounds (Figure 7D). The capability of the three identified compounds to interfere with the QS cascade was assessed in *E. coli* cell-

cultures through the β-galactosidase assay (Figure 6E). 21 and 22 showed an IC_{50} of 11 and 14 μM, respectively. Interestingly, 21 is a metabolite produced by *Harpagophytum procumbens*, popularly known as devil's claw, used in African traditional medicine as an anti-inflammatory and antirheumatic drug. Moreover, besides 21 and 25, other natural compounds such as stictic acid (24), fumarprotocetaric acid (26), and celastrol (27, from *Tripeterygium wilfordii*) resulted from the HTS as promising LsrK inhibitors with IC_{50} of 3, 7, and 3 μM, respectively (Figure 7). Of note, the last two compounds are both produced by many lichen species, which makes these organisms fascinating sources of LsrK inhibitors.[102−105]

■ CURRENT CHALLENGES AND FUTURE PERSPECTIVES

The WHO has identified AMR as a significant threat to public health and the economy. Superbug bacteria are responsible for about 25% of infections and almost 30% of AMR-related deaths. Conventional antibacterial drugs usually interfere with bacterial cell wall biosynthesis, protein synthesis, or DNA replication, and the search for new antimicrobials is still mainly focused on these approaches. However, the massive evolutive pressure, consequent to the misuse of antibiotics performed in the last decades, forced bacteria to develop strategies to overcome the antibiotics' efficacy. Thus, the hunt for new targets and innovative weapons to treat these superbug infections has become a priority. Although the WHO delineated global strategies to contain the spread of resistance, funding, and lack of resources remain significant obstacles in achieving this goal.[106] For cell−cell communication, bacteria use QS signaling, a mechanism that allows them to release and detect extracellular signals. As the QS signaling system is involved in bacterial resistance development, QS inhibition could become a new promising antibacterial strategy to prevent bacterial resistance and repress the expression of virulence factor genes related to population density. These virulence factors are not essential for bacterial growth and survival. Thus, focused treatment would not inhibit bacterial growth, not generate selective pressure, and, therefore, is expected to be associated with a much lower risk of resistance development. Advances in the research of QS may lead to the development of novel antibacterial compounds with new modes of action and, in consequence, may provide a paradigm shift in the fight against AMR. In the entire QS process, the bacterial LsrK kinase plays a key role, representing an attractive target. The relationship between LsrK and AMR has been well established. Thus, the exploitation of LsrK as a target to develop drugs to be used alone or in combination with current antimicrobials is at a pioneering stage and may represent an innovative strategy for fighting AMR.

Since the LsrK pathway has been discovered relatively recently, LsrK is still poorly explored from a pharmaceutical standpoint. At present, only a few molecules showing significant interactions with LsrK are known. In this scenario, nature-aided drug discovery can be considered a successful approach to discovering new LsrK inhibitors. Thus, results reported by Gatta et al. in 2019 pave the way to identify new hits from nature. Indeed, as a future perspective, the over 600 iridoid glycosides belonging class of harpagoside and identified in 57 families of different plants can be assessed for inhibition of LsrK.[107] On the other hand, both fumarprotocetraric acid and stictic acid belong to the class of depsidones, which are ubiquitous metabolites in lichens world. These data should push researchers to consider superior plants and lichens as exciting and innovative sources of

active metabolites. However, this research field is still in its infancy.

Although the knowledge about LsrK structure is still limited, the pilot studies described in this perspective offer an overview of the protein's behavior and highlight all the elements essential to understand better the protein—substrate dynamics and how to interfere with it. The comprehensive consideration of LsrK and related pathways may be an important strategy in developing a new generation of antimicrobials with unprecedented modes of actions and complementary to the currently available antibacterial agents. This strategy could allow fighting the projected worldwide occurrences of superbugs infections. This approach will be novel and nonincremental. The ability of this new generation of antimicrobial drug candidates to surpass any current or in-development technological paradigm is summarized in the following highlights:

- The identified lead compounds will divert from the conventional bacterial targets exploited by pharmaceutical companies to develop antibacterial drugs approved for humans.

- They will not directly kill the bacteria by inhibiting vital targets, but they will attenuate their virulence by interfering with their ability to communicate and organize in communities.

- They will not promote the AMR phenomenon as they will not act on vital targets for bacteria but instead interfere directly with the origin's resistance development process.

- They may restore the efficacy of currently available antibacterial drugs against resistant bacterial strains through their coadministration.

An in-depth structural insight into the kinase's structure and function, the generation of a portfolio of LsrK inhibitors, and the consequent in vivo demonstration of the engagement between LsrK and AMR will represent a breakthrough in the fight against antimicrobial resistance.

■ AUTHOR INFORMATION

Corresponding Author

Simona Collina — *Department of Drug Sciences, University of Pavia, 27100 Pavia, Italy;* ● orcid.org/0000-0002-2954-7558; Phone: 00390382422975; Email: simona.collina@unipv.it

Authors

Pasquale Linciano — *Department of Drug Sciences, University of Pavia, 27100 Pavia, Italy;* ● orcid.org/0000-0003-0382-7479

Valeria Cavalloro — *Department of Earth and Environmental Science, University of Pavia, 27100 Pavia, Italy*

Emanuela Martino — *Department of Earth and Environmental Science, University of Pavia, 27100 Pavia, Italy*

Johannes Kirchmair — *Department of Pharmaceutical Chemistry, Faculty of Life Sciences, University of Vienna, 1090 Vienna, Austria;* ● orcid.org/0000-0003-2667-5877

Roberta Listro — *Department of Drug Sciences, University of Pavia, 27100 Pavia, Italy*

Daniela Rossi — *Department of Drug Sciences, University of Pavia, 27100 Pavia, Italy*

Complete contact information is available at:
https://pubs.acs.org/10.1021/acs.jmedchem.0c01282

Author Contributions

The manuscript was written through the contributions of all authors. All authors have approved the final version of the manuscript.

Notes

The authors declare no competing financial interest.

Biographies

Pasquale Linciano received his Ph.D. in Pharmaceutical Sciences from the University of Chieti-Pescara in 2014. He spent six years as a postdoctoral research fellow at the University of Modena. Here, he had the opportunity to collaborate in a European and an AIRC project coordinated by Prof. Costi. His interests mainly focused on the drug design and synthesis of compounds with anti-infective, anticancer, and neuroprotective activity. One of his main research topics focuses on β-lactamase inhibitors for the treatment of bacterial AMR. He was a visiting student at the University of Siena in 2012 and the University of Genéve in 2013. Since March 2020, he is an Assistant Professor at the Department of Drug Science at the University of Pavia, working in the group of Prof. S. Collina.

Valeria Cavalloro graduated *cum laude* in Chemical and Pharmaceutical Sciences at the University of Pavia in 2017 under the supervision of Prof. Simona Collina. After that, she attended the postgraduate Master Course in Drug Design and Development at the same University. She is currently pursuing her Ph.D. in Earth and Environmental Sciences at the University of Pavia, mentored by Prof. Emanuela Martino. She was a visiting student at Inte: ligand (Vienna) under the supervision of Dr. Sharon Bryant. She is currently involved in the discovering of novel anticancer and antimicrobial agents from natural sources.

Emanuela Martino is an Assistant Professor at the University of Pavia. Graduated in Natural Science, she received her Ph.D. in Experimental Ecology and Geobotany in 2006 at the University of Pavia. She attended the postgraduate Master Course in Drug Design and Development at the same University, spending a training period in Indena (R&D, Settala, Milan). Since 2011, she is an Assistant Professor at the Earth and Environmental Sciences Department, University of Pavia, Italy. Her research activities are mainly focused on drug discovery from plant sources. The development of methodologies for the extraction of biologically active secondary metabolites, physicochemical characterization, and quantification is her main interest.

Johannes Kirchmair is an Assistant Professor in cheminformatics at the Department of Pharmaceutical Chemistry of the University of Vienna. He also is a group leader at the Center for Bioinformatics (ZBH) of the University of Hamburg. After earning his Ph.D. from the University of Innsbruck (2007), he started his career as an application scientist at Inte: Ligand GmbH (Vienna) and as a university assistant (University of Innsbruck). In 2010, he joined BASF SE (Ludwigshafen) as a postdoctoral research fellow. After that, he worked as a research associate at the University of Cambridge (2010—2013) and ETH Zurich (2013—2014). Johannes held a junior professorship in applied bioinformatics at the University of Hamburg (2014—2018) and an associate professorship in bioinformatics at the University of Bergen (2018—2019).

Roberta Listro graduated *cum laude* in Pharmacy at the University of Palermo in 2018, under the supervision of Dr. Valeria Raimondi, discussing a thesis about pyrrolomycins as antimicrobial agents. She is currently pursuing her Ph.D. in Chemical and Pharmaceutical Sciences and Industrial Innovation at the University of Pavia, under the supervision of Prof. Simona Collina. Her research activity is focused on the synthesis of novel compounds to combat cancer and microbial infections.

Daniela Rossi is an Assistant Professor at the Department of Drug Sciences of the University of Pavia since 2006. After her Ph.D. (2003), she spent four years in the pharmaceutical industry. Her research activity mainly focuses on rational drug design and structure–activity relationship studies of new biologically active compounds. Specifically, the identification and biological investigation of new modulators of sigma receptors and small molecules able to affect the protein kinase C (PKC)/ELAV proteins/mRNA system are the main topics of her research. The development of methodologies suitable for the preparation of homochiral compounds is another key interest.

Simona Collina is a Full Professor and Laboratory Head of the Medicinal Chemistry Laboratory (MedChemLab) at the Department of Drug Sciences at the University of Pavia, Italy. Her broad interest in medicinal chemistry and drug discovery encompasses the design and synthesis of new chemical entities and their therapeutic application, particularly cancer, pain, neurodegenerative, and infectious diseases.

ABBREVIATIONS USED

2-AA, 2-amino acetophenone; 6PGD, 6-phosphogluconate dehydrogenase; 6PLG, 6-phosphogluconolactonase; ADHP, 10-acetyl-3,7-dihydroxyphenoxazine; ADP, adenosine diphosphate; AHL, N-acyl homoserine lactones; AI-2, autoinducer-2; AMR, antimicrobial resistance; ATP, adenosine triphosphate; cAMP, cyclic adenosine monophosphate; CCR, carbon catabolite repression; CRP, cAMP receptor protein; DHAP, dihydroxyacetone phosphate; DSF, diffusible signal factor; EI, enzyme E I; EII, enzyme E II; EP, enolpyruvate; G6PD, glucose-6-phosphate dehydrogenase; GLASS, Global Antimicrobial Resistance Surveillance System; HPr, histidine protein; LuxS, S-ribosylhomocysteinase; P-DPD, S-3,3,4,5-tetrahydroxy-2-pentanone-5-phosphate; PEP, phosphoenol-pyruvate; Pfs, 5′-methylthioadenosine nucleosidase; PQS, *Pseudomonas* quinolone signal; P-TPO, 3,4,4-trihydroxy-2-pentanone-5-phosphate; PTS, dependent sugar phosphotransferase system; QS, quorum sensing; qTLC, thin-layer chromatography; R-DHMF, (2R,4S)-2,4-dihydroxy-2-methyldihydrofuran-3-one; R-THMF, (2R,4S)-2-methyl-2,3,3,4- tetrahydroxytetrahydrofuran; Ru5P, ribulose 5-phosphate; SAH, S-adenosylhomocysteine; SAM, S-adenosylmethionine; S-DHMF, (2S,4S)-2,4-dihydroxy-2-methyl-dihydrofuran-3-one; S-DPD, S-4,5-dihydroxy-2,3-pentanedione; SRH, S-ribosylhomocisteine; S-THMF, (2S,4S)-2-methyl-2,3,3,4-tetrahydroxytetrahydrofuran; S-THMF-borate, (2S,4S)-2-methyl-2,3,3,4-tetrahydroxytetrahydrofuranborate; S-THP, S-3,3,4,5-tetrahydroxy-2-pentanone; WHO, World Health Organization

REFERENCES

(1) *Antimicrobial Resistance: Global Report on Surveillance*; World Health Organization 2014.

(2) *Global Action Plan on Antimicrobial Resistance*; World Health Organization 2015.

(3) O' Neil, J. *Review on Antibiotic Resistance: Tackling a Crisis for the Health and Wealth of Nations*; Wellcome Trust, 2014.

(4) O'Neill, J. *Tackling Drug-Resistance Infection Globally: Final Report and Recommendation*; Wellcome Trust, 2016.

(5) Goff, D. A.; Kullar, R.; Bauer, K. A.; File, T. M. Eight Habits of Highly Effective Antimicrobial Stewardship Programs to Meet the Joint Commission Standards for Hospitals. *Clin. Infect. Dis.* **2017**, *64* (8), 1134–1139.

(6) *Drug-Resistant Infections: A Threat to Our Economic Future*; World Bank, 2017; https://openknowledge.worldbank.org/handle/10986/26707 (accessed on 2020-10).

(7) *Global Antimicrobial Resistance Surveillance System (GLASS) Report*; World Health Organization, 2017.

(8) McEwen, S. A.; Collignon, P. J. Antimicrobial Resistance: A One Health Perspective. *Microbiol. Spectr.* **2018**, *6* (2), 521–547.

(9) Munita, J. M.; Arias, C. A. Mechanisms of Antibiotic Resistance. *Microbiol. Spectrum* **2016**, *4* (2), 1–37.

(10) Mayers, D. L.; Sobel, J. D.; Ouellette, M.; Kaye, K. S.; Marchaim, D., Eds.; *Antimicrobial Drug Resistance*; Springer International Publishing: Cham, 2017.

(11) Ali, J.; Rafiq, Q. A.; Ratcliffe, E. Antimicrobial Resistance Mechanisms and Potential Synthetic Treatments. *Futur. Sci. OA* **2018**, *4*, FSO290.

(12) Ghai, I.; Ghai, S. Understanding Antibiotic Resistance via Outer Membrane Permeability. *Infect. Drug Resist.* **2018**, *11*, 523–530.

(13) Masi, M.; Réfregiers, M.; Pos, K. M.; Pagès, J.-M. Mechanisms of Envelope Permeability and Antibiotic Influx and Efflux in Gram-Negative Bacteria. *Nat. Microbiol.* **2017**, *2* (3), 17001.

(14) Linciano, P.; Cendron, L.; Gianquinto, E.; Spyrakis, F.; Tondi, D. Ten Years with New Delhi Metallo-β-Lactamase-1 (NDM-1): From Structural Insights to Inhibitor Design. *ACS Infect. Dis.* **2019**, *5* (1), 9–34.

(15) Gutkind, G. O.; Di Conza, J.; Power, P.; Radice, M. β-Lactamase-Mediated Resistance: A Biochemical, Epidemiological and Genetic Overview. *Curr. Pharm. Des.* **2012**, *19*, 164–208.

(16) Ramirez, M. S.; Tolmasky, M. E. Aminoglycoside Modifying Enzymes. *Drug Resist. Updates* **2010**, *13* (6), 151–171.

(17) Rabin, N.; Zheng, Y.; Opoku-Temeng, C.; Du, Y.; Bonsu, E.; Sintim, H. O. Biofilm Formation Mechanisms and Targets for Developing Antibiofilm Agents. *Future Med. Chem.* **2015**, *7* (4), 493–512.

(18) Tolker-Nielsen, T. Biofilm Development. *Microbiol. Spectrum* **2015**, *3*, MB-0001-2014.

(19) Khatoon, Z.; McTiernan, C. D.; Suuronen, E. J.; Mah, T.-F.; Alarcon, E. I. Bacterial Biofilm Formation on Implantable Devices and Approaches to Its Treatment and Prevention. *Heliyon* **2018**, *4* (12), No. e01067.

(20) Davies, D. Understanding Biofilm Resistance to Antibacterial Agents. *Nat. Rev. Drug Discovery* **2003**, *2* (2), 114–122.

(21) Rutherford, S. T.; Bassler, B. L. Bacterial Quorum Sensing: Its Role in Virulence and Possibilities for Its Control. *Cold Spring Harbor Perspect. Med.* **2012**, *2*, No. a012427.

(22) LaSarre, B.; Federle, M. J. Exploiting Quorum Sensing To Confuse Bacterial Pathogens. *Microbiol. Mol. Biol. Rev.* **2013**, *77* (1), 73–111.

(23) Papenfort, K.; Bassler, B. L. Quorum Sensing Signal-Response Systems in Gram-Negative Bacteria. *Nat. Rev. Microbiol.* **2016**, *14* (9), 576–588.

(24) Diggle, S. P.; Griffin, A. S.; Campbell, G. S.; West, S. A. Cooperation and Conflict in Quorum-Sensing Bacterial Populations. *Nature* **2007**, *450*, 411–414.

(25) Solano, C.; Echeverz, M.; Lasa, I. Biofilm Dispersion and Quorum Sensing. *Curr. Opin. Microbiol.* **2014**, *18*, 96–104.

(26) Rumbaugh, K. P.; Sauer, K. Biofilm Dispersion. *Nat. Rev. Microbiol.* **2020**, *18*, 571–586.

(27) Miller, M. B.; Bassler, B. L. Quorum Sensing in Bacteria. *Annu. Rev. Microbiol.* **2001**, *55* (1), 165–199.

(28) Waters, C. M.; Lu, W.; Rabinowitz, J. D.; Bassler, B. L. Quorum Sensing Controls Biofilm Formation in Vibrio Cholerae through Modulation of Cyclic Di-GMP Levels and Repression of VpsT. *J. Bacteriol.* **2008**, *190* (7), 2527–2536.

(29) Ahmed, N. A. A. M.; Petersen, F. C.; Scheie, A. A. AI-2 Quorum Sensing Affects Antibiotic Susceptibility in Streptococcus Anginosus. *J. Antimicrob. Chemother.* **2007**, *60* (1), 49–53.

(30) Zhu, J.; Miller, M. B.; Vance, R. E.; Dziejman, M.; Bassler, B. L.; Mekalanos, J. J. Quorum-Sensing Regulators Control Virulence Gene Expression in Vibrio Cholerae. *Proc. Natl. Acad. Sci. U. S. A.* **2002**, *99* (5), 3129–3134.

L

(31) Antunes, L. C. M.; Ferreira, R. B. R.; Buckner, M. M. C.; Finlay, B. B. Quorum Sensing in Bacterial Virulence. *Microbiology* **2010**, *156* (8), 2271−2282.

(32) Morrison, D. A. Streptococcal Competence for Genetic Transformation: Regulation by Peptide Pheromones. *Microb. Drug Resist.* **1997**, *3* (1), 27−37.

(33) Engebrecht, J.; Nealson, K.; Silverman, M. Bacterial Bio-luminescence: Isolation and Genetic Analysis of Functions from Vibrio Fischeri. *Cell* **1983**, *32* (3), 773−781.

(34) Bassler, B. L.; Wright, M.; Silverman, M. R. Multiple Signalling Systems Controlling Expression of Luminescence in Vibrio Harveyi: Sequence and Function of Genes Encoding a Second Sensory Pathway. *Mol. Microbiol.* **1994**, *13* (2), 273−286.

(35) Patzelt, D.; Wang, H.; Buchholz, I.; Rohde, M.; Gröbe, L.; Pradella, S.; Neumann, A.; Schulz, S.; Heyber, S.; Münch, K.; Münch, R.; Jahn, D.; Wagner-Döbler, I.; Tomasch, J. You Are What You Talk: Quorum Sensing Induces Individual Morphologies and Cell Division Modes in Dinoroseobacter Shibae. *ISME J.* **2013**, *7* (12), 2274−2286.

(36) Perchat, S.; Talagas, A.; Poncet, S.; Lazar, N.; Li de la Sierra-Gallay, I.; Gohar, M.; Lereclus, D.; Nessler, S. How Quorum Sensing Connects Sporulation to Necrotrophism in Bacillus Thuringiensis. *PLoS Pathog.* **2016**, *12* (8), No. e1005779.

(37) Zhu, L.; Chen, T.; Xu, L.; Zhou, Z.; Feng, W.; Liu, Y.; Chen, H. Effect and Mechanism of Quorum Sensing on Horizontal Transfer of Multidrug Plasmid RP4 in BAC Biofilm. *Sci. Total Environ.* **2020**, *698*, 134236.

(38) Givskov, M.; de Nys, R.; Manefield, M.; Gram, L.; Maximilien, R.; Eberl, L.; Molin, S.; Steinberg, P. D.; Kjelleberg, S. Eukaryotic Interference with Homoserine Lactone-Mediated Prokaryotic Signal-ling. *J. Bacteriol.* **1996**, *178* (22), 6618−6622.

(39) Chen, X.; Zhang, L.; Zhang, M.; Liu, H.; Lu, P.; Lin, K. Quorum Sensing Inhibitors: A Patent Review (2014−2018). *Expert Opin. Ther. Pat.* **2018**, *28* (12), 849−865.

(40) Brackman, G.; Coenye, T. Quorum Sensing Inhibitors as Anti-Biofilm Agents. *Curr. Pharm. Des.* **2014**, *21* (1), 5−11.

(41) Kalia, V. C. Quorum Sensing Inhibitors: An Overview. *Biotechnol. Adv.* **2013**, *31* (2), 224−245.

(42) Galloway, W. R. J. D.; Hodgkinson, J. T.; Bowden, S.; Welch, M.; Spring, D. R. Applications of Small Molecule Activators and Inhibitors of Quorum Sensing in Gram-Negative Bacteria. *Trends Microbiol.* **2012**, *20* (9), 449−458.

(43) Brackman, G.; Breyne, K.; De Rycke, R.; Vermote, A.; Van Nieuwerburgh, F.; Meyer, E.; Van Calenbergh, S.; Coenye, T. The Quorum Sensing Inhibitor Hamamelitannin Increases Antibiotic Susceptibility of Staphylococcus Aureus Biofilms by Affecting Peptidoglycan Biosynthesis and EDNA Release. *Sci. Rep.* **2016**, *6* (1), 20321.

(44) Kalia, D. Synthetic Quorum Sensing Inhibitors: Signal Analogues. In *Quorum Sensing vs Quorum Quenching: A Battle with No End in Sight*; Springer India: New Delhi, 2015; pp 285−302.

(45) Ji, G.; Beavis, R. C.; Novick, R. P. Cell Density Control of Staphylococcal Virulence Mediated by an Octapeptide Pheromone. *Proc. Natl. Acad. Sci. U. S. A.* **1995**, *92* (26), 12055−12059.

(46) Pearson, J. P.; Feldman, M.; Iglewski, B. H.; Prince, A. Pseudomonas Aeruginosa Cell-to-Cell Signaling Is Required for Virulence in a Model of Acute Pulmonary Infection. *Infect. Immun.* **2000**, *68* (7), 4331−4334.

(47) Bassler, B. L.; Losick, R. Bacterially Speaking. *Cell* **2006**, *125* (2), 237−246.

(48) Suga, H. Molecular Mechanisms of Bacterial Quorum Sensing as a New Drug Target. *Curr. Opin. Chem. Biol.* **2003**, *7* (5), 586−591.

(49) Geske, G. D.; Wezeman, R. J.; Siegel, A. P.; Blackwell, H. E. Small Molecule Inhibitors of Bacterial Quorum Sensing and Biofilm Formation. *J. Am. Chem. Soc.* **2005**, *127* (37), 12762−12763.

(50) Rasmussen, T. B.; Givskov, M. Quorum-Sensing Inhibitors as Anti-Pathogenic Drugs. *Int. J. Med. Microbiol.* **2006**, *296* (2−3), 149−161.

(51) Clatworthy, A. E.; Pierson, E.; Hung, D. T. Targeting Virulence: A New Paradigm for Antimicrobial Therapy. *Nat. Chem. Biol.* **2007**, *3* (9), 541−548.

(52) Allen, R. C.; Popat, R.; Diggle, S. P.; Brown, S. P. Targeting Virulence: Can We Make Evolution-Proof Drugs? *Nat. Rev. Microbiol.* **2014**, *12* (4), 300−308.

(53) Whiteley, M.; Diggle, S. P.; Greenberg, E. P. Progress in and Promise of Bacterial Quorum Sensing Research. *Nature* **2017**, *551* (7680), 313−320.

(54) Fuqua, W. C.; Winans, S. C.; Greenberg, E. P. Quorum Sensing in Bacteria: The LuxR-LuxI Family of Cell Density-Responsive Tran-scriptional Regulators. *J. Bacteriol.* **1994**, *176* (2), 269−275.

(55) Schuster, M.; Joseph Sexton, D.; Diggle, S. P.; Peter Greenberg, E. Acyl-Homoserine Lactone Quorum Sensing: From Evolution to Application. *Annu. Rev. Microbiol.* **2013**, *67* (1), 43−63.

(56) Parsek, M. R.; Val, D. L.; Hanzelka, B. L.; Cronan, J. E.; Greenberg, E. P. Acyl Homoserine-Lactone Quorum-Sensing Signal Generation. *Proc. Natl. Acad. Sci. U. S. A.* **1999**, *96* (8), 4360−4365.

(57) Kleerebezem, M.; Quadri, L. E. N.; Kuipers, O. P.; De Vos, W. M. Quorum Sensing by Peptide Pheromones and Two-component Signal-transduction Systems in Gram-positive Bacteria. *Mol. Microbiol.* **1997**, *24* (5), 895−904.

(58) Dunny, G. M.; Leonard, B. A. B. Cell-Cell Communication in Gram-Positive Bacteria. *Annu. Rev. Microbiol.* **1997**, *51* (1), 527−564.

(59) Pereira, C. S.; Thompson, J. A.; Xavier, K. B. AI-2-Mediated Signalling in Bacteria. *FEMS Microbiol. Rev.* **2013**, *37* (2), 156−181.

(60) Pesci, E. C.; Milbank, J. B. J.; Pearson, J. P.; McKnight, S.; Kende, A. S.; Greenberg, E. P.; Iglewski, B. H. Quinolone Signaling in the Cell-to-Cell Communication System of Pseudomonas Aeruginosa. *Proc. Natl. Acad. Sci. U. S. A.* **1999**, *96* (20), 11229−11234.

(61) Dubern, J.-F.; Diggle, S. P. Quorum Sensing by 2-Alkyl-4-Quinolones in Pseudomonas Aeruginosa and Other Bacterial Species. *Mol. BioSyst.* **2008**, *4* (9), 882.

(62) Barber, C. E.; Tang, J. L.; Feng, J. X.; Pan, M. Q.; Wilson, T. J. G.; Slater, H.; Dow, J. M.; Williams, P.; Daniels, M. J. A Novel Regulatory System Required for Pathogenicity of Xanthomonas Campestris Is Mediated by a Small Diffusible Signal Molecule. *Mol. Microbiol.* **1997**, *24* (3), 555−566.

(63) Deng, Y.; Wu, J.; Tao, F.; Zhang, L.-H. Listening to a New Language: DSF-Based Quorum Sensing in Gram-Negative Bacteria. *Chem. Rev.* **2011**, *111* (1), 160−173.

(64) Takano, E. γ-Butyrolactones: Streptomyces Signalling Molecules Regulating Antibiotic Production and Differentiation. *Curr. Opin. Microbiol.* **2006**, *9* (3), 287−294.

(65) Kesarwani, M.; Hazan, R.; He, J.; Que, Y.; Apidianakis, Y.; Lesic, B.; Xiao, G.; Dekimpe, V.; Milot, S.; Deziel, E.; Lépine, F.; Rahme, L. G. A Quorum Sensing Regulated Small Volatile Molecule Reduces Acute Virulence and Promotes Chronic Infection Phenotypes. *PLoS Pathog.* **2011**, *7* (8), No. e1002192.

(66) Loh, J.; Carlson, R. W.; York, W. S.; Stacey, G. Bradyoxetin, a Unique Chemical Signal Involved in Symbiotic Gene Regulation. *Proc. Natl. Acad. Sci. U. S. A.* **2002**, *99* (22), 14446−14451.

(67) Taga, M. E.; Semmelhack, J. L.; Bassler, B. L. The LuxS-Dependent Autoinducer AI-2 Controls the Expression of an ABC Transporter That Functions in AI-2 Uptake in Salmonella Typhimu-rium. *Mol. Microbiol.* **2001**, *42* (3), 777−793.

(68) Rhoads, M. K.; Hauk, P.; Terrell, J.; Tsao, C. Y.; Oh, H.; Raghavan, S. R.; Mansy, S. S.; Payne, G. F.; Bentley, W. E. Incorporating LsrK AI-2 Quorum Quenching Capability in a Functionalized Biopolymer Capsule. *Biotechnol. Bioeng.* **2018**, *115* (2), 278−289.

(69) Quan, D. N.; Bentley, W. E. Gene Network Homology in Prokaryotes Using a Similarity Search Approach: Queries of Quorum Sensing Signal Transduction. *PLoS Comput. Biol.* **2012**, *8* (8), No. e1002637.

(70) Stotani, S.; Gatta, V.; Medda, F.; Padmanaban, M.; Karawajczyk, A.; Tammela, P.; Giordanetto, F.; Tzalis, D.; Collina, S. A Versatile Strategy for the Synthesis of 4,5-Dihydroxy-2,3-Pentanedione (DPD) and Related Compounds as Potential Modulators of Bacterial Quorum Sensing. *Molecules* **2018**, *23* (10), 2545.

(71) Stotani, S.; Gatta, V.; Medarametla, P.; Padmanaban, M.; Karawajczyk, A.; Giordanetto, F.; Tammela, P.; Laitinen, T.; Poso, A.; Tzalis, D.; Collina, S. DPD-Inspired Discovery of Novel LsrK Kinase Inhibitors: An Opportunity to Fight Antimicrobial Resistance. *J. Med. Chem.* **2019**, *62* (5), 2720−2737.

(72) Federle, M. J.; Bassler, B. L. Interspecies Communication in Bacteria. *J. Clin. Invest.* **2003**, *112* (9), 1291−1299.

(73) Singh, V.; Lee, J. E.; Núñez, S.; Howell, P. L.; Schramm, V. L. Transition State Structure of 5′-Methylthioadenosine/ S -Adenosylhomocysteine Nucleosidase from Escherichia Coli and Its Similarity to Transition State Analogues †. *Biochemistry* **2005**, *44* (35), 11647−11659.

(74) Chen, X.; Schauder, S.; Potier, N.; Van Dorsselaer, A.; Pelczer, I.; Bassler, B. L.; Hughson, F. M. Structural Identification of a Bacterial Quorum-Sensing Signal Containing Boron. *Nature* **2002**, *415* (6871), 545−549.

(75) Globisch, D.; Lowery, C. A.; McCague, K. C.; Janda, K. D. Uncharacterized 4,5-Dihydroxy-2,3-Pentanedione (DPD) Molecules Revealed Through NMR Spectroscopy: Implications for a Greater Signaling Diversity in Bacterial Species. *Angew. Chem., Int. Ed.* **2012**, *51* (17), 4204−4208.

(76) Pereira, C. S.; McAuley, J. R.; Taga, M. E.; Xavier, K. B.; Miller, S. T. Sinorhizobium Meliloti, a Bacterium Lacking the Autoinducer-2 (AI-2) Synthase, Responds to AI-2 Supplied by Other Bacteria. *Mol. Microbiol.* **2008**, *70* (5), 1223−1235.

(77) Miller, S. T.; Xavier, K. B.; Campagna, S. R.; Taga, M. E.; Semmelhack, M. F.; Bassler, B. L.; Hughson, F. M. Salmonella Typhimurium Recognizes a Chemically Distinct Form of the Bacterial Quorum-Sensing Signal AI-2. *Mol. Cell* **2004**, *15* (5), 677−687.

(78) Kavanaugh, J. S.; Gakhar, L.; Horswill, A. R. The Structure of LsrB from Yersinia Pestis Complexed with Autoinducer-2. *Acta Crystallogr., Sect. F: Struct. Biol. Cryst. Commun.* **2011**, *67* (12), 1501−1505.

(79) Li, J.; Wang, L.; Hashimoto, Y.; Tsao, C.; Wood, T. K.; Valdes, J. J.; Zafiriou, E.; Bentley, W. E. A Stochastic Model of Escherichia Coli AI-2 Quorum Signal Circuit Reveals Alternative Synthesis Pathways. *Mol. Syst. Biol.* **2006**, *2* (1), 67.

(80) Xavier, K. B.; Bassler, B. L. Interference with AI-2-Mediated Bacterial Cell-Cell Communication. *Nature* **2005**, *437* (7059), 750−753.

(81) Herzberg, M.; Kaye, I. K.; Peti, W.; Wood, T. K. YdgG (TqsA) Controls Biofilm Formation in Escherichia Coli K-12 through Autoinducer 2 Transport. *J. Bacteriol.* **2006**, *188* (2), 587−598.

(82) Li, J.; Attila, C.; Wang, L.; Wood, T. K.; Valdes, J. J.; Bentley, W. E. Quorum Sensing in Escherichia Coli Is Signaled by AI-2/LsrR: Effects on Small RNA and Biofilm Architecture. *J. Bacteriol.* **2007**, *189* (16), 6011−6020.

(83) Ha, J.-H.; Eo, Y.; Grishaev, A.; Guo, M.; Smith, J. A. I.; Sintim, H. O.; Kim, E.-H.; Cheong, H.-K.; Bentley, W. E.; Ryu, K.-S. Crystal Structures of the LsrR Proteins Complexed with Phospho-AI-2 and Two Signal-Interrupting Analogues Reveal Distinct Mechanisms for Ligand Recognition. *J. Am. Chem. Soc.* **2013**, *135* (41), 15526−15535.

(84) Zhu, J.; Hixon, M. S.; Globisch, D.; Kaufmann, G. F.; Janda, K. D. Mechanistic Insights into the LsrK Kinase Required for Autoinducer-2 Quorum Sensing Activation. *J. Am. Chem. Soc.* **2013**, *135* (21), 7827−7830.

(85) Marques, J. C.; Lamosa, P.; Russell, C.; Ventura, R.; Maycock, C.; Semmelhack, M. F.; Miller, S. T.; Xavier, K. B. Processing the Interspecies Quorum-Sensing Signal Autoinducer-2 (AI-2). *J. Biol. Chem.* **2011**, *286* (20), 18331−18343.

(86) Marques, J. C.; Oh, I. K.; Ly, D. C.; Lamosa, P.; Ventura, M. R.; Miller, S. T.; Xavier, K. B. LsrF, a Coenzyme A-Dependent Thiolase, Catalyzes the Terminal Step in Processing the Quorum Sensing Signal Autoinducer-2. *Proc. Natl. Acad. Sci. U. S. A.* **2014**, *111* (39), 14235−14240.

(87) Xavier, K. B.; Bassler, B. L. Regulation of Uptake and Processing of the Quorum-Sensing Autoinducer AI-2 in Escherichia Coli. *J. Bacteriol.* **2005**, *187* (1), 238−248.

(88) Roy, V.; Fernandes, R.; Tsao, C. Y.; Bentley, W. E. Cross Species Quorum Quenching Using a Native AI-2 Processing Enzyme. *ACS Chem. Biol.* **2010**, *5* (2), 223−232.

(89) Ha, J. H.; Hauk, P.; Cho, K.; Eo, Y.; Ma, X.; Stephens, K.; Cha, S.; Jeong, M.; Suh, J. Y.; Sintim, H. O.; Bentley, W. E.; Ryu, K. S. Evidence of Link between Quorum Sensing and Sugar Metabolism in Escherichia Coli Revealed via Cocrystal Structures of LsrK and HPr. *Sci. Adv.* **2018**, *4* (6), No. eaar7063.

(90) Xavier, K. B.; Miller, S. T.; Lu, W.; Kim, J. H.; Rabinowitz, J.; Pelczer, I.; Semmelhack, M. F.; Bassler, B. L. Phosphorylation and Processing of the Quorum-Sensing Molecule Autoinducer-2 in Enteric Bacteria. *ACS Chem. Biol.* **2007**, *2* (2), 128−136.

(91) Ha, J.-H.; Eo, Y.; Ahn, H.-C.; Ryu, K.-S. Increasing the Soluble Expression and Crystallization of the Escherichia Coli Quorum-Sensing Protein LsrK. *Acta Crystallogr., Sect. F: Struct. Biol. Commun.* **2017**, *73* (5), 253−258.

(92) Horstmann, N.; Seidel, G.; Aung-Hilbrich, L.-M.; Hillen, W. Residues His-15 and Arg-17 of HPr Participate Differently in Catabolite Signal Processing via CcpA. *J. Biol. Chem.* **2007**, *282* (2), 1175−1182.

(93) Medarametla, P.; Gatta, V.; Kajander, T.; Laitinen, T.; Tammela, P.; Poso, A. Structure-Based Virtual Screening of LsrK Kinase Inhibitors to Target Quorum Sensing. *ChemMedChem* **2018**, *13* (22), 2400−2407.

(94) Taga, M. E.; Miller, S. T.; Bassler, B. L. Lsr-Mediated Transport and Processing of AI-2 in Salmonella Typhimurium. *Mol. Microbiol.* **2003**, *50* (4), 1411−1427.

(95) Viht, K.; Vaasa, A.; Raidaru, G.; Enkvist, E.; Uri, A. Fluorometric TLC Assay for Evaluation of Protein Kinase Inhibitors. *Anal. Biochem.* **2005**, *340* (1), 165−170.

(96) Tsuchikama, K.; Zhu, J.; Lowery, C. A.; Kaufmann, G. F.; Janda, K. D. C4-Alkoxy-HPD: A Potent Class of Synthetic Modulators Surpassing Nature in AI-2 Quorum Sensing. *J. Am. Chem. Soc.* **2012**, *134* (33), 13562−13564.

(97) Gatta, V.; Ilina, P.; Porter, A.; McElroy, S.; Tammela, P. Targeting Quorum Sensing: High-Throughput Screening to Identify Novel Lsrk Inhibitors. *Int. J. Mol. Sci.* **2019**, *20* (12), 3112.

(98) Bell, R. A. V.; Storey, K. B. Novel Detection Method for Chemiluminescence Derived from the Kinase-Glo Luminescent Kinase Assay Platform: Advantages over Traditional Microplate Luminometers. *MethodsX* **2014**, *1*, 96−101.

(99) Charter, N. W.; Kauffman, L.; Singh, R.; Eglen, R. M. A Generic, Homogenous Method for Measuring Kinase and Inhibitor Activity via Adenosine 5′-Diphosphate Accumulation. *J. Biomol. Screening* **2006**, *11* (4), 390−399.

(100) Ilina, P.; Ma, X.; Sintim, H. O.; Tammela, P. Miniaturized Whole-Cell Bacterial Bioreporter Assay for Identification of Quorum Sensing Interfering Compounds. *J. Microbiol. Methods* **2018**, *154*, 40−45.

(101) Gatta, V.; Tomašič, T.; Ilaš, J.; Zidar, N.; Peterlin Mašič, L.; Barančoková, M.; Frlan, R.; Anderluh, M.; Kikelj, D.; Tammela, P. A New Cell-Based Al-2-Mediated Quorum Sensing Interference Assay in Screening of LsrK-Targeted Inhibitors. *ChemBioChem* **2020**, *21*, 1918.

(102) Mišić, M.; Ranković, B.; Sukdolak, S. Antimicrobial Activity of Fumarprotocetraric Acid, Lecanoric Acid, Protocetraric Acid and Stictic Acid Isolated from Different Species of Lichen. *Planta Med.* **2008**, *74* (09), PA228.

(103) Ranković, B.; Mišić, M.; Sukdolak, S. The Antimicrobial Activity of Substances Derived from the Lichens Physcia Aipolia, Umbilicaria Polyphylla, Parmelia Caperata and Hypogymnia Physodes. *World J. Microbiol. Biotechnol.* **2008**, *24* (7), 1239−1242.

(104) Kosanić, M.; Ranković, B.; Stanojković, T.; Rančić, A.; Manojlović, N. Cladonia Lichens and Their Major Metabolites as Possible Natural Antioxidant, Antimicrobial and Anticancer Agents. *LWT - Food Sci. Technol.* **2014**, *59* (1), 518−525.

(105) Yılmaz, M.; Türk, A. Ö.; Tay, T.; Kıvanç, M. The Antimicrobial Activity of Extracts of the Lichen Cladonia Foliacea and Its (−)-Usnic Acid, Atranorin, and Fumarprotocetraric Acid Constituents. *Z. Naturforsch., C: J. Biosci.* **2004**, *59* (3−4), 249−254.

N

(106) *Antibacterial Agents in Clinical Development*; World Health Organization **2019**.

(107) Yamane, H.; Konno, K.; Sabelis, M.; Takabayashi, J.; Sassa, T.; Oikawa, H. *Chemical Defence and Toxins of Plants*; Liu, H.-W., Mander, L., Eds.; Elsevier: Oxford, 2010; Chapter 4.08, pp 339−385 .

O

Paper 5

![molecules logo] **molecules**

Article

Microwave-Assisted Extraction and HPLC-UV-CD Determination of (S)-usnic Acid in *Cladonia foliacea*

Valeria Cavalloro [1,†], Giorgio Marrubini [2,†], Rita Stabile [2], Daniela Rossi [2], Pasquale Linciano [2,*], Gabriele Gheza [3], Silvia Assini [1], Emanuela Martino [1,*] and Simona Collina [2]

1 Department of Earth and Environmental Sciences, University of Pavia, 27100 Pavia, Italy; valeria.cavalloro01@universitadipavia.it (V.C.); silviapaola.assini@unipv.it (S.A.)
2 Department of Drug Sciences, University of Pavia, 27100 Pavia, Italy; giorgio.marrubini@unipv.it (G.M.); rita.stabile01@universitadipavia.it (R.S.); daniela.rossi@unipv.it (D.R.); simona.collina@unipv.it (S.C.)
3 Department of Biological Geological and Environmental Sciences University of Bologna, 40126 Bologna, Italy; gheza.gabriele@gmail.com
* Correspondence: pasquale.linciano@unipv.it (P.L.); emanuela.martino@unipv.it (E.M.)
† Authors contributed equally to this work.

Abstract: During the years, many usnic acid (UA) conjugates have been synthesized to obtain potent endowed with biological properties. Since (S)-UA is less abundant in nature than (R)-enantiomer, it is difficult to source, thus precluding a deeper investigation. Among the lichens producing UA, *Cladonia foliacea* is a valuable (S)-UA source. In the present work, we report on a rapid HPLC-UV/PAD-CD protocol suitable for the analysis and the identification of the main secondary metabolites present in *C. foliacea* extract. Best results were achieved using XBridge Phenyl column and acetonitrile and water, which were both added with formic acid as mobile phase in gradient elution. By combining analytical, spectroscopical, and chiroptical analysis, the most abundant analyte was unambiguously identified as (S)-UA. Accordingly, a versatile microwave-assisted extractive (MAE) protocol, assisted by a design of experiment (DoE), to quantitatively recover (S)-UA was set up. The best result in terms of UA extraction yield was obtained using ethanol and heating at 80 °C under microwave irradiation for 5 min. Starting from 100 g of dried *C. foliacea*, 420 mg of (S)-UA were achieved. Thus, our extraction method resulted in a suitable protocol to produce (S)-UA from *C. foliacea* for biological and pharmaceutical investigation or commercial purposes.

Keywords: *Cladonia foliacea*; usnic acid; chiroptical properties; absolute configuration; HPLC-UV/PAD-CD; DoE; MAE; lichens

1. Introduction

Metabolites produced by lichens are still poorly investigated, although these organisms are commonly used in folk medicine to treat pathological conditions [1–9]. Among the most investigated metabolites, usnic acid (UA) deserved attention due to its intrinsic properties and its potential use as chiral synthon. UA is a dibenzofuran derivative, and it is characterized by the presence of a stereogenic center (Figure 1). Both enantiomers occur in nature, depending on the producing organism. The (R)-configured enantiomer of UA is the most abundant in nature, and *Cladonia arbuscula*, *C. mitis*, *Ramalina boninensis*, *R. pacifica*, *R. roesleri*, *R. farinacea*, *Usnea diffracta*, *U. longissima*, *U. hirta*, *U. steineri*, *Flavoparmelia caperata*, and *Xanthoparmelia chlorochroa* were identified as valuable source for its extraction. Conversely, (S)-UA was isolated as an exclusive enantiomer in few species of *Cladonia* (*C. uncialis* and *C. foliacea*) and *Alectoria* (*A. lata* and *A. ochroleuca*) [10]. In another few species of lichens, UA was detected as a mixture of (R)- and (S)-isomers in different ratios [10].
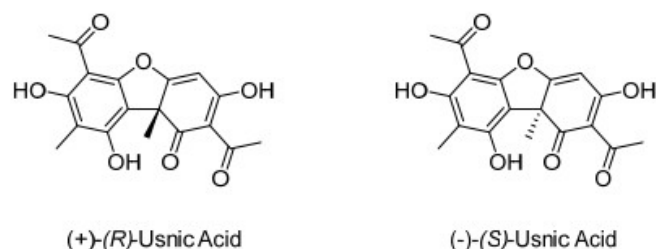
Figure 1. Chemical structure of usnic acid (UA) enantiomers.

UA has demonstrated interesting bioactivity from a biological standpoint, with antimicrobial, cytotoxic, or anti-inflammatory properties [10]. Moreover, UA was exploited as a useful intermediate to obtain potent analogs with improved biological profiles [11–14]. The chemical modifications introduced in the main scaffold of UA are resumed in Figure 2 [13,15–25]. All these chemical modifications preserve the stereochemistry of the UA used as starting material.
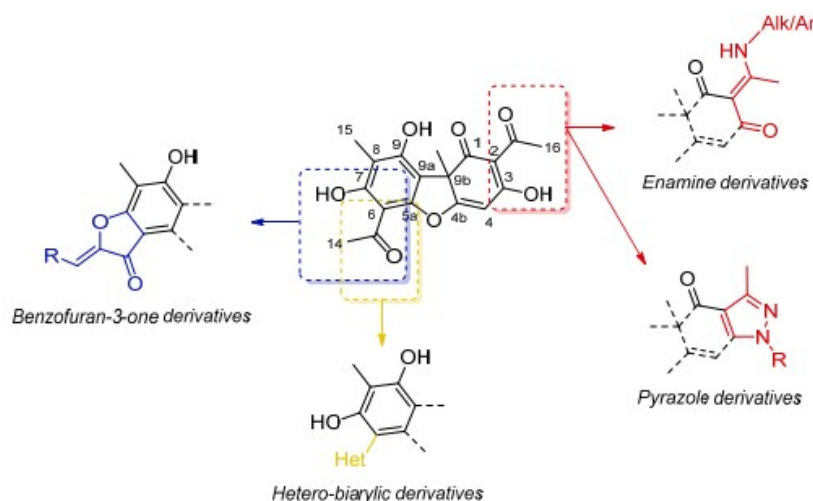
Figure 2. Chemical modifications of the main core scaffold of UA apported in the derivatives described in the literature [13,15–25].

However, most of the published data concern (*R*)-UA, whereas only a few studies regarding (*S*)-UA are described. Moreover, only a small number of reports refer to (R)- and (S)-UA activity when examined in comparison. The discrepancy about the investigations around the (*R*)- and (*S*)-UA results from the different accessibility and availability of the two enantiomers. Indeed, (*R*)-UA is commercially available due to the high abundance of accessible natural sources. In contrast, (*S*)-UA is less naturally abundant. It is not available from the leading chemical suppliers; otherwise, it is sold at a retail cost 30 times higher than the (*R*)-enantiomer. Therefore, the prior extraction of (*S*)-UA was required before proceeding with the biological or pharmacological investigation or the further chemical modification, thus hugely limiting the use and investigation of the (*S*)-UA so far.

As an alternative to the extractive procedure for the production of UA, only two synthetic strategies have been reported (Figure 3) [26,27].
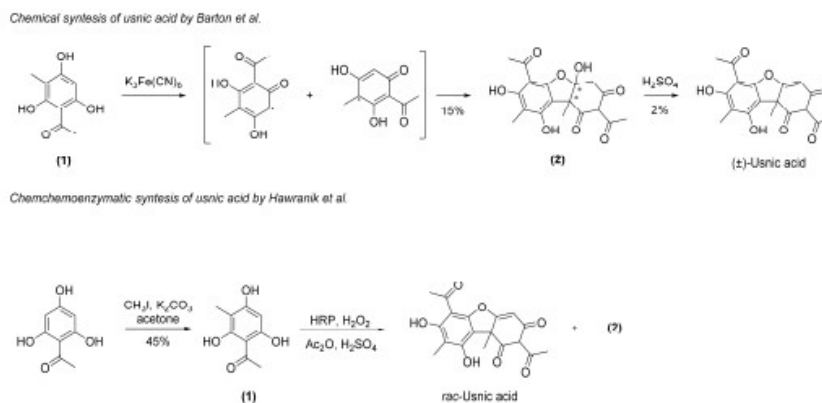
164

Chemical syntesis of usnic acid by Barton et al.

Chemchemoenzymatic syntesis of usnic acid by Hawranik et al.

Figure 3. Chemical and chemoenzymatic synthesis of UA.

These processes suffer from several drawbacks such as the availability of the starting materials, the employment of hazardous reactive or of hard to handle enzymes, the cumbersome purification procedures, and the difficulty to control the stereochemistry. Indeed, following these two procedures, UA was obtained exclusively as a racemic mixture and in poor yield (overall yield 2%) or in mixture with the hydrated derivative (2). Thus, the extraction of enantiomeric (*R*)- or (*S*)-UA from lichens remains the preferred procedure. To the best of our knowledge, the extraction protocols for UA reported in the literature mainly exploit maceration, Soxhlet, or supercritical CO_2 extraction, using diverse solvents such as water, methanol, ethanol, acetone, or benzene and with an extraction time ranging between 1 and 6 h. Several analytical procedures aimed at identifying and quantifying UA in the dry extract or biological fluids, including High-Performance Liquid Chromatography (HPLC)/HPLC coupled with MS or UV detector, High-Performance Thin Layer Chromatography (HPTLC) and Thin Layer Chromatography (TLC), were developed [28–37].

Starting from these considerations, herein, we focused on *Cladonia foliacea* as a valuable source of this metabolite [38–40]. *C. foliacea* (*Cladoniaceae*, *Lecanorales*, lichenized *Ascomycota*) is a soil-dwelling lichen with a leafy appearance, being its thallus composed of squamules organized in pads (Figure 4). *C. foliacea* has been already reported as one of the few lichen species able to exclusively produce the (S)-enantiomer of UA. Moreover, *C. foliacea* is widespread in Eurasia, occurring only in open dry habitats on oligotrophic soils in lowlands and hills, mostly under temperate climate. *C. foliacea* spontaneously grows in inland sand dunes in the western Po Plain (Lombardy region, Nord Italy). Considering this, studies about this interesting species can lead not only to the valorization of our biodiversity but also to the conservation and protection of the open dry habitats, which typically host this and other *Cladonia* species [41–43].

In the present work, we report on a rapid HPLC-UV/PAD-CD analytical methodology suitable for the analysis and the identification of the main secondary metabolites present in *C. foliacea* crude extract. By combining spectroscopical and chiroptical analysis, the main secondary metabolites present in the crude extract have been identified, with (*S*)-UA resulting in the most abundant. To exhaustively recover (*S*)-UA from *C. foliacea*, A versatile microwave-assisted extractive (MAE) protocol, developed by a design of experiment (DoE), was then set up.

Figure 4. *Cladonia foliacea*, photo snapped.

2. Results

2.1. Isolation and Characterization of the Main Metabolites Present in C. foliacea Extract

Thalli of *C. foliacea* were harvested from a lowland dry grassland located at *Bosco della Ghisolfa* (Province of Pavia, Northern Italy). They were used to prepare a pilot extract by an in-house consolidated microwave-assisted extraction (MAE) protocol [44–51]. The natural matrix was subjected to microwave irradiation, using acetone as extractive solvent [52].

The solvent was evaporated. The obtained crude was used to set up a rapid and economic HPLC-UV/PAD-CD protocol that was suitable for the analysis of the content of the lichen extract and for gaining information on the stereochemical properties of the analytes present within. Two different stationary phases with complementary selectivity were investigated: a classical C-18 reversed-phase and an XBridge Phenyl stationary phase. The latter contains bonded aromatic ligands, and therefore, it is useful for analyzing polyaromatic compounds. The best results in terms of the time of analysis, peak shape, and peak resolution were achieved using the XBridge Phenyl (5 μm, 4.6 × 150 mm) column. Acetonitrile (A) and water (B), both added with formic acid (0.1%, *v/v*), were used as mobile phase. A gradient elution was set up: from 75% to 100% of A in 7 min, followed by a 100% isocratic of A for 1 min.

The chromatographic HPLC-UV/PAD-CD profile of the crude extract is reported in Figure 5A. Three prominent and fully resolved peaks were detected in the UV trace at 2.8, 4.3, and 4.9 min (Figure 5A, above). To investigate the chiroptical properties of the analytes present in the crude extract, the in-line circular dichroism of the eluate was registered at 270 nm. The CD traces of the crude extract showed that the two peaks at 2.8 and 4.3 min were optically inactive, whereas the peak at 4.9 min registered a positive Cotton effect (Figure 5A, below).

The chemical identification of the three detected secondary metabolites was investigated, combining analytical and spectroscopical approaches [53]. Therefore, the crude extract was subjected to HPLC-ESI-MS to determine the m/z ratio of the three metabolites, which resulted in 473, 375, and 344 m/z for the compounds eluting at 2.8, 4.3, and 4.9 min, respectively. The ESI mass spectra of the three analytes are reported in Figure 5B. By querying online spectral databases for natural product identification, the molecular mass and mass spectra of the three analytes detected in the crude extract of *C. foliacea* were compatible with those of fumarprotocetraric acid (t_R = 2.8 min, ESI-MS [M-H]$^-$ calcd for $C_{22}H_{15}O_{12}^-$: 471.1; found 471.8; MW = 472.4), atranorin (t_R = 4.3 min, ESI-MS [M-H]$^-$ calcd for $C_{19}H_{17}O_8^-$: 373.1; found 372.9; MW = 374.1), and UA (t_R = 4.9 min, ESI-MS [M-H]$^-$ calcd for $C_{18}H_{15}O_7^-$: 343.1; found 343.0; MW = 344.3). These three proposed secondary metabolites are highly plausible, since fumarprotocetraric acid, atranorin, and in particular UA have been already detected in *C. foliacea*. Moreover, the proposed structures are in accordance with the results observed in the HPLC-CD analysis: fumarprotocetraric

acid and atranorin are achiral compounds, whereas UA, unless in a racemic mixture, may exert a Cotton effect in CD spectra.
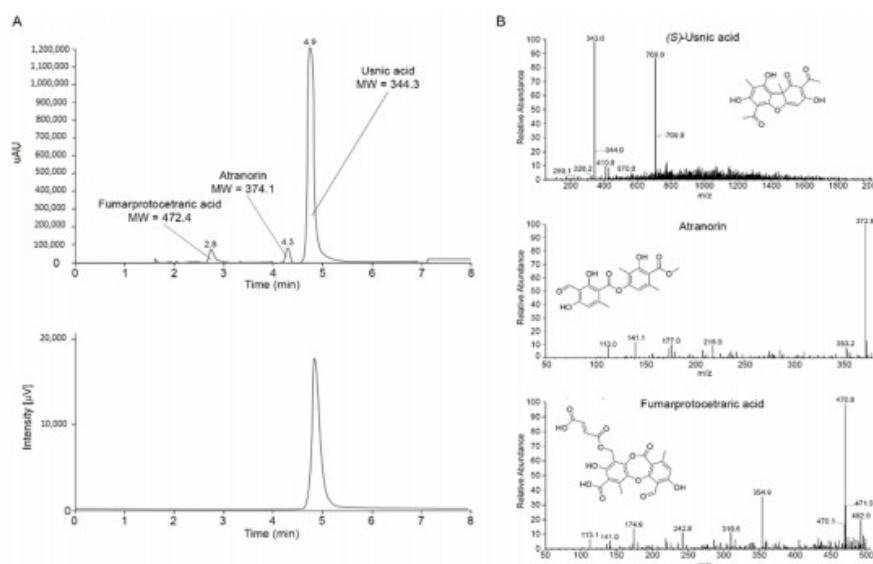

Figure 5. (**A**) HPLC-PAD profile of the crude acetone extract of *C. foliacea* recorded at λ = 254 nm (above) and the corresponding HPLC-CD profile recorded at λ = 270 nm (below); (**B**) ESI-MS spectra of the peaks at 4.9, 4.3, and 2.8 min and ascribable to UA, atranorin, and fumarprotocetraric acid, respectively.

The three analytes were purified from the crude extract to confirm the identity of the main three secondary metabolites and the stereochemistry of the putative UA. The crude was precipitated first over dichloromethane, and the precipitated was collected by filtration. By HPLC-UV/PAD-CD analysis, it resulted in the analyte eluting at 4.3 min and therefore was ascribable to atranorin. Later, the organic phase was concentrated, and the residue was partitioned between water and hexane. After collection and evaporation of the organic phase, the secondary crude obtained was further purified over silica gel to achieve two analytic samples of the compound eluting at 2.8 min (putative fumarprotocetraric acid) and 4.9 min (putative UA). The purity of the three analytes was assessed by HPLC analysis, and the chemical identification was achieved by mono- and bidimensional NMR spectroscopy. The comparison of the NMR spectra of compounds eluted at 2.8 min ($m/z = 473$) and 4.3 min ($m/z = 375$) with the data reported in the literature confirmed them as fumarprotocetraric acid and atranorin, respectively (Figure S1-2), [54,55].

The most abundant analyte identity, hypothesized to be UA, was instead thoroughly investigated by comparing its analytical, spectroscopical, and chiroptical properties with those of the commercially available (R)-UA, which was purchased and used as reference standard. A perfect superimposition between the analytical HPLC-UV profile (Figure 6A) and proton chemical shifts of both (R)-UA standard (blue spectra, Figure 6B) and extracted metabolite (red spectra, Figure 6B) was observed, thus confirming the identity of the most abundant analyte as UA. In addition, a full spectroscopic NMR characterization, comprising ^{13}C, HSQC, and HMBC, supported this conclusion (Figure S3). Chiroptical analysis, such as electronic circular dichroism (ECD) and optical rotatory power, was performed to assign the absolute configuration of the extracted UA.
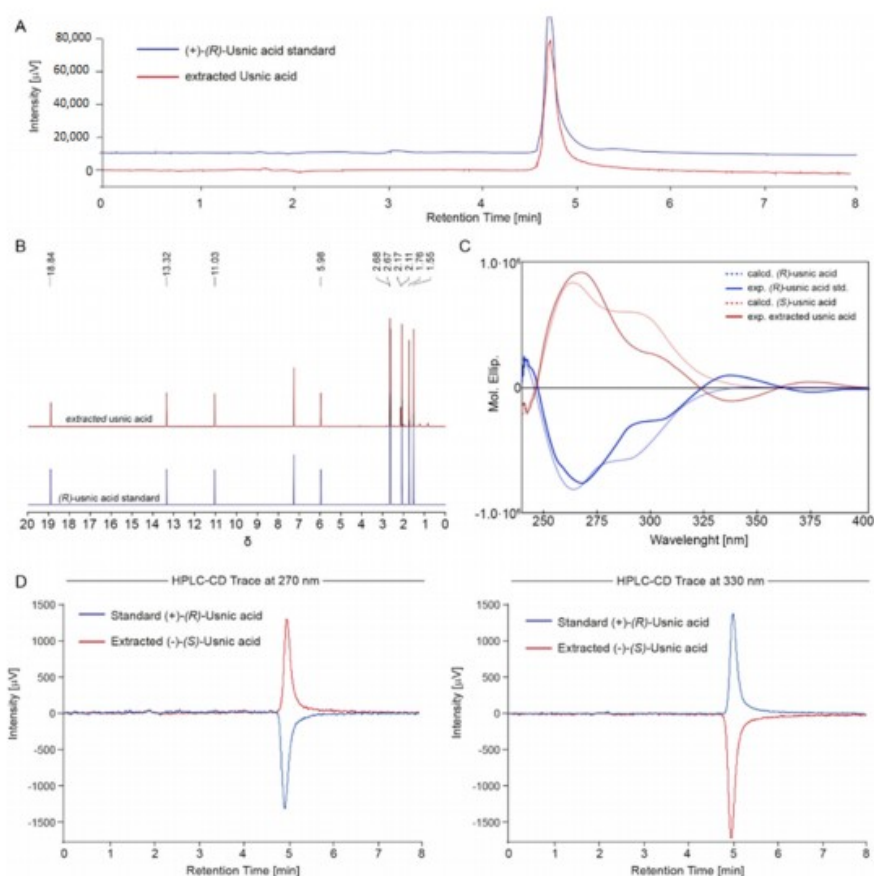
Figure 6. Superimposition of the (**A**) HPLC-UV chromatogram, (**B**) ^{1}H NMR spectra, (**C**) electronic circular dichroism (ECD) spectra in chloroform and (**D**) HPLC-CD traces acquired at 270 and 330 nm of extracted (S)-UA (in red) and (R)-UA standard.

The ECD spectra of extracted UA in chloroform were acquired and compared with the ECD spectra of the standard (R)-UA. As depicted in Figure 6C, the UA from *C. foliacea* (red line) showed an ECD profile entirely specular with respect to the standard (blue line). In detail, the ECD spectra of extracted UA showed two positive Cotton effects at 270 and 300 nm and one negative Cotton effect at 330 nm. In contrast, the standard (R)-UA presented the same prominent bands but with an opposite profile. Moreover, the ECD spectra for both (S)- and (R)-UA were computationally calculated. The results were in accordance with the experimental ECD spectra, thus supporting the right assignment of the absolute configuration.

Since the ECD profile of UA shows a main Cotton effect (CE) at 250 nm with a shoulder at 325 nm and an opposite CE at 360 nm, the HPLC-CD spectra have been recorded at 275 and 320 nm. Wavelengths below and around 250 nm have been avoided due to excessive CD noise observed in the region. This noise is due to the absorbance of acetonitrile, which was added to the HPLC mobile phase. According to experimental and calculated EDC spectra, the HPLC-CD chromatograms recorded at 275 nm showed a negative CE for the standard (R)-UA and a positive CE for the extracted UA (Figure 6D, left). Conversely, at 330 nm, the HPLC-CD traces were positive for (R)-UA and negative for (S)-UA (Figure 6D, right). Taken together, these data confirm that it is essential to record the ECD spectra, or at least to calculate them, prior to setting the in-line CD wavelength,

especially when the enantiomeric analyte is responsible for CEs of opposite sign, depending on the selected wavelength.

The (S)-enantiomer of UA herein isolated was used as an external standard, and an instrumental calibration via a six-point calibration curves, each replicated three times, was performed. The extracted (S)-UA showed an $[\alpha]_D^{25}$ of $-476°$ (c = 0.5%, chloroform), which is in line with the absolute $[\alpha]_D^{25}$ value of the standard (R)-enantiomer reported in the datasheet of the supplier ($[\alpha]_D^{25}$ of + 488°, c = 0.7%, chloroform, from Carbosynth, Staad, Switzerland). By comparison of the absolute value of the optical rotation, we can state that the optical purity of the herein extracted UA is c.a. 99% (based on the assumption that the optical purity of the standard was about 100%) and that no racemization occurred during the extraction procedure [56].

To conclude, the (S) absolute configuration can be undoubtedly assigned to the UA extracted from *C. foliacea*. The fully characterized (S)-UA and was used as standard in further experiments.

2.2. Microwave-Assisted Extraction (MAE) Protocol

To assess the experimental conditions suitable to extract exhaustively (S)-UA, a design of experiments (DoE) methodology was applied [57,58]. Briefly, the DoE approach is a collection of systematic statistical-based tools to study chemical processes both in the academic and industrial fields. Initially developed by Sir Ronald A. Fisher [59,60], many authors have continuously implemented it to provide the scientific community with tools that could minimize the investments in labor and time while maximizing the information obtainable by rigorous experimentation [61–63]. DoE is increasingly used and can be applied to several kinds of experiments, i.e., organic synthesis [64], analytical method development [65], and sample preparation [66]. Particularly, factorial designs represent an attractive approach for natural matrices extraction [48] and the systematic evaluation of plant secondary metabolism [67].

In contrast with the classic "one factor at a time" approach, DoE permits the study of the influence of multiple factors simultaneously. Specifically, two responses were studied varying three different parameters: solvent, extraction time, and temperature. Acetone, ethyl acetate, and ethanol characterized by different polarity and dielectric constant have been selected as extraction solvent, since it is well known that the microwave heating response depends on the solvent used.

We considered the total extraction yield percentage (Y_1) and the (-)-(S)-UA % recovered (Y_2).

The quantitative UA determination was performed by HPLC-UV/PAD using the same protocol exploited for the identification of UA in the lichen dry extract. The (S)-enantiomer of UA herein isolated was used as an external standard and six-point calibration curves, each replicated three times, were determined. The method response function was linear with a good correlation coefficient (R) of 0.9996 (y = (2.58 ± 0.04) × 10^7x − (3 ± 2) × 10^5). The statistical control of the method was assessed by performing three injections of external standard at the beginning of every measurement session on different days. The limits of detection and quantification were also estimated during the validation procedure using the S/N ratio. S was at least 3N in the peak region of the chromatogram for the limit of detection (LOD), whereas S > 10N for the limit of quantification (LOQ). The values resulted in being 0.0063 mg/mL and 0.0022 mg/mL, respectively, and were also experimentally confirmed. The method repeatability and accuracy were assessed by performing three injections on different days and assessing the UA recovery by a double-point standard addition method, spiking two aliquots of 0.30 g of sample with 12 mg and 9 mg of (-)-(S)-UA. Good recovery has been obtained, being the comparison between the spiked amount of UA and the amount found in the non-spiked samples as high as 99%. To sum up, the method is suitable for (S)-UA quantification in *C. foliacea* extracts. Results are reported in Table 1.

Table 1. Experimental plan and response data.

Exp#	Solvent	N° of Cycles × Minutes	T°C	Y₁ Extraction Yield (%)	Y₂ (−)-(S)-UA Yield [1]
1	Acetone	2 × 5	60	4.16	12.86
2	Acetone	3 × 5	60	3.40	12.88
3	Acetone	2 × 5	80	3.60	13.07
4	Acetone	3 × 5	80	3.31	11.73
5	Ethyl Acetate	2 × 5	60	3.93	12.49
6	Ethyl Acetate	3 × 5	60	2.76	10.28
7	Ethyl Acetate	2 × 5	80	2.50	13.04
8	Ethyl Acetate	3 × 5	80	1.70	11.64
9	Ethanol	2 × 5	60	6.63	12.78
10	Ethanol	3 × 5	60	5.84	11.54
11	Ethanol	2 × 5	80	6.73	13.51
12	Ethanol	3 × 5	80	7.29	12.79
13 *	Ethanol	2 × 5	70	6.15 ± 0.01	13.2 ± 0.7
Predicted **	Ethanol	2 × 5	70	7 ± 2	13 ± 2

LEGEND: Exp#, experiment number in standard order; [1] (-)-(S)-UA yield is reported as mg of extracted metabolite per g of lichen. * exp13 has been repeated three times, and results are reported as a mean ± confidence interval at the 95% level of probability. ** Model's predicted data was reported as a mean ± confidence interval at the 95% probability level.

The best results in terms of UA extraction yield (Y₂), whose quantification is the primary goal of the present study, were obtained using ethanol, applying two cycles of microwave heating of 5 min each at 80 °C (experiment number 11, Table 1).

To obtain an insight into thermal (S)-UA degradation, an additional MAE experiment (70°C, two cycles of 5 min, ethanol) was carried out, adding known amounts of (S)-UA to the natural matrix. The good recoveries obtained (about 90%) confirmed the chemical stability of UA under the experimental conditions. With the extraction method in hand, the extraction procedure was scaled up. In detail, 100 g of dried *C. foliacea* were extracted, exploiting the parameters of experiment 11, thus obtaining 420 mg of (-)-(S)-UA (yield, 0.42%, HPLC purity, 99.9%). The extracted (-)-(S)-UA was analyzed by HPLC-UV/PAD-CD, the optical rotation was measured, and the analytical data were compared with those of the commercial (R)-UA standard and the (S)-UA standard previously prepared and characterized as described above. Based on the results obtained, we can state that the applied extraction protocol does not induce racemization.

3. Materials and Methods

3.1. Lichen Material

Thalli of *C. foliacea* were harvested from a lowland dry grassland located at Bosco della Ghisolfa (Province of Pavia, Northern Italy) in Spring 2018.

Plant material was reduced to a homogenous powder by grounding it with a blade-mill (A10 IKA-Werke GmbH & Co. Staufen, Germany) just before performing the extractions.

3.2. Chemicals

Formic acid and deuterated solvents were purchased from Sigma-Aldrich (Milan, Italy).

HPLC-grade solvents were supplied by Honeywell (Seelze, Germany), while analytical grade solvents were supplied by PanReac (Barcelona, Spain).

Standard (R)-UA was purchased by Carbosynth (Staad, Switzerland).

3.3. Instruments

The evaporation procedures were performed under reduced pressure using a Heidolph Laborota 4000 instrument (Heidolph Instruments GmbH & Co., Schwabach, Germany). Analytical thin-layer chromatography (TLC) was carried out on silica gel pre-coated glass-backed plates (Fluka Kieselgel 60 F254, Merck, Darmstadt, Germany). The detection

was conducted with UV light (λ = 254 nm). Flash chromatography was performed with silica gel 60 (particle size 230–400 mesh) purchased from Nova Chimica (Cinisello Balsamo, Italy). Separations were carried out at room temperature, and separations were obtained using two different columns from Waters (Waters Corporation, Milford, MA, USA), namely a Symmetry C-18, 5 μm, 150 × 3.9 mm and an XBridge Phenyl 5 μm, 4.6 × 150 mm. Analyses were carried out using the following systems. HPLC-UV/PAD-CD: a Jasco (Tokyo, Japan) system consisting of a PU-1580 pump and a MD-1510 photodiode array (PDA) detector. Chromatogram acquisitions and elaborations were performed using the ChromNAV software (Tokyo, Japan). HPLC-UV/PAD-ESI/MS: Finnigan LCQ fleet ion trap system, controlled by Xcalibur software 1.4 (Thermo Finnigan, San Jose, CA, USA). Optical rotation was recorded using a Jasco photoelectric polarimeter DIP 1000. Electronic circular dichroism (ECD) spectra were recorded on a Jasco J-1500 Circular Dichroism Spectrophotometer from 400 to 240 nm. Nuclear magnetic resonance spectra were recorded on Bruker Avance 400 spectrometers operating at 400 MHz. Chemical shifts (δ) are reported in parts per million with the solvent reference relative to tetramethylsilane (TMS) internal standard.

3.4. Isolation and Identification of Main Metabolites

3.4.1. Isolation and Identification of Main Metabolites

A preliminary extract was prepared by applying an MAE methodology on 10 g of natural matrix using acetone as a solvent (2 min ramping, maximum pressure 120 psi, maximum potency 100 W, 80 °C) for three cycles of 5 min each. Then, the extract was filtered, and the solvent was evaporated under reduced pressure. The green syrup so obtained was suspended in dichloromethane (DCM). The suspension was filtered, and the solid residue was washed two times with DCM, thus obtaining atranorin as white powder, as confirmed by NMR analysis. Then, the combined organic phases were concentrated under reduced pressure and purified by L/L extraction (water/hexane). The aqueous phase was discarded, and the combined organic phases were concentrated under reduced pressure. After flash chromatography (diethyl ether: n-hexane (6: 4, *v/v*) added with formic acid (0.1%, *v/v*)), (−)-(S)-UA as yellow powder and 3 mg of fumarprotocetraric acid have been isolated.

Fumarprocetraric acid, 5 mg, mp 257°C, *m/z* 473; ^{1}H-NMR in DMSO-d_6, δ (ppm): 10.57 (s, 1H, COH), 6.82 (s, 1H, CH), 6.62 (s, 1H, CHCH), 6.62 (s, 1H, CHCH), 5.28 (s, 2H, **CH₂**), 2.46 (s, 3H, **CH₃**), 2.42 (s, 3H, **CH₃**).

Atranorin, 2mg, mp 190°C, *m/z* 375; ^{1}H-NMR in CDCl$_3$, δ (ppm): 12.59 (s, 1H, **OH**), 12.53 (s, 1H, **OH**), 11.98 (s, 1H, **OH**), 10.40 (s, 1H, **COH**), 6.55 (s, 1H, **CH**), 6.44 (s, 1H, **CH**), 4.02 (s, 3H, **OCH₃**), 2.72 (s, 3H, **CH₃**), 2.58 (s, 3H, **CH₃**), 2.13 (s, 3H, **CH₃**).

(-)-S-UA, 15 mg, mp 204 °C, *m/z* 344, $[\alpha]_D^{25}$= −476°, c 0.5% CHCl$_3$, ^{1}H-NMR in CDCl$_3$ δ (ppm): 18.86 (s, 1H, **OH**), 13.33 (s, 1H, **OH**), 11.05 (s, 1H, **OH**), 6.00 (s, 1H, **OCCH**), 2.70 (s, 3H, **COCH₃**), 2.68 (s, 3H, **COCH₃**), 2.13 (s, 3H, **CCCH₃**), 1.78 (s, 3H, **COCCH₃**) (see Figure S3 for complete NMR characterization).

3.4.2. HPLC-UV/PAD-CD and HPLC-UV/PAD-ESI/MS Analysis

A proper high-performance liquid chromatography-electrospray-tandem mass spectrometry (RP-HPLC-UV/PAD-ESI/MS) method was set up, analyzing the crude extract, atranorin, (-)-(S)-UA and fumarprotocetraric acids isolated, as described in Section 3.4.1.

The best results in terms of time of analysis and peak resolution were obtained at 1 mL/min flow rate at room temperature using an XBridge Phenyl column (5 μm, 4.6 × 150 mm). The mobile phase consisted of water (A) and acetonitrile (B), which were both added with 0.1% (*v/v*) of formic acid. The eluent was applied onto the column in gradient mode from 75% to 100% B in 7 min, which was followed by an isocratic elution step for 1 min. The column was reconditioned by eluting from 100% B to 75% B in 1 min and with a final 4 min isocratic elution at the initial conditions. Mass spectra were generated in positive and negative ion mode (mass range: 50–2000 Da, capillary temperature 120 °C): ion spray voltage 3 kV, capillary voltage 10 V, aux gas flow rate 10,

sheath gas flow rate 20, and tube lens voltage 75 V for positive mode and ion spray voltage 5 kV, capillary voltage −45 V, aux gas flow rate 10, sheath gas flow rate 20, and tube lens voltage −125 V for negative mode. MS/MS data were acquired in dependent scan mode (full-scan MS followed by MS/MS of the most intense ion). The identification of (S)-UA was unequivocally accomplished by comparing its HPLC retention time, UV, and MS spectra with those of the standard analyzed in the same conditions.

The same method was also applied to a HPLC-UV/PAD-CD system. Analytes were detected photometrically at 220 and 254 nm.

3.4.3. Electronic Circular Dichroism

The chloroform solutions of (–)-(S)-UA (c: 1.09×10^{-6} M) and (+)-(R)-UA (c: 1.37×10^{-6} M) were analyzed in a nitrogen atmosphere with an optical pathway of 1 cm. ECD spectra were scanned at 200 nm/min with a spectral bandwidth of 1 nm and a data resolution of 1 nm. For each measurement, 10 scans were taken and averaged, considering both enantiomers. ECD spectra of the solvent in the same experimental conditions were subtracted. Data are reported in $\Delta\varepsilon$ versus λ (nm) from knowledge of the cell path length and solution concentration (Figure 6C).

3.4.4. Computer-Assisted Conformational Analyses and ECD Calculations

Conformational analyses of (R)- and (S)-UA were performed with Merck Molecular Force Field (MMFF) by using Maestro 10.3 of the Schrödinger Suite. The lowest energy conformers of (R)- and (S)-UA were subjected to ECD calculation, which was carried out with the B3LYP/6-31G(d,p) level of time-dependent density functional theory (TDDFT). The polarizable continuum model (PCM) was used to take into account the solvent effects of chloroform. The calculated ECD spectra of (R)- and (S)-UA were the result of a weighted average of the calculated ECD spectra of each conformer based on Boltzmann distribution.

3.4.5. Quantitative Determination of (−)-(S)-UA in the Extract

Quantitative determination of (−)-(S)-UA was performed using the (−)-(S)-enantiomer isolated in the preliminary part of this work as an external standard, exploiting the HPLC/UV-PAD protocol used for the UA identification in the dry extract. The calibration curve was built through six points, each replicated three times. The limits of detection (LOD) and quantification (LOQ) were estimated using the S/N ratio. S was at least 3N in the peak region of the chromatogram for the LOD, whereas S > 10N for the LOQ. The values resulted in being 0.0063 mg/mL and 0.0022, respectively. These data were also experimentally confirmed. However, the calibration curve was studied in the range of 0.75–0.1 mg/mL. The method response function was linear with a correlation coefficient (R) of 0.9996 (y = $(2.58 \pm 0.04) \times 10^7$ x $- (3 \pm 2) \times 10^5$). The statistical control of the method was assessed by performing three injections of external standard at the beginning of every measurement session on different days. The method accuracy was evaluated by assessing the UA recovery by a double-point standard addition method, spiking two aliquots of 0.30 g of sample with 12 mg and 9 mg of (−)-(S)-UA, respectively. Each experiment has been repeated in triplicate. The recovery found by comparing the spiked amount of UA to the amount found in the non-spiked samples was 99.3 ± 0.2% for samples spiked with 12 mg of UA and 99.1 ± 0.3% for samples spiked with 9 mg of UA.

3.4.6. Experimental Design of the Extraction Procedure

The experimental design of the extraction procedure was aimed at the screening of the factors that influenced two responses, namely the total extraction yield (%, Y_1) and the yield of (−)-(S)-UA extracted per unit amount of source material (mg (−)-(S)-UA/g of lichen, Y_2).

Three process factors were considered. These parameters are all known to strongly influence the extraction procedures and are also strictly related to microwave power. The first factor was the extraction solvent. Three solvents were selected having different responses

to microwave heating, namely ethyl acetate (S_1, polarity index = 4.4, LogP 0.71, low microwave absorbance), acetone (S_2, polarity index = 5.1, LogP −0.24, medium microwave absorbance), and ethanol (S_3, polarity index = 5.2, LogP −0.31, high microwave absorbance).

These solvents have also been chosen because they are suitable for the scaling-up process, being considered the safest among the available.

The second factor was the time of extraction ($2 \times 5 - 3 \times 5$ number of cycles of microwaves irradiation per minute, X_2).

The third factor was the extraction temperature (60–80°C, X_3).

Given these factors and levels, a full factorial design, including $2^2 \times 3 = 12$ experiments, was used as an experimental plan (Table 1).

A weight of 0.30 g of ground plant material was dispersed in 6 mL of solvent (acetone, ethyl acetate, or ethanol (Table 1)) under magnetic stirring and subjected to microwave heating (2 min ramping, maximum pressure 120 psi, maximum potency 100 W, at 60°C or 80°C (Table 1)) for 2 to 3 cycles of 5 min each (Table 1). Then, the samples were cooled to 40°C and filtered through a paper filter. The solvent was evaporated under reduced pressure to obtain a yellow-green oil (yield, Table 1).

3.5. Experimental Design Analysis and Extraction Efficiency Enhancement

The full factorial $2^2 \cdot 3$ experimental design selected counted twelve experiments. One additional test experiment was performed in three independent replicates and kept apart from those used to build the model (Table 1, Exp#13). The test experiment was used to verify whether the models computed for the two responses could reliably represent the responses and assess the overall method standard deviation in the experimental domain center. This procedure represents the model's validation and consists of comparing the results predicted by the models with the outcome of the test experiment. The models will be accepted as reliable if the predicted data agree with the test experiment results within limits of uncertainty acceptable for the method application (Table 1).

The response Y_1, extraction yield percentage, is modeled reliably by the linear model, according to the equation:

$$Y_1 = 6.62 - 0.27 \cdot X_2 - 0.13 \cdot X_3 - 3.00 \cdot S_1 - 3.90 \cdot S_2 + 0.18 \cdot X_2 X_3.$$

The (−)-(S)-UA yield (Y_2) results were modeled by the equation

$$Y_2 = 12.66 - 0.57 X_2 + 0.25 \cdot X_3 - 0.02 \cdot S_1 - 0.79 \cdot S_2 + 0.00 X_2 X_3.$$

Both models predict reliably the experimental results with the predicted data, which refer to the experiment with ethanol irradiated with two cycles of 5 min each, at 70°C, i.e., in the test point having coded coordinates $S_1 = S_2 = 0$, $X_2 = -1$, and $X_3 = 0$. However, while the model for Y_1 (yield%) shows a good fit (r = 0.935), the model for (−)-(S)-UA yield (Y_2) shows limited fitting ability (r = 0.661). However, the model for Y_2 provides sufficient evidence of a linear dependence on the parameters X_2, time of extraction, and X_3, temperature, and no significant dependence on the interaction term $X_2 X_3$ accounting for the combined effect of extraction time and temperature.

Based on these results, we can consider the models for Y_1 and Y_2 validated. The difference between the predicted data and the experimental data is within the uncertainty limits associated with the used experimental procedure.

The results of our experiments showed that the proposed models could predict the trend of the expected extraction yield and (−)-(S)-UA recovery. According to our results, ethanol is the best solvent both for the extraction yield (Y_1) and for UA recovery (Y_2), while extraction time (X_2) and temperature (X_3) affect the responses to a lower extent. In particular, high temperature (80°C) and low extraction times (2 cycles x 5 min each) enhance (−)-(S)-UA recovery (Y_2) and do not affect the extraction yield (Y_1).

4. Conclusions

To sum up, in the present work, a suitable microwave-assisted extraction (MAE) coupled with HPLC-UV/PAD-CD protocol was set up for the stereochemical identification of UA content in the lichen extracts and to achieve a complete recovery of UA from *C. foliacea*. To the best of our knowledge, this is the first time microwaves have been exploited to extract UA. By combining analytical (HPLC), spectroscopical (mono- and bidimensional NMR), and chiroptical analysis (ECD and optical rotation value) and by comparison with the corresponding commercially available (R)-enantiomer used as standard, the UA produced by the *C. foliacea* was unambiguously identified as (S)-UA with an optical purity > 99%. Moreover, the herein proposed HPLC-UV/PAD protocol is suitable for the quantitative determination of UA in lichen extracts, and the association of an in-line CD allows us to obtain at the same time information about the stereochemistry of the UA, thus discriminating between the two enantiomers of UA that the different lichen species may produce.

Afterward, a versatile microwave-assisted extractive (MAE) protocol, assisted by a design of experiment (DoE), was optimized to recover (S)-UA from *C. foliacea* quantitatively. The best result in terms of UA extraction yield was obtained using ethanol and heating twice at 80°C under microwave irradiation for 5 min. The herein proposed procedure is simple, rapid, low cost, and applicable to evaluate the content of UA also in other lichen extracts. Of note, the optimized protocol requires less than 20 min in total to perform (−)-(S)-UA extraction and quantification. The optimized MAE protocol was assessed for the scale-up extraction of UA, and it represents a suitable procedure to produce (S)-UA for biological or pharmaceutical studies or commercial purposes.

Supplementary Materials: The following are available online, Figure S1: Fumarprotocetraric acid ^{1}H-NMR spectrum; Figure S2: Atranorin ^{1}H-NMR spectrum; Figure S3: 1H-NMR (A), HSQC (B), 13C-DEPT (C) and 13C-NMR (D) of (−)-UA after MAE procedure.

Author Contributions: Conceptualization, P.L., E.M. and S.C.; Formal analysis, P.L.; Funding acquisition, S.A.; Investigation, V.C., G.M. and G.G.; Methodology, V.C., G.M., R.S., D.R. and P.L.; Project administration, S.C.; Software, G.M. and P.L.; Supervision, E.M. and S.C.; Writing—original draft, V.C., G.M., D.R., P.L., G.G. and S.A.; Writing—review and editing, P.L., E.M. and S.C. All authors have read and agreed to the published version of the manuscript.

Conflicts of Interest: The authors declare no conflict of interest.

Sample Availability: Samples of the compounds ... are available from the authors.

References

1. Bonny, S.; Hitti, E.; Boustie, J.; Bernard, A.; Tomasi, S. Optimization of a microwave-assisted extraction of secondary metabolites from crustose lichens with quantitative spectrophoto densitometry analysis. *J. Chromatogr. A* **2009**, *1216*, 7651–7656. [CrossRef]
2. Malhotra, S.; Subban, R.; Singh, A. lichens-role in traditional medicine and drug discovery. *Inter. J. Altern. Med.* **2007**, *5*, 1–6.
3. Weissbuch, B.K. Medicinal Lichens: The Final Frontier. *J. Am. Herb. Guild* **2014**, *12*, 23–28.
4. Freysdottir, J.; Omarsdottir, S.; Ingólfsdóttir, K.; Vikingsson, A.; Olafsdottir, E.S. In vitro and in vivo immunomodulating effects of traditionally prepared extract and purified compounds from *Cetraria islandica*. *Int. Immunopharmacol.* **2008**, *8*, 423–430. [CrossRef] [PubMed]
5. Ingólfsdóttir, K.; Wiedemann, B.; Birgisdóttir, M.; Nenninger, A.; Jónsdóttir, S.; Wagner, H. Inhibitory effects of baeomycesic acid from the lichen *Thamnolia subuliformis* on 5-lipoxygenase in vitro. *Phytomedicine* **1997**, *4*, 125–128. [CrossRef]
6. Martins, M.; Silva, M.; Silva, H.; Silva, L.; Albuquerque, M.; Aires, A.; Falcão, E.; Pereira, E.; de Melo, A.; da Silva, N. Barbatic acid offers a new possibility for control of biomphalaria glabrata and schistosomiasis. *Molecules* **2017**, *22*, 568. [CrossRef] [PubMed]
7. Jeon, Y.J.; Kim, S.; Kim, J.H.; Youn, U.J.; Suh, S.S. The comprehensive roles of ATRANORIN, A secondary metabolite from the antarctic lichen *Stereocaulon caespitosum*, in HCC tumorigenesis. *Molecules* **2019**, *24*, 1414. [CrossRef]

8. Foden, F.R.; McCormick, J.; O'Mant, D.M. Vulpinic acids as potential antiinflammatory agents. 1. Vulpinic acids with substituents in the aromatic ring. *J. Med. Chem.* **1975**, *18*, 199–203. [CrossRef]
9. Kumar, K.C.S.; Müller, K. Depsides as non-redox inhibitors of leukotriene B4 biosynthesis and HaCaT cell growth. 2. Novel analogs of obtusatic acid. *Eur. J. Med. Chem.* **2000**, *35*, 405–411. [CrossRef]
10. Galanty, A.; Paśko, P.; Podolak, I. Enantioselective activity of usnic acid: A comprehensive review and future perspectives. *Phytochem. Rev.* **2019**, *18*, 527–548. [CrossRef]
11. Luzina, O.A.; Salakuthdinov, N.F. Usnic acid and its derivatives for pharmaceutical use: A patent review (2000–2017). *Expert Opin. Ther. Pat.* **2018**, *28*, 477–491. [CrossRef] [PubMed]
12. Luzina, O.; Filimonov, A.; Zakharenko, A.; Chepanova, A.; Zakharova, O.; Ilina, E.; Dyrkheeva, N.; Likhatskaya, G.; Salakhutdinov, N.; Lavrik, O. Usnic Acid conjugates with monoterpenoids as potent Tyrosyl-DNA phosphodiesterase 1 Inhibitors. *J. Nat. Prod.* **2020**, *83*, 2320–2329. [CrossRef] [PubMed]
13. Shi, C.-J.; Peng, W.; Zhao, J.H.; Yang, H.L.; Qu, L.L.; Wang, C.; Kong, L.Y.; Wang, X.B. Usnic acid derivatives as tau-aggregation and neuroinflammation inhibitors. *Eur. J. Med. Chem.* **2020**, *187*, 111961. [CrossRef] [PubMed]
14. Mallavadhani, U.V.; Vanga, N.R.; Rao, K.B.; Jain, N. Synthesis and antiproliferative activity of novel (+)- usnic acid analogues. *J. Asian Nat. Prod. Res.* **2020**, *22*, 562–577. [CrossRef] [PubMed]
15. Luzina, O.A.; Sokolov, D.N.; Pokrovskii, M.A.; Pokrovskii, A.G.; Bekker, O.B.; Danilenko, V.N.; Salakhutdinov, N.F. Synthesis and Biological Activity of Usnic Acid Enamine Derivatives. *Chem. Nat. Compd.* **2015**, *51*, 646–651. [CrossRef]
16. Zakharenko, A.; Luzina, O.; Koval, O.; Nilov, D.; Gushchina, I.; Dyrkheeva, N.; Švedas, V.; Salakhutdinov, N.; Lavrik, O. Tyrosyl-DNA phosphodiesterase 1 inhibitors: Usnic acid enamines enhance the cytotoxic effect of camptothecin. *Nat. Prod.* **2016**, *79*, 2961–2967. [CrossRef]
17. Shtro, A.A.; Zarubaev, V.V.; Luzina, O.A.; Sokolov, D.N.; Kiselev, O.I.; Salakhutdinov, N.F. Novel derivatives of usnic acid effectively inhibiting reproduction of influenza A virus. *Bioorg. Med. Chem.* **2014**, *22*, 6826–6836. [CrossRef]
18. Bruno, M.; Trucchi, B.; Monti, D.; Romeo, S.; Kaiser, M.; Verotta, L. Synthesis of a potent antimalarial agent through natural products conjugation. *ChemMedChem* **2013**, *8*, 221–225. [CrossRef]
19. Cirillo, D.; Borroni, E.; Festoso, I.; Monti, D.; Romeo, S.; Mazier, D.; Verotta, L. Synthesis and antimycobacterial activity of (+)-usnic acid conjugates. *Arch. Pharm. Chem. Life Sci.* **2018**, *351*, e1800177. [CrossRef]
20. Pastrana-Mena, R.; Mathias, D.K.; Delves, M.; Rajaram, K.; King, J.G.; Yee, R.; Trucchi, B.; Verotta, L.; Dinglasan, R.R. A malaria transmission-blocking (+)-usnic acid derivative prevents plasmodium zygote-to-ookinete maturation in the mosquito midgut. *ACS Chem. Biol.* **2016**, *11*, 3461–3472. [CrossRef]
21. Pyrczak-Felczykowska, A.; Narlawar, R.; Pawlik, A.; Guzow-Krzemińska, B.; Artymiuk, D.; Haĉ, A.; Ryś, K.; Rendina, L.M.; Reekie, T.A.; Herman-Antosiewicz, A.; et al. Synthesis of usnic acid derivatives and evaluation of their antiproliferative activity against cancer cells. *J. Nat. Prod.* **2019**, *82*, 1768–1778. [CrossRef] [PubMed]
22. Zakharova, O.; Luzina, O.; Zakharenko, A.; Sokolov, D.; Filimonov, A.; Dyrkheeva, N.; Chepanova, A.; Ilina, E.; Ilyina, A.; Klabenkova, K.; et al. Synthesis and evaluation of aryliden- and hetarylidenfuranone derivatives of usnic acid as highly potent Tdp1 inhibitors. *Bioorg. Med. Chem.* **2018**, *26*, 4470–4480. [CrossRef] [PubMed]
23. Luzina, O.A.; Sokolov, D.N.; Shernyukov, A.V.; Salakhutdinov, N.F. Synthesis of aurones based on usninic acid. *Chem. Nat. Compd.* **2012**, *48*, 385–391. [CrossRef]
24. Filimonov, A.S.; Chepanova, A.A.; Luzina, O.A.; Zakharenko, A.L.; Zakharova, O.D.; Ilina, E.S.; Dyrkheeva, N.S.; Kuprushkin, M.S.; Kolotaev, A.V.; Khachatryan, D.S.; et al. New hydrazinothiazole derivatives of usnic acid as potent Tdp1 inhibitors. *Molecules* **2019**, *24*, 3711. [CrossRef] [PubMed]
25. Zakharenko, A.L.; Luzina, O.A.; Sokolov, D.N.; Kaledin, V.I.; Nikolin, V.P.; Popova, N.A.; Patel, J.; Zakharova, O.D.; Chepanova, A.A.; Zafar, A.; et al. Novel tyrosyl-DNA phosphodiesterase 1 inhibitors enhance the therapeutic impact of topotecan on in vivo tumor models. *Eur. J. Med. Chem.* **2019**, *161*, 581–593. [CrossRef]
26. Barton, D.H.R.; Deflorin, A.M.; Edwards, O.E. The synthesis of usnic acid. *J. Chem. Soc.* **1956**, 530–534. [CrossRef]
27. Hawranik, D.J.; Anderson, K.S.; Simmonds, R.; Sorensen, J.L. The chemoenzymatic synthesis of usnic acid. *Bioorg. Med. Chem. Let.* **2009**, *19*, 2383–2385. [CrossRef]
28. Singh, S.; Khatoon, S.; Joshi, Y.; Prgyadeep, S.; Upreti, D.K.; Rawat, A.K.S. A validated HPTLC densitometric method for simultaneous determination of evernic and usnic acids in four usnea species and comparison of their antioxidant potential. *J. Chromatogr. Sci.* **2016**, *54*, 1670–1677. [CrossRef]
29. Kosanić, M.; Ristić, S.; Stanojković, T.; Manojlović, N.; Ranković, B. Extracts of five cladonia lichens as sources of biologically active compounds. *Farmacia* **2018**, *66*, 644–651. [CrossRef]
30. Oran, S.; Sahin, S.; Sahinturk, P.; Ozturk, S.; Demir, C. Antioxidant and antimicrobial potential, and HPLC analysis of stictic and usnic acids of three Usnea species from Uludag mountain (Bursa, Turkey). *Iran. J. Pharmac. Res.* **2016**, *15*, 527–535.
31. Popovici, V.; Bucur, L.; Popescu, A.; Caraiane, A.; Badea, V. Determination of the content in usnic acid and polyphenols from the extracts of *Usnea barbata* L. and the evaluation of their antioxidant activity. *Farmacia* **2018**, *66*, 337–341.
32. Popovici, V.; Bucur, L.; Costache, T.; Gherghel, D.; Vochita, G.; Mihai, C.T.; Rotinberg, P.; Schroder, V.; Badea, F.C.; Badea, V. Studies on preparation and UHPLC analysis of the *Usnea barbata* (L) F.H.Wigg dry acetone extract. *Revista de Chimie* **2019**, *70*, 3775–3777. [CrossRef]

33. Zugic, A.; Jeremic, I.; Isakovic, A.; Arsic, I.; Savic, S.; Tadic, V. Evaluation of anticancer and antioxidant activity of a commercially available CO$_2$ supercritical extract of old man's beard (*Usnea barbata*). *PLoS ONE* **2016**, *11*, e0146342. [CrossRef] [PubMed]

34. Chaowuttikul, C.; Thitikornpong, W.; Palanuvej, C.; Ruangrungsi, N. Quantitative determination of usnic acid content in *Usnea siamensis* by TLC-densitometry and TLC image analysis. *Res. J. Pharmac. Bio. Chem. Sci.* **2014**, *5*, 118–125.

35. Kiliç, N.; Islakoğlu, Y.Ö.; Büyük, İ.; Gür-Dedeoğlu, B.; Cansaran-Duman, D. Determination of usnic acid responsive mirnas in breast cancer cell lines. *Anti-Cancer Agen. Med. Chem.* **2016**, *19*, 1463–1472. [CrossRef]

36. Kyslychenko, O.A.; Protska, V.V.; Zhuravel, I.O. HPLC determination of phenolic compounds content in *Parmelia sulcata* and *Parmelia vagans* thalli. *Pharmacia* **2019**, *66*, 161–164. [CrossRef]

37. Wang, H.; Yang, T.; Cheng, X.; Kwong, S.; Liu, C.; An, R.; Li, G.; Wang, X.; Wang, C. Simultaneous determination of usnic, diffractaic, evernic and barbatic acids in rat plasma by ultra-high-performance liquid chromatography–quadrupole exactive Orbitrap mass spectrometry and its application to pharmacokinetic studies. *Biomed. Chromatogr.* **2018**, *32*, e4123. [CrossRef]

38. Varol, M.; Tay, T.; Candan, M.; Türk, A.; Koparal, A.T. Evaluation of the sunscreen lichen substances usnic acid and atranorin. *Biocell* **2015**, *39*, 25–31.

39. Koparal, A.T. Anti-angiogenic and antiproliferative properties of the lichen substances (-)-usnic acid and vulpinic acid. *Z. Naturforsch C* **2015**, *70*, 159–164. [CrossRef]

40. Koparal, A.T.; Ayaz Tüylü, B.; Türk, H. In vitro cytotoxic activities of (+)-usnic acid and (−)-usnic acid on V79, A549, and human lymphocyte cells and their non-genotoxicity on human lymphocytes. *Nat. Prod. Res.* **2006**, *20*, 1300–1307. [CrossRef]

41. Gheza, G.; Assini, S.; Valcuvia-Passadore, M. Contribution to the knowledge of lichen flora of inland sand dunes in the western Po Plain (N Italy). *Plant. Biosyst.* **2015**, *149*, 307–314. [CrossRef]

42. Nimis, P.L. *The Lichens of Italy—A Second Annotated Catalogue*; EUT: Trieste, Italy, 2016; p. 740.

43. Gheza, G.; Assini, S.; Lelli, C.; Marini, L.; Mayrhofer, H.; Nascimbene, J. Biodiversity and conservation of terricolous lichens and bryophytes in continental lowlands of northern Italy: The role of different dry habitat types. *Biodive. Conser.* **2020**, *29*, 3533–3550. [CrossRef]

44. Malacrida, A.; Cavalloro, V.; Martino, E.; Cassetti, A.; Nicolini, G.; Rigolio, R.; Cavaletti, G.; Mannucci, B.; Vasile, F.; Di Giacomo, M.; et al. Anti-multiple myeloma potential of secondary metabolites from hibiscus sabdariffa. *Molecules* **2019**, *24*, 2500. [CrossRef] [PubMed]

45. Vigani, B.; Rossi, S.; Gentile, M.; Sandri, G.; Bonferoni, M.C.; Cavalloro, V.; Martino, E.; Collina, S.; Ferrari, F. Development of a mucoadhesive and an in situ gelling formulation based on κ-carrageenan for application on oral mucosa and esophagus walls. II. Loading of a bioactive hydroalcoholic extract. *Mar. Drugs* **2019**, *17*, 153. [CrossRef] [PubMed]

46. Martino, E.; Collina, S.; Rossi, D.; Bazzoni, D.; Gaggeri, R.; Bracco, F.; Azzolina, O. Influence of the extraction mode on the yield of hyperoside, vitexin and vitexin-2″-O-rhamnoside from *Crataegus monogyna* Jacq. (hawthorn). *Phytochem. Anal.* **2008**, *19*, 534–540. [CrossRef]

47. Granata, M.U.; Bracco, F.; Catoni, R.; Martino, E. Secondary metabolites profile and physiological leaf traits in wild and cultivated Corylus avellana under different nutritional status. *Nat. Prod. Res.* **2019**, *56*, 1–8. [CrossRef]

48. Martino, E.; Della Volpe, S.; Cavalloro, V.; Amri, B.; Kaab, L.B.B.; Marrubini, G.; Rossi, D.; Collina, S. The use of a microwave-assisted solvent extraction coupled with HPLC-UV/PAD to assess the quality of *Marrubium vulgare* L. (white horehound) herbal raw material. *Phytochem. Anal.* **2019**, *30*, 377–384. [CrossRef]

49. Amri, B.; Martino, E.; Vitulo, F.; Corana, F.; Ben-Kaâb, L.B.; Rui, M.; Rossi, D.; Mori, M.; Rossi, S.; Collina, S. *Marrubium vulgare* L. leave extract: Phytochemical composition, antioxidant and wound healing properties. *Molecules* **2017**, *22*, 1851. [CrossRef]

50. Rossi, D.; Ahmed, K.M.; Gaggeri, R.; Volpe, S.D.; Maggi, L.; Mazzeo, G.; Longhi, G.; Abbate, S.; Corana, F.; Martino, E.; et al. (R)-(-)-Aloesaponol III 8-methyl ether from eremurus persicus: A novel compound against leishmaniosis. *Molecules* **2017**, *22*, 519. [CrossRef]

51. Gaggeri, R.; Rossi, D.; Christodoulou, M.S.; Passarella, D.; Leoni, F.; Azzolina, O.; Collina, S. Chiral flavanones from *Amygdalus lycioides* Spach: Structural elucidation and identification of TNFalpha inhibitors by bioactivity-guided fractionation. *Molecules* **2012**, *17*, 1665–1674. [CrossRef]

52. Popovici, V.; Bucur, L.A.; Schröder, V.; Gherghel, D.; Mihai, C.T.; Caraiane, A.; Badea, F.C.; Vochiţa, G.; Badea, V. Evaluation of the Cytotoxic Activity of the *Usnea barbata* (L.) F. H. Wigg Dry Extract. *Molecules* **2020**, *25*, 1865. [CrossRef]

53. Rossi, D.; Nasti, R.; Collina, S.; Mazzeo, G.; Ghidinelli, S.; Longhi, G.; Memo, M.; Abbate, S. The role of chirality in a set of key intermediates of pharmaceutical interest, 3-aryl-substituted-γ-butyrolactones, evidenced by chiral HPLC separation and by chiroptical spectroscopies. *J. Pharmac. Biomed. Analy.* **2017**, *144*, 41–51. [CrossRef] [PubMed]

54. Carvalho, M.-G.; Carvalho, G.J.A.; Braz-Filho, R. Chemical constituents from *Ouratea floribunda*: Complete ^{1}H- and ^{13}C-NMR assignments of atranorin and its new acetyl derivative. *J. Brazil. Chem. Soc.* **2000**, *11*, 143–147. [CrossRef]

55. Su, B.-N.; Cuendet, M.; Nikolic, D.; Kristinsson, H.; Ingólfsdóttir, K.; van Breemen, R.B.; Fong, H.H.S.; Pezzuto, J.M.; Kinghorn, A.D. NMR study of fumarprotocetraric acid, a complex lichen depsidone derivative from *Cladonia furcate*. *Mag. Res. Chem.* **2003**, *41*, 391–394. [CrossRef]

56. Yang, Y.; Nguyen, T.T.; Jeong, M.-H.; Crişan, F.; Yu, Y.H.; Ha, H.-H.; Choi, K.H.; Jeong, H.G.; Jeong, T.C.; Lee, K.Y.; et al. Inhibitory Activity of (+)-Usnic Acid against Non-Small Cell Lung Cancer Cell Motility. *PLoS ONE* **2016**, *11*, e0146575. [CrossRef] [PubMed]

57. Marrubini, G.; Fattorini, P.; Previderé, C.; Goi, S.; Sorçaburu Cigliero, S.; Grignani, P.; Serra, M.; Biesuz, R.; Massolini, G. Experimental design applied to the optimization of microwave-assisted DNA hydrolysis. *J. Chromatogr. A* **2012**, *1249*, 8–16. [CrossRef]

58. Moldovan, M.L.; Iurian, S.; Puscas, C.; Silaghi-Dumitrescu, R.; Hanganu, D.; Bogdan, C.; Vlase, L.; Oniga, I.; Benedec, D. A Design of Experiments Strategy to Enhance the Recovery of Polyphenolic Compounds from *Vitis vinifera* By-Products through Heat Reflux Extraction. *Biomolecules* **2019**, *9*, 529. [CrossRef]

59. Fisher, R.A. and Mackenzie, W.A. Studies in crop variation. II. The manurial response of different potato varieties. *J. Agric. Sci.* **1923**, *13*, 311–320. [CrossRef]

60. Yates, F. Sir Ronald Fisher and the Design of Experiments. *Biometrics* **1964**, *20*, 307–332. [CrossRef]

61. Box, G.E.P.; Allen, J.L. *An Accidental Statistician: The life and memories of George E.P. Box*; John Wiley & Sons: Hoboken, NJ, USA, 2013.

62. Box, G.E.P.; Hunter, J.S.; Hunter, W.G. *Statistics for experimenters: Design, Innovation, and Discovery*; John Wiley & Sons: Hoboken, NJ, USA, 2005.

63. Montgomery, D.J. *Design and Analysis of Experiments*; John Wiley & Sons: Hoboken, NJ, USA, 2019.

64. Carlson, R. *Design and Optimization in Organic Synthesis*, 3rd ed.; Elsevier Science: Amsterdam, The Netherlands, 2012.

65. Hibbert, D.B. Experimental design in chromatography: A tutorial review. *J. Chromatogr. B* **2012**, *910*, 2–13. [CrossRef]

66. Marrubini, G.; Dugheri, S.; Cappelli, G.; Arcangeli, G.; Mucci, N.; Appelblad, P.; Melzi, C.; Speltini, A. Experimental designs for solid-phase microextraction method development in bioanalysis: A review. *Anal. Chim. Acta* **2020**, *1119*, 77–100. [CrossRef] [PubMed]

67. Vasilev, N.; Boccard, J.; Lang, G.; Grömping, U.; Fischer, R.; Goepfert, S.; Rudaz, S.; Schillberg, S. Structured plant metabolomics for the simultaneous exploration of multiple factors. *Sci. Rep.* **2016**, *6*, 37390. [CrossRef] [PubMed]

Paper 6

RESEARCH ARTICLE

WILEY Phytochemical Analysis

The use of a microwave-assisted solvent extraction coupled with HPLC-UV/PAD to assess the quality of *Marrubium vulgare* L. (white horehound) herbal raw material

Emanuela Martino[1] | Serena Della Volpe[2] | Valeria Cavalloro[1] | Bedis Amri[3] | Leila Bettaeib Been Kaab[3] | Giorgio Marrubini[2] | Daniela Rossi[2] | Simona Collina[2]

[1] Department of Earth and Environmental Sciences, University of Pavia, Pavia, Italy

[2] Department of Drug Sciences, University of Pavia, Pavia, Italy

[3] Département de Biologie, Faculté des Sciences de Tunis el Manar, Unité de recherche "Nutrition et métabolismes azoté et protéines de stress", Tunis, Tunisia

Correspondence

Simona Collina, Department of Drug Sciences, University of Pavia, Viale Taramelli 12, 27100 Pavia, Italy.

Email: simona.collina@unipv.it

Abstract

Introduction: *Marrubium vulgare* is a herbal remedy presents in several European Pharmacopoeias and commonly marketed as white horehound. The chemotaxonomic marker of Marrubium genus is marrubiin and its content may change in response to biotic and abiotic stress.

Objective: Development of a microwave-assisted solvent extraction (MASE) methodology suitable for exhaustively extracting marrubiin from *M. vulgare* leaves, easily applicable to large sets of samples. Evaluation of the influence of copper(II) on marrubiin production.

Material and methods: *M. vulgare* leaves were dried, extracted exploiting MASE and analysed *via* high-performance liquid chromatography ultraviolet photodiode array detection (HPLC-UV/PAD) system. A design of experiments approach was adopted to select the best extraction conditions. Extraction parameters (solvent composition, extraction time and temperature), were studied applying two full factorial experimental designs in a sequential approach. To analyse samples, a rapid HPLC-UV/PAD method was set up.

Results: The best results in terms of marrubiin extraction yield were obtained extracting samples at 120°C with 100% ethanol, for 15 min (3 × 5 min microwave cycles). The developed methodology was successfully applied to matrices grown in Greenhouse conditions and under stress induced by copper(II), selected as model agent for abiotic stress. Progressively decreasing production of marrubiin was evidenced in connection with treatment with 80, 200 and 300 mg/L copper sulphate.

Conclusion: An efficient methodology for the extraction and determination of the amount of marrubiin in large sets of samples of *M. vulgare* plants was developed. Results demonstrated that marrubiin is an easily detectable marker useful for evaluating *M. vulgare* reaction to stress.

KEYWORDS

copper(II)-induced stress, DoE, HPLC-UV/PAD analysis, *Marrubium vulgare* L. leave extract, MASE

1 | INTRODUCTION

Nature contributes greatly to the history and landscape of drugs. Around half of the drugs currently in clinical use are of natural origin, about 30% ofdrugs approved by the FDA (US Food and Drug Administration) over the past three decades are nature-inspired and nearly one-quarter derive from the vegetal kingdom.[1] By their very nature, plants protect themselves producing compounds commonly known as secondary metabolites.[2] These compounds are characterised by a high degree of structural variability, including terpenes, phenols, alkaloids, also in their glycosidic forms. Secondary metabolites produced in nature have survival functions for producing organisms and are able to set off physiological and pharmacological effects within living cells. For this reason, on one hand, natural compounds play a relevant role in the nature-aided drug-discovery process and, on the other hand, given their involvement in the plant defence system, they are useful markers for evaluating the plant adaptation to environmental stress factors (i.e. growth, geographical position, climate change, waste deposition or agricultural practices).

The extensive use of plants for millennia for healthcare purposes has found renewed interest due to recent advances in modern biology, pharmacology, chemistry and related disciplines.[3] The integration of traditional and modern medicine has given birth to "Green Medicine"; which has been proven to be more effective with fewer side effects on human beings. Within this context, we can mention white horehound whose great interest as a herbal remedy is testified by its presence in Pharmacopoeias and the Merck Index of Phytotherapy since 1910. Recent literature has evidenced that *Marrubium vulgare* shows several *in vivo* and *in vitro* activities including antihypertensive, antioxidant, antiinflammatory, antidiabetic, effects on respiratory system, digestive stimulant, antiasthmatic, hypolipidemic, antibacterial, and antifungal effects. Within this context, and as a part of our current research in this field, in the present contribution we focused on *M. vulgare* L. (white/common horehound), an annual herbaceous plant belonging to Lamiaceae family, native to Eurasia and northern Africa zones.[4-17] Due to its biological activities, the European Medicines Agency has published a monograph for *M. vulgare* in which all the traditional, non-clinical and clinical data are reported.[18] The main secondary metabolite of the plant is marrubiin, a furane labdane diterpenoid, isolated for the first time from *M. vulgare* in 1930 and considered a chemotaxonomic marker of *Marrubium* genus.[19] During the last 20 years, a plethora of works has highlighted that marrubiin can be related to pharmacological effects such as antinociceptive, antioxidant,

antigenotoxic, cardioprotective, vasorelaxant, gastroprotective, antispasmodic, immunomodulating, antioedematogenic, analgesic, and antidiabetic properties (Figure 1).[10,12,20-29]

Aim of our general project is to understand whether culture and environmental conditions may affect the growth and quality of white horehound. We have already demonstrated that copper(II)-induced stress reduced the uptake and translocation of cationic elements, like iron(II), potassium(I) and calcium(II), whereas increased the content of total phenols and flavonoids. It is worth noting that in connection with waste deposition and agricultural practices, copper(II), commonly present at low concentrations in the soil, tends to accumulate to high and toxic concentrations, leading to an alteration of vital physiological or biochemical functions. These effects may have a great impact on human health, since *M. vulgare* is commonly used worldwide for its medicinal properties. As a continuation of our research, the aim of the herein presented work is to develop a rapid and reproducible microwave-assisted solvent extraction (MASE) methodology for exhaustively extracting marrubiin from *M. vulgare* leaves. In the last decades, MASE has gained increasing importance for isolation and extraction of metabolites from vegetal matrices, since it entails low solvent consumption, gives high and fast extraction performances and offers protection to thermo-labile constituents. To date, MASE is considered a robust alternative to traditional extraction techniques, especially for analytical purposes. [4-7]

In detail, we herein describe the development of a MASE methodology easily applicable to the extraction of marrubiin from *M. vulgare*, and the evaluation of the impact of copper(II) concentration in the soil on the production of marrubiin. It is worth noting that in connection with waste deposition and agricultural practices, copper(II), commonly present at low concentration in the soil, tends to accumulate to high and toxic concentrations, leading to an alteration of vital physiological or biochemical functions. These effects may have a great impact on human health, since *M. vulgare* is used worldwide for its medicinal properties.

To set up the experimental conditions suitable to ensure the exhaustive extraction of marrubiin from the vegetal matrix, a design of experiments (DoE) approach was adopted. Moreover, a proper high-performance liquid chromatography (HPLC) method allowed the rapid analysis of the samples. The proposed MASE methodology allowed the exhaustive extraction of marrubiin from *M. vulgare* leaves and may be successfully applied for evaluating the marrubiin content in a wide number of samples. Until now, such approach for evaluating the production of marrubiin in *M. vulgare* had not been reported.
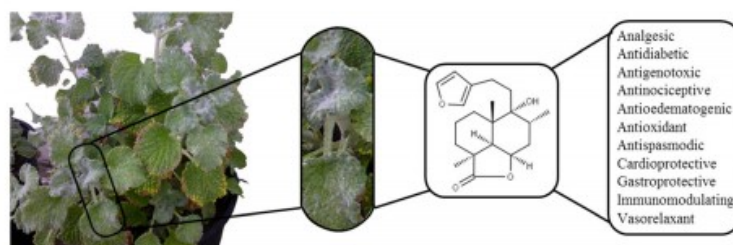

FIGURE 1 Marrubiin natural source, chemical structure and biological activities [Colour figure can be viewed at wileyonlinelibrary.com]

2 | EXPERIMENTAL

2.1 | Plant material and copper treatment

Seeds of *M. vulgare* were issued from a non-contaminated wild population in the region of Béja (north-western Tunisia; latitude 36°43′30″ (N), longitude 9°10′51″ (E), altitude 255 m). Voucher specimen of *M. vulgare* was deposited in the herbarium unit for the research of Plant Ecology, Department Biology, Faculty of Sciences of Tunisia, under the registration number MV-N-20.

The experiments started in August 2014, and lasted four months. Initially, three replicates of 20 seeds for each treatment were sown at a depth of 2 cm in plastic pots (26 cm × 22 cm) fitted with commercial peat and sand (1:2, *v/v*) and maintained under Greenhouse conditions (naturally exposed to sunlight, with a temperature range 20–25°C, and relative humidity range 50–80%). Seedlings were separately transplanted into individual pots (18.2 cm × 14.2 cm) and treated with 0 (control), 80, 200 and 300 mg/L copper sulphate ($CuSO_4$) for eight weeks. Nutrient solutions were renewed every 4 days.[3] At the end of the treatment (in December), the fresh leaves were separated, and dried in a drying room with active ventilation at room temperature (about 26–28°C) until constant weight. The aerial parts were stored in closed glass jars and preserved in dark conditions. The plant material was thus ground with a blade-mill (A10 IKA-Werke GmbH & Co., Staufen, Germany) to obtain a homogenous powder, just before performing the extractions.

2.2 | Chemicals and standards

Solvents for both HPLC (HPLC grade) and extraction procedures (analytical grade) were supplied by Carlo Erba (Milan, Italy). The reference standard of marrubiin (> 98% purity) was obtained from Carbosynth, while charcoal from Sigma Aldrich (Milan, Italy).

2.3 | Instruments and apparatus

All extraction experiments were conducted under microwave irradiation in a microwave mono-mode oven (Discover® Lab-Mate instrument, CEM Corporate, Buckingham, UK) equipped with a power and temperature controller. Extract analyses were carried out on a Jasco (Tokyo, Japan) high-performance liquid chromatography ultraviolet photodiode array detection (HPLC-UV/PAD) system equipped with a Jasco AS-2055 plus autosampler, a PU-2089 plus pump and a -2010 plus multi-wavelength detector. Experimental data were acquired and interpreted with Borwin PDA and Borwin chromatograph software (Tokyo, Japan).

2.4 | HPLC-UV/PAD analysis

We prepared the hydroalcoholic leaves extract by applying the MASE methodology we had previously developed and reported[3] and analysed by HPLC-UV/PAD, at 1 mL/min flow rate, at room temperature using a Phenyl X-Bridge endcapped column (50 mm

× 4.6 mm, length × inner diameter, 3 μm particle size, macropore size 2 μm, mesopore size 13 nm, Merck, Darmstadt, Germany). The mobile phase consisted of water containing 0.1% (v/v) formic acid (A) and methanol containing 0.1% (v/v) formic acid (B). The eluent was applied onto the column in gradient mode from 10% to 90% B in 14 min, followed by an isocratic elution step for 6 min. Reconditioning of the column was accomplished by eluting the column with the mobile phase from 90% B to 10% B in 5 min, followed by a re-equilibration step of 5 min under isocratic conditions with 10% B. The analytical conditions reported earlier ensure a good resolution of marrubiin (unequivocally identified comparing its HPLC retention time and UV spectrum with those of the standard analysed in the same conditions, Figure 2 and Supporting Information Figure S1) with respect to the other analytes present in the extract. A representative chromatographic profile of the extract is reported in Figure 2. Quantitative determination of marrubiin was performed using the external standard procedure by means of a six-point calibration curve with three replicate measurements for each calibration point (Figure S1).

The limits of detection (LOD) and limits of quantification (LOQ) were estimated using the calibration curves calculated during the validation procedure, from which the average of slope (S) and the standard deviation of intercept (δ) were calculated. LOD and LOQ were obtained as follows: $LOD = 3.3\delta/S$, $LOQ = 10\delta/S$, thus the values were 0.016 mg/mL and 0.032 mg/mL, respectively. The calibration curve in the range 1.00–0.003 mg/mL was linear with a correlation coefficient (R) of 0.9878 ($y = 7E + 06x - 434459$). The statistical control of the method was assessed by performing three injections of reference standard at the beginning of every measurement session on different days. The method accuracy was evaluated by assessing the marrubiin recovery by single-point standard addition method, spiking 0.30 g of samples with 3.2 mg of marrubiin. The recovery found by comparison of the spiked amount of marrubiin to the amount found in the non-spiked samples was as high as 99%.
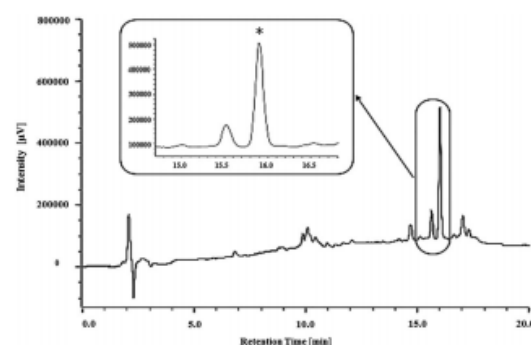

FIGURE 2 High-performance liquid chromatography ultraviolet photodiode array detection (HPLC-UV/PAD) profile at λ = 220 nm of ethanol microwave-assisted solvent extraction (MASE) obtained from plant grown in Greenhouse conditions. The star * identifies the marrubiin peak

2.5 | MASE parameters determination: DoE

The experimental extraction plan was designed to study three responses, i.e. total extraction yield percentage (computed as milligrams of dried extract per milligrams of dried plant material × 100, Y_1), total area of the peaks recorded in the HPLC-UV/PAD chromatograms (mAU-s, Y_2), and marrubiin yield (expressed in milligrams of marrubiin per gram of dried plant material, Y_3). Three experimental parameters were evaluated in the first set of experiments; the parameters were solvent composition (%volume of solvent/volume of water, X_1), time of extraction (in minutes, X_2) and temperature (in Celsius degrees, X_3). All other parameters including the operator were kept constant (e.g. amount of dried material, solvent volume, type of vessel, etc.). The selected parameters were varied within defined ranges according to Tables 1 and 2 for methanol and ethanol.

2.6 | Statistical analysis

All collected data were studied using Microsoft Excel 2010 and R for Microsoft Windows version 3.2.3, Copyright© 2014. The R Foundation for Statistical Computing R-based chemometric software routines were used for DoE calculations.

The R-based software has been developed by the Group of Chemometrics of the Italian Chemical Society (http://gruppochemiometria.it/gruppo-lavoro-r-inchemiometria.html).

2.7 | Sample extraction and analysis

2.7.1 | *Marrubium vulgare* matrices obtained from plant grown in Greenhouse conditions

Here 0.30 g of matrix were dispersed in 10 mL of solvent (Tables 1 and 2) under magnetic stirring and subjected to microwave heating (2 min ramping, maximum pressure 120 psi, maximum potency 100 W, temperature – Tables 1 and 2) for one to three cycles of 5 min with solvent renewal (Tables 1 and 2). The mixture was left to cool at room temperature, charcoal (0.090 g) was added, stirred for 5 min and filtered over paper; the last procedure was repeated once and the solvent was evaporated under reduced pressure to obtain a yellow-green oil (yield, Tables 1 and 2).

2.7.2 | *Marrubium vulgare* matrices from plants treated with copper(II)

Here 0.30 g of matrix in 10 mL of ethanol under magnetic stirring were subjected to microwave heating (2 min ramping, maximum pressure 120 psi, maximum potency 100 W, temperature 120°C) for three cycles of 5 min. The mixture was left to cool at room temperature, added with 0.090 g of charcoal, stirred for 5 min, and filtered over paper; the filtration was repeated once and the solvent was evaporated under reduced pressure to obtain a yellow-green oil (yield, Table 3).

All samples were analysed by HPLC-UV/PAD. Each extract was dissolved in a 90:10 methanol/water mixture (12.5 mg/mL) and filtered with a 0.45 μm GH Polypro (GHP- PerkinElmer, China) membrane before injection into the HPLC-system. The different extracts were analysed exploiting the chromatographic conditions described earlier.

3 | RESULTS AND DISCUSSION

To establish a powerful approach for the determination of marrubiin in *M. vulgare* leaves, the research activity was organised as follows:

i. a HPLC-UV/PAD methodology for marrubiin quantitation was properly set up, using marrubiin as external standard;

ii. the dried samples of *M. vulgare* leaves were ground and extracted using microwave irradiation; and a screening of the factors relevant to the MASE procedure was conducted;

iii. the best MASE parameters were determined by DoE, quickly allowing the identification of the best extraction conditions;

iv. samples of *M. vulgare* leaves grown under abiotic stress induced by $CuSO_4$ (80–200-300 mg/L) were analysed;

every step is discussed hereinafter.

3.1 | Optimisation of the HPLC method

Relying on the results obtained in our previous work, a rapid and economic chromatographic method suitable for the complete resolution

TABLE 1 Experimental parameters used on unstressed matrix to set up the extraction method

Entry number	Solvent composition $v_m{:}v_w$	Number of cycles × minutes	Temperature (°C)	Y_{1m} Extraction yield (%)	Y_{2m} Total area (mAU-s)	Y_{3m} Marrubiin yield (mg/g dried plant)
1	80:20	1 × 5	40	16.29	7831107	2.20
2	20:80	1 × 5	40	13.86	7706809	0.15
3	80:20	3 × 5	40	14.60	10681435	2.03
4	20:80	3 × 5	40	16.84	9326463	0.23
5	80:20	1 × 5	80	20.82	16897393	5.17
6	20:80	1 × 5	80	22.29	14019358	3.39
7	80:20	3 × 5	80	25.22	22448046	8.01
8	20:80	3 × 5	80	17.31	13538365	2.52
9	50:50	2 × 5	60	23.66	13058322	1.22
10	50:50	2 × 5	60	24.00	14430454	1.40

Note: the solvents used are m, methanol and w, water.

TABLE 2 Experimental parameters used on unstressed matrix to set up the extraction method

Entry number	Solvent composition v_e:v_w	Number of cycles × minutes	Temperature (°C)	Y_{1e} Extraction yield (%)	Y_{2e} Total area (mAU-s)	Y_{3e} Marrubiin yield (mg/g dried plant)
1	80:20	1 × 5	40	13.84	10563133	2.92
2	20:80	1 × 5	40	18.77	6679179	1.61
3	80:20	3 × 5	40	17.85	9005601	5.25
4	20:80	3 × 5	40	23.05	7063361	2.25
5	80:20	1 × 5	80	19.27	10828100	5.39
6	20:80	1 × 5	80	20.87	7498999	2.78
7	80:20	3 × 5	80	17.35	13320100	6.24
8	20:80	3 × 5	80	22.37	6644688	4.82
9	50:50	2 × 5	60	21.45	7927552	3.49
10	50:50	2 × 5	60	19.40	12993662	4.12
11	75:25	3 × 5	80	21.27	10753422	5.89
12	100	3 × 5	120	14.53	14040263	9.20
13	100	3 × 5	80	10.10	9167573	4.98
14	80:20	3 × 5	120	21.42	11635041	8.47
15	90:10	3 × 5	100	15.47	13380524	6.45

Note: the solvents used are e, ethanol and w, water.

TABLE 3 Experimental parameters used on stressed matrices

Copper sulphate (mg/L)	Solvent composition v_e:v_w	Number of cycles × minutes	Temperature (°C)	Extraction yield (%)	Extract total area (mAU-s)	Marrubiin yield (mg/g dried plant)
80	100	3 × 5	120	12.87	10200575	4.97
200	100	3 × 5	120	12.50	9509691	3.88
300	100	3 × 5	120	10.23	21595277	2.79

Note: the solvents used are e, ethanol and w, water.

of marrubiin was developed.[3] The optimised method allowed us to obtain a shorter time of analysis exploiting an XBridge Phenyl (5 μm, 4.6 mm × 150 mm) column under gradient elution conditions, using a mobile phase composed of water and methanol both with 0.1% (v/v) formic acid. Marrubiin was identified comparing its HPLC retention time and UV spectrum with those of the standard analysed in the same conditions.

Quantitative determinations of this secondary metabolite were performed using external standard by means of a six-point calibration curve. The equation was obtained over a wide concentration range, in accordance with the level of marrubiin expected in the drug powder. The calibration equation thus attained was then used to compare the chromatographic marrubiin peak areas of the extracted samples with the external standard to achieve this secondary metabolite quantification. The chromatographic method response resulted a linear equation in the concentration range considered.

3.2 | Screening of the factors relevant for marrubiin extraction

The set up of the extraction method was conducted on the dry matrix of unstressed *M. vulgare* according to the experimental procedure described in sections 2.1–2.7. Based on our previous experience, we applied a DoE approach for identifying the best experimental

conditions.[30] The application of a DoE strategy for the development of optimised MASE procedures on natural matrices is a recent approach.[31]

Three responses were studied varying three different parameters. As responses, we considered the total extraction yield percentage (Y_1), the total area of the peaks recorded in the HPLC-UV/PAD chromatograms (Y_2), and the marrubiin yield (Y_3). It is well known that the efficiency of MASE strongly relies on the selection of operating conditions and parameters affecting the extraction mechanisms and yield: the main factors affecting MASE performance are, together with sample characteristics, solvent nature and composition, extraction time and temperature (strictly related to microwave power). Accordingly, we studied the parameters, solvent composition (X_1), extraction time (X_2) and temperature (X_3), applying two full factorial experimental designs in a sequential approach. The selected parameters were varied within defined ranges, as reported in Tables 1 and 2. The first eight experiments constituted the initial screening, followed by three test experiments in which the computed models were validated. The second set of four experiments was designed following the observations collected in the first phase of the study. Experiment numbers 7, 12, 13, and 14 of Table 2 were used to compute a 2^2 full factorial design, and experiment number 15 was used to validate this latter design. The detailed DoE experimental plan is reported in the Supporting Information.

Results of experiments with methanol (Table 1) showed that the proposed model is able to predict the trend of the expected extract

yield, total area of the chromatograms and marrubiin yield. Accordingly, we moved to the second set of experiments (Table 2), using ethanol, generally recognised as an eco-friendly and green solvent.

Results of the screening phase showed that:

- the extraction yield (Y_{1e}) obtained using ethanol reaches higher values when factor X_1 (solvent%) is kept at its minimum level (ethanol at the 80% level), while extraction time and temperature are not important to enhance the extraction yield;

- the total area of the peaks (Y_{2e}) is greater when factors X_1 and X_3 at their highest levels (ethanol 100% and temperature 120°C, respectively), whereas the extraction time seems to have no effect on the response;

- the marrubiin yield (Y_{3e}) seems higher when all three factors X_1, X_2, and X_3, are at the highest levels simultaneously (i.e. ethanol 100%, time of extraction 15 min, and temperature 120°C).

To assess whether the responses could be improved, one additional set of four experiments was then performed at the extremes of the experimental domain. The results are reported in Table 2 (experiment numbers 7, 12, 13, 14 for model computation and 15 for model validation). The response Y_{1e}, extraction yield %, is modelled very accurately by the simplified linear model without interactions of the solvent composition and temperature, according to the equation

$$Y_{1e} = (15.85 \pm 0.09) - (3.54 \pm 0.09)X_1 + (2.12 \pm 0.09)X_2$$

which provides a good fit ($r = 0.9993$) and accurate prediction of the experimental extraction yield percentage found (Table 2, experiment number 15, relative error percentage equal to 2.5%). The marrubiin

yield (Y_3) results, turned out instead to be better modelled by the simplified linear equation

$$Y_{3e} = (7.2 \pm 0.4) + (1.6 \pm 0.4)X_3$$

which showed only a simple dependence of the marrubiin yield from the extraction temperature and that the time of extraction and solvent composition do not actually influence the results. The model correctly predicts the marrubiin extraction yield found in the centre of the experimental domain (Table 2, experiment number 15, measured yield 6.45 mg/g, with a relative error of 12% versus predicted value of 7.2 ± 0.4 mg/g). Conversely, the total area of the peak in the chromatograms (Y_{2e}) is not described by a valid model and the mean value of the total area found, (1.20 ± 0.1)107 mAU-s, is independent of the variations made to the factors solvent composition and temperature studied (experiment numbers 7, 12, 13, and 14, Table 2).

Based on the results discussed earlier, we can consider validated the models for Y_{1e} and Y_{3e}, since the error is within the uncertainty limits associated with the used experimental procedure.

The best results in terms of marrubiin extraction yield (Y_3), whose quantification is the main goal of the work, were obtained using 100% ethanol, applying three cycles of microwave heating of 5 min each at 120°C (experiment number 12, Table 2). To exclude thermal marrubiin degradation at the extraction conditions, an additional MASE experiment (experiment number 12, Table 2) was carried out, adding known amounts of marrubiin to vegetal matrix (obtained from plant grown in Greenhouse conditions). The good recoveries obtained (99%) confirmed the chemical stability of marrubiin under the experimental conditions. Accordingly, these conditions have been applied for evaluating the effect of the treatment with copper(II) to the marrubiin production.
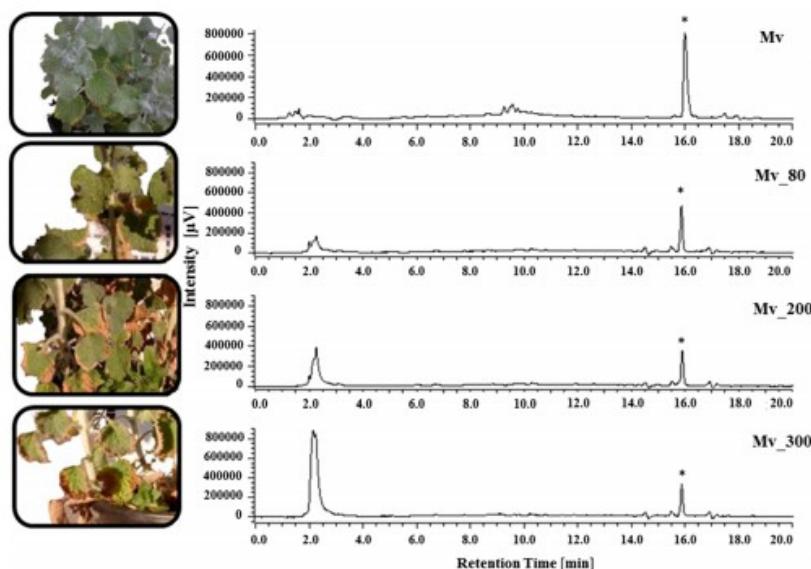

FIGURE 3 Chromatographic profile (λ = 220 nm) and morphology of the aerial part of *Marrubium vulgare* grown in Greenhouse conditions (Mv) and subsequently to an increasing stress caused by 80 (Mv_80), 200 (Mv_200) and 300 (Mv_300) mg/L of CuSO₄. The star * identifies the marrubiin peak [Colour figure can be viewed at wileyonlinelibrary.com]

FIGURE 4 Total area, extraction yield and marrubiin concentration in *Marrubium vulgare* grown in Greenhouse conditions (Mv) and subsequently to an increasing stress caused by 80 (Mv_80), 200 (Mv_200) and 300 (Mv_300) mg/L of CuSO₄. Boxes and error bars represent the mean ± standard deviation over repeated measurements
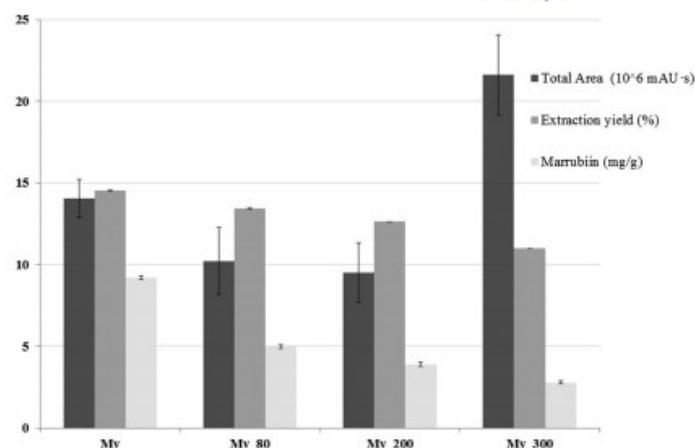
3.3 | MASE extraction of *M. vulgare* samples grown in Greenhouse conditions and treated with copper(II)

The optimised MASE protocol (experiment number 12, Table 2) was applied to *M. vulgare* leaves obtained from plants grown in Greenhouse conditions and treated with 80, 200 and 300 mg/L of CuSO₄ and the ethanolic extracts analysed using the HPLC-UV/PAD method developed here. The chromatographic profiles are shown in Figure 3, and the results are summarised in Figure 4.

Our results showed that raw materials originating from unstressed plant contained more marrubiin compared to leaves harvested from plants grown in stressed conditions. In detail, the plants were treated with CuSO₄ (80, 200 and 300 mg/L) for eight weeks according to the related literature.[32-34] As highlighted in Figure 4, there are significant differences ($P < 0.05$) in the amount of marrubiin, depending on the growth conditions. Furthermore, the concentration of marrubiin ranged from a maximum amount of 9.20 mg/g of dried plant grown in Greenhouse conditions and progressively decreased to 4.97 mg/g, 3.88 mg/g and 2.79 mg/g subsequently to an increasing stress caused by 80, 200 and 300 mg/L of CuSO₄, respectively. A similar trend was observed for total extraction yields (differences are significant at a statistical level, $P < 0.05$), suggesting a modification of the composition of secondary metabolites in the raw materials. This hypothesis may be corroborated by the chromatographic profiles of the extracts: the peak area corresponding to the first compounds eluted, the most polar, increased with stress. Therefore, we can state that there is a negative relation between copper(II) concentration, selected as test model substance responsible for soil pollution, and marrubiin content.

To conclude, we developed a cost effective MASE methodology to exhaustively extract marrubiin from *M. vulgare* leaves. The HPLC-UV/PAD analysis of the raw extract allows a rapid and reliable quantification of marrubiin in *M. vulgare* leaves and can be applied to evaluate the quality of a wide range of samples of white horehound. To optimise the process, we used the statistical DoE approach. DoE findings indicated that the highest extraction efficiency of marrubiin with high repeatability were obtained using 100% ethanol at 120°C for 15 min, with significant benefits in terms of extraction times and

environmental impact, given that ethanol is completely biodegradable. The developed methodology was applied to evaluate the quality of white horehound, grown under Greenhouse as well as under copper(II)-mediated stress conditions. We demonstrated that growth conditions may affect the marrubiin content and therefore the quality of the herbal drug.

We propose this methodology for the characterisation of *M. vulgare* herbal drug samples, thus evaluating their exposure to abiotic stress, revealing their phytochemical status, and facilitating the identification of raw materials obtained from plant grown under stress conditions.

ORCID

Simona Collina https://orcid.org/0000-0002-2954-7558

REFERENCES

1. Newman DJ, Cragg GM. Natural products as sources of new drugs over the 30 years from 1981 to 2010. *J Nat Prod*. 2012;75(3):311-335.
2. Bartwal A, Mall R, Lohani P, Guru SK, Arora S. Role of secondary metabolites and Brassinosteroids in plant defense against environmental stresses. *J Plant Growth Regul*. 2013;32(1):216-232.
3. Martino E, Casamassima G, Castiglione S, et al. Vinca alkaloids and analogues as anti-cancer agents: looking back, peering ahead. *Bioorg Med Chem Lett*. 2018;28(17):2816-2826.
4. Amri B, Martino E, Vitulo F, et al. *Marrubium vulgare* L. leave extract: phytochemical composition, antioxidant and wound healing properties. *Molecules*. 2017;22(11):1851-1869.
5. Martino E, Collina S, Rossi D, et al. Influence of the extraction mode on the yield of hyperoside, vitexin and vitexin-2-O-rhamnoside from *Crataegus monogyna* Jacq. (hawthorn). *Phytochem Anal*. 2008;19(6):534-540.
6. Rossi D, Ahmed KM, Gaggeri R, et al. (R)-(−)-Aloesaponol III 8-methyl ether from *Eremurus persicus*: a novel compound against leishmaniosis. *Molecules*. 2017;22(4):519-534.
7. Martino E, Ramaiola I, Urbano M, Bracco F, Collina S. Microwave-assisted extraction of coumarin and related compounds from *Melilotus officinalis* (L.) Pallas an alternative to Soxhlet and ultrasound-assisted extraction. *J Chromatogr A*. 2006;1125(2):147-151.
8. Lucconi G, Chlapanidas T, Martino E, et al. Formulation of microspheres containing *Crataegus monogyna* Jacq. extract with free radical scavenging activity. *Pharm Dev Technol*. 2014;19(1):65-72.

9. Sahpaz S, Garbacki N, Tits M, Bailleu F. Isolation and pharmacological activity of phenylpropanoid esters from *Marrubium vulgare*. *J Ethnopharmacol*. 2002;79(3):389-392.

10. El Bardai S, Morel N, Wibo M, et al. The vasorelaxant activity of marrubenol and marrubiin from *Marrubium vulgare*. *Planta Med*. 2003;69(1):75-77.

11. El Bardai S, Lyoussi B, Wibo M, Morel N. Comparative study of the antihypertensive activity of *Marrubium vulgare* and of the dihydropyridine calcium antagonist amlodipine in spontaneously hypertensive rat. *Clin Exp Hypertens*. 2004;26(6):465-474.

12. Meyre-Silva C, Yunes RA, Schlemper V, Campos-Buzzi F, Cechinel-Filho V. Analgesic potential of marrubiin derivatives, a bioactive diterpene present in *Marrubium vulgare* (Lamiaceae). *IL Farmaco*. 2005;60(4):321-326.

13. Stulzer HK, Tagliari MP, Zampirolo JA, Cechinel-Filho V, Schlemper V. Antioedematogenic effect of marrubiin obtained from *Marrubium vulgare*. *J Ethnopharmacol*. 2006;108(3):379-384.

14. Masoodi MH, Bahar A, Zagar IM, Khan SA, Khan S, Singh P. Antibacterial activity of whole plant extract of *Marrubium vulgare*. *Afr J Biotechnol*. 2008;7:86-87.

15. Boudjelal A, Henchiri C, Siracusa L, Sari M, Ruberto G. Compositional analysis and *in vivo* anti-diabetic activity of wild Algerian *Marrubium vulgare* L. infusion. *Fitoterapia*. 2012;83(2):286-292.

16. Akther N, Shawl AS, Sultana S, Chandan BK, Akhter M. Hepatoprotective activity of *Marrubium vulgare* against paracetamol induced toxicity. *J Pharm Res*. 2013;7(7):565-570.

17. Boulila A, Sanaa A, Ben Salem I, et al. Antioxidant properties and phenolic variation in wild populations of *Marrubium vulgare* L. (Lamiaceae). *Ind Crop Prod*. 2015;76:616-622.

18. 9 July 2013 EMA/HMPC/604273/2012 Committee on Herbal Medicinal Products (HMPC).

19. McCrea A. Comparative marrubiin content in *Marrubium vulgare* from European vs. American seed. *J Am Pharm Assoc*. 1930;19(3):231.

20. De Jesus RAP, Cechinel-Filho V, Oliveira AE, Schlemper V. Analysis of the antinociceptive properties of marrubiin isolated from *Marrubium vulgare*. *Phytomedicine*. 2000;7(2):111-115.

21. Mnonopi N, Levendal RA, Davies-Coleman RT, Frost CL. The cardioprotective effects of marrubiin, a diterpenoid found in *Leonotis leonurus* extracts. *J Ethnopharmacol*. 2011;138(1):67-75.

22. Laonigro G, Lanzetta R, Parrilli M, Adinolfi M, Mangoni L. The configuration of the diterpene spiro ethers from *Marrubium vulgare* and from *Leonotis leonurus*. *Gazz Chim Ital*. 1979;109:145-150.

23. Paula de Olivera A, Santin JR, Lemos M, et al. Gastroprotective activity of methanol extract and marrubiin obtained from leaves of *Marrubium vulgare* L. (Lamiaceae). *J Pharm Pharmacol*. 2011;63(9):1230-1237.

24. Zaabat N, Hay AE, Michalet S, et al. Antioxidant and antigenotoxic properties of compounds isolated from *Marrubium deserti* de Noe. *J Food Chem Toxicol*. 2011;49(12):3328-3335.

25. Karioti A, Skopeliti M, Tsitsilonis O, Heilmann J, Skaltsa H. Cytotoxicity and immunomodulating characteristics of labdane diterpenes from *Marrubium cylleneum* and *Marrubium velutinum*. *Phytochemistry*. 2007;68(11):1587-1594.

26. Hellen K, Stulzer HK, Tagliari MP, Zampirolo JA, Cechinel-Filho V, Schlemper V. Antioedematogenic effect of marrubiin obtained from *Marrubium vulgare*. *J Ethnopharmacol*. 2006;108:379-384.

27. De Souza MM, De Jesus RAP, Cechinel-Filho V, Schlemper V. Analgesic profile of hydroalcoholic extract obtained from *Marrubium vulgare*. *Phytomedicine*. 1998;5(2):103-107.

28. Mnonopi N, Levendal RA, Mzilikezi N, Frost CL. Marrubiin, a constituent of *Leonotus leonurus*, alleviates diabetic symptoms. *Phytomedicine*. 2012;19(6):488-493.

29. Popoola OK, Elbagory AM, Ameer F, Hussein AA. Marrubiin. *Molecules*. 2016;18:9049-9060.

30. Marrubini G, Fattorini P, Previderé C, et al. Experimental design applied to the optimization of microwave-assisted DNA hydrolysis. *J Chromatogr A*. 2012;1249:8-16.

31. Leone A, Tamborrino A, Zagaria R, Sabella E, Romaniello R. Plant innovation in the olive oil extraction process: a comparison of efficiency and energy consumption between microwave treatment and traditional malaxation of olive pastes. *J Food Eng*. 2015;146:44-52.

32. Amri B, Kaab SB, Gouia H, Martino E, Collina S, Ben-Kaâb LB. Copper-induced changes in nutrient uptake, enzymatic and non-enzymatic antioxidant systems in horehound (*Marrubium vulgare* L.). *Botan Sci*. 2017;95(3):565-575.

33. Gupta D. Abdullah. Toxicity of copper and cadmium on germination and seedling growth of maize (*Zea mays* L.) seeds. *Ind J Sci Res*. 2011;2:67-70.

34. Tóth G, Hermann T, Da Silva MR, Montanarella L. Heavy metals in agricultural soils of the European Union with implications for food safety. *Environ Int*. 2016;88:299-309.

SUPPORTING INFORMATION

Additional supporting information may be found online in the Supporting Information section at the end of the article.

Paper 7

MDPI

Article

Development of a Mucoadhesive and an in Situ Gelling Formulation Based on κ-Carrageenan for Application on Oral Mucosa and Esophagus Walls. II. Loading of a Bioactive Hydroalcoholic Extract

Barbara Vigani [1], Silvia Rossi [1,*], Matteo Gentile [1], Giuseppina Sandri [1], Maria Cristina Bonferoni [1], Valeria Cavalloro [2], Emanuela Martino [2], Simona Collina [1] and Franca Ferrari [1]

[1] Department of Drug Sciences, University of Pavia, Viale Taramelli, 12-27100 Pavia, Italy; barbara.vigani@unipv.it (B.V.); matteo.gentile01@universitadipavia.it (M.G.); giuseppina.sandri@unipv.it (G.S.); cbonferoni@unipv.it (M.C.B.); simona.collina@unipv.it (S.C.); franca.ferrari@unipv.it (F.F.)

[2] Department of Earth and Environmental Science, University of Pavia, Via S. Epifanio, 14-27100 Pavia, Italy; valeria.cavalloro01@universitadipavia.it (V.C.); emanuela.martino@unipv.it (E.M.)

* Correspondence: silvia.rossi@unipv.it; Tel.: +39-0382-987357; Fax: +39-0382-422975

check for **updates**

Abstract: The aim of the present work was to load a *Hibiscus sabdariffa* (HS) hydroalcoholic extract into in situ gelling formulations for the treatment of oral mucositis and esophagitis. Such formulations, selected as the most promising options in a previous work of ours, were composed by κ-carrageenan (κ-CG), a sulfated marine polymer able to gelify in presence of saliva ions, hydroxypropyl cellulose (HPC), used as mucoadhesive agent, and $CaCl_2$, salt able to enhance the interaction κ-CG/saliva ions. HS extract, which is rich in phytochemicals such as polyphenols, polysaccharides and organic acids, was selected due to its antioxidant and anti-inflammatory properties. For HS extraction, three different methodologies (maceration, Ultrasound Assisted Extraction (UAE) and Microwave Assisted Extraction (MAE)) were compared in terms of extraction yield and extract antioxidant activity, revealing that MAE was the best procedure. Rheological and mucoadhesive properties of HS-loaded formulations were investigated. Such formulations were characterized by a low viscosity at 25 °C, guaranteeing an easy administration, a proper in situ gelation behavior and marked elastic and mucoadhesive properties at 37 °C, functional to a protective action towards the damaged mucosa. Finally, the biocompatibility and the proliferative effect of HS-loaded formulations, as well as their antioxidant and anti-inflammatory properties, were proved in vitro on human dermal fibroblasts.

Keywords: oral mucositis; *Hibiscus sabdariffa* extract; κ-carrageenan; in situ gelation; mucoadhesion; antioxidant; anti-inflammatory properties

---

1. Introduction

Carrageenans (CGs) are an important class of hydrophilic pharmaceutical polymeric excipients obtained by extraction with water or aqueous alkali from some members of marine red seaweeds of the class Rhodophyceae, such as *Chondrus*, *Eucheuma*, *Gigartina* and *Hypnea*. CGs are sulfated polysaccharides, consisting of an alternating linear chain of galactose and 3,6-anydrogalactose, which can be classified according to the degree of substitution on their free hydroxyl groups. Depending on the number and position of the ester sulfate groups, three primary classes of CGs, named kappa (κ), iota (ι) and lambda (λ), are recognized. In particular, κ-CG, having one negative charge per

disaccharide residue, is well known to obtain gels in presence of certain cations, such as K^+, Na^+, Mg^{2+} and Ca^{2+} [1–3].

In a previous work of ours [4], in situ gelling formulations based on κ-CG were developed for the treatment of oral mucositis and esophagitis. κ-CG was chosen for its ability to gelify in presence of saliva ions. The formulations also contained hydroxypropyl cellulose (HPC), employed as mucoadhesive agent, and $CaCl_2$ that was proved to enhance, at a low concentration (0.04% w/w), the interaction between κ-CG and saliva ions. Different κ-CG, HPC and $CaCl_2$ concentrations were investigated in order to obtain formulations able to interact with saliva ions, producing a gel capable of adhering to the damaged mucosa. The developed formulations were characterized by: (i) an easy administration, due to their low viscosity at room temperature, (ii) a protective action towards the mucosa, related to their marked elastic properties at 37 °C, and (iii) mucoadhesion properties.

These promising results prompted us to investigate the possibility of loading the previously developed formulations with a bioactive hydroalcoholic extract intended for the treatment of the oral mucositis and esophagitis.

Hibiscus sabdariffa Linn. (HS), also named roselle, red sorrel or karcadè, is an annual herbaceous subshrub belonging to the family of Malvaceae and is commonly distributed in tropical and subtropical regions [5–7]. The pharmacological properties of HS have been extensively studied for years, preparing extracts using several solvents (water, alcohols alone or in mixtures) and evaluating their biological effects [8–15]. All the HS extracts are characterized by the presence of phenols, polyphenols, anthocyanins and organic acids, such as citric, tartaric, malic, ascorbic acids and others, which are responsible for high antioxidant and anti-inflammatory properties [16–19]. These functions enhance the healing process by modulating the production of reactive oxygen species and pro-inflammatory cytokines that are responsible for the amplification of the damage [20]. In the present work, on the basis of our experience [21–25], we experimented different HS extraction methodologies (maceration, Ultrasound Assisted Extraction (UAE) and Microwave Assisted Extraction (MAE)), using a hydroalcoholic solvent. To obtain extracts rich in antioxidant metabolites, the mixture ethanol/water 80/20 v/v was used as extracting solvent in accordance with literature [26]. The different extracts were compared in terms of both extraction yield and antioxidant activity in order to select the most convenient approach.

Two formulations, indicated with the name BLANK 1 and BLANK 2, containing 0.04% w/w $CaCl_2$, 1% w/w HPC and different κ-CG concentrations (0.6% and 0.4% w/w, respectively) were loaded with HS extract (0.2% w/w). Such formulations, after dilution to a 3: 1 weight ratio with artificial saliva or distilled water [4,27,28], were subjected to viscosity measurements at increasing shear rates in order to verify if the presence of the extract affects the formulation gelling capability. In addition to viscosity, the viscoelasticity of the vehicle could play an important role on its ability, once administered, to withstand the physiological removal action exerted by saliva and by the mechanical stress produced by the movement of the walls of the oral cavity [29]. For this reason, all formulations, loaded and not, have been subjected to dynamic oscillatory measurements at 37 °C after dilution in artificial saliva [30–35].

Thereafter, the mucoadhesive properties of all the formulations under investigation were studied: the samples were submitted to mucoadhesion measurements by means of a tensile test, using porcine gastric mucin as biological substrate [36,37].

In order to verify the biocompatibility of the developed formulations, the vehicle containing the highest concentration of κ-CG, unloaded and after loading with HS extract, was subjected to cytotoxicity and cell proliferation tests on human fibroblasts [38,39]. The developed formulations should be able to deliver HS bioactive substances without impairing their biological activity. Therefore, the capability of the formulations to protect cells from oxidative stress induced by hydrogen peroxide was also investigated in comparison with HS extract [40]. Moreover, the anti-inflammatory properties of the HS extract and HS-loaded formulations have been evaluated on fibroblasts inflamed with lipopolysaccharide (LPS) [41].

2. Results and Discussion

2.1. Preparation and Characterization of HS Extracts

HS extracts were prepared performing maceration (Mac), Ultrasound Assisted Extraction (UAE) and Microwave Assisted Extraction (MAE) exploiting ethanol/water 80/20 v/v as solvent. Mac and UAE were performed both in light and dark conditions at different temperatures. Extraction time and temperature were chosen according to literature, taking into account the stability of anthocyanins [26]. For the analytical characterization of the HS extracts, an appropriate reverse phase HPLC/UV-PAD method under gradient condition was set up. All the extracts give rise to chromatograms with a similar profile, indicating that they are characterized by a similar composition.

In Figure 1, chromatographic profiles of MAE and UAE extracts are reported as an example.
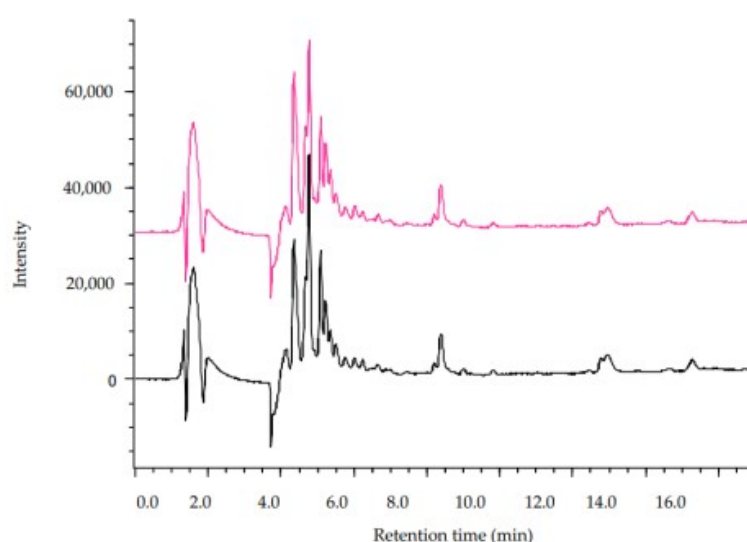
Figure 1. Chromatographic profiles recorded at λ = 274 nm of HS extracts obtained by Microwave Assisted Extraction (MAE, red line) and Ultrasound Assisted Extraction (UAE, black line).

The three extraction methodologies were then compared considering both extraction yield and free radical scavenging (FRS) activity (Table 1), evaluated by means of DPPH test, a chemical assay widely used as primary screening of antioxidant activity of natural compounds [42,43]. Overall results showed that the methodology used as well as the operating conditions (light or dark) do not affect the extraction efficiency, giving rise to extraction yields ranging from 34.6 to 40.7%. A different trend was observed for the FRS properties. Indeed, FRS% seems to be related to both extraction temperature and light or dark status, rather than the methodology applied: Mac, UAE and MAE at 45 °C under dark conditions give rise to extracts with FRS% values very close to 60%.

The results obtained highlighted that MAE is the most convenient extraction method, allowing to obtain an extract with yield and FRS activity % comparable with Mac and UAE at 45 °C under dark conditions, but in very shorter times. For this reason, such an extract was chosen for the continuation of the work.

Table 1. Extraction yields and antioxidant activity of the different HS extracts obtained. Antioxidant activity is expressed as a percent compared with the control.

Extraction	T (°C)	Time (min × Cycles)	Extraction Yield (g/g of Dried Calyces)	FRS %
Mac Light	r.t.	60 × 3	36.1	50.1
Mac Light	45	60 × 3	38.3	58.1
Mac Dark	r.t.	60 × 3	34.6	42.3
Mac Dark	45	60 × 3	35.2	58.9
UAE Light	r.t.	45 × 3	39.4	46.3
UAE Light	45	45 × 3	40.7	55.1
UAE Dark	r.t.	45 × 3	38.4	54.1
UAE Dark	45	45 × 3	40.1	57.5
MAE	45	5 × 3	36.3	58.9

r.t.: room temperature.

2.2. Rheological Properties

In a previous work of ours [4], in situ gelling formulations, intended for the treatment of oral mucositis and esophagitis induced by cancer therapies, were developed. In particular, the formulations consisted of κ-CG, a hydrophilic sulfate marine polymer with wound healing properties and able to gelify in presence of saliva ions, hydroxypropyl cellulose (HPC) as mucoadhesive agent and $CaCl_2$ as salt able to enhance the interaction κ-CG/saliva ions.

In the present work, the formulations characterized by the best rheological and mucoadhesive performances, containing κ-CG 0.4 or 0.6% w/w, HPC 1% w/w and $CaCl_2$ 0.04% w/w, were loaded with HS extract at 0.2% w/w.

Figure 2 compares the viscosity values measured at 25 °C and 300 s^{-1} shear rate of the formulations BLANK 1 (containing κ-CG 0.6% w/w) and BLANK 2 (containing κ-CG 0.4% w/w), before and after HS loading (LOADED 1 and LOADED 2). Such results represent the mean values obtained from three aliquots collected in different regions of each formulation. The low variability of the data proves the homogeneity of the samples under investigation. The same rheological measurements were performed 1h, 24h and 1 week after sample preparation and no significant viscosity variation was pointed out (data not shown). In the case of the loaded formulations, such results indicate their physical stability in the time period considered.
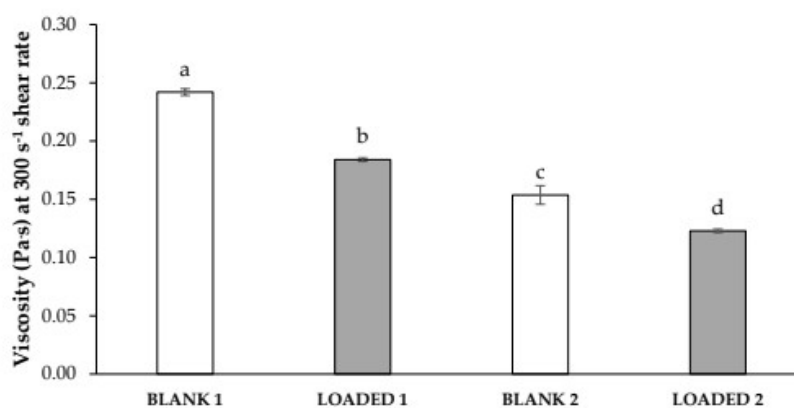
Figure 2. Viscosity values measured at 25 °C and 300 s^{-1} shear rate of the formulations BLANK 1 (containing 0.6% w/w κ-CG) and BLANK 2 (containing 0.4% w/w κ-CG) before and after loading of HS extract at the concentration of 0.2% w/w (LOADED 1 and 2) (mean values ± s.d.; n = 3). Anova one-way, Multiple Range Test (p < 0.05): a vs. b–d; b vs. c, d; c vs. d.

The presence of HS is responsible for a decrease of the formulation viscosity (Figure 2). This decrease is functional to an easy administration: a low viscosity is accompanied by a better distribution of the formulation on the application mucosa. In addition, the presence of HS is responsible for a greater capability of both the formulations to interact with saliva ions, as indicated by the normalized rheological synergism parameter (ΔSYN) calculated for LOADED 1 and LOADED 2, that was equal, respectively, to 1.44 ± 0.09 and 1.19 ± 0.06 (mean values $\pm$ s.d.; n = 3). ΔSYN values higher than 1 indicate a greater capability of the formulations to interact with saliva ions with respect to the relevant blank vehicles. Between the two loaded formulations, LOADED 1 is characterized by the highest ΔSYN value; its performance in terms of increase in viscosity when in contact with saliva ions is about one and a half times the gelling capability of BLANK 1.

In Figure 3, loss tangent (tgδ) values of HS-loaded and blank formulations upon contact with artificial saliva are compared. It can be observed that both the loaded formulations are characterized by lower loss tangent values with respect to the relevant blanks. Since the loss tangent is calculated as the ratio between the loss (G″) and the storage (G′) moduli that represent, respectively, the viscous and the elastic components, a lowering of tgδ indicates that the presence of HS produces a strengthening of the formulation elasticity. Moreover, the LOADED 1 formulation is characterized by a loss tangent value lower than 1, indicating that the elastic behavior is higher than the viscous one. This means that the interaction with saliva ions produces a polymeric network that, when subjected to a mechanical stress, mainly responds deforming itself and recovering the strain undergone when the stress is removed. As stated in a previous work [44], this behavior functions as a protective action of the solution towards the application site.
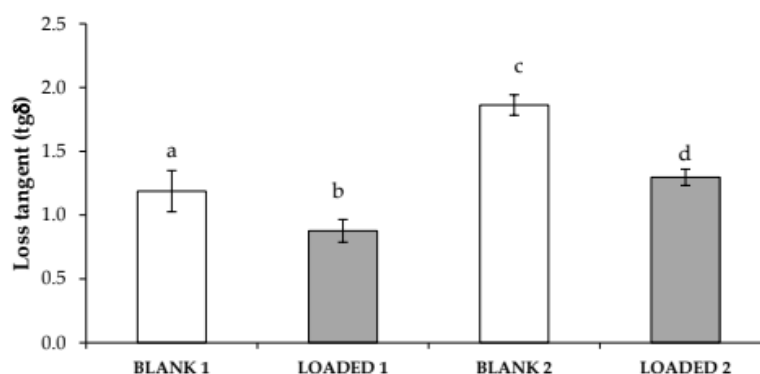
Figure 3. Loss tangent (tgδ) values of blank and loaded formulations upon dilution 3:1 w/w in artificial saliva (mean value $\pm$ s.d.; n = 3). Anova one-way, Multiple Range Test ($p < 0.05$): a vs. b, c; b vs. c, d; c vs. d.

2.3. Mucoadhesion Properties

As reported in the Part I of this research work [4], the presence of HPC at 1% w/w into the formulations is responsible for their mucoadhesive properties. To compare the mucoadhesion behavior of the blank and HS-loaded formulations on homogeneous basis, the normalized mucoadhesion interaction parameter (ΔFmax/Fmax) was calculated by normalizing the difference between the maximum detachment force in the presence and absence of mucin for the maximum force in the absence of biological substrate [36,37]. In Figure 4, ΔFmax/Fmax values of all the formulations are reported. It can be observed that the presence of HS does not significantly affect the mucoadhesive properties of the formulation.
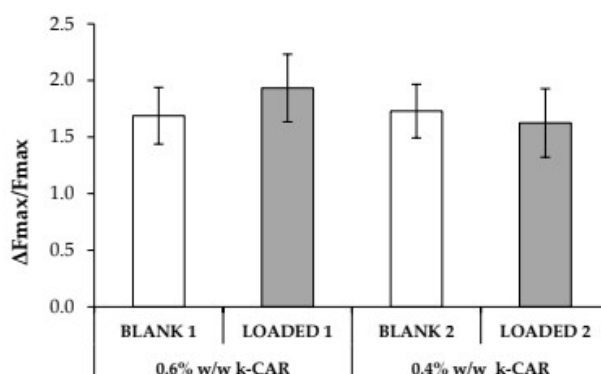
Figure 4. Comparison of the values of the normalized mucoadhesion parameter (ΔFmax/Fmax), observed for the blank and loaded formulations (mean value $\pm$ s.d.; n = 6). Anova one way: no significant differences.

On the basis of the results obtained, LOADED 1 formulation was chosen for the continuation of the work because it was characterized by the greatest capability to interact with the saliva ions, forming a gel with marked elastic properties and able to adhere to the mucosa.

2.4. In Vitro Functional Properties of LOADED 1 Formulation

The cytotoxic effect of both BLANK 1 and LOADED 1 formulations was investigated on human dermal fibroblasts. Figure 5 shows the percentage of living cells after treatment with the samples, upon dilution 1: 1 and 1: 3 v/v in complete culture medium (CM). All the samples tested are characterized by viability % values higher than 80%. Such a result highlights that the polymers used for the preparation of the in situ gelling formulations considered in the study are biocompatible [45]. These results demonstrate that the addition of HS extract improves the formulation compatibility with the cell substrate. In particular, LOADED 1, regardless of the dilution considered, shows viability % values that are comparable to CM and statistically higher than those obtained for BLANK 1.
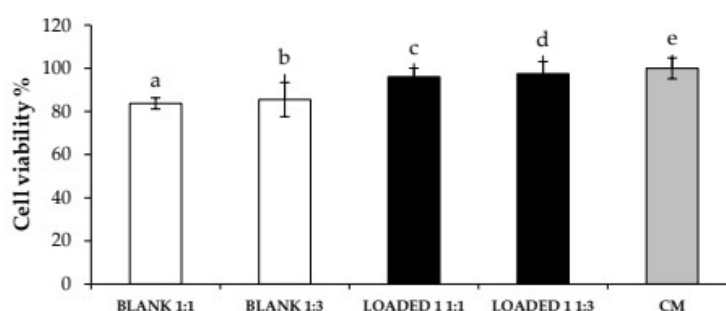
Figure 5. Viability % values calculated after cell contact with BLANK 1 and LOADED 1 formulations for 24 h. Two different dilutions, 1:1 and 1:3 v/v, in CM were considered. CM was used as reference (mean values $\pm$ s.d.; n = 3). Anova one-way, Multiple Range Test (p < 0.05): a vs. b–e; b vs. c–e.

In order to verify if the LOADED 1 formulation was not only biocompatible, but also able to promote cell growth, a proliferation test was performed on both blank and HS-loaded formulations. In such a test, all the samples were diluted in medium without serum (M w/s). Since serum is the medium component principally involved in promoting cell proliferation, the use of M w/s should allow to investigate the actual sample capability to enhance cell growth. Fibroblasts were seeded in

the medium without serum (M w/s) and, simultaneously, put in contact with the samples in order to verify if their presence could interfere on cell growth. An aqueous solution of HS, at the same concentration used for the preparation of LOADED 1 formulation (0.2% w/w), was investigated for a better understanding of the proliferative effect of HS extract.

Figure 6 highlights a significant difference between cell proliferation % values of CM and M w/s, indicating the discriminating power of the test. Both blank and HS-loaded formulations, when diluted 1:1 v/v in M w/s, show viability percentages statistically higher than those obtained for the references, CM and M w/s, proving their capability to promote cell proliferation. Moreover, LOADED 1 formulation is characterized by a cell proliferation % value significantly higher than that obtained for HS, suggesting that the polymers used to prepare the formulations are able to improve extract capability to promote cell proliferation.
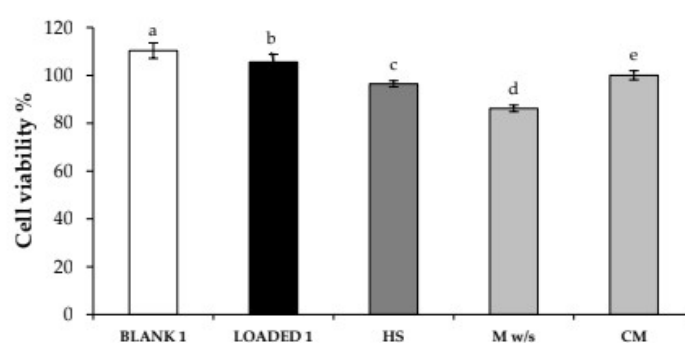
Figure 6. Proliferation % values calculated after cell contact with BLANK 1 and LOADED 1 formulations (diluted 1:1 v/v in M w/s) for 24 h. A solution of HS extract prepared in distilled water at the concentration of 0.2% w/w (diluted 1:1 v/v in M w/s) was also investigated (HS). M w/s and CM were used as references (mean values ± s.d.; n = 3). Anova one-way, Multiple Range Test ($p < 0.05$): a vs. b–e; b vs. c–e; c vs. d–e; d vs. e.

The capability of BLANK 1 and LOADED 1 formulations to protect cells against the oxidative damage was assessed. In particular, the antioxidant properties of HS extract, as proven above by DPPH assay, were investigated on fibroblasts treated with H_2O_2: both HS aqueous solution (0.2% w/w) and HS-loaded formulation were considered.

Figure 7 shows the optical density values measured after cell contact with increasing H_2O_2 concentrations. It can be observed that H_2O_2 concentrations higher than 1.25 mM are responsible for a statistically significant decrease of the optical density, when compared to the untreated cells (H_2O_2 concentration equal to 0). In an attempt to evaluate the antioxidant properties of the samples, 1.25 mM was selected as the H_2O_2 concentration necessary to induce a proper oxidative damage, without a complete cell death. Therefore, fibroblasts were treated with the samples for 24 h and, then, subjected to an oxidative stress with H_2O_2 at the concentration of 1.25 mM. Figure 8 points out that LOADED 1 formulation and HS solution exert an antioxidant effect, since they are characterized by optical density values higher than those observed for the cells subjected to H_2O_2 in absence of the samples (CTR). No statistical difference is observed between the values of LOADED 1 and HS, indicating that the vehicle does not disturb the anti-oxidant properties of HS.
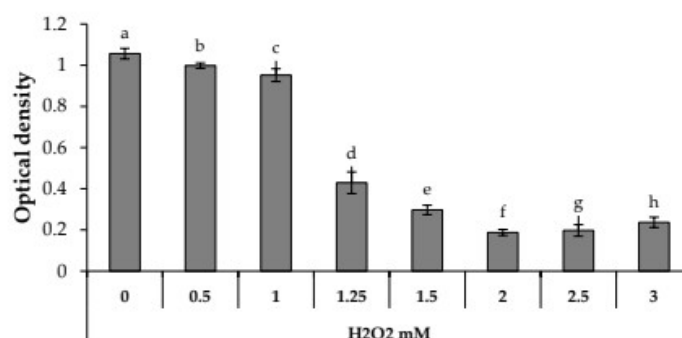
Figure 7. Optical density values measured after cell treatment with increasing H_2O_2 solutions for 24 h (mean values ± s.e.; n = 6). Anova one-way, Multiple Range Test (p < 0.05): a vs. c–h; b vs. d–h; c vs. d–h; d vs. e–h; e vs. f–g; f vs. h.
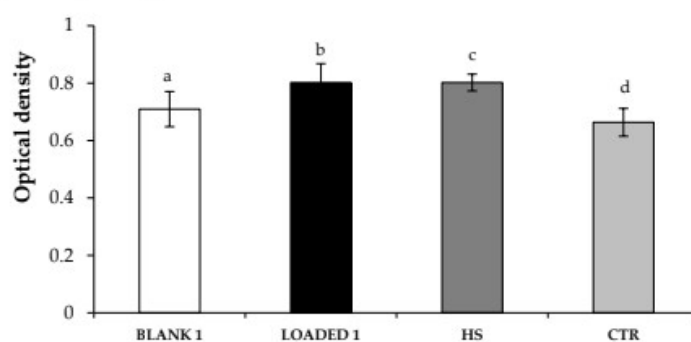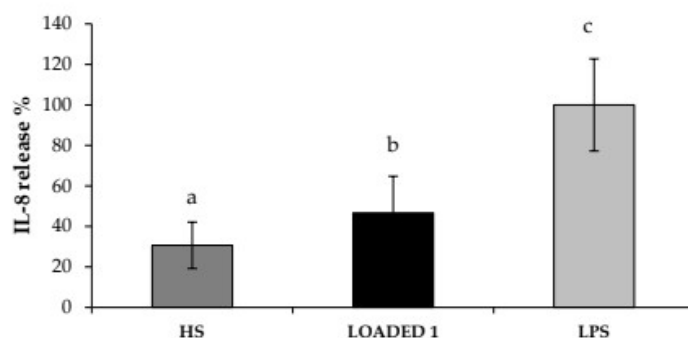

Figure 8. Optical density values measured after cell treatment with the samples (diluted 1:1 v/v in CM) for 24 h and, then, with H_2O_2 (1.25 mM) for other 24 h. Cells subjected to the oxidative stress in absence of the samples were considered as control (CTR) (mean values ± s.e.; n = 3). Anova one-way, Multiple Range Test (p < 0.05): b vs. d; c vs. d.

As expected, BLANK 1 formulation is not characterized by an antioxidant effect, showing an optical density value similar to that measured for the CTR.

Such results can be explained considering the composition of the aqueous extract of *Hibiscus sabdariffa*, which is rich in anthocyanins and other phenolic compounds, such as chlorogenic acids. Beltràn-Debón and colleagues (2010) demonstrated that the use of HS aqueous extract preserved peripheral blood mononuclear cells (PBMCs) from the cellular death induced by H_2O_2. In particular, a dose-dependent resistance to the oxidative damage was observed after PBMCs co-incubation with HS and H_2O_2, confirming the presence of antioxidant compounds in the HS extract. The same effect was observed when PBMCs were pre-treated with HS and, subsequently, with H_2O_2 [46].

Finally, the anti-inflammatory effect of HS extract and LOADED 1 formulation was investigated on cells inflamed with lipopolysaccharide (LPS). Figure 9 reports cell viability % of the inflamed cells untreated (LPS) and treated with the formulations (BLANK and LOADED 1). It can be observed that cell viability is not affected neither by the LPS-treatment nor by the samples: no statistically significant differences are observed between the viability % values of inflamed cells in presence of the samples (HS and LOADED 1), inflamed cells in absence of the samples (LPS) and not inflamed cells (CM) (Figure 9). This result is in line with what reported in the literature [41].
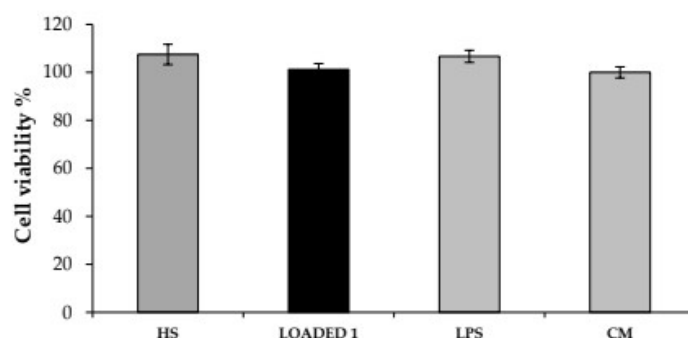
Figure 9. Viability % values calculated after cell treatment with the samples (diluted 1:1 v/v in CM) for 24 h and, then, with LPS solution (10 µg/mL) for other 24 h. Cells subjected to LPS-inflammation in absence of samples were considered as the negative control (LPS). CM, not inflamed cells, was used as reference (mean values ± s.d.; n = 3).

In Figure 10, IL-8 release % values observed in presence of HS extract and LOADED 1 formulation are reported. When fibroblasts were pre-treated for 24 h with LOADED 1 formulation, the LPS-induced inflammation leads to a lower IL-8 release. In particular, the percentage of IL-8 released after treatment with both HS solution and LOADED 1 formulation is statistically lower than 100% (CTR, inflamed cells in absence of samples). This indicates that HS and LOADED 1 are characterized by anti-inflammatory properties. No statistical difference is observed between the values of LOADED 1 and HS, indicating that the vehicle does not disturb the anti-inflammatory properties of HS.

Figure 10. IL-8 release % values calculated after cell treatment with the samples (diluted 1:1 v/v in CM) for 24 h and, then, with LPS solution (10 µg/mL) for other 24 h. Cells subjected to LPS-inflammation in absence of samples were considered as negative control (LPS) and corresponds to 100% (mean values ± s.e.; n = 3). Anova one-way, Multiple Range Test (p < 0.05): a vs. c; b vs. c.

3. Materials and Methods

3.1. Materials

The solvents for the extraction and the high performance liquid chromatography (HPLC grade) were supplied by Carlo Erba (Milan, Italy). Formic acid and 2,2-diphenyl-1-picrylhydrazyl radical (DPPH) were purchased from Sigma Aldrich (Milan, Italy). All solvents were evaporated under reduced pressure using a Heidolph Laborota 4000 instrument (Heidolph Instruments GmbH & Co, Schwabach, Germany).

For the preparation of all the formulations and their characterization in terms of rheological and mucoadhesive properties, the materials hereafter reported were used. κ-carrageenan (κ-CG),

porcine gastric mucin type II and calcium chloride ($CaCl_2$) were purchased from Sigma-Aldrich (Milan, Italy). Potassium chloride (KCl), sodium chloride (NaCl), sodium bicarbonate ($NaHCO_3$) and sodium phosphate monobasic ($NaH_2PO_4 \cdot H_2O$) were purchased from Carlo Erba Reagents (Milan, Italy). Klucel™ hydroxypropylcellulose (HPC) was from Ashland (Schaffhausen, Switzerland).

For experiments with Normal Human Dermal Fibroblasts (NHDF) from juvenile foreskin (PromoCell GmbH, VWR, Milan, Italy), the materials hereafter reported were used. Dimethyl sulfoxide (DMSO), Dulbecco's Phosphate Buffer Solution (PBS), MTT (3-(4,5-dimethylthiazol-2-yl)-2,5-diphenyltetrazolium bromide), antibiotic/antimycotic solution (100×; stabilized with 10,000 units penicillin, 10 mg streptomycin, and 25 µg amphotericin B per mL), trypan blue solution, trypsin– EDTA solution and lipopolysaccharide from *Escherichia coli* O55: B5 were purchased from Sigma-Aldrich (Milan, Italy). DMEM was purchased from Corning Incorporated (Corning, NY, USA) and inactivated fetal bovine serum from Biowest (Nuaillé, France).

3.2. Plant Material and Extraction Procedure

Dried calyces of *Hibiscus sabdariffa* Linn were cultivated in Burkina Faso and bought in a local market. The matrix was stored in dark conditions and, at the time of use, it was cut to small size and grounded with a blade mill (A10 IKA-Werke GmbH & Co., Staufen, Germany) to obtain a homogeneous fine powder.

HS extracts were prepared by extracting 10 g of powder with 200 mL of ethanol/water 80/20 v/v for three times and comparing three different approaches: dynamic maceration, ultrasound assisted extraction (UAE) and microwave assisted extraction (MAE).

In detail, maceration and UAE (Elma Transsonic T420, Singen, Germany) were performed in four different conditions alternating light and dark, room and hot temperature (heating plate with magnetic stirring, VELP Scientifica, Milan, Italy).

On the other side, MAE was performed in a multimode microwave apparatus, using a closed-vessel system (MARSX press, CEM Corporation, Matthews, NC, USA), at 50 °C for 5 min (ramp time 1.30 min), with a power of 400 W.

3.3. High Performance Liquid Chromatography Analyses

High performance liquid chromatography-photodiode array (HPLC-UV/PAD) analyses were performed on a Jasco system (Cremella (LC), Italy) equipped with a Jasco AS-2055 plus autosampler, a PU-2089 plus pump and a MD-2010 plus multi-wavelength detector. Experimental data were acquired and processed by Jasco Borwin PDA and Borwin Chromatograph Software (ChromNAV 2.0 HPLC Software, Jasco-Europe, Cremella (LC), Italy).

Reverse phase chromatographic analyses were carried out at room temperature (r.t.) under gradient conditions, using a Symmetry RP-18 column (150 mm × 3.9 mm, macropore size 5 µm, mesopore size 300 Å, Waters).

The HPLC analysis conditions were initially set up to allow comparison among different HS extracts. The mobile phase was water containing 0.1% formic acid and the composition gradient was: from 10% to 75% of B in 16 min, 10% B until 3 min, followed by a re-equilibration step of 4 min; total run time of 23 min. The chromatographic run was monitored at wavelength of 245 nm.

For all analyses the flow rate was set at 1 mL/min. When necessary samples were dissolved in water (1 mg/mL) and filtered with a 0.45 µm GH Polypro (GHP) membrane before injection into the HPLC-system.

3.4. Free Radical Scavenging Activity

The free radical scavenging activity (FRS) of the extracts was determined by using a 2,2-diphenyl-1-picrylhydrazyl (DPPH). Briefly, dried HS extracts and a commercially available standardized green tea extract (Green Select®, Indena S.p.A., Milan, Italy) were dissolved in MeOH at a concentration of 2 mg/mL. 100 µL of each solution were, then, added to 3.9 mL of DPPH solution, freshly prepared

by dissolving DPPH in methanol/KH$_2$PO$_4$ and NaOH buffer (50/50 v/v) at a concentration of 6×10^{-5} M, giving test solutions with final concentrations of 50 µg/mL. After 30 min of incubation at room temperature, the absorbance was measured at 515 nm by the UV-Visible.

FRS was expressed as a percent compared with the control, consisting of 3.9 mL of DPPH solution and 100 µL of methanol. The percent inhibition of the DPPH radical by the test solution was calculated using the following formula:

$$FRS\% = [(Abs\ control - Abs\ sample)/Abs\ control] \times 100$$

The analyses were carried out in triplicate.

3.5. Preparation of Unloaded and HS-Loaded κ-CG/HPC/CaCl$_2$ Solutions

In the present work, two formulations, named as BLANK 1 and BLANK 2, containing κ-CG at 0.6 and 0.4% w/w respectively, HPC 1% w/w and CaCl$_2$ 0.04% w/w, were prepared as detailed below. Briefly, κ-CG was dissolved in distilled water at 80 °C; HPC and CaCl$_2$ were, then, sequentially added to each κ-CG solution and maintained under magnetic stirring at room temperature until complete dissolution of all the components occurred.

Both the formulations were loaded with dried HS extract at the concentration of 0.2% w/w and maintained under mild stirring for 3 h. Loaded formulations were, therefore, labelled as LOADED 1, when derived from BLANK 1, and as LOADED 2, when derived from BLANK 2.

Prior to each analysis, all polymeric solutions were maintained at rest for 24 h at 4 °C.

3.6. Preparation of Artificial Saliva

Artificial saliva was prepared dissolving KCl 1.5%, NaCl 0.43%, CaCl$_2$ 0.22%, NaHCO$_3$ 0.42% and NaH$_2$PO$_4 \cdot$H$_2$O w/v in distilled water [34].

3.7. Viscosity Measurements

Rheological analyses were carried out by means of a rotational rheometer (MCR 102, Anton Paar, Turin, Italy) equipped with a cone plate combination (CP50-1, diameter = 50 mm; angle = 1°) as measuring system. Viscosity measurements were performed at increasing shear rates in the range 1–300 s^{-1} at 25 °C on the sample as such. In particular, three aliquots were collected in different regions of each sample and subjected to rheological characterization. Each measure was performed in triplicate. Such measurements were carried out 1 h, 24 h and 1 week after sample preparation (storage temperature: 4 °C).

In order to investigate the rheological interaction between sample and saliva ions, each formulation was diluted 3:1 w/w in artificial saliva (S) or in distilled water (W) and subjected to viscosity measurement at 37 °C.

The normalized rheological synergism parameter (ΔSYN) was calculated at 50 s^{-1}, according to Equation (1):

$$ASYN = [(\eta_S - \eta_W)/\eta_W]_{LOADED}/[(\eta_S - \eta_W)/\eta_W]_{BLANK} \quad (1)$$

where: η_S = viscosity measured at 37 °C upon dilution 3:1 w/w in artificial saliva; η_W = viscosity measured at 37 °C upon dilution 3:1 w/w in deionized water.

Three replicates were considered for each sample.

3.8. Viscoelastic Measurements

Rheological analyses were performed by means of a rotational rheometer (MCR102, Anton Paar, Turin, Italy), using a C50-1 cone (Ø = 50 mm and ϑ = 1°) as measuring system.

Sample viscoelasticity was assessed by dynamic oscillatory measurements, such as stress sweep test and oscillation test. In the stress sweep test, increasing stresses were applied at a constant frequency

(0.1 Hz) and the elastic response of the sample, expressed as storage modulus G′, was measured. Such a test allows us to identify the "linear viscoelastic region". In the oscillation test, a shear stress, chosen in the linear viscoelastic region previously determined, was applied at increasing frequencies (0.1 to 10 Hz) and G′ (storage modulus) and G″ (loss modulus) profiles were recorded. Loss tangent value (tgδ) was calculated as G″/G′ at 1 Hz. Measurements were performed at 37 °C on solutions upon dilution 3:1 w/w in artificial saliva. Three replicates were considered for each sample.

3.9. Mucoadhesion Measurements

The mucoadhesive properties of blank and loaded formulations, after 3:1 w/w dilution in artificial saliva, were assessed at 37 °C by means of a TA.XT plus Texture Analyzer (Stable Micro Systems, Godalming, UK), equipped with 1 kg load cell and with a cylindrical movable probe (P/10C). A porcine gastric mucin dispersion (8% w/w) was prepared in artificial saliva as biological substrate.

Each sample (30 μL) was layered on a filter paper disc (Ø = 10 mm) and fixed on the movable probe. 30 μL of mucin dispersion were fixed, faced to the solution, on the sample holder. A preload of 2500 mN was applied for 300 s. The probe was then lowered to put in contact mucin dispersion and diluted sample. The probe was, then, raised at a constant speed (2.5 mm/s) up to the complete mucin-sample separation. Blank measurements were also carried out using 30 μL of artificial saliva instead of mucin dispersion. Six replicates were considered for each sample.

The maximum detachment force (Fmax, mN) was measured and the differential parameter ΔFmax was calculated according to the following Equation (2):

$$\Delta Fmax = (Fmax_{mucin} - Fmax_{blank})/Fmax_{blank} \qquad (2)$$

where: $Fmax_{mucin}$ was the maximum force measured in presence of mucin and $Fmax_{blank}$ the maximum force measured in absence of mucin (blank measurements).

3.10. In Vitro Studies on Fibroblast Cell Line

3.10.1. Cytotoxicity Test

The cytotoxicity of BLANK 1 and LOADED 1 formulations was assessed on NHDF. Briefly, cells (100,000 cells/cm²) were seeded in the basolateral chamber of Transwell® Permeable Supports (Corning Incorporated, Corning, NY, USA) for 24 h. The samples, diluted 1:1 and 1:3 v/v in complete culture medium (CM), were, then, placed in the apical chamber for other 24 h. CM was used as reference. An MTT assay was performed 24 h later.

Briefly, apical chambers were removed from each well and the medium in the basolateral chamber was discarded; the cells were rinsed with PBS. Subsequently, 150 μL of MTT 7.5 μM in 300 μL of DMEM without phenol red was added to each well and incubated for 3 h (37 °C and 5% CO_2). Finally, 300 μL of DMSO, used as solubilizing agent, was added to each well, in order to promote the complete dissolution of formazan crystals, obtained from MTT dye reduction by mitochondrial dehydrogenases of living cells. The solution absorbance was measured by means of an iMark® Microplate reader (Bio-Rad Laboratories Inc., Hercules, CA, USA) at 570 nm and 690 nm wavelengths after 60 s of mild shaking. Results were expressed as % cell viability by normalizing the absorbance measured after contact with each sample with that measured for CM. Three replicates were performed for each sample.

3.10.2. Proliferation Test

The capability of BLANK 1 and LOADED 1 formulations to promote NHDF proliferation was assessed. Briefly, cells (50,000 cells/cm²) were seeded in the basolateral chamber of Transwell® System (Corning Incorporated, Corning, NY, USA) and, simultaneously, the samples, diluted 1:1 v/v in medium without serum (M w/s), were placed in the apical chamber. An aqueous solution of HS extract at 0.2% w/w, diluted 1:1 v/v in M w/s, was also investigated. M w/s and CM were used as

references. An MTT assay was performed 24 h later as previously described. Three replicates were performed for each sample.

3.10.3. Assessment of Antioxidant Properties

The antioxidant properties of BLANK 1 and LOADED 1 formulations and HS solution were assessed on NHDF. The concentration of H_2O_2 necessary to induce a proper oxidative damage, without leading to a complete cell death, was identified as follows. Cells were seeded (50,000 cells/cm^2) overnight into a 96-well plate (Greiner Bio-One Italia S.r.l., Cassina de Pecchi, Italy) and, then, put in contact for 24 h with different H_2O_2 solutions, prepared in sterile distilled water with increasing concentrations (0 mM, 0.5 mM, 1 mM, 1.25 mM, 1.5 mM and 3 mM). Untreated (without samples) cells subjected to the oxidative stress were considered as the control (CTR). An MTT assay was performed 24 h later as previously described. Eight replicates were performed for each sample.

Thereafter, cells (50,000 cells/cm^2) were treated with the samples for 24 h and, then, with H_2O_2 at the concentration of 1.25 mM for another 24 h. An MTT assay was performed as previously described; three replicates were performed for each sample.

3.10.4. Assessment of Anti-Inflammatory Properties

The levels of IL-8 in the culture medium of NHDF (50,000 cells/cm^2), treated with LOADED 1 formulation and HS solution for 24 h and, then, with lipopolysaccharide (LPS) at the concentration of 10 µg/mL for another 24 h, were detected by means of Human IL-8/CXCL8 ELISA kit (Sigma Aldrich, St. Louis, MO, USA) according to the manufacturer's instructions.

Untreated (without samples) cells subjected to LPS-inflammation were considered as the negative control (LPS), while untreated cells not subjected to LPS-inflammation (CM) was used as reference. An MTT assay was also performed in order to evaluate if the inflammation could alter cell viability %; three replicates were performed for each sample.

3.11. Statistical Analysis

Whenever possible, experimental values of the various type of measures were subjected to statistical analysis, carried out by means of the statistical package Statgraphics 5.0 (Statistical Graphics Corporation, Rockville, MD, USA). In particular, one-way ANOVA—Multiple Range Test and Student's t-test were used.

4. Conclusions

In this study, an in situ gelling formulation loaded with *Hibiscus sabdariffa* extract intended for the treatment of oral mucositis and esophagitis was developed.

Different methodologies of extraction of HS calyces were compared to evaluate the best procedure in terms of extraction yield and antioxidant activity. In this phase, a proper HPLC method was set up to compare the chromatographic profile of different extracts. The Microwave Assisted Extraction (MAE) technique was chosen because it combines a shorter extraction time and a good extraction yield, obtaining an extract characterized by good antioxidant properties.

The investigation of the formulation gelling capability by means of the rheological analysis and of the mucoadhesion properties has driven the choice of the LOADED 1 formulation as optimal. The presence of HS produces a lowering of the formulation viscosity at room temperature (behavior functional to an easy administration) and enhances κ-CG interaction with saliva ions (behavior functional to a prolonged permanence of the formulation on the action site).

The in vitro biological tests proved that the formulation was biocompatible and did not disturb the anti-oxidant and anti-inflammatory properties of the extract releasing HS substances, which were free to carry out their biological activity.

References

1. Li, L.; Ni, R.; Shao, Y.; Mao, S. Carrageenan and its application in drug delivery. *Carbohydr. Polym.* **2014**, *103*, 1–11. [CrossRef] [PubMed]

2. Campo, V.L.; Kawano, D.F.; Silva, D.B., Jr.; Caevahlo, D.J. Carrageenans: Biological properties, chemical modifications and structural analysis—A review. *Carbohydr. Polym.* **2009**, *77*, 167–180. [CrossRef]

3. Jiao, G.; Yu, G.; Zhang, J.; Ewart, H.S. Chemical structure and bioactivities of sulfated polysaccharides from marine algae. *Mar. Drugs* **2011**, *9*, 196–223. [CrossRef] [PubMed]

4. Vigani, B.; Rossi, S.; Faccendini, A.; Sandri, G.; Bonferoni, M.C.; Gentile, M.; Ferrari, F. Development of a mucoadhesive and in situ gelling formulation based on k-carrageenan for the treatment of the oral mucositis. I. A functional in vitro characterization. *Mar. Drugs* **2018**, *17*, 112. [CrossRef] [PubMed]

5. Riaza, G.; Chopra, R. A review on phytochemistry and therapeutic uses of *Hibiscus sabdariffa* L. *Biomed. Pharmacother.* **2018**, *102*, 575–582. [CrossRef] [PubMed]

6. Mohamed, R.; Fernandez, J.; Pineda, M.; Augilar, M. Roselle (*Hibiscus sabdariffa*) seed oil is a rich source of gamma-tocopherol. *J. Food Sci.* **2007**, *72*, 207–210. [CrossRef] [PubMed]

7. Mahadevan, N.; Kamboj, P. *Hibiscus sabdariffa* Linn.—An overview. *Nat. Prod. Radiance* **2009**, *8*, 77–83.

8. Qi, Y.; Chin, K.L.; Malekian, F.; Berhane, M.; Gager, J. Biological characteristics, nutritional and medicinal value of roselle, *Hibiscus sabdariffa*. *Circ. Urban For. Nat. Resour. Environ.* **2005**, *604*, 1–2.

9. Faraji, M.H.; Tarkhani, A.H.H. The effect of sour tea (*Hibiscus sabdariffa*) on essential hypertension. *J. Ethnopharmacol.* **1999**, *65*, 231–236. [CrossRef]

10. Peng, C.H.; Yang, Y.S.; Chan, K.C.; Wang, C.J.; Chen, M.L.; Huang, C.N. *Hibiscus sabdariffa* polyphenols alleviate insulin resistance and renal epithelial to mesenchymal transition: A novel action mechanism mediated by type 4 dipeptidyl peptidase. *J. Agric. Food Chem.* **2014**, *62*, 9736–9743. [CrossRef] [PubMed]

11. Lin, H.H.; Chen, J.H.; Kuo, W.H.; Wang, C.J. Chemopreventive properties of *Hibiscus sabdariffa* L. on human gastric carcinoma cells through apoptosis induction and JNK/p38 MAPK signaling activation. *Chem. Biol. Interact.* **2007**, *165*, 59–75. [CrossRef] [PubMed]

12. Wu, C.H.; Huang, C.C.; Hung, C.H.; Yao, F.Y.; Wang, C.J.; Chang, Y.C. Delphinidin-rich extracts of *Hibiscus sabdariffa* L. trigger mitochondria-derived autophagy and necrosis through reactive oxygen species in human breast cancer cells. *J. Funct. Foods* **2016**, *25*, 279–290. [CrossRef]

13. Malacrida, A.; Maggioni, D.; Cassetti, A.; Nicolini, G.; Cavaletti, G.; Miloso, M. Antitumoral effect of *Hibiscus sabdariffa* on human squamous cell carcinoma and multiple myeloma cells. *Nutr. Cancer* **2016**, *68*, 1161–1170. [CrossRef] [PubMed]

14. Hassan, S.T.S.; Berchová, K.; Majerová, M.; Pokorná, M.; Švajdlenka, E. In vitro synergistic effect of *Hibiscus sabdariffa* aqueous extract in combination with standard antibiotics against Helicobacter pylori clinical isolates. *Pharm. Biol.* **2016**, *54*, 1736–1740. [CrossRef] [PubMed]

15. Chen, C.C.; Hsu, J.D.; Wang, S.F.; Chiang, H.C.; Yang, M.Y.; Kao, E.S.; Ho, Y.C.; Wang, C.J. *Hibiscus sabdariffa* extract inhibits the development of atherosclerosis in cholesterol-fed rabbits. *J. Agric. Food Chem.* **2003**, *51*, 5472–5477. [CrossRef] [PubMed]

16. Haroon, E.T.; Zou, X.; Shi, J.; Abdalbasit, A. Rapid Determination of Antioxidant Compounds and Antioxidant Activity of Sudanese Karkade (*Hibiscus sabdariffa* L.) Using Near Infrared Spectroscopy. *Food Anal. Methods* **2016**, *9*, 1228–1236. [CrossRef]

17. Duh, P.D.; Yen, G.C. Antioxidant activity of three herbal water extracts. *Food Chem.* **1997**, *60*, 639–645. [CrossRef]

18. Sogo, T.; Terahara, N.; Hisanaga, A.; Kumamoto, T.; Yamashiro, T.; Wu, S.; Sakao, K.; Hou, D.-X. Anti-inflammatory activity and molecular mechanism of delphinidin 3-sambubioside, a Hibiscus anthocyanin. *Res. Commun.* **2015**, *41*, 58–65. [CrossRef]

19. Kao, E.-S.; Hsu, J.-D.; Wang, C.-J.; Yang, S.-H.; Cheng, S.-Y.; Lee, H.-J. Polyphenols Extracted from *Hibiscus sabdariffa* L. Inhibited Lipopolysaccharide-Induced Inflammation by Improving Antioxidative Conditions and Regulating Cyclooxygenase-2 Expression. *Biosci. Biotechnol. Biochem.* **2009**, *73*, 385–390. [CrossRef] [PubMed]

20. Rossi, S.; Ferrari, F.; Sandri, G.; Bonferoni, M.C.; Del Fante, C.; Perotti, C.; Caramella, C. Wound Healing: Hemoderivatives and Biopolymers. Concise Encyclopedia of Biomedical Polymers and Polymeric Biomaterials. In *Encyclopedia of Biomedical Polymers and Polymeric Biomaterials*, 1st ed.; Mishra, M., Ed.; Taylor & Francis: New York, NY, USA, 2015; Volume 11, pp. 8280–8298.

21. Gaggeri, R.; Rossi, D.; Christodoulou, M.S.; Passarella, D.; Leoni, F.; Azzolina, O.; Collina, S. Chiral flavanones from Amygdalus lycioides spach: Structural elucidation and identification of TNFalpha inhibitors by bioactivity-guided fractionation. *Molecules* **2012**, *17*, 1665–1674. [CrossRef] [PubMed]

22. Martino, E.; Collina, S.; Rossi, D.; Bazzoni, D.; Gaggeri, R.; Bracco, F.; Azzolina, O. Influence of the extraction mode on the yield of hyperoside, vitexin and vitexin-2-O-rhamnoside from Crataegus monogyna Jacq. (Hawthorn). *Phytochem. Anal.* **2008**, *19*, 534–540. [CrossRef] [PubMed]

23. Amri, B.; Martino, E.; Vitulo, F.; Corana, F.; Ben-Kaâb, L.B.; Rui, M.; Rossi, D.; Mori, M.; Rossi, S.; Collina, S. *Marrubium vulgare* L. leave extract: Phytochemical composition, antioxidant and wound healing properties. *Molecules* **2017**, *22*, 1851. [CrossRef] [PubMed]

24. Martino, E.; Ramaiola, I.; Urbano, M.; Bracco, F.; Collina, S. Microwave-assisted extraction of coumarin and related compounds from *Melilotus officinalis* (L.) Pallas as an alternative to Soxhlet and ultrasound-assisted extraction. *J. Chromatogr. A* **2006**, *1125*, 147–151. [CrossRef] [PubMed]

25. Arpini, S.; Fuzzati, N.; Giori, M.A.; Martino, E.; Mombelli, G.; Pagni, L.; Ramaschi, G. HPLC-DAD-MS fingerprint of Andrographis paniculata (Burn. f.) Nees (Acanthaceae). *Nat. Prod. Commun.* **2008**, *3*, 1981–1985.

26. Almahy, H.A.; Abdel-Razik, H.H.; Yaser, A. El-Badry and Elhadi, M. Ibrahim. Ultrasonic extraction of anthocyanins as natural dyes from *Hibiscus sabdariffa* (karkade) and its application on dying foodstuff and beverages in kingdom of Saudi Arabia. *Am. J. Biol. Pharm. Res.* **2015**, *2*, 168–174.

27. Lagerlof, F.; Dawes, C. The Volume of Saliva in the Mouth Before and After Swallowing. *J. Dent. Res.* **1984**, *63*, 618–621. [CrossRef] [PubMed]

28. Gittings, S.; Turnbull, N.; Henry, B.; Roberts, C.J.; Gershkovich, P. Characterisation of human saliva as a platform for oral dissolution medium development. *Eur. J. Pharm. Biopharm.* **2015**, *91*, 16–24. [CrossRef] [PubMed]

29. Jones, D.S.; Laverty, T.P.; Morris, C.; Andrews, G.P. Statistical modelling of the rheological and mucoadhesive properties of aqueous poly(methylvinylether-co-maleic acid) networks: Redefining biomedical applications and the relationship between viscoelasticity and mucoadhesion. *Colloids Surf. B Biointerfaces* **2016**, *144*, 125–134. [CrossRef] [PubMed]

30. Karavana, S.Y.; Güneri, P.; Ertan, G. Benzydamine hydrochloride buccal bioadhesive gels designed for oral ulcers: Preparation, rheological, textural, mucoadhesive and release properties. *Pharm. Dev. Technol.* **2009**, *14*, 623–631. [CrossRef] [PubMed]

31. Tenci, M.; Rossi, S.; Aguzzi, C.; Carazo, E.; Sandri, G.; Bonferoni, M.C.; Grisoli, P.; Viseras, C.; Caramella, C.M.; Ferrari, F. Carvacrol/clay hybrids loaded into in situ gelling films. *Int. J. Pharm.* **2017**, *53*, 676–688. [CrossRef] [PubMed]

32. Rossi, S.; Ferrari, F.; Bonferoni, M.C.; Sandri, G.; Faccendini, A.; Puccio, A.; Caramella, C. Comparison of poloxamer-and chitosan-based thermally sensitive gels for the treatment of vaginal mucositis. *Drug Dev. Ind. Pharm.* **2014**, *40*, 352–360. [CrossRef] [PubMed]

33. Sandri, G.; Bonferoni, M.C.; Ferrari, F.; Rossi, S.; Del Fante, C.; Perotti, C.; Gallanti, A.; Caramella, C. An in situ gelling buccal spray containing platelet lysate for the treatment of oral mucositis. *Curr. Drug Discov. Technol.* **2011**, *8*, 277–285. [CrossRef] [PubMed]

34. Rossi, S.; Marciello, M.; Bonferoni, M.C.; Ferrari, F.; Sandri, G.; Dacarro, C.; Grisoli, P.; Caramella, C. Thermally sensitive gels based on chitosan derivatives for the treatment of oral mucositis. *Eur. J. Pharm. Biopharm.* **2010**, *74*, 248–254. [CrossRef] [PubMed]

35. Rossi, S.; Vigani, B.; Bonferoni, M.C.; Sandri, G.; Caramella, C.; Ferrari, F. Rheological analysis and mucoadhesion: A 30 year-old and still active combination. *J. Pharm. Biomed. Anal.* **2018**, *156*, 232–238. [CrossRef] [PubMed]

36. Sandri, G.; Rossi, S.; Bonferoni, M.C.; Ferrari, F.; Mori, M.; Caramella, C. The role of chitosan as a mucoadhesive agent in mucosal drug delivery. *J. Drug Deliv. Sci. Technol.* **2012**, *22*, 275–284. [CrossRef]

37. Rossi, S.; Ferrari, F.; Bonferoni, M.C.; Caramella, C. Characterization of chitosan hydrochloride–mucin rheological interaction: Influence of polymer concentration and polymer: Mucin weight ratio. *Eur. J. Pharm. Sci.* **2001**, *12*, 479–485. [CrossRef]

38. Rossi, S.; Vigani, B.; Puccio, A.; Bonferoni, M.C.; Sandri, G.; Ferrari, F. Chitosan ascorbate nanoparticles for the vaginal delivery of antibiotic drugs in atrophic vaginitis. *Mar. Drugs* **2017**, *15*, 319. [CrossRef] [PubMed]

39. Rossi, S.; Mori, M.; Vigani, B.; Bonferoni, M.C.; Sandri, G.; Riva, F.; Caramella, C.; Ferrari, F. A novel dressing for the combined delivery of platelet lysate and vancomycin hydrochloride to chronic skin ulcers: Hyaluronic acid particles in alginate matrices. *Eur. J. Pharm. Sci.* **2018**, *118*, 87–95. [CrossRef] [PubMed]

40. Mori, M.; Rossi, S.; Ferrari, F.; Bonferoni, M.C.; Sandri, G.; Chlapanidas, T.; Torre, M.L.; Caramella, C. Sponge-Like Dressings Based on the Association of Chitosan and Sericin for the Treatment of Chronic Skin Ulcers. I. Design of Experiments-Assisted Development. *J. Pharm. Sci.* **2016**, *105*, 1180–1187. [CrossRef] [PubMed]

41. Qi, F.; Sun, J.; Yan, J.; Li, C.; Lv, X. Anti-inflammatory effects of isorhamnetin on LPS-stimulated human. gingival fibroblasts by activating Nrf2 signaling pathway. *Microb. Pathog.* **2018**, *120*, 37–41. [CrossRef] [PubMed]

42. Chlapanidas, T.; Perteghella, S.; Leoni, F.; Faragò, S.; Marazzi, M.; Rossi, D.; Martino, E.; Gaggeri, R.; Collina, S. TNF-α blocker effect of naringenin-loaded sericin microparticles that are potentially useful in the the treatment of psoriasis. *Int. J. Mol. Sci.* **2014**, *15*, 13624–13636. [CrossRef] [PubMed]

43. Lucconi, G.; Chlapanidas, T.; Martino, E.; Gaggeri, R.; Perteghella, S.; Rossi, D.; Faragò, S.; Vigo, D.; Faustini, M.; Collina, S.; et al. Formulation of microspheres containing Crataegus monogyna Jacq. extract with free radical scavenging activity. *Pharm. Dev. Technol.* **2014**, *19*, 65–72. [CrossRef] [PubMed]

44. Mori, M.; Rossi, S.; Ferrari, F.; Bonferoni, M.C.; Sandri, G.; Riva, F.; Tenci, M.; Del Fante, C.; Nicoletti, G.; Caramella, C.M. Sponge-like dressings based on the association of chitosan and sericin for the treatment of chronic skin ulcers. II. Loading of the hemoderivative platelet lysate. *J. Pharm. Sci.* **2016**, *105*, 1180–1187. [CrossRef] [PubMed]

45. ISO 10993-6:1994. *Biological Evaluation of Medical Devices—Part 5: Tests for In Vitro Cyto-Toxicity*; International Organization for Standardization: Geneva, Switzerland, 1994.

46. Beltràn-Debón, R.; Alonso-Villaverde, C.; Aragonès, G.; Rodríguez-Medina, I.; Rull, A.; Micol, V.; Segura-Carretero, A.; Fernández-Gutiérrez, A.; Camps, J.; Joven, J. The aqueous extract of *Hibiscus sabdariffa* calices modulates the production of monocyte chemoattractant protein-1 in humans. *Phytomedicine* **2010**, *17*, 186–191. [CrossRef] [PubMed]

Paper 8

Article

Anti-Multiple Myeloma Potential of Secondary Metabolites from *Hibiscus sabdariffa*

Alessio Malacrida [1,2,†], Valeria Cavalloro [3,†], Emanuela Martino [3,*], Arianna Cassetti [4], Gabriella Nicolini [1,2], Roberta Rigolio [1,2], Guido Cavaletti [1,2], Barbara Mannucci [5], Francesca Vasile [6], Marcello Di Giacomo [7], Simona Collina [7,*] and Mariarosaria Miloso [1,2,*]

[1] School of Medicine and Surgery, University of Milan-Bicocca, 20900 Monza, Italy
[2] Experimental Neurology Unit, University of Milano-Bicocca, 20900 Monza, Italy
[3] Department of Earth and Environmental Sciences, University of Pavia, 27100 Pavia, Italy
[4] CREA, Research Centre for Vegetable and Ornamental Crops, 18038 Sanremo, Italy
[5] Center of Large Equipment, University of Pavia, 27100 Pavia, Italy
[6] Department of Chemistry, University of Milan, 20133 Milano, Italy
[7] Department of Drug Sciences, University of Pavia, 27100 Pavia, Italy
* Correspondence: emanuela.martino@unipv.it (E.M.); simona.collina@unipv.it (S.C.); mariarosaria.miloso@unimib.it (M.M.); Tel.: +39-0382-986810 (E.M.); +39-0382-987379 (S.C.); +39-0264-488123 (M.M.)
† Authors contributed equally to this work.

Abstract: Multiple myeloma (MM) belongs to hematological cancers and its incidence is increasing worldwide. Despite recent advances in its therapy, MM still causes many deaths every year. In fact, current therapies sometimes fail and are associated with severe adverse effects, including neurotoxicity. As a part of our ongoing efforts to discover new potential therapies against MM, we prepared *Hibiscus sabdariffa* extracts obtained by a microwave-assisted solvent extraction and investigate their activity by in vitro assays on the RPMI-8226 cell line. The bioguided fractionation of the crude ethanolic extract allowed the identification of HsFC as the most effective extract. We assessed cell viability (MTT and Tripan blue test), cell migration (Boyden chamber assay), and neurotoxicity (DRG neurotoxicity assay). The promising results prompted us to further fractionate HsFC and we obtained two molecules effective against RPMI-8226 cells without neurotoxic effects at their active concentrations. Moreover, both compounds are able to significantly reduce cell migration.

Keywords: Multiple myeloma; *Hibiscus sabdariffa*; nature-aided drug discovery; bioguided assay fractionation; Hib-ester; Hib-carbaldehyde

---

1. Introduction

Multiple myeloma (MM) is a plasma cell neoplastic disorder causing severe bone pain and bone fractures, hypercalcemia, anemia, and kidney damage. This disease is characterized by clonal proliferation of malignant plasma cells in bone marrow and by overproduction of monoclonal protein (M protein) [1]. MM represents 1% of all cancer diseases and 10% of hematological cancers and its incidence is highly variable among age, sex, and countries [2]. MM is prevalent among the elderly and the male sex and the most affected countries are the industrialized regions of Australia, Europe, and North America. MM is still considered an incurable disease causing 110,000 deaths every year worldwide. To date, different therapeutic options are available and over the last decade, the five-year relative survival of patients raised approximately to 56% [3]. Nevertheless, the high heterogeneity of MM leads to numerous cases of refractory/relapsing MM. Moreover, since bone marrow is the

ideal support for homing and progression of MM cells [4], 70% of patients presents bones metastasis at diagnosis and the percentage further increases to 90% during the development of the disease. These patients suffer from osteolytic lesions caused by osteoblast differentiation suppression and inhibition of bone matrix deposition [5]. Therefore, MM still represents an unmet medical need.

During the last five years, new targets in MM have been proposed as therapeutic options (Figure 1), thus broadening the MM therapeutic landscape. Several drugs are now available and new molecules have recently been approved (Table 1) other therapies, including a peptide-based vaccination, are under validation [6]. Briefly, the main MM therapies consist of:

- DNA damaging agents. Alkylating agents such as melphalan and other DNA damaging agents such as doxorubicin as well as pan-HDAC inhibitors such as panobinostat are still important MM drugs [7].
- Proteasome inhibitors [8]. The proteasome is a multicatalytic target responsible for the degradation of 80–90% of proteins during cell life. Until now, three proteasome inhibitors have been approved for clinical use: Bortezomib, Carfilzomib, and Ixazomib. Particularly, Bortezomib was the first FDA-approved proteasome inhibitor and represents one of the most important discoveries for fighting MM of recent years. Of note, these agents can stimulate bone formation in MM patients [9]. Proteasome modulation can be also achieved by employing small molecules such as lenalidomide, structurally related to thalidomide and acting as E3-Ligasi inhibitors [10].
- Immunomodulators [11]. MM was among the first tumors wherein the therapeutic efficacy of blockade of inhibitory immune receptors, particularly the PD-1 axis, was demonstrated in preclinical models.
- Monoclonal antibodies [12]. There are only two FDA-approved monoclonal antibodies for the treatment of MM: daratumumab, targeting the CD38 pathway, and elotuzumab, targeting the SLAMF7 pathway. Despite the efficacy of this strategy in long term cancer remission, monoclonal antibodies still remain very expensive, thus limiting their diffusion.

It has to be pointed out that treatments currently available are often unsuccessful, lead to drug resistance [13], and cause adverse effects [14]. One of the major side effects related to MM therapies is a dose-limiting neurotoxicity, often linked to chemotherapy-induced peripheral neuropathy, which generally presents several sensory symptoms, including hypersensitivity, dysesthesia, and paresthesia [15,16]. At least 60% of patients treated with Bortezomib shows this severe side effect, leading to dose reduction or complete suspension of the therapy.

Therefore, despite the efforts of the scientific community, MM therapy is still considered an unmet medical need and new effective therapies are needed.
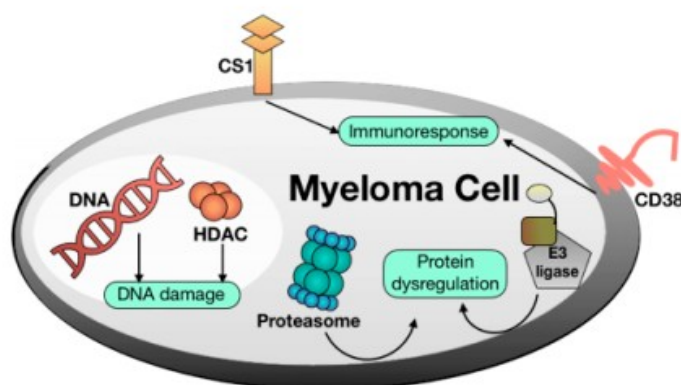

Figure 1. Molecular targets of multiple myeloma drugs.

Table 1. Drugs approved for multiple myeloma and their molecular targets.

Drug	Trade Name	Target
Melphalan	Alkeran®	DNA
Bendamustine	Levact®, Ribomustin®, Treanda®	DNA
Doxorubicin	Adriamycin®	DNA
Carmustine	BiCNU®	DNA
Cyclophosphamide	Cytoxan®, Neosar®	DNA
Panobinostat	Faridak®	HDAC
Elotuzumab	Empliciti®	CS1
Daratumumab	Darzalex®	CD38
Bortezomib	Velcade®	Proteasome
Ixazomib	Ninlaro®	Proteasome
Carfilzomib	Kyprolis®	Proteasome
Thalidomide	Thalidomide Celgene®	E3 ligase
Lenalidomide	Revlimid®	E3 ligase
Pomalidomide	Imnovid®	E3 ligase

Our research group has been studying MM from a pharmacological point of view for several years [17–19] and only recently we have focused on the identification of new therapeutic opportunities. Following a nature-aided drug discovery approach, we demonstrated the beneficial effects of *Hibiscus sabdariffa* Linn against MM [20]. *H. sabdariffa* is an annual herbaceous subshrub belonging to the Malvaceae family that is also known as Roselle, Red Sorrel or Karkadè. This plant is commonly distributed in tropical and subtropical regions and it is originally native to India and Saudi Arabia. It is cultivated in different regions such as Sudan, Egypt, Nigeria, Mexico, Saudi Arabia, Taiwan, West Indies, Central America, and European countries [21–23]. *H. sabdariffa* calyces are commonly used for the preparation of tea and infusions. The red drink is widely consumed directly or it is an ingredient in the preparation of some foods, such as juice, jam, pudding, gelatin, and desserts [24]. Moreover, it is well known in traditional medicine for its diuretic and mild laxative effects. Along the years, the phytochemical composition *H. sabdariffa* calyces as well as their pharmacological properties have been extensively studied. Different *H. sabdariffa* extracts have been prepared and the main constituents are phenols, polyphenols, anthocyanins, and organic acids, such as citric, tartaric, malic, ascorbic acids, and others [24,25]. Several studies demonstrated that *H. sabdariffa* calyces possess high antioxidant and anti-inflammatory properties and are able to counteract hypertension [26], diabetic status [27], microbial infections [28], as well as to slow down the development of atherosclerosis [29].

H. sabdariffa is known to possess antiproliferative properties and to be a possible source of new bioactive compounds for cancer treatment; it shows an antiproliferative effect against MCF-7 and MDA-MB-231 breast carcinoma cells, CaoV-3 ovarian cancer cells, Hela cervical cancer cells, and K-562 leukemia cells [30–33]. Moreover, anthocyanins extracted from *H. sabdariffa* are able to induce apoptosis of promyelocytic leukemia HL-60 cells via the p38 MAP kinase pathway [34].

To continue the study on the anticancer potential of *H. sabdariffa* calyces, specially focusing on MM, in this work we focused on the preparation and bioassay-guided fractionation of its ethanolic extract. Herein we report the isolation, structure elucidation, and evaluation of the potential of Hibiscus acid dimethyl ester and of a new aldehydic compound against multiple myeloma. In detail, their cytotoxicity and effect on cell migration and invasion of RPMI-8226 MM cells as well as their neurotoxicity on embryo rats dorsal root were evaluated.

2. Results and discussion

The dried and powdered *H. sabdariffa* calyces were extracted following a microwave-assisted solvent extraction (MASE) procedure exploiting 80% ethanol as the extracting solvent [35–38]. The obtained ethanolic extract (HsEE) was then fractionated via a liquid/liquid extraction, suspending

Appendice

the extract in water and sequentially extracting with hexane (A), dichloromethane (B), ethyl acetate (C), and butanol (D), yielding four organic fractions (HsFA–D) and an aqueous one.

To obtain the analytical fingerprint, useful both as a control of the extracts' quality and as a starting point for future purification studies, we set up a proper RP-HPLC-UV/PAD-ESI/MS method [39]. Specifically, different elution conditions (methanol, acetonitrile, water, with or without formic acid) adopting several gradient modes were tested on two different columns (Symmetry C18 and Chromolith Performance RP-18 endcapped). The best results in terms of peak resolution, peak shape, and time of analysis were achieved using a Symmetry C18 (5 μm, 3.9 × 150 mm) column in gradient elution conditions, using water and ACN added with formic acid. The HsEE HPLC-UV chromatograms (λ = 325 nm) together with the reconstructed ion chromatograms (RIC) in negative ion mode are shown in Figure 2.
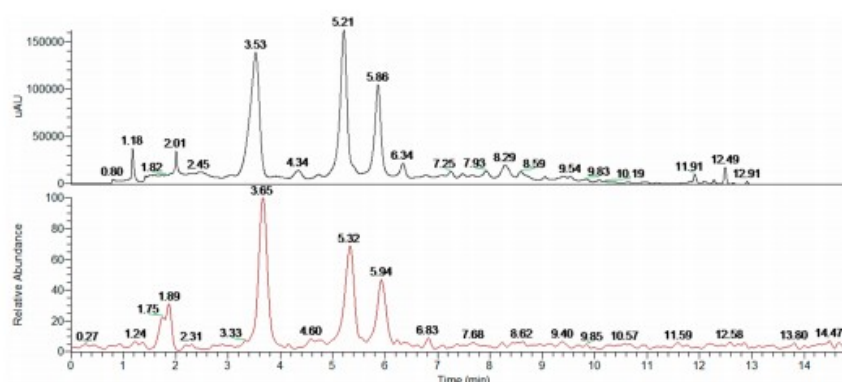
Figure 2. HPLC-UV/PAD-ESI/MS profile recorded at λ = 325 nm (black line) and reconstructed ion chromatograms (red line) of *H. sabdariffa* ethanolic extract (HsEE).

With the HPLC-UV-ESI/MS analytical methodology in hands, the profiles of fractions A–D were drawn: HsFA and HsFB contain only compounds with low polarity (retention time >12 min), HsFC presents acidic components (hibiscus acid, 5-caffeoylquinic acid and isomers, caffeic acid), while HsFD shows only few peaks at low intensity. The chromatographic profiles of HsFA–D and the MS associated with the peaks (total ion content) are reported in the Supplementary Material (Figure S1, Table S1).

In the meantime, the effect of HsEE and HsFA-D on cell viability of RPMI 8226 cells was assessed by MTT vital count assay. Cells were treated with different concentrations of HsEE (1–50 mg/mL) or HsFA-D (1–10 mg/mL) for 24, 48, and 72 h. Untreated cells were used as control.

HsEE and HsFC are able to impair cell viability of RPMI 8226 cells in a dose- and time-dependent manner with IC_{50} at 24 h of 21.3 mg/mL and 3.5 mg/mL for HsEE and HsFC, respectively (Figure 3). The other fractions were not active and therefore were discarded (data not shown).

The in vitro neurotoxicity of the crude extract, HsEE, and of the most effective fraction, HsFC, was then assessed by the well consolidated embryo rats dorsal root ganglia (DRG) neurotoxicity model [40]. Briefly, DRG explants from E15 Sprague Dawley rat embryos are able to sprout neurites when cultured with prodifferentiation agents, and the neurite outgrowth is blocked or slowed by neurotoxic agents. DRG were treated with different concentrations of HsEE (1–50 mg/mL) or HsFC (1–10 mg/mL) for 24 and 48 h and then the neurite outgrowth was measured. Results showed that HsEE and HsFC are non-neurotoxic at doses lower than 7.5 mg/mL and 3 mg/mL, respectively, after both 24 h and 48 h of treatment (Figure 4). At these time points, neurotoxicity was evident for both extracts at higher concentrations. HsEE is highly neurotoxic at its active concentrations (IC_{50} = 21.3 mg/mL), while HsFC can be considered safe at concentrations near its IC_{50} (IC_{50} = 3.5 mg/mL).
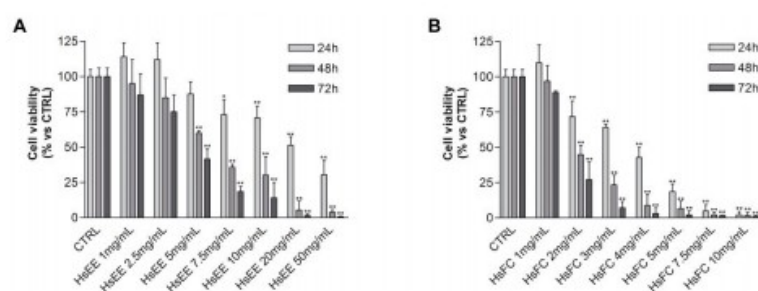
Figure 3. RPMI 8226 cell viability after HsEE or HsFC treatment. (**A**) MTT assay of RPMI 8226 cells treated with different concentrations (1–50 mg/mL) of HsEE for 24, 48, and 72 h. (**B**) MTT assay of RPMI 8226 cells treated with different concentrations (1–10 mg/mL) of HsFC for 24, 48, and 72 h. Untreated cells (CTRL) are control. Graphs represent the mean percentage ± SD of viable cells of three independent experiments (* $p < 0.05$, ** $p < 0.01$ vs. CTRL).
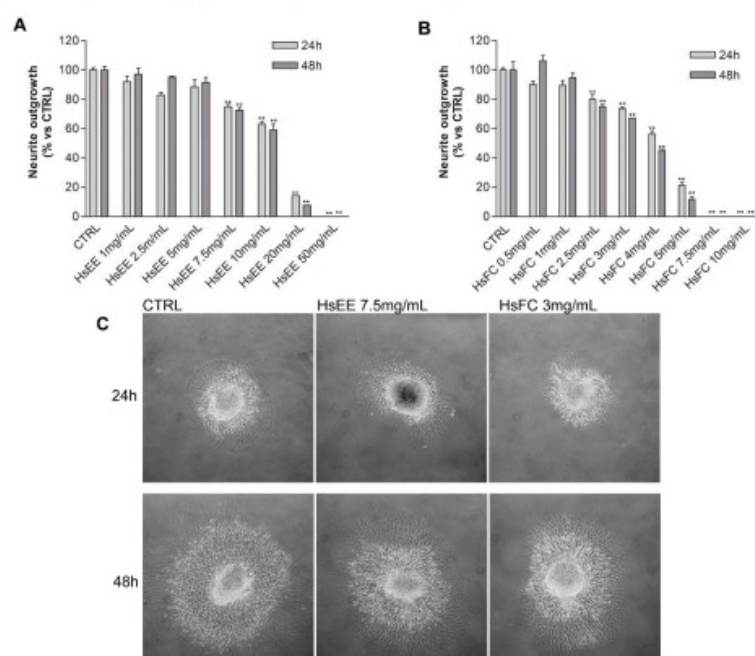

Figure 4. In vitro DRG neurotoxicity of HsEE and HsFC. (**A**) Neurite outgrowth from DRG treated with HsEE for 24 and 48 h. (**B**) Neurite outgrowth from DRG treated with HsFC for 24 and 48 h. Graphs represent mean neurite length ± SD of three independent experiments. (** $p < 0.01$ vs. CTRL). (**C**) Representative images of DRG treated with HsEE or HsFC for 24 and 48 h. Untreated DRG represent the controls.

We decided to further investigate HsFC at the effective and non-neurotoxic concentration of 3 mg/mL, evaluating the cell viability/cell death (RPMI 8226 cells) by Trypan blue vital count assay and the cell migration and invasion properties by Boyden chamber assay.

Results of Trypan blue assay after treatment of RPMI 8226 cells with HsFC (3 mg/mL for 24, 48 and 72 h) highlighted that this fraction reduced cell viability and increased the number of dead cells from 8% (of untreated cells) to 20% (at 24 h), 43% (at 48 h), and 61% (at 72 h) (Figure 5). Moreover, the replacing of the culture medium after 24 h of treatment with fresh medium without HsFC generated

a growing curve comparable to that obtained with continuous treatment; therefore, the HsFC effect is not reversible. (Figure 6). Regarding the cell migration and invasion, assessed by Boyden chamber assay, the treatment with HsFC significantly inhibited the ability of untreated RPMI 8226 cells in the presence of FBS as chemoattractant to pass through the gelatin-coated membrane. The HsFC effect was similar to that observed when untreated RPMI 8226 cells are in the absence of the chemoattractant FBS (Figure 7). Seventy percent of patients presents bone metastasis at diagnosis of MM and the percentage further increases during the development of the disease and can reach 90% of patients. For these reasons, it is important to identify drugs that are not only toxic to MM but that are also effective against MM bone metastasis formation.
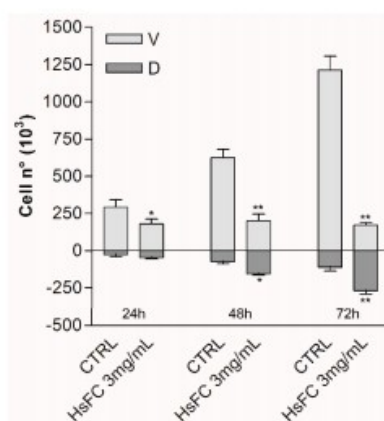
Figure 5. Trypan blue vital count assay of RPMI 8226 cells treated with HsFC 3 mg/mL. Untreated cells (CTRL) are control. Graphs represent the mean ± SD number of counted viable (V) and dead (D) cells of three independent experiments. (** $p < 0.01$ vs. CTRL).
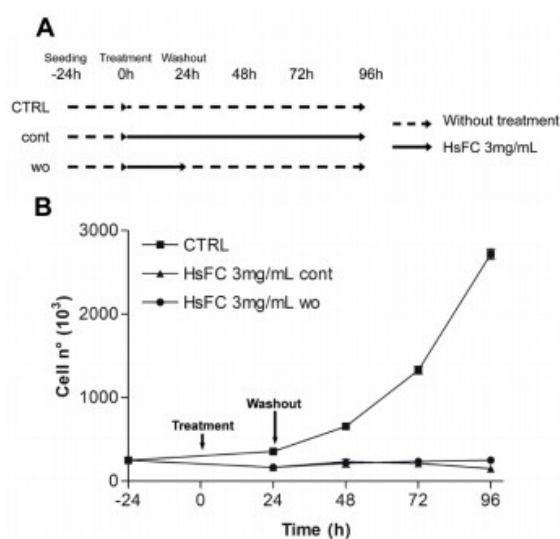
Figure 6. Effect of RPMI 8226 cells treated with HsFC 3 mg/mL in continuous (cont) or in washout (wo) culture medium. (**A**) Time schedule of HsFC treatment. Black arrows represent the presence of HsFC in culture medium of cont or wo treatment. Dashed lines represent culture medium without treatment. (**B**) Graphs represent the mean ± SD number of viable cells counted in three independent experiments.
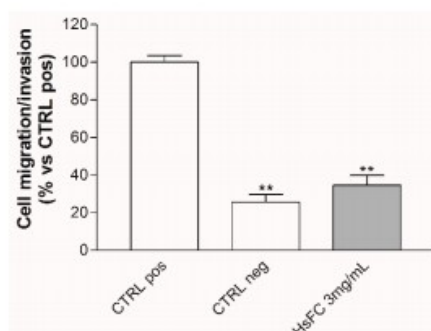
Figure 7. RPMI 8226 cell migration/invasion after HsFC treatment. The migration/invasion ability of RPMI 8226 cells was assessed by Boyden chamber assay. Cells were treated with HsFC 3 mg/mL. Untreated cells with or without FBS as chemoattractant represent positive controls (CTRL pos) and negative controls (CTRL neg), respectively. Data represent the percentage of migrating cells with respect to CTRL pos, arbitrarily set to 100%, and are expressed as mean ± SD of three independent experiments. (** $p < 0.01$ vs. CTRL pos).

To identify the main metabolites responsible for the cytotoxic properties, HsFC was then further fractionated. A first purification with polymer-supported carbonate (PS-carbonate) of HsFC was performed. Briefly, the fraction dissolved in methanol was treated with PS-carbonate, the solvent removed, and the resin washed with fresh methanol and dichloromethane. The washing solvent was collected and evaporated under reduced pressure, obtaining the wash fraction (WF). The PS-carbonate was then treated with 0.1% HCl in methanol, thus obtaining a simplified fraction. The subsequent purification by flash chromatography allowed the isolation of six fractions which underwent a preliminary cytotoxicity screening (MTT test). Only one fraction was active against MM in the initial screening. The HPLC-MS analysis showed that the white solid obtained corresponded to a pure compound with *m/z* 218.

The ^{1}H-NMR spectrum recorded in DMSO is consistent with that reported in literature for hibiscus acid dimethylester [41]. To confirm the γ-lactonic structure of this compound, bidimensional NMR (^{1}H-^{13}C HSQC *J* = 8 Hz, HSQC *J* = 2 Hz and ^{1}H-^{13}C HMBC) in CDCl$_3$ was recorded (Figure S8). Basing on this data and on the positive value of its specific optical rotatory power recorded in chloroform and acetonitrile ($[\alpha]^D_{20}$ = + 57.0 and + 84,1, respectively), the compound has been identified as (2S,3R)-hibiscus acid dimethylester (Figure 8A), by now on called *Hib-ester* [41].
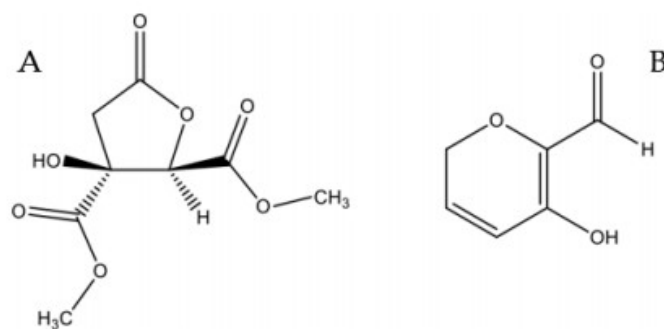

Figure 8. Chemical structure of *Hib-ester* (**A**) and *Hib-carbaldehyde* (**B**).

It has to be noted that, according to the purification procedure, PS-carbonate caught acid compounds present in HsFC, including the hibiscus acid.

Further fractionation of WF by flash chromatography yielded four main fractions, which underwent MTT cytotoxicity screening. A yellow oil, corresponding to new pure compound showing an interesting MTT value, was isolated. This compound was identified by NMR techniques (^{1}H-NMR, ^{1}H-^{13}C HSQC J = 8 Hz, HSQC J = 2 Hz and 1H-13C HMBC) and MS analysis (*m/z* 126) as 5-hydroxy-2*H*-pyran-6-carbaldehyde, hereafter called *Hib-carbaldehyde* (Figure 8B). This compound has not been isolated from natural sources before.

The effect of *Hib-ester* and *Hib-carbaldehyde* on cell viability of RPMI 8226 cells was evaluated by MTT and trypan blue vital count assay. Cells were treated with increasing concentrations of the compounds (3 µg/mL–3 mg/mL) for 24, 48, and 72 h and untreated cells were used as control.

Both compounds significantly reduced cell viability of RPMI 8226 cells (MTT test) in a dose- and time-dependent manner (Figure 9A,B). After 24 h of treatment, *Hib-ester* and *Hib-carbaldehyde* are about ten and 20 times more active than HsFC, showing IC_{50} values of 0.45 and 0.21 mg/mL, respectively. Results of the trypan blue vital count assay highlighted a similar trend (Figure 9C,D).

The evaluation of the in vitro neurotoxicity of *Hib-ester* and *Hib-carbaldehyde* using our DRG model showed that both compounds are non-neurotoxic at doses near the IC_{50} values, after both 24 h and 48 h of treatment. *Hib-carbaldehyde* at 0.3 mg/mL and 1 mg/mL reduced the length of neurites, but at a non-neurotoxic percentage (about 20%) (Figure S8).
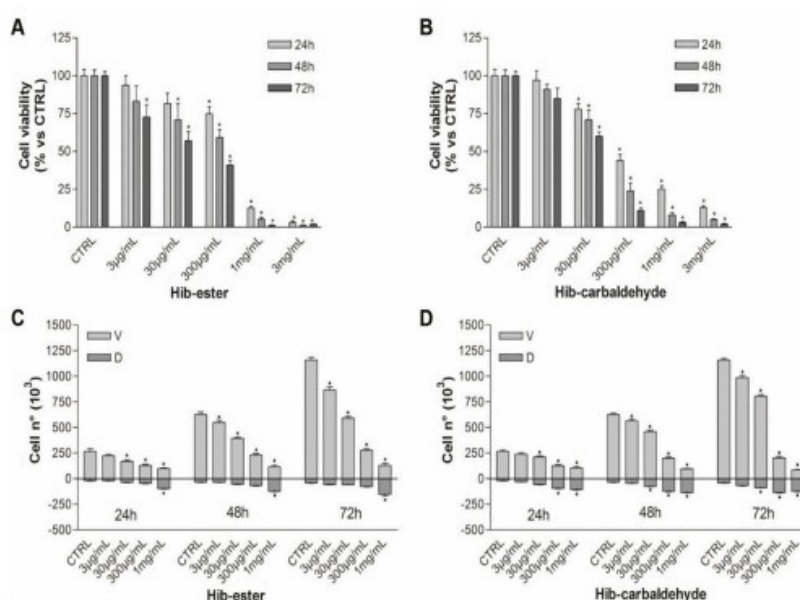

Figure 9. Cell viability and neurotoxicity after treatment with *Hib-ester* and *Hib-carbaldehyde*. (**A**) MTT assay of RPMI 8226 cells treated with *Hib-ester* (3 µg/mL–3 mg/mL) for 24, 48, and 72 h. (**B**) MTT assay of RPMI 8226 cells treated with *Hib-carbaldehyde* (3 µg/mL–3 mg/mL) for 24, 48, and 72 h. (**C**) Trypan blue vital count assay of RPMI 8226 cells treated with *Hib-ester* (3 µg/mL–1 mg/mL) for 24, 48, and 72 h. **D**) Trypan blue vital count assay of RPMI 8226 cells treated with different concentrations of *Hib-carbaldehyde* (3 µg/mL–1 mg/mL) for 24, 48, and 72 h.

Regarding the ability to impair cell migration and invasion, both compounds are effective at their respective IC_{50} values. Particularly, *Hib-ester* inhibits cell migration and invasion by more than 50% at 30 µg/mL (Figure 10A,B).
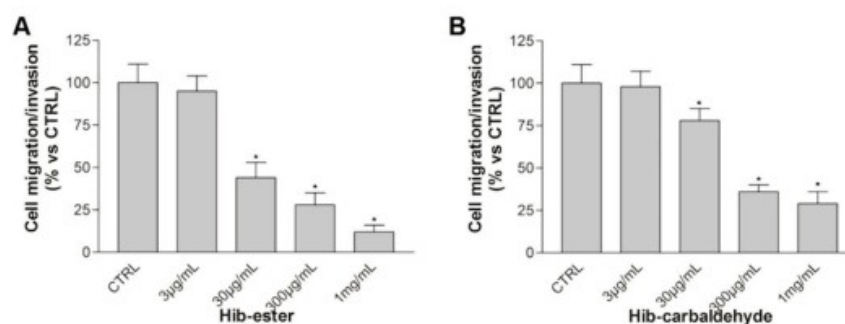
Figure 10. RPMI 8226 cells' migration/invasion after *Hib-ester* and *Hib-carbaldehyde* treatment. Migration/invasion ability of RPMI 8226 cells was assessed by Boyden chamber assay. (**A**) Cells were treated with *Hib-ester* (3 µg/mL–1 mg/mL). (**B**) Cells were treated with *Hib-carbaldehyde* (3 µg/mL–1 mg/mL). Data represent the percentage of migrating cells with respect to CTRL, arbitrarily set to 100%, and are expressed as mean ± SD of three independent experiments. (** $p < 0.01$ vs. CTRL pos).

3. Conclusions

In this paper, we prepared a hydroalcoholic *H. sabdariffa* extract by adopting a MASE-based methodology, an efficient method to extract secondary metabolites from raw matrices with high yields and in short time. Microwave oven parameters (temperature, power, and time) were chosen according to literature data concerning the stability of the main metabolites of *H. sabdariffa* [42]. The bioguided fractionation of the crude ethanolic extract (HsEE) (sequential liquid/liquid extraction using organic solvents with growing polarities, followed by chromatographic fractionation) allowed the identification of two active compounds, named *Hib-ester* and *Hib-carbaldehyde* (Figure 8).

Both compounds are effective against the tested MM cell line at non-neurotoxic µg/mL concentrations. Moreover, they are able to reduce cell migration and invasion, events involved in the process of metastasis. Compounds identified in this study may be the starting point for the antineoplastic medicinal chemistry field. We expect that our results can offer useful information for the identification of next-generation drugs against multiple myeloma.

4. Materials and Methods

4.1. Chemicals and Standards

Solvents for both HPLC (HPLC grade) and extraction procedures (analytical grade) were supplied by Carlo Erba (Milan, Italy). Chlorogenic acid was purchased from Indena S.p.A. (Milan, Italy).

Analytical thin-layer chromatography (TLC) was carried out on silica gel precoated glass-backed plates (Fluka Kieselgel 60 F254, Merck, Darmstadt, Germany) and visualized by UV light or ceric ammonium molibdate (IV) stain (Hanessian's Stain).

Flash chromatography was performed with silica gel 60 (particle size 230–400 mesh) purchased from Nova Chimica (Cinisello Balsamo, Italy).

Deuterated solvent for NMR spectroscopy, RPMI-1640 Medium, Phosphate Buffered Saline (PBS), 3-(4,5-dimethylthiazol-2-yl)-2,5-diphenyltetrazolium bromide (MTT), dimethylsulfoxide (DMSO) were purchased from Sigma Aldrich (Milan, Italy).

Fetal bovine serum (FBS; GibcoR) was purchased from ThermoFisher Scientific (Lisbon, Portugal).

4.2. Instruments

H. sabdariffa calyces were powdered using a blade mill (A10 IKA-Werke GmbH & Co., Staufen, Germany) and then extracted exploiting a Multimode Microwave apparatus (MARSX press, CEM Corporation, Matthews, NC, USA).

All solvents were evaporated under reduced pressure using a Heidolph Laborota 4000 instrument (Heidolph Instruments GmbH & Co., Schwabach, Germany).

^{1}H-NMR, ^{13}C-NMR, and bidimensional experiments were performed at 400.0 MHz and 100.6 MHz, respectively, on the Bruker Avance 400 MHz FT NMR spectrometer (Bruker, Leipzig, Germany) with a multinuclear BBO probe. CDCl$_3$ was used as solvent. 1H chemical shift values were reported on the δ scale in ppm, relative to TMS (δ = 0.0 ppm) and in ^{13}C-NMR, chemical shift values were reported posing CDCl3 (δ = 77.36 ppm) as reference.

High performance liquid chromatography-electrospray-tandem mass spectrometry (RP-HPLC-UV/PAD-ESI/MS) analyses were carried out on Finnigan LCQ fleet ion trap system, controlled by Xcalibur software 1.4 (ThermoFinnigan, San Jose, CA, USA).

4.3. Plant Material and Extraction Procedure

H. sabdariffa plants obtained from seeds were cultivated in pots under greenhouse conditions (mean temperature 25.9 °C) at CREA institute (43°49′05″N, 7°45′30″E, Sanremo, IM, Italy).

H. sabdariffa calyces from five-month-old plants were harvested at the end of September, separated from the seedpod, and after a rapid wash with tap water, dried in a ventilated oven at 45 °C for three days. Voucher samples of dry calyces (ca. 100 g) are conserved under room conditions at the Plant Propagation Laboratory of the CREA, Sanremo, Italy. Seeds of this HS line are also kept for regular use.

The obtained matrix was stored in dark conditions and, at the time of use, it was cut to small size and grounded with a blade mill. Then, 10 g of the obtained homogeneous fine powder were dispersed in 200 mL of ethanol 80% and subjected to microwave heating (2 min ramping, 5 min hold time, maximum pressure 120 psi, maximum potency 200 W, temperature 50 °C, one cycle). The mixture was left to cool at room temperature filtrated and concentrated under reduced pressure to obtain HsEE as a red thick oil.

4.4. Extract Fractionation and Analysis

The crude extract HEE was resolubilized in water and sequentially extracted three times. with hexane (A), dichloromethane (B), ethyl acetate (C), and butanol (D) as organic solvents. The combined organic phases were dried with anhydrous NaSO$_4$ and the solvent removed under reduced pressure, yielding four organic fractions (HsFA–D) and an aqueous fraction. All dry extracts obtained were stored at 4 °C until analysis. Each extraction experiment was carried out in triplicate. HsEE and HsFA–D were analyzed using high-performance liquid chromatography-electrospray-tandem mass spectrometry. Each sample was dissolved in water (4 mg/mL) and filtered with a 0.45 μm GH Polypro (GHP) membrane before injection into the HPLC system. The sample was analyzed on a Symmetry C18 (5 μm, 3.9 × 150 mm) column. The mobile phase is composed by Water (A) and ACN (B), both containing 0.1% (*v/v*) formic acid and the composition gradient was: an initial isocratic elution of 10% B for 2min, from 10 to 25% B in 8 min, from 25 to 90% B in 5 min, 10% B until 3 min, followed by a re-equilibration step of 4 min. The flow rate was 1 mL/min and the elution was performed at room temperature. The UV detection was fixed at 325 nm. Mass spectra were generated in negative ion mode under constant instrumental conditions (ion spray voltage 5 kV, capillary voltage −12 V, capillary temperature 220 °C, and tube lens voltage −60 V). MS/MS data were acquired in Dependent scan mode (Full-scan MS followed by MS/MS of the most intense ion).

HsFC (2.5 g) was dissolved in 50 mL of methanol and then subjected to a treatment with PS-carbonate (5 g). The mixture was shaken at room temperature for 40 min, then filtered and washed with methanol (30 mL) and dichloromethane (150 mL). The combined filtrates were evaporated

Appendice

Molecules **2019**, *24*, 2500

11 of 15

under reduced pressure. The resin was then recovered and 50 mL of MeOH + 0.1% HCl was added. The system was shaken for 1 h at room temperature, and the solvent filtered. The procedure was performed twice. The combined methanolic filtrates were evaporated under reduced pressure and then subjected to a flash chromatography on silica gel with 50% Toluene, 30% hexane, and 20% isopropyl-alcohol as mobile phase. Six fractions were collected on the basis of the TLC profile. Fraction 2 (18 mg) corresponds to a single spot (TLC: MP = 5 Toluene: 3 hexane: 2 isopropyl-alcohol RF = 0.41). It underwent Nuclear Magnetic Resonance (1H- and 13C-NMR) and Mass Spectral (MS) analysis and it has been identified as dimethyl 3-hydroxy-5-oxotetrahydrofuran-2,3-dicarboxylate. All the spectra are reported in supplementary material, Figure S2. ESI-MS: m/z 218 [M + H]+. 1H-NMR (CDCl$_3$, 400 MHz): δH: 5.1 (1H, s), 3.9 (3H, s), 3.8 (3H, s), 3.0 (1H, d, J = 17.4 Hz), 2.8 (1H, d, J = 17.4 Hz). 13C-NMR (CDCl$_3$): δC: 172, 168, 165, 82, 77, 55, 54, 40.

HsFC (5 g) was dissolved in 100 mL of methanol and then subjected to a treatment with PS-carbonate (10 g). The mixture was shaken at room temperature for 40 min, then filtered and washed with dichloromethane (300 mL). The filtrate was concentrated in vacuo and then subjected to a flash chromatography on silica gel with 70% dichloromethane and 30% ethyl acetate as mobile phase. Four fractions were collected on the basis of the TLC profile. The second fraction corresponds to a pure compound (TLC: MP = 7 DCM: 3 AcOEt RF = 0.37; 9 mg) as a yellow oil. Its structure was then incestigated with Nuclear Magnetic Resonance (^{1}H- and ^{13}C-NMR) and Mass Spectral (MS) techniques and elucidated as 5-hydroxy-2*H*-pyran-6-carbaldehyde (see supplementary material S2). ESI-MS: m/z 127 [M + H]+, 149 [M + Na]+. 1H-NMR (CDCl$_3$, 400 MHz): δH: 9.6 (1H, s), 7.2 (1H, m), 6.4 (1H, m), 4.6 (2H, d).13C-NMR (CDCl$_3$): δC: 178, 160, 155, 125, 110, 58.

4.5. Cell Culture

RPMI 8226 human multiple myeloma cells (ATCC, Manassas, VA, USA) were cultured in RPMI 1640 medium (Euroclone, Pero, Italy) supplemented with 10% fetal bovine serum (FBS), 1% glutamine, 1% Penicillin and Streptomycin (Euroclone, Pero, Italy). Cells were incubated at 37 °C and 5% CO$_2$ in a humidified incubator.

HsEE and HsFC were dissolved in phosphate-buffered saline (PBS) at 1 g/mL concentration and then diluted directly into culture medium to working concentrations.

4.6. Biological Assays

4.6.1. MTT Assay

RPMI 8226 cells were seeded in 96-well plates at 10×10^3 cells/well density and were treated with different concentrations of HsEE (1–50 mg/mL) and HsFC (1–10 mg/mL). Untreated cells represented the controls. After 24, 48, and 72 h of treatment, a 5 mg/mL solution of 3-(4,5-dimethylthiazol-2-yl)-2,5-diphenyltetrazolium bromide (MTT) (Sigma-Aldrich, St. Louis, MO, USA) was added directly to culture medium, at final concentration of 0.5 mg/mL. After 4 h of incubation at 37 °C, plates were centrifuged at 2×10^3 RPM and culture medium was removed, formazan crystals were solubilized in acidified 2-propanol (HCl 0.3%), and absorbance was read at 560 nm in a microplate reader (BMG-Labtech, Offenburg, Germany).

4.6.2. Trypan Blue Vital Count

RPMI 8226 cells were seeded in six-well plates at 250×10^3 cells/well density and were treated with different concentrations of HsFC. Untreated cells represented the controls. After 24, 48, and 72 h of treatment cells were harvested and stained with Trypan blue vital dye (Sigma-Aldrich, USA). Viable and dead cells were counted in a Burker hemocytometer under a light microscope (Eclipse TS100, Nikon, Tokyo, Japan).

The reversibility of HsFC was evaluated by Trypan blue vital count. Cells were plated and treated as previously described. After 24 h of treatment cells were harvested. Culture medium was removed

215

after centrifugation at 1200 RPM and it was replaced with fresh medium without HsEE/HsFC. After 24, 48, and 72 h cells were stained and counted as previously described.

4.6.3. Boyden Chamber Assay

Boyden chamber assay was used to assess RPMI 8226 cell migration and invasion as previously described [20]. Briefly, 5×10^3 RPMI 8226 cells were plated in HsEE/HsFC serum free medium in the upper compartment of the Boyden chamber. Culture medium supplemented with 10% FBS as chemo-attractant was placed in the lower compartment of the chamber. Compartments were separated by a polycarbonate membrane with 8 μm pores (Biomap, Agrate Brianza, MB, Italy). The membrane was coated with gelatin at 0.2 mg/mL concentration.

After 16 h of incubation at 37 °C, the membrane was removed, fixed with cold methanol, and stained with Diff quick staining kit (Biomap, Agrate Brianza, MB, Italy). Cells on the lower surface of the membrane were counted under a light microscope.

4.6.4. DRG Neurotoxicity Assay

All experimental procedures were approved by the Ethics Committee for Animal Studies of the University of Milan Bicocca.

A pregnant Sprague Dawley rat (Envigo, Udine, Italy) was sacrificed after a deep anesthesia. Embryos were collected in L15 medium (Euroclone, Pero, Italy) and DRG were removed after dissection.

DRGs were seeded in 35 mm dishes previously coated with collagen and filled with AN2 medium (MEM (Euroclone, Pero, Italy), 10% Calf Bovine Serum (Euroclone, Pero, Italy), 1.4 mM L-Glutamine (Euroclone, Pero, Italy), 0.6% Glucose (Sigma-Aldrich, USA), and 5 ng/mL Nerve Growth Factor (NGF) (Thermo Fisher, Waltham, MA, USA). After 2 h, culture medium was removed and replaced with treatment medium (HsEE 1–10 mg/mL or HsFC 1–5 mg/mL). Untreated DRG represented the controls. After 24 and 48 h, micrographs of DRG were taken under a light microscope (Nikon Eclipse TS100) and the length of DRGs neurites was measured with ImageJ software (National Institutes of Health, Bethesda, MD, USA, http://imagej.nih.gov/ij).

4.7. Statistical Analysis

Data are reported as mean ± standard deviation (SD) from at least three independent experiments. Statistical analysis was performed using GraphPad Prism 3 software. The differences between control and treated cells were evaluated using One Way ANOVA analysis of variance followed by Dunnet's multiple comparison test. Statistical significance was set at $p < 0.05$ or $p < 0.01$.

References

1. Bergsagel, P.L.; Kuehl, W.M. Chromosome translocations in multiple myeloma. *Oncogene* **2001**, *20*, 5611–5622. [CrossRef] [PubMed]

2. Rajkumar, S.V. Multiple Myeloma: 2016 update on Diagnosis, Risk-stratification and Management. *Am. J. Hematol.* **2016**, *91*, 719–734. [CrossRef] [PubMed]

3. Kazandjian, D. Multiple myeloma epidemiology and survival, a unique malignancy. *Semin. Oncol.* **2016**, *43*, 676–681. [CrossRef] [PubMed]

4. Moschetta, M.; Sacco, A.; Belotti, A.; Ribolla, R.; Chiarini, M.; Giustini, V.; Bertoli, D.; Sottini, A.; Valotti, M.; Ghidini, C.; et al. Bone Marrow Stroma and Vascular Contributions to Myeloma Bone Homing. *Curr. Osteoporos. Rep.* **2017**, *15*, 499–506. [CrossRef] [PubMed]

5. Shupp, A.B.; Kolb, A.D.; Mukhopadhyay, D.; Bussard, K.M. Cancer Metastases to Bone: Concepts, Mechanisms, and Interactions with Bone Osteoblasts. *Cancers* **2018**, *10*, 182. [CrossRef] [PubMed]

6. Klausen, U.; Holmberg, S.; Holmström, M.O.; Jørgensen, N.G.D.; Grauslund, J.H.; Svane, I.M.; Andersen, M.H. Novel Strategies for Peptide-Based Vaccines in Hematological Malignancies. *Front. Immunol.* **2018**, *9*, 2264. [CrossRef] [PubMed]

7. López-Iglesias, A.A.; González-Méndez, L.; San-Segundo, L.; Herrero, A.B.; Hernández-García, S.; Martín-Sánchez, M.; Gutiérrez, N.C.; Paíno, T.; Avilés, P.; Mateos, M.V.; et al. Synergistic DNA-damaging effect in multiple myeloma with the combination of zalypsis, bortezomib and dexamethasone. *Haematologica* **2017**, *102*, 168–175. [CrossRef] [PubMed]

8. Moreau, P.; Richardson, P.G.; Cavo, M.; Orlowski, R.Z.; Miguel, J.F.S.; Palumbo, A.; Harousseau, J.-L. Proteasome inhibitors in multiple myeloma: 10 years later. *Blood* **2012**, *120*, 947–959. [CrossRef] [PubMed]

9. Pennisi, A.; Li, X.; Ling, W.; Khan, S.; Zangari, M.; Yaccoby, S. The proteasome inhibitor, bortezomib suppresses primary myeloma and stimulates bone formation in myelomatous and nonmyelomatous bones in vivo. *Am. J. Hematol.* **2009**, *84*, 6–14. [CrossRef] [PubMed]

10. Driscoll, J. Expression of E3 Ubiquitin Ligases in Multiple Myeloma Patients after Treatment with the Proteasome Inhibitor Bortezomib. *Cancer Transl. Med.* **2015**, *1*, 153. [CrossRef]

11. Costa, F.; Das, R.; Bailur, J.K.; Dhodapkar, K.; Dhodapkar, M.V. Checkpoint Inhibition in Myeloma: Opportunities and Challenges. *Front. Immunol.* **2018**, *9*, 2204. [CrossRef] [PubMed]

12. Ishida, T. Therapeutic antibodies for multiple myeloma. *Jpn. J. Clin. Oncol.* **2018**, *48*, 957–963. [CrossRef] [PubMed]

13. Robak, P.; Drozdz, I.; Szemraj, J.; Robak, T. Drug resistance in multiple myeloma. *Cancer Treat. Rev.* **2018**, *70*, 199–208. [CrossRef] [PubMed]

14. Gay, F.; Palumbo, A. Multiple myeloma: Management of adverse events. *Med. Oncol.* **2010**, *27*, 646–653. [CrossRef] [PubMed]

15. Meregalli, C. An Overview of Bortezomib-Induced Neurotoxicity. *Toxics* **2015**, *3*, 294–303. [CrossRef] [PubMed]

16. Tacchetti, P.; Terragna, C.; Galli, M.; Zamagni, E.; Petrucci, M.T.; Pezzi, A.; Montefusco, V.; Martello, M.; Tosi, P.; Baldini, L.; et al. Bortezomib- and thalidomide-induced peripheral neuropathy in multiple myeloma: Clinical and molecular analyses of a phase 3 study. *Am. J. Hematol.* **2014**, *89*, 1085–1091. [CrossRef] [PubMed]

17. Argyriou, A.A.; Cavaletti, G.; Bruna, J.; Kyritsis, A.P.; Kalofonos, H.P. Bortezomib-induced peripheral neurotoxicity: An update. *Arch. Toxicol.* **2014**, *88*, 1669–1679. [CrossRef]

18. Meregalli, C.; Chiorazzi, A.; Carozzi, V.A.; Canta, A.; Sala, B.; Colombo, M.; Oggioni, N.; Ceresa, C.; Foudah, D.; La Russa, F.; et al. Evaluation of tubulin polymerization and chronic inhibition of proteasome as citotoxicity mechanisms in bortezomib-induced peripheral neuropathy. *Cell Cycle* **2014**, *13*, 612–621. [CrossRef]

19. Cavaletti, G.; Jakubowiak, A.J. Peripheral neuropathy during bortezomib treatment of multiple myeloma: A review of recent studies. *Leuk. Lymphoma* **2010**, *51*, 1178–1187. [CrossRef]

20. Malacrida, A.; Maggioni, D.; Cassetti, A.; Nicolini, G.; Cavaletti, G.; Miloso, M. Antitumoral Effect of Hibiscus sabdariffa on Human Squamous Cell Carcinoma and Multiple Myeloma Cells. *Nutr. Cancer* **2016**, *68*, 1–10. [CrossRef]

21. Riaz, G.; Chopra, R. A review on phytochemistry and therapeutic uses of Hibiscus sabdariffa L. *Biomed. Pharmacother.* **2018**, *102*, 575–586. [CrossRef] [PubMed]

22. Mohamed, R.; Fernández, J.; Pineda, M.; Aguilar, M. Roselle (Hibiscus sabdariffa) Seed Oil Is a Rich Source of? Tocopherol. *J. Food Sci.* **2007**, *72*, S207–S211. [CrossRef] [PubMed]

23. Mahadevan, N.; Shivali; Kamboj, P. Hibiscus sabdariffa Linn.-An overview. *Nat. Prod. Radiance* **2009**, *8*, 77–83.

24. Tahir, H.E.; Xiaobo, Z.; Jiyong, S.; Mariod, A.A.; Wiliam, T. Rapid Determination of Antioxidant Compounds and Antioxidant Activity of Sudanese Karkade (Hibiscus sabdariffa L.) Using Near Infrared Spectroscopy. *Food Anal. Methods* **2016**, *9*, 1228–1236. [CrossRef]

25. Duh, P.-D.; Yen, G.-C. Antioxidative activity of three herbal water extracts. *Food Chem.* **1997**, *60*, 639–645. [CrossRef]

26. Hajifaraji, M.; Tarkhani, A.H. The effect of sour tea (Hibiscus sabdariffa) on essential hypertension. *J. Ethnopharmacol.* **1999**, *65*, 231–236. [CrossRef]

27. Peng, C.-H.; Yang, Y.-S.; Chan, K.-C.; Wang, C.-J.; Chen, M.-L.; Huang, C.-N. Hibiscus sabdariffa Polyphenols Alleviate Insulin Resistance and Renal Epithelial to Mesenchymal Transition: A Novel Action Mechanism Mediated by Type 4 Dipeptidyl Peptidase. *J. Agric. Food Chem.* **2014**, *62*, 9736–9743. [CrossRef]

28. Hassan, S.T.S.; Berchová, K.; Majerová, M.; Pokorná, M.; Švajdlenka, E. In vitro synergistic effect of Hibiscus sabdariffa aqueous extract in combination with standard antibiotics against Helicobacter pylori clinical isolates. *Pharm. Biol.* **2016**, *54*, 1736–1740. [CrossRef]

29. Chen, C.-C.; Hsu, J.-D.; Wang, S.-F.; Chiang, H.-C.; Yang, M.-Y.; Kao, E.-S.; Ho, Y.-C.; Wang, C.-J. Hibiscus sabdariffaExtract Inhibits the Development of Atherosclerosis in Cholesterol-Fed Rabbits. *J. Agric. Food Chem.* **2003**, *51*, 5472–5477. [CrossRef]

30. Khaghani, S.; Razi, F.; Yajloo, M.M.; Paknejad, M.; Shariftabrizi, A.; Pasalar, P. Selective Cytotoxicity and Apoptogenic Activity of Hibiscus Sabdariffa Aqueous Extract Against MCF-7 Human Breast Cancer Cell Line. *J. Cancer Ther.* **2011**, *2*, 394–400. [CrossRef]

31. Akim, A.M.; Ling, L.C.; Rahmat, A. Antioxidant and anti-proliferative activities of Roselle juice on Caov-3, MCF-7, MDA-MB-231 and HeLa cancer cell lines. *African J. Pharm. Pharmacol.* **2011**, *5*, 957–965.

32. Olvera-García, V.; Castaño-Tostado, E.; Rezendiz-Lopez, R.I.; Reynoso-Camacho, R.; González de Mejía, E.; Elizondo, G.; Loarca-Piña, G. Hibiscus sabdariffa L. extracts inhibit the mutagenicity in microsuspension assay and the proliferation of HeLa cells. *J. Food Sci.* **2008**, *73*, T75–T81. [CrossRef] [PubMed]

33. Adanlawo, I.; Ajibade, V. Nutritive Value of the Two Varieties of Roselle (Hibiscus Sabdariffa) Calyces and Soaked with Wood Ash. *Pak. J. Nutr.* **2007**, *1*, 38–46.

34. Chang, Y.-C.; Huang, H.-P.; Hsu, J.-D.; Yang, S.-F.; Wang, C.-J. Hibiscus anthocyanins rich extract-induced apoptotic cell death in human promyelocytic leukemia cells. *Toxicol. Appl. Pharmacol.* **2004**, *205*, 201–212. [CrossRef] [PubMed]

35. Amri, B.; Martino, E.; Vitulo, F.; Corana, F.; Ben-Kaâb, L.B.; Rui, M.; Rossi, D.; Mori, M.; Rossi, S.; Collina, S. Marrubium vulgare L. leave extract: Phytochemical composition, antioxidant and wound healing properties. *Molecules* **2017**, *22*, 1851. [CrossRef]

36. Martino, E.; Collina, S.; Rossi, D.; Bazzoni, D.; Gaggeri, R.; Bracco, F.; Azzolina, O. Influence of the extraction mode on the yield of hyperoside, vitexin and vitexin-2-O-rhamnoside from Crataegus monogyna Jacq. (Hawthorn). *Phytochem. Anal.* **2008**, *19*, 534–540. [CrossRef] [PubMed]

37. Martino, E.; Ramaiola, I.; Urbano, M.; Bracco, F.; Collina, S. Microwave-assisted extraction of coumarin and related compounds from Melilotus officinalis (L.) Pallas an alternative to Soxhlet and ultrasound-assisted extraction. *J. Chromatogr. A* **2006**, *1125*, 147–151. [CrossRef]

38. Rossi, D.; Ahmed, K.M.; Gaggeri, R.; Volpe, S.D.; Maggi, L.; Mazzeo, G.; Longhi, G.; Abbate, S.; Corana, F.; Martino, E.; et al. (R)-(-)-Aloesaponol III 8-methyl ether from Eremurus persicus: A novel compound against leishmaniosis. *Molecules* **2017**, *22*, 519. [CrossRef]

39. Martino, E.; Della Volpe, S.; Cavalloro, V.; Amri, B.; Kaab, L.B.B.; Marrubini, G.; Rossi, D.; Collina, S. The use of a microwave-assisted solvent extraction coupled with HPLC-UV/PAD to assess the quality of Marrubium vulgare L. (white horehound) herbal raw material. *Phytochem. Anal.* **2019**, *30*, 377–384. [CrossRef]

40. Scuteri, A.; Nicolini, G.; Miloso, M.; Bossi, M.; Cavaletti, G.; Windebank, A.J.; Tredici, G. Paclitaxel toxicity in post-mitotic dorsal root ganglion (DRG) cells. *Anticancer. Res.* **2006**, *26*, 1065–1070.

41. Polavarapu, P.L.; Donahue, E.A.; Shanmugam, G.; Scalmani, G.; Hawkins, E.K.; Rizzo, C.; Ibnusaud, I.; Thomas, G.; Habel, D.; Sebastian, D. A Single Chiroptical Spectroscopic Method May Not Be Able To Establish the Absolute Configurations of Diastereomers: Dimethylesters of Hibiscus and Garcinia Acids. *J. Phys. Chem. A* **2011**, *115*, 5665–5673. [CrossRef] [PubMed]
42. Almahy, H.A.; Abdel-Razik, H.H.; El-Badry, Y.A.; Ibrahim, E.M. Ultrasonic extraction of anthocyanin's natural dyes from Hibiscus sabdariffa (Karkade) and its application on dying foodstuff and beverages in kingdom of Saudi Arabia. *Am. J. Biol. Pharm. Res.* **2015**, *2*, 168–174.

Samples of the compounds *Hib-ester* and *Hib-carbaldeyde* are available from the authors.